

Characterization and Identification of Bituminous Materials

Modified with Montmorillonite Nanoclay

Gang Liu

**Karakterisering en Identificatie van met Montmorillonite Nanoklei
gemodificeerde Bitumineuze Materialen**

Proefschrift

ter verkrijging van de graad van doctor
aan de Technische Universiteit Delft,
op gezag van de Rector Magnificus prof. ir. K.C.A.M. Luyben,
voorzitter van het College voor Promoties,
in het openbaar te verdedigen op maandag 12 december 2011 om 10:00uur

door

Gang LIU

Master of Science in Materials Science & Engineering
Wuhan University of Technology, P.R. China
geboren te Jingmen, Hubei, P.R. China

Dit proefschrift is goedgekeurd door de promotoren:

Prof.dr.ir. A.A.A. Molenaar

Prof. S.P. Wu, BSc., MSc., PhD.

Copromotor:

Ir. M.F.C van de Ven

Samenstelling promotiecommissie:

Rector Magnificus

Prof.dr.ir. A.A.A. Molenaar

Prof. S.P. Wu, BSc., MSc., PhD.

Ir. M.F.C. van de Ven

Prof. B. Birgisson, BSc., MSc.,
PhD.

Prof. J.Y.Yu, BSc., MSc., PhD.

Prof. dr. S. J. Picken

Dr. Z. Su, BSc., MSc.

Technische Universiteit Delft, voorzitter

Technische Universiteit Delft, promotor

Technische Universiteit Wuhan, promotor

Technische Universiteit Delft, copromotor

Royal Institute of Technology, Sweden

Technische Universiteit Wuhan

Technische Universiteit Delft

ESHA Group bv, R&D

Prof.dr.ir. K. van Breugel

Technische Universiteit Delft, reservelid

Published and distributed by:

Gang Liu

Road and Railway Engineering Section

Faculty of Civil Engineering and Geosciences

Delft University of Technology

P.O. Box 5048, 2600 GA Delft, the Netherlands

E-mail: liugang102129@hotmail.com

ISBN 978-90-8570-779-0

Key words: Bitumen; Montmorillonite; Ageing; Rheology; Fatigue; Structure

Printing: Wohrmann Print Service, Zutphen, the Netherlands

©2011 by Gang Liu

All rights reserved. No part of this publication may be reproduced, stored in a retrieval system or transmitted in any form or by any means, electronic, mechanical, photocopying, recording, or otherwise without the prior permission of the proprietor

To my mother who is always there for me

ACKNOWLEDGEMENT

This PhD research was mainly carried out at the Laboratory of Road and Railway Engineering (80%), the Delft University of Technology (DUT) in cooperation with the Key Laboratory of Silicate Materials Science and Engineering of Ministry of Education (20%), Wuhan University of Technology (WHUT, my Alma Mater). When writing this acknowledgment, I realized that so many people have been involved in my work and generously offered me lots of help. Without their support, it would have been hard for me to make all these things happen. I would like to convey them my most grateful acknowledgement.

I would first of all like to thank my promotor, Prof. A.A.A. Molenaar who gave me the opportunity to do this research at TUD. He gave me invaluable guidance and encouragement and shared with me his extensive experience in the academic and industrial world. These are useful for my entire life.

I am very grateful to Prof. Shaopeng Wu who was my supervisor in my master study and also my promotor in my PhD study. Without his contribution to the international scientific cooperation between DUT and WHUT, I would have no such an important chance to study abroad.

I also would like to thank associate Prof. Martin van de Ven who was my daily supervisor and co-promotor. His experience, unique knowledge in the road engineering and the attitude to the life benefit me a lot. Each day I highly appreciated the fact that he has lent me his bicycle.

I would like to thank Prof. Jianying Yu for his personal guidance during the first year of my PhD study. He provided me a lot of important insight into the research.

I am very grateful to Dr. Zhao Su for his help and suggestions on my research, especially for his careful review of my thesis manuscript during the time he was ill.

I also like to acknowledge Prof. Zhonghe Shui for his contribution to the cooperation between the DUT and the WHUT.

For the work done at WHUT, I express my special gratitude to my colleagues, Jingang Wang, Yuan Zhang, Man Yu and Juntao Lin for their hard work on the experimental tests.

I would like to thank the staff of the Laboratory of Road and Railway Engineering of the DUT, Jan Moraal, Jan-Willem Bientjes, Marco Poot, ex-manager Abdol Miradi, secretary Jacqueline Barnhoorn and former secretary Sonja van den Bos for their assistance and help.

It has been my fortune to meet so many talented colleagues and friends at DUT. Socializing with them brought me happiness. Therefore, many thanks go to Jian, Dongxing, Yue, Ning, Quantao, Diederik, Milliyan, Mohamad, Dongya, Shaoguang, Xiangyun, Sadegh, Chang, Xin, Mingliang, Mauricio, Punkgy, as well as my officemates Marija and Pengpeng. My special gratitude goes to my senior

colleague Liantong Mo and his wife Xuming Shan who offered me their hospitality when I just arrived in Delft and helped me to get used to the life in this city.

Finally, I would like to thank my mother for her unswerving support and encouragement. Most importantly, my last thanks go to my wife Juan for her love, understanding and continuous support from my bachelor to PhD studies for almost ten years.

Gang Liu

31st, October, 2011, Delft

Summary

Montmorillonite (Mt) nanoclay is a layered silicate mineral with a 2:1-type layer structure, two tetrahedrals sandwiching one octahedral. In recent decades, it is successfully introduced into polymer systems to form polymer-clay nanocomposites (PCN) in which the silicate layers of the Mt are randomly and homogeneously dispersed at a molecular level in the polymer matrix. Due to the addition of Mt, some properties of PCN, such as the mechanical, thermal and gas barrier properties, were superior to those of pristine polymers.

Based on this idea, natural and organo Mts were used to modify bitumens with different penetration grades in this study. Some rheological, ageing and fatigue properties of the modified bitumens and mortars were characterized. High-shearing mixing method was used to prepare the modified bitumen; X-ray diffraction and micro-CT scanning were employed to observe structures of Mts in bitumen; DSR equipment was adopted to characterize the rheological properties; the rolling thin film oven (RTFO) and pressure ageing vessel (PAV) methods were used to simulate the short term and long term ageing on base and Mt modified bitumens, respectively. Fatigue tests were performed on bitumen and mortar samples which consisted of bitumen, filler and sand at a weight ratio of 0.34:0.30:0.36, as well as on a dense graded asphalt mixture.

XRD results indicated an intercalated structure of organo Mts in the bituminous matrix. A phase separated structure of natural Mt was found in the base bitumen. Micro-CT images further proved that natural Mt acted like a conventional filler at micrometer level. The interaction between the Mts layers and bitumen changed its viscosity and dynamic response as characterized by means of the DSR. Reinforced shear thinning was observed on the modified bitumens at a liquid state, which implies a better drainage resistance of asphalt mixture during transportation.

The results indicated that organo Mts improve the short term ageing resistance of base bitumen. The main reason for this improvement is that the barrier properties of Mt particles hinder the penetration of oxygen. Meanwhile, the reduction of volatilization of the oil components of bitumen due to these barrier properties can be another reason. However, a less effective improvement was observed for the long term ageing using the PAV. That is because organo Mt platelets automatically accumulated to reduce their surface area under tough testing conditions in the PAV. This accumulation weakened the barrier properties of the Mts. It is believed however that organo Mts will improve the long term ageing

behaviour of bitumen in the field because the state of the Mt will be very stable and no accumulation as occurred in the PAV will happen.

The addition of organo Mts can change the fatigue properties of bitumen and even mortar. This change was influenced by the type of the surfactant on the Mt which determined the interfacial interaction between the bitumen and the Mt. Because of the heterogeneous character of asphalt mixtures and their complicated failure mechanism, the fatigue test on the asphalt mixture with the modified bitumen only gave a limited improvement of this property.

Finally, some important aspects are given for further research. Based on the present research results, the organo Mt can be an alternative to modifiers used in the bitumen to sustain the durability of asphalt pavements.

Samenvatting

Montmorillonite (Mt) nanoklei is een gelaagd silicaat material met een zogenaamde 2:1 type lagen structuur, waarbij een octaeder zit tussen twee tetraeders. De laatste decennia is deze nanoklei succesvol toegepast in polymeer systemen en deze klei/polymeermengsels worden wel clay-polymer nanocomposites (PCN) genoemd. De silicaat lagen van de Mt zijn op moleculair niveau willekeurig en homogeen gedispergeerd in de polymeer matrix. Dankzij de toevoeging van Mt kunnen sommige eigenschappen van PCN zoals mechanische, thermische en gas barrière eigenschappen, superieur zijn ten opzichte van de polymeer zonder Mt.

Op basis van de ervaringen met polymeren zijn in deze studie zowel natuurlijke als organo Mts gebruikt voor het modifieren van penetratie bitumen. De invloed van toevoeging van Mts op een aantal rheologische eigenschappen, alsmede het vermoeiingsgedrag en de veroudering van penetratie bitumen en bitumineuze mortels is onderzocht. Een speciale mengmethode is ontwikkeld voor het inbrengen van de Mts. X-ray diffractie en micro-CT scanning zijn gebruikt om de structuur van Mts in bitumen te bestuderen. De dynamic shear rheometer (DSR) is gebruikt voor het bepalen van de rheologisch eigenschappen; de rolling thin film oven (RTFOT) en de pressure aging vessel (PAV) zijn gebruikt om de korte termijn veroudering en de lange termijn veroudering na te bootsen. Vermoeiingsproeven zijn uitgevoerd op de gemodificeerde bitumen, gemodificeerde bitumineuze mortels en een met organoklei gemodificeerd dichtasfaltbeton mengsel

De XRD resultaten toonden dat de organo Mts volgens een zogenaamde intercalated structuur zijn verdeeld in de bitumen matrix. Micro CT scans toonden aan dat de natuurlijke Mt functioneert als een conventionele vulstof op micrometer niveau. Met de DSR kon een duidelijke verandering van de viscositeit en de dynamische reactie van het gemodificeerde bindmiddel worden waargenomen dankzij de interactie tussen de Mt lagen en het bitumen. Versterkte “shear thinning” werd waargenomen voor de gemodificeerde bitumen in de vloeistoffase, hetgeen een betere weerstand tegen afdruipten van het bindmiddel in een asfaltmengsel tijdens transport suggereert.

De korte termijn veroudering vermindert aanzienlijk ten gevolge van het toevoegen van Mt aan bitumen. De belangrijkste verklaring voor deze verbetering kan worden gevonden in de barrière werking van de Mt plaatjes waardoor indringing van zuurstof wordt verhinderd. Ook is het mogelijk dat door de barrière

werking de bij hoge temperaturen vluchtige componenten beter in de bitumen vast worden gehouden. Voor de lange termijn veroudering uitgevoerd met de PAV kon deze trend niet worden bevestigd. Het is echter aannemelijk dat de organo Mt plaatjes spontaan aan elkaar gaan zitten ten gevolge van de agressieve proefcondities in de PAV, waardoor het specifiek oppervlak sterk afneemt. Hierdoor worden de barrière eigenschappen zoals geïndiceerd door afzonderlijke plaatjes sterk verminderd. Omdat in de praktijk geen samenvoeging van de Mt plaatjes zoals waargenomen in de PAV zal optreden, wordt verwacht dat organo Mts ook de lange termijn veroudering van bitumen in de praktijk sterk zullen verbeteren.

Toevoeging van organo Mt beïnvloedt de vermoeiingseigenschappen van bitumen en de mortel. De invloed op de vermoeiingseigenschappen hangt af van de soort surfactant die op de Mt is aangebracht, omdat deze de interactie tussen de bitumen en de Mt bepaalt. Vanwege het heterogene karakter van asfalt mengsels en het complexe bezwijkmechanisme bij vermoeiing bleek de toevoeging van Mt aan bitumen slechts geringe verbetering van het vermoeiingsgedrag van een mengsel te geven. Wel werd een duidelijke verbetering van de weerstand tegen permanente deformatie waargenomen.

Op basis van de huidige onderzoeksresultaten kan worden gesteld dat toevoeging van organo Mt aan bitumen een uitstekend middel kan zijn om de veroudering en het afdruipe van het bindmiddel in asfaltmengsels tegen te gaan. Met name voor zoab is dit een zeer belangrijke eigenschap.

Abbreviations

AA	Amino acid
ABS	Acrylonitrile butadiene styrene
AFM	Atomic force microscopy
AI	Ageing index
BE	Electron binding energy
BET	Specific surface area
CEC	Cation exchange capacity
CLSM	Confocal laser-scanning microscope
CPS	Photoelectron counts per second
CT	Computed tomography
DSC	Differential scanning calorimetry
DSR	Dynamic shear rheometer
DTG	Derivative thermogravimetric
ESEM	Environmental scanning electron microscopy
EVA	Ethylene vinyl acetate
FBA	Fluorescent brightening agent
FM	Fluorescence microscopy
FTIR	Fourier transform infrared
H/C	Hydrogen/carbon
GPC	Gel permeation chromatography
KE	Kinetic energy
Mt	Montmorillonite
NCH	Nylon-6 clay hybrid
NMR	Nuclear magnetic resonance
NRTFOT	Nitrogen rolling thin film oven test
PAC	Porous asphalt
PAV	Pressure ageing vessel
PB	Polybutylene
PCN	Polymer-clay nanocomposites
PE	Polyethylene
PMMA	Poly (methyl methacrylate)
PMB	Polymer modified bitumen
PP	Polypropylene
PS	Polystyrene
RDEC	Ratio of dissipated energy change
RTFOT	Rolling thin film oven test
SBR	Styrene butadiene rubber

SBS	Styrene butadiene styrene
SEBS	Styrene-(ethylene-butylene)-styrene
SEM	Scanning electron microscopy
SIS	Styrene-isoprene-styrene
SMA	Stone matrix asphalt
S-model	Sigmoid model
TEM	Transmission electron microscopy
TFOT	The thin film oven test
TGA	Thermogravimetric
TUD	Delft University of Technology
UV	Ultraviolet
WLF	Williams-Landel-Ferry
WHUT	Wuhan University of Technology
XPS	X-ray photoelectron spectrometry
XRD	X-ray diffraction

TABLE OF CONTENTS

1 INTRODUCTION.....	- 1 -
1.1 Background	- 1 -
1.2 Objectives.....	- 3 -
1.3 Structure of this dissertation	- 4 -
1.4 References	- 6 -
2 LITERATURE REVIEW.....	- 7 -
2.1 Application of nanoclay in polymers	- 7 -
2.1.1 Montmorillonite nanoclay	- 8 -
2.1.2 Processing of polymer-clay nanocomposites.....	- 12 -
2.1.3 Properties of polymer-clay nanocomposite (PCN)	- 13 -
2.1.3.1 Mechanical	- 13 -
2.1.3.2 Barrier	- 17 -
2.1.3.3 Thermal	- 18 -
2.2 Bitumen	- 19 -
2.2.1 Chemical composites in the bitumen	- 19 -
2.2.2 Colloidal nature.....	- 23 -
2.2.3 Modification to bitumen	- 24 -
2.2.4 Bitumen's natural relation with clays	- 25 -
2.3 Summary.....	- 26 -
2.4 References	- 27 -
3 PREPARATION OF MONTMORILLONITE MODIFIED BITUMEN - 31 -	
3.1 Introduction.....	- 31 -
3.2 Characteristics of montmorillonites	- 32 -
3.2.1 Thermal stability	- 32 -
3.2.2 Density	- 36 -
3.2.3 Basal spacing (d_{001}).....	- 37 -
3.2.4 Particle size	- 39 -
3.3 Specimen preparation	- 41 -
3.3.1 Equipments.....	- 41 -
3.3.2 Preparation protocol.....	- 42 -
3.4 Summary and conclusions.....	- 45 -
Appendix A.1	- 47 -

<i>Appendix A.2</i>	- 49 -
<i>3.5 References</i>	- 54 -
4 STRUCTURE OF NANOCLAY IN MODIFIED BITUMEN.....	- 55 -
<i>4.1 Introduction</i>	- 55 -
4.1.1 Structures of base and modified bitumens	- 55 -
4.1.2 Structures of clay in the polymer	- 58 -
4.1.3 Summary	- 60 -
<i>4.2 Methods</i>	- 60 -
4.2.1 XRD	- 60 -
4.2.2 X-ray computed tomography (CT) scanning	- 61 -
4.2.3 Fluorescence microscope and other methods	- 62 -
<i>4.3 Results and analyses</i>	- 63 -
4.3.1 XRD	- 63 -
4.3.2 Micro-CT Scanning.....	- 66 -
4.3.3 Fluorescence image.....	- 68 -
4.3.4 Other methods	- 69 -
<i>4.4 Summary and conclusions</i>	- 70 -
<i>4.5 Reference</i>	- 71 -
5 AGEING PROPERTIES	- 73 -
<i>5.1 Introduction</i>	- 73 -
5.1.1 Ageing effect.....	- 73 -
5.1.2 Improvement of bitumen ageing	- 76 -
<i>5.2 Characterization methods</i>	- 77 -
5.2.1 Simulation in the lab	- 77 -
5.2.2 Ageing evaluation	- 81 -
5.2.2.1 Rheological methods.....	- 81 -
5.2.2.2 Chemical characterization on ageing	- 82 -
5.2.2.3 Summary	- 83 -
<i>5.3 Ageing results and analyses</i>	- 84 -
5.3.1 Empirical rheological properties.....	- 84 -
5.3.2 Fundamental rheological properties.....	- 89 -
5.3.3 FTIR method	- 95 -
5.3.4 Morphology change after ageing	- 99 -
<i>5.4 Summary and conclusions</i>	- 100 -
<i>Appendix B</i>	- 102 -
<i>5.5 Reference</i>	- 104 -

6 RHEOLOGICAL PROPERTIES	- 107 -
6.1 Introduction.....	- 107 -
6.2 Methods.....	- 108 -
6.2.1 Materials.....	- 108 -
6.2.2 Cone and plate rheometer	- 108 -
6.2.3 Dynamic shear rheometer	- 111 -
6.3 Results and analyses	- 116 -
6.3.1 Properties characterized by the cone and plate rheometer.....	- 116 -
6.3.1.1 Dynamic viscosity.....	- 116 -
6.3.1.2 Shear rate sweeps	- 117 -
6.3.2 Master curves by DSR	- 121 -
6.3.3 Composite model	- 128 -
6.3.3.1 Theory	- 128 -
6.3.3.2 Volume fraction	- 131 -
6.3.3.3 Results and analysis	- 132 -
6.4 Summary and conclusions.....	- 136 -
Appendix C.....	- 137 -
6.5 Reference.....	- 139 -
7 FATIGUE-----FROM BINDER TO MIXTURE.....	- 141 -
7.1 Introduction.....	- 141 -
7.1.1 Fatigue in asphalt mixtures	- 141 -
7.1.1.1 Fatigue phenomenon	- 141 -
7.1.1.2 Fatigue failure mechanism.....	- 142 -
7.1.1.3 Laboratory methods and criteria	- 143 -
7.1.2 Fatigue in polymer-clay nanocomposites (PCN).....	- 152 -
7.1.3 Conclusion	- 152 -
7.2 Experimental program.....	- 153 -
7.2.1 Raw materials.....	- 153 -
7.2.1.1 Bitumens	- 153 -
7.2.1.2 Montmorillonite nanoclay (Mt)	- 153 -
7.2.1.3 Filler and sand.....	- 154 -
7.2.1.4 Stones	- 154 -
7.2.1.5 Specimen preparation.....	- 155 -
7.2.2 Test description and interpretation.....	- 158 -
7.2.2.1 Testing of the bitumen	- 158 -
7.2.2.2 Testing of the mortar.....	- 163 -
7.2.2.3 Testing of the mixture	- 165 -
7.3 Fatigue results and analyses.....	- 168 -

7.3.1 Binder fatigue.....	- 168 -
7.3.2 Mortar fatigue	- 174 -
7.3.3 Mixture fatigue.....	- 180 -
7.3.4 Resilient modulus.....	- 183 -
7.4 <i>Summary and conclusions</i>	- 187 -
7.5 <i>Reference</i>	- 189 -
8 CONCLUSIONS AND RECOMMENDATIONS.....	- 193 -
8.1 <i>Introduction</i>	- 193 -
8.2 <i>Conclusions</i>	- 193 -
8.3 <i>Recommendations</i>	- 194 -
Publications.....	- 197 -
Curriculum Vitae	- 199 -

1

INTRODUCTION

1.1 Background

Bitumen is one of human's oldest engineering materials and is used at the beginning of civilization as a water proofing and bonding agent. It is defined in the Wikipedia as a mixture of organic liquids that are highly viscous, black, sticky, entirely soluble in carbon disulfide (CS_2), and composed primarily of highly condensed polycyclic aromatic hydrocarbons.

The earliest record about natural bitumens was to bind the stone blocks in the wall of the water tank in the Sumerian empire which existed from around 3500 B.C. to approximately 2000 B.C. As early as 2600 B.C., Egyptians used natural bitumen for waterproofing, mummification and building structures. These bitumens were laid down in a geologic stratum and occurred in veins of rock formations, or impregnated in various limestone, sandstone formations and lakes (Roberts, Kandhal et al. 1996). Trinidad Lake Bitumen is one of the largest natural bitumen deposits in the world.

In modern industrial society, bitumen is manufactured by the distillation process of crude oil in refineries, and has been widely used in the construction of asphalt pavements all over the world. A schematic representation of the components in an asphalt mixture is shown in Figure 1.1.1a. To stabilize the stone aggregate skeleton in an asphalt pavement, mortar consisting of bitumen, filler, and sand at a certain ratio acts as a real glue in the asphalt mixture. Bitumen is a viscoelastic material and makes the asphalt pavement flexible and comfortable.

Figure 1.1.1b shows the worldwide bitumen consumption per year which increases year by year. It is more prominent in some developing countries due to the economic growth. Statistic data indicates that 19 million tons of bitumen was used in the construction of asphalt pavement in 2010 in China, which is almost one fifth of total consumption in the world (104.3 million tons in this year).

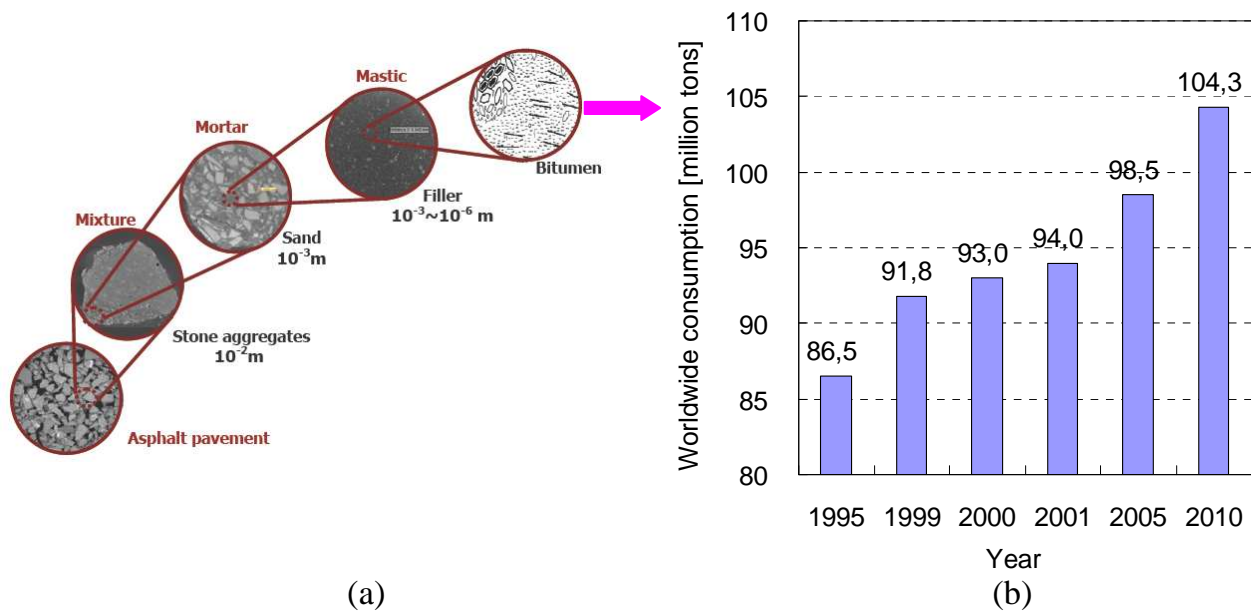


Figure 1.1.1 (a) Schematic components of asphalt mixture and (b) bitumen's worldwide consumption every year

In practice, the properties of bitumen change during its service life due to vehicle loads and environmental factors (Petersen 1984 ; Halstead 1985). At high temperatures, low frequency of loading, bitumen could become soft with a low stiffness and susceptible to permanent deformation. As a complex mixture of aliphatic, aromatic and naphthenic hydrocarbons, bitumen easily gets aged due to the diffusion of oxygen and UV radiation. Repeated loads will result in decreasing strength because of fatigue. Rainwater can influence the adhesion between bitumen and the aggregate and the brittleness of bitumen at low temperatures often causes thermal cracking. All these factors can lead to failure of the asphalt pavement.

On the other hand, society's development demands better performing pavements as the number and axle loading of vehicles increase year by year. Good structural design and high construction quality are necessary to provide safety and comfort to the road user. The use of modified bitumen is an important solution to reduce the frequency of maintenance and sustain the pavement's durability. According to practical needs and requirements on site, different modifiers are available to improve properties of the bitumen. For example, improvements in deformation resistance can be achieved using thermoplastic polymers and rubbers, as well as some chemicals, such as sulphur. Thermoplastic elastomers could improve the thermal cracking and fatigue resistance. Hydrated lime and some antioxidants could increase the ageing resistance and some adhesion improvers are available in

the market to reduce moisture damage (Read and Whiteoak 2003). Some mechanisms of these improvements will be introduced in Chapter 2.

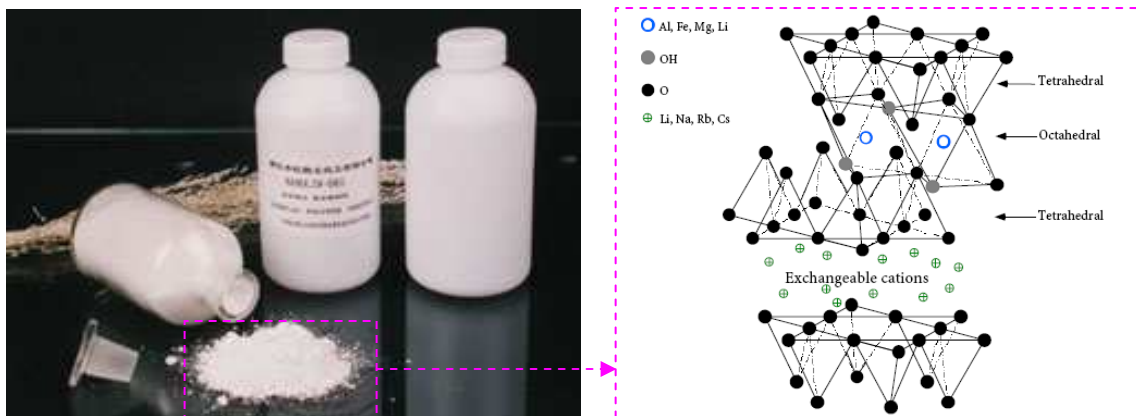


Figure 1.1.2 Montmorillonite available from the market and its molecular structure (Giannelis, Krishnamoorti et al. 1999)

In recent decades, montmorillonite nanoclay (Mt), a member of the smectite family, has been successfully used to modify polymers. As shown in Figure 1.1.2, Mt is a layered silicate mineral with a 2:1-type layer structure, two tetrahedrals sandwiching one octahedral (F.Bergaya, Theng et al. 2006; Okada and Usuki 2006). The single Mt layer has a thickness of around 1 nm and a cross-sectional area of 100 nm². There are some hydrated cations, such as Na⁺, residing between the layers. In order to make the Mt more compatible with the polymer, some surfactants, such as quaternary ammonium salt, are usually used to modify them in which organic cations will replace the interlayer hydrated cations. In this way, the normally hydrophilic silicate surface becomes organophilic (Giannelis 1996).

The Mts help polymer systems to form polymer-clay nanocomposites (PCN) in which Mt layers are randomly and homogeneously dispersed at a molecular level in the polymer matrix (Pinnavaia and Beall 2000; Koo 2006). With only a small amount of Mt about 1-5 wt.%, some properties of PCN are superior to those of virgin polymers. This concerns improved mechanical properties, thermal and chemical resistance, decreased gas and moisture permeability, etc. The first PCN of Nylon 6-clay hybrid invented in 1985 has to be mentioned (Okada and Usuki 2006).

1.2 Objectives

The main goal of this research is to investigate how different montmorillonites influence the properties of base bitumens, and consequently find possibilities of how these modifications can be used in practice. To achieve this goal, following objectives were defined:

- Determine the most accessible method to manufacture montmorillonite modified bitumen in the lab.
- Observe and characterize the structures of Mts at micro- and nano-scale levels in the bitumen which could determine the final properties.
- Investigate the effect of Mts on the rheological, ageing and fatigue properties of base bitumen.
- Develop a relation between the characteristics of Mt (such as the surfactants on the Mt, its structures in the bitumen etc.) and properties of modified bitumen.

Figure 1.2.1 shows the simplified schematic of whole research work.

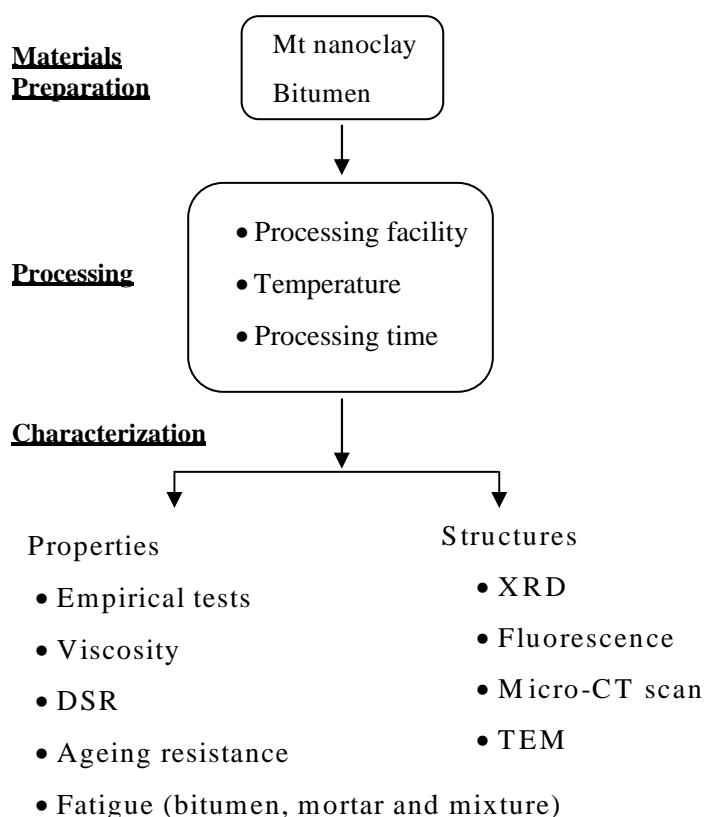


Figure 1.2.1 Simplified schematic of whole research work

1.3 Structure of this dissertation

This dissertation is divided into seven chapters. Chapter 2 summarizes the present knowledge about bitumen, its modification, nanoclays (e.g. montmorillonite) and their application in the polymer-clay nanocomposites.

Chapter 3 gives a detailed description of the materials used in this study, including base bitumens and montmorillonites (Mts) with and without surfactants. The

manufacturing method and its conditions (e.g. time and temperature) are also presented.

In Chapter 4, different methods are described to observe the structures of inorganic and organo Mts in the base bitumen, including X-ray diffraction (XRD), Micro-CT scanning, fluorescence microscope and atomic force microscope (AFM).

The ageing behaviour of modified bitumens is discussed in Chapter 5. The rolling thin film oven test (RTFOT) and the pressure air vessel (PAV) are used to simulate the short term and long term ageing on base and Mt modified bitumens, respectively. Rheological tests and Fourier transform infrared spectroscopy (FTIR) tests are performed to evaluate the effect of ageing on the physical and chemical properties of bitumens. The change in the Mt structure after the ageing of bitumen is also observed using the XRD.

In Chapter 6, the dynamic shear rheometer (DSR) equipment is used to characterize the rheological properties of bitumen modified by the Mts in terms of viscosity and dynamic response. The aspect ratio of Mt in the bitumen is evaluated using a composite model.

Fatigue tests are performed on bitumen, mortar, and mixture; this is discussed in Chapter 7. First, the cone and plate device is used to characterize the fatigue properties of bitumens modified by two organo Mts, Mt1 and Mt2. Next, the standard mortar and the one modified with Mt2 before and after short time ageing are subjected to fatigue tests using a column type specimen. The dissipated energy ratio (DER) method is adopted to define the fatigue life. Finally, the indirect tensile fatigue test is used to characterize the fatigue properties of mixtures.

Finally, Chapter 8 gives conclusions and some recommendations.

1.4 References

- F.Bergaya, B. K. G. Theng, et al. (2006). Handbook of clay science, Elsevier Science Ltd.
- Giannelis, E., R. Krishnamoorti, et al. (1999). "Polymer-silicate nanocomposites: model systems for confined polymers and polymer brushes." Polymers in confined environments: 107-147.
- Giannelis, E. P. (1996). "Polymer layered silicate nanocomposites." Advanced materials 8(1): 29-35.
- Halstead, W. J. (1985). "Relation of asphalt chemistry to physical properties and specification." Journal of the association of asphalt paving technologist 54 91-117.
- Koo, J. H. (2006). Polymer nanocomposites: processing, characterization, and applications, McGraw-Hill Professional.
- Okada, A. and A. Usuki (2006). "Twenty Years of Polymer Clay Nanocomposites." Macromolecular Materials and Engineering 291(12): 1449-1476.
- Petersen, J. C. (1984). Chemical Composition of Asphalt as Related to Asphalt Durability: State of the Art. Transport Research Record Washington, DC. No. 999.
- Pinnavaia, T. J. and G. W. Beall (2000). Polymer-clay Nanocomposites. . Chichester, John Wiley & Sons Ltd.
- Read, J. and D. Whiteoak (2003). The shell bitumen handbook, Thomas Telford Ltd, London.
- Roberts, F. L., P. S. Kandhal, et al. (1996). Hot Mix Asphalt Materials, Mixture Design, and Construction, National Asphalt Pavement Association Education Foundation. Lanham, MD.

2

LITERATURE REVIEW

2.1 Application of nanoclay in polymers

In recent decades, layered silicate montmorillonite nanoclay (Mt) has been successfully introduced into polymer systems to form polymer-clay nanocomposites (PCN) in which Mt layers are randomly and homogeneously dispersed at a molecular level (Pinnavaia and Beall 2000; Koo 2006). Because of their ultrafine phase dimensions (see Figure 2.1.1), PCNs possess unique properties which are superior to those of virgin polymers, in terms of improved mechanical properties, thermal and chemical resistance, decreased gas and moisture permeability, etc. Therefore, PCN materials offer a new technology and business opportunities in the industry.

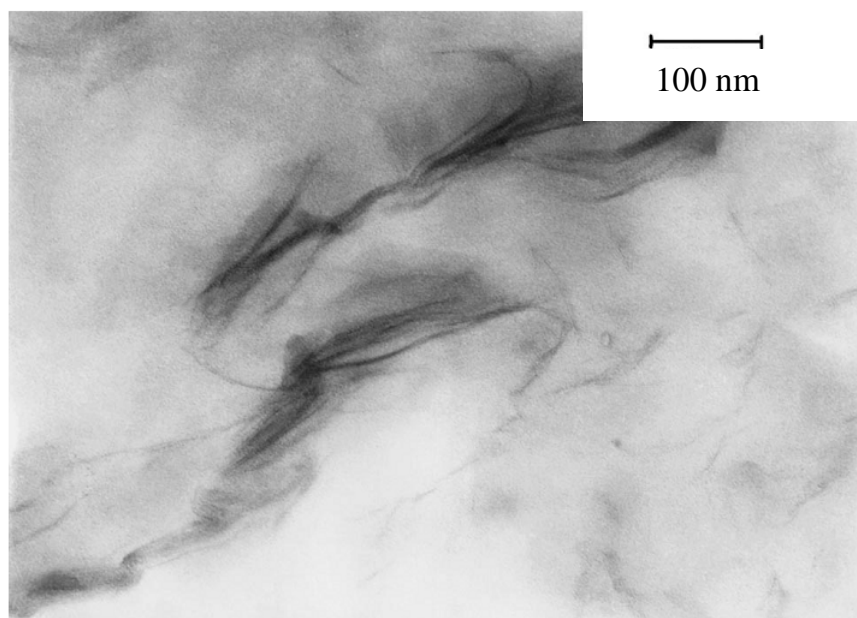


Figure 2.1.1 TEM micrograph of organo montmorillonite exfoliated in a polymer matrix (Alexandre and Dubois 2000)

Since the first nanocomposite nylon 6-clay hybrid was invented at Toyota Central R&D Lab in 1985, extensive researches about nanocomposites have been performed in the industrial and the academic world (Okada and Usuki 2006). Some possible polymer matrices which can be synthesized with the clay into nanocomposites are listed below:

- Polypropylene (PP) (Kurokawa, Yasuda et al. 1996)
- Polyethylene (PE) (Su, Jiang et al. 2004)
- Polybutylene (PB) (Zhang, Manias et al. 2009)
- Polystyrene (PS) (Gilman, Jackson et al. 2000)
- Acrylonitrile butadiene styrene (ABS) terpolymer (Zheng and Wilkie 2003)
- Poly styrene butadiene styrene (SBS) (Laus, Francescangeli et al. 1997)
- Styrene butadiene rubber (SBR) (Zhang, Wang et al. 2000)
- Poly (methyl methacrylate) (PMMA) (Okamoto, Morita et al. 2000)
- Poly (ethylene glycidyl methacrylate) (Alyamac and Yilmazer 2007)

2.1.1 Montmorillonite nanoclay

Layered silicate Montmorillonite (Mt) is a type of clay mineral which refers to materials which have a layered structure or a structure substantially derived from or containing major features of such layer structures (Giese and Van Oss 2002). Clay minerals normally form in an environment of low temperatures, low pressure and abundant presence of water. Under these conditions, it is impossible to form a perfect crystal structure and consequently these materials are highly disordered and amorphous. However, a short range order exists.

Montmorillonite originates from bentonite which is most commonly formed by the in-situ alternation of volcanic ash (Koo 2006). Besides of montmorillonite, bentonite also contains other minerals and clays, such as illite, kaolinite, quartz, zeolite, etc. Based on its molecular structures, montmorillonite belongs to a member of the smectite family which includes dioctahedral smectites such as montmorillonite and nontronite, and trioctahedral smectites for example saponite (Bergaya, Theng et al. 2006).

The Mts are produced in several countries, such as China and USA which are two of the largest not only producers, but also consumer and exporters. The consumption has reached several million tons per year and is continuously increasing. The price of Mt varies from 100 dollar per ton to several thousands dollar per ton, depending on the quality and the application. The rapid expansion of the Mt's consumption implies a promising future for the nanocomposites based on Mts.

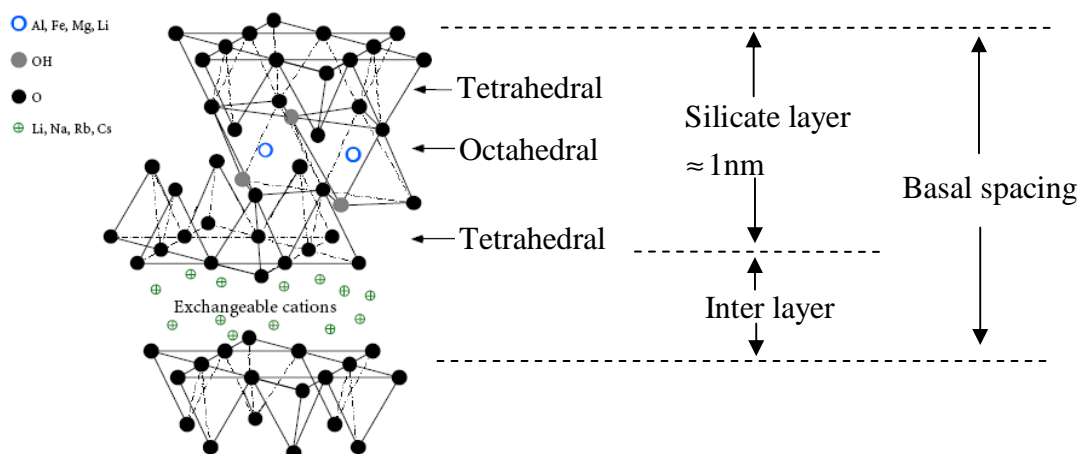


Figure 2.1.2 Structure of montmorillonite (Giannelis, Krishnamoorti et al. 1999)

The chemical structure of montmorillonite clay is illustrated in Figure 2.1.2. As shown, its sheet structure consists of tetrahedral silicate layers and octahedral alumina layers. The tetrahedral silicate layer consists of SiO_4 groups linked together to form a hexagonal network of repeating units of Si_4O_{10} . The alumina layer consists of two sheets of closely packed oxygens or hydroxyls, between which octahedrally coordinated aluminum atoms are imbedded in such a position that they are equidistant from six oxygens or hydroxyls. The two tetrahedral layers sandwich the octahedral layer, sharing their apex oxygens with the latter (Koo 2006). A single silicate layer with a sandwiched structure has a thickness of around 1 nm and a cross-sectional area of about 100 nm^2 (Okada and Usuki 2006).

The chemical formula of the montmorillonite is $(\text{Na},\text{Ca})_{0.33}(\text{Al},\text{Mg})_2(\text{Si}_4\text{O}_{10})(\text{OH})_2$. Besides of Na^+ and Ca^{2+} , there are other possible cations, such as Li^+ , K^+ , Mg^{2+} residing in the interlayer space of the montmorillonite. These inorganic cations make the montmorillonite hydrophilic.

To be more compatible with polymers, ion exchange reactions towards these exchangeable cations (Figure 2.1.2) are necessary. The schematic process of this reaction is shown in Figure 2.1.3.

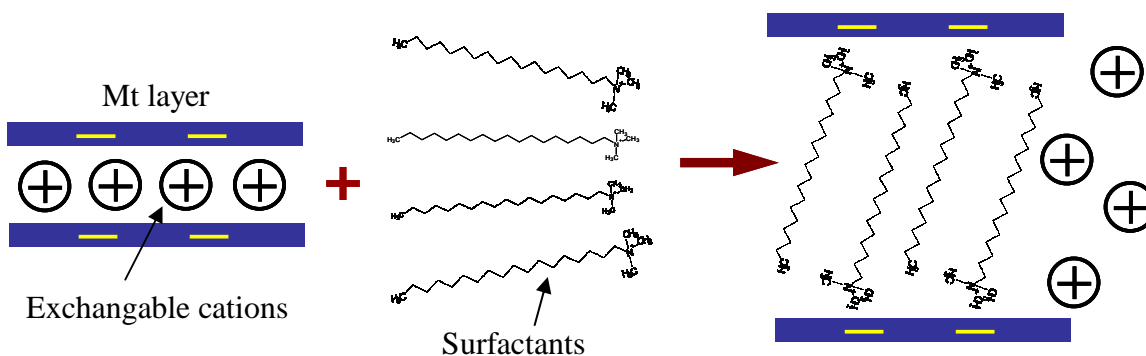


Figure 2.1.3 Schematic process of ion exchange reaction

During this exchange reaction, some organic surfactants replace inorganic cations, and render the normally hydrophilic silicate surface organophilic (Giannelis 1996). The optimum cation exchange capacity (CEC) of montmorillonite is between 80 and 150 meq/100g (milliequivalent of hydrogen per 100 g). If this value is too low, it is hard to exchange inorganic cations with organic ones; on the other hand, high CEC makes two layers connected with each other with a strong bond, and organic cations hardly enter the interlayer space to replace the inorganic cations (Qi and Shang 2002).

Due to the negative charge on the surface of the silicate layer, the cationic heads of surfactant molecules prefer to reside at this surface, leaving the organic tail radiating away from the surface. According to X-ray diffraction, the organic alkyl chains have been thought to lie either parallel to the silicate layer, or forming bilayers, or paraffin-type monolayers, which are illustrated in the top of Figure 2.1.4. Depending on the packing density, temperature and chain length, more structures can develop and some idealized ones are shown at the bottom of Figure 2.1.4.

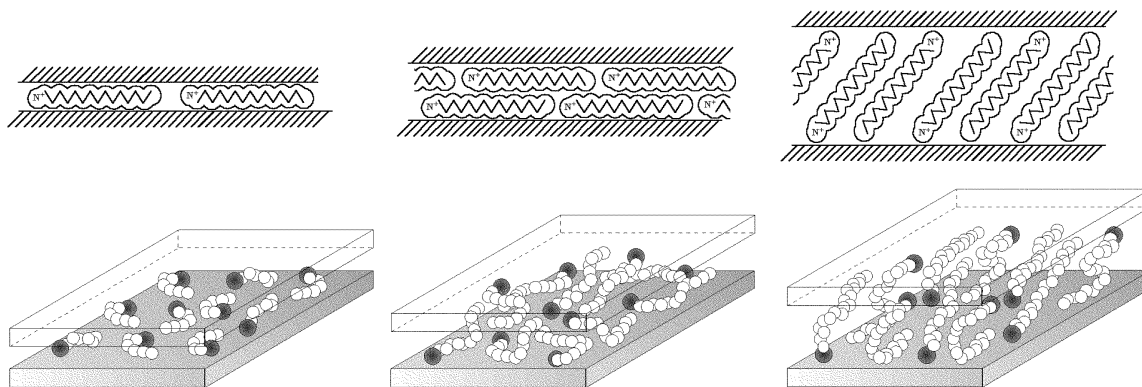


Figure 2.1.4 Idealized structures of organically modified silicates (top) and the structure of organically modified silicates as summarized by Giannelis, Krishnamoorti et al. (1999)

Koo (2006) summarized main types of surfactants which are used to modify the montmorillonite. They are:

- Quaternary ammonium
- Alky imidazoles
- Coupling and tethering agents
- Amide acids
- Others consisting of cation types containing phosphorous ionic compounds.

Amide acids were the first surface modifiers used in the synthesis of the nanocomposite nylon 6-clay hybrid. Figure 2.1.5 shows some quaternary ammonium surfactants used in the nanoclay from Southern Clay Company, U.S.A. Due to the commercial confidentiality, parts of their molecular structures are replaced using “T”.

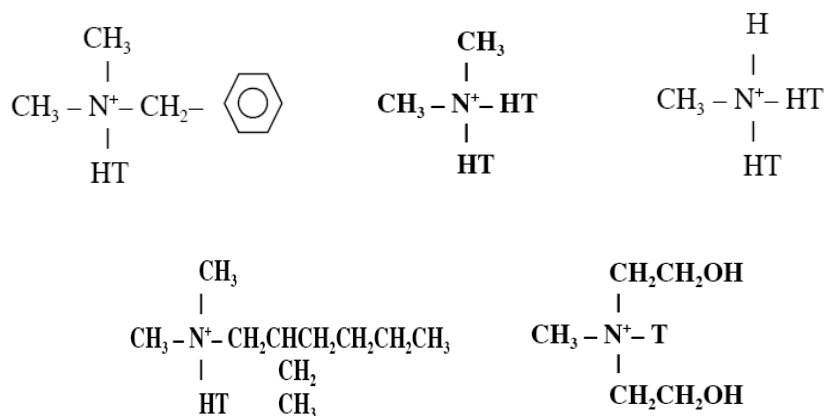


Figure 2.1.5 Quaternary ammonium surfactant cations from Southern Clay Company (www.nanoclay.com)

Surfactant cations lower the surface energy of the silicate surface and improve wetting with the polymer matrix. Meanwhile, they increase the basal spacing and make polymer molecules conveniently enter the interlayer space. Table 2.1.1 gives an example of how the surfactant's structures influences the basal spacing (Usuki, Kojima et al. 1993). However, the final interaction between the matrix and clay is determined by their compatibility.

Sometimes, the organic cations may contain various functional groups that react with the polymer to improve adhesion between the inorganic phase and the matrix (Alexandre and Dubois 2000).

Table 2.1.1 Change of montmorillonite's basal spacing as the function of surfactant's molecular structure (Usuki, Kojima et al. 1993)

n value in ${}^+\text{H}_3\text{N}-(\text{CH}_2)_{n-1}-\text{COOH}_{(n)}$	Interlayer spacing of the modified clay (nm)
2	1.27
3	1.31
4	1.32
5	1.32
6	1.32
8	1.34
11	1.74
12	1.72
18	2.82

2.1.2 Processing of polymer-clay nanocomposites

In total, there are six methods to process polymer-clay nanocomposites which are summarized by Koo (2006).

Solution intercalation

The Mt is exfoliated into single layers using a solvent in which the polymer is also soluble. Due to the weak forces that stack the layers, such Mt could be easily dispersed in an adequate solvent. The polymer then absorbs onto the delaminated sheets, and when evaporated (or the mixture precipitated), the sheet reassembles, sandwiching the polymer to form an ordered, multilayered structures.

Melt intercalation

In this method, polymer and nanoparticles are directly mixed in the extruder machine and are then melt-extruded together to prepare the nanocomposite (Ke and Stroeve 2005). During the whole process, the solid polymer matrix is in the molten state. If the layer surface is sufficiently compatible with the selected

polymer, the polymer can be inserted into the interlayer space and form either an intercalated or an exfoliated nanocomposite. No solvent is required.

Roll milling

Three-roll milling is considered as low shear mixing for incorporating the nanoclay into a polymer. The compounding of nanoclay composites with a three-roll mill machine is found to be highly appealing and environmentally friendly since no solvent is required. Compared with the solution method, it is more efficient in achieving a higher degree of intercalation/exfoliation within a short period of time. The definition of different structure of nanoclay in the matrix is introduced in the section 4.1.2 of Chapter 4. The longer the mixing time, the higher the degree of intercalation (Yasmin 2003).

Emulsion polymerization

In a manner analogous to the solution intercalation technique, the layered silicate is dispersed in the aqueous phase, and the polymer nanocomposites are formed.

In-situ polymerization

The layered silicate is swollen within the liquid monomer (or a monomer solution) so that the polymer formation can occur between the intercalated sheets. Polymerization can be initiated by different polymerization methods such as heat or radiation, diffusion of a suitable initiator, or an organic initiator or catalyst fixed through cationic exchange inside the interlayer before the swelling step of the monomer.

High shearing mixing

The nanoclays are mixed with the liquid polymer matrix using high-shearing equipment. Under these conditions and if the surface treated nanoclays are comparable with the selected polymer, the high-shear mixing will disrupt the nanoclays and disperse the polymer matrix into the clay layers. An intercalated or an exfoliated nanocomposite will result. This technique may or may not, (especially in the case of water-based polymers) require solvent.

2.1.3 Properties of polymer-clay nanocomposite (PCN)

In polymer clay nanocomposites (PCN), a small amount of layered silicate triggers a tremendous improvement in the properties of pristine polymers. In this literature review, we focused on the mechanical, thermal and barrier properties of PCN because they could be linked to the modification of bitumen. Other properties, such as conductivity, thermal expansion, et al., are not discussed.

2.1.3.1 Mechanical

As the first nanocomposite invented by Toyota Central R&D lab in 1985, mechanical properties of Nylon-6 clay hybrid (NCH) have to be introduced. Due

to the discovery on the NCH, an extensive world wide research on PCN has been continuing to the present day, not only in the industrial but also in the academic field (Okada and Usuki 2006).

Nylon-6 is a typical engineering polymer and normally reinforced by glass fiber. It is obtained through the intercalative ring opening polymerization of caprolactam and its reaction process is shown in Figure 2.1.6.

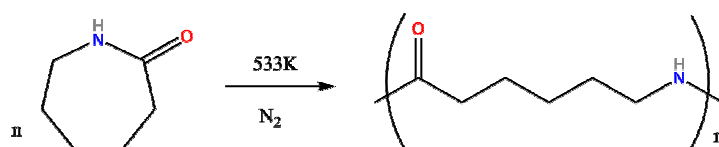


Figure 2.1.6 Schematic to obtain Nylon 6 by ring opening polymerization of caprolactam molecule

Kojima, Usuki et al. (1993) adopted the melt intercalation method to synthesize the exfoliated nylon-6 clay nanocomposites with different clay contents. The montmorillonite nanoclay was modified by amino acid (AA) hydrogen chloride with carbon numbers from 2 to 18. According to the ASTM D638M, mechanical properties of Nylon-6 and its nanocomposites were tested and results are shown in Table 2.1.2. Compared with pristine nylon 6, addition of only a few percent of clay by weight improved its strength and modulus. These properties were saturated at 5 wt. % of clay. If clay content was increased to 8 wt. %, few improvements were observed. Note that the elongation at break is reduced. Especially at 23 °C, it dropped from higher than 100 % for the pristine down to 7.3 % and 2.5 % for the nanocomposite filled with 5 wt. % and 8 wt. %, respectively.

Table 2.1.2 Mechanical properties of pristine Nylon-6 and its nanocomposites with 2 wt.%, 5 wt.% and 8 wt.%, respectively (Kojima, Usuki et al. 1993)

Properties	Temperature [°C]	Unit	Pristine	2 wt.%	5 wt.%	8 wt.%
Tensile strength	23	MPa	68.6	76.4	97.2	93.6
	120		26.6	29.7	32.3	31.4
Tensile modulus	23	GPa	1.11	1.43	1.87	2.11
	120		0.19	0.32	0.61	0.72
Flexural strength	23	MPa	89.3	107	143	122
	120		12.5	23.8	32.7	37.4
Flexural modulus	23	GPa	1.94	2.99	4.34	5.32
	120		0.29	0.75	1.16	1.87
Elongation	23	%	>100	>100	7.30	2.5
	120		>100	>100	>100	51.6

However, such a loss in ultimate elongation does not occur in elastomeric epoxy (Wang and Pinnavaia 1998). Furthermore, the addition of nanoclay in cross-linked matrix triggers an increase of the elongation at break as clearly depicted in Figure 2.1.7. The strain-at-break is substantially increased for exfoliated and intercalated nanocomposites, whereas conventional clay composites exhibit normal behavior and become less elastic than the pristine polymer. In the case of the exfoliated nanocomposites, the authors attributed this improvement partly to the plasticizing effect of the dangling chains in the polymer matrix and the reinforcement effect of the clay layers. However, they did not give a good explanation in the case of intercalated nanocomposite. For the conventional clay composites, the high filler content makes these composites much more brittle which results in less elongation. The clustering of nanoclay as well as nano- or micro-size voids in the microstructure due to inadequate degassing of the mixture could also lead to less elongation.

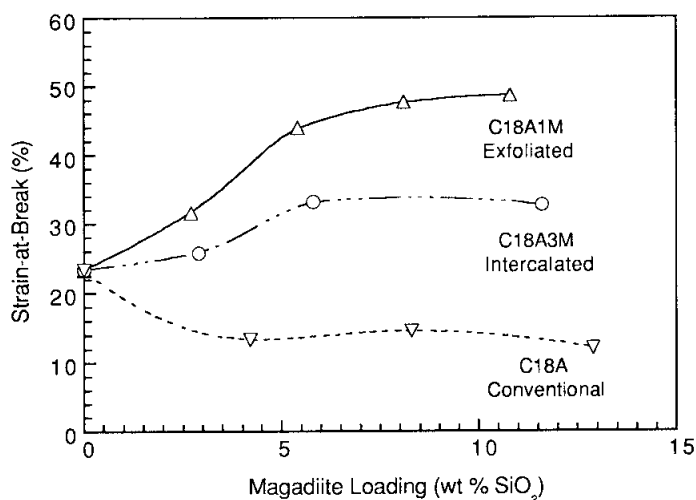


Figure 2.1.7 Comparison of the strain at break values for an exfoliated epoxy/clay nanocomposite prepared from a hydrous sodium silicate mineral modified with methyl octadecyl ammonium ion (C18A1M), an intercalated nanocomposite prepared from the silicate modified with trimethyl octadecyl ammonium ion (C18A3M) and a conventional composite prepared from the silicate modified with octadecyl ammonium ion (C18A) (Wang, Lan et al. 1996)

As shown in Figure 2.1.8, Liu, Qi et al. (1999) found that the tensile modulus of nylon 6 clay nanocomposites increases rapidly with the clay content in the range of 0–15 wt %, but changes little for a clay content higher than 15 wt. %. The montmorillonite with octadecyl ammonium surfactant was used in their research.

For the dynamic modulus, some research has been done on polypropylene (PP) which is one of the most widely used polyolefin polymers (Kawasumi, Hasegawa

et al. 1997). Figure 2.1.9 presents the storage moduli of the PPCHs-PP-MA-1001 relative to those of the matrix, obtained by sinusoidally vibrating the samples in the tensile mode at 10 Hz. Here, PPCH-C18-Mt/1001 refers to one type of PP oligomers plus 5 wt.% of montmorillonite nanoclay intercalated with stearyl ammonium surfactant; PPCH-C18-Mc/1001 means the same type of PP oligomers plus 5 wt. % of synthetic fluorinated mica nanoclay intercalated by the same surfactant. Apparently, the moduli of the PPs are higher than the matrix over the whole temperature range. This is considered to be due to the real reinforcement effect of the clays. PPCH-C18-Mc/1001 exhibited 2.4 times higher modulus at 90 °C by using only 5 wt. % clay.

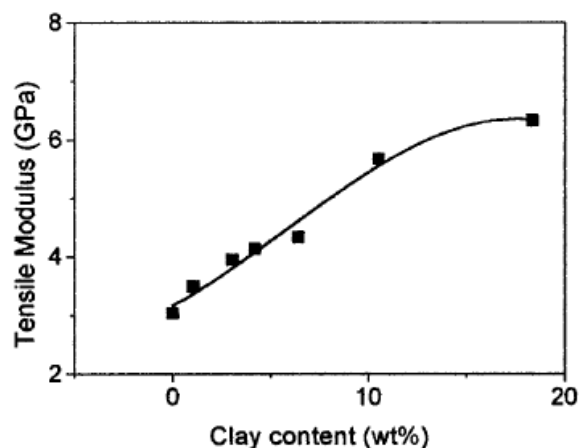


Figure 2.1.8 Effect of nanoclay content on tensile modulus of nylon 6 clay nanocomposites (Liu, Qi et al. 1999)

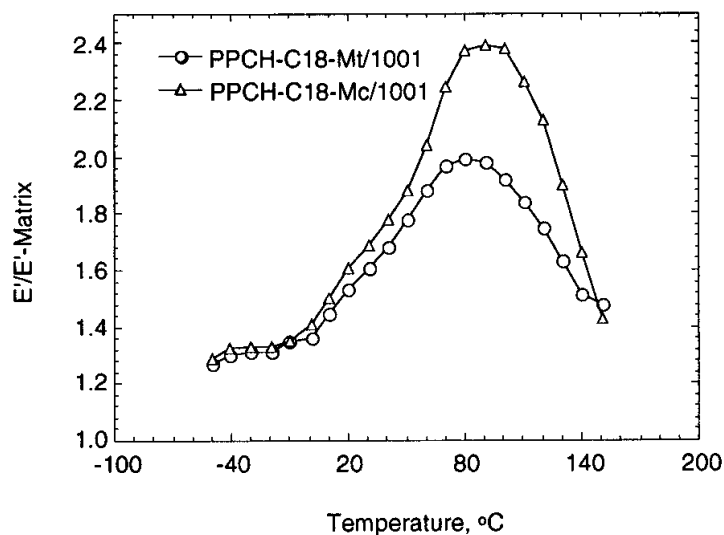


Figure 2.1.9 Relative dynamic storage moduli (E'/E' -matrix) of the polypropylene nanocomposites to that of the matrix (Kawasumi, Hasegawa et al. 1997)

2.1.3.2 Barrier

The high aspect ratio of silicate layers in nanocomposites has been found to highly reduce the gas permeability in films prepared from such nanomaterials (Lan, Kaviratna et al. 1994; Messersmith and Giannelis 1995). As indicated in Table 2.1.3, a decrease in gas permeability of nylon nanocomposite is independent of the type of gas (H_2 , O_2 , and H_2O) (Okada and Usuki 2006).

Table 2.1.3 Gas permeability of nylon nanocomposite (Okada and Usuki 2006)

Permeability	Temperature [$^{\circ}C$]	Relative permeability*, P_c / P_p
O_2	23	0.25
CO_2	23	0.50
Water	40	0.45

* means a ratio of the permeability of the composite to the permeability of the pristine, P_c / P_p

Figure 2.1.10 shows the comparison of the relative permeability of water defined in Table 2.1.3 as a function of the silicate content between a nanocomposite and two conventionally filled silicate composites (A and B) (Giannelis 1996). The permeability in the nanocomposite is much lower compared to the unfilled polymer; the decrease in permeability is much more pronounced in the nanocomposites compared to the conventionally filled polymers with much higher filler content.

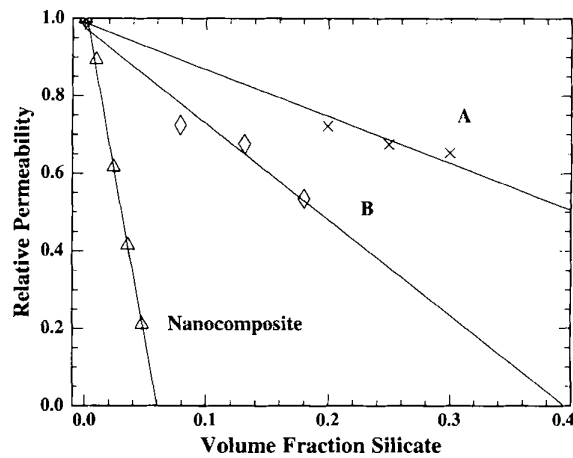


Figure 2.1.10 Relative permeability, P_c / P_p as a function of filler content for polycaprolactone nanocomposites and conventionally filled silicate composites (A and B) (Giannelis 1996).

The barrier property can be explained by Nielsen's permeability model which is illustrated in Figure 2.1.11 and expressed by the following Equation:

$$P_c / P_p = 1/[1 + (L/2W)V_f] \quad 2.1.1$$

Here, P_c and P_p are the permeability coefficient of the nanocomposite and the pristine; L , W and V_f represent the plate length, width and volume fraction of silicate clay, respectively.

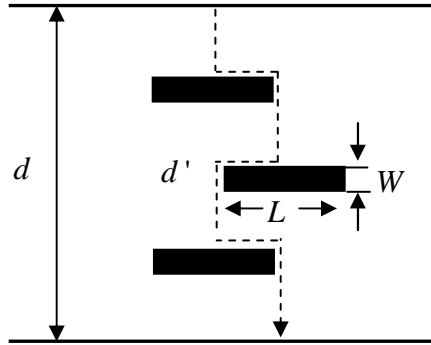


Figure 2.1.11 Nielsen permeability model (Nielsen 1967)

The dramatic reduction of permeability in the nanocomposites is due to the presence of dispersed large aspect ratio silicate layers in the polymer matrix which are impermeable to gas molecules and moisture. This forces them traversing nanoclay particles to follow a tortuous path through the polymer matrix surrounding the silicate particles, thereby increasing the effective path length for diffusion (Giannelis 1996).

2.1.3.3 Thermal

The nanocomposites often exhibit markedly improved thermal properties when compared with the pristine or microcomposites. The thermal stability of a material is usually assessed by thermogravimetric analysis (TGA) where the sample mass loss due to volatilization of degraded by-products is monitored as a function of a temperature ramp. When heating is done under an inert gas flow (nitrogen, helium), a non-oxidative degradation occurs while the use of air or oxygen allows to determine the oxidative degradation of the sample (Alexandre and Dubois 2000).

Figure 2.1.12 shows the TGA traces of silicone rubber and its nanocomposites with 8.1% vol. % of organo montmorillonite and aerosilica, respectively (Wang, Long et al. 1998). Decomposition temperatures of both nanocomposites (433 °C and 440 °C) are higher than that of the pristine (381 °C). The authors proposed possible origins for the observed thermal improvement such as some inactivation of the centers active in silicone main chain decomposition by interaction with the clay or by prevention of the unzipping degradation occurring through physical and chemical cross-linking points built up between polymer chains and particles.

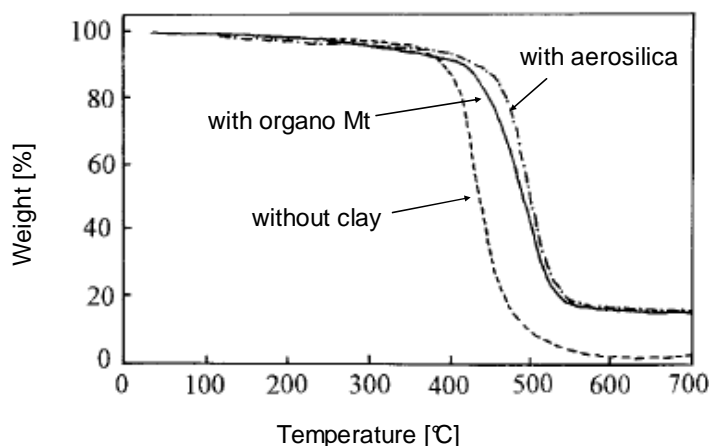


Figure 2.1.12 TGA traces for silicone rubber and its nanocomposites with 8.1% vol. % of organo montmorillonite and aerosilica, respectively (Wang, Long et al. 1998)

Another important reason for the better thermal stability is that the evaporation of the volatile decomposition by-products is hindered as a direct result of the decrease in permeability, which is usually observed in exfoliated nanocomposites (Burnside and Giannelis 1995).

2.2 Bitumen

Bitumen is widely used as a binder in the construction of asphalt pavements. It is refined from crude oil which originates from the remains of plant life at certain conditions of temperature and pressure. Its chemical composition and properties are variable from source to source due to the complexity of the crude oil itself.

2.2.1 Chemical composites in the bitumen

Table 2.2.1 gives typical elements contained in bitumens from different sources (Plancher, Green et al. 1976). The main content by weight is carbon and hydrogen. In so-called heteroatoms, sulfur is the most abundant element while nitrogen and oxygen exist in relatively small amounts. These heteroatoms impart functionality and polarity to the molecules and may disproportionately contribute to the properties of bitumen (Petersen 1984). Heavy metals like vanadium and nickel usually exist in trace amounts in the form of inorganic salts and oxides or in porphyrinic structures (Morgen and Mulder 1995).

In bitumen, heteroatoms like nitrogen, sulfur, and oxygen are attached to the carbon as part of the bitumen molecules in different configurations. The imbalance of electrical forces within heteroatoms produces a dipole which imparts these configurations with functionality and polarity. Therefore, these configurations are called functional or polar groups

Some important functional groups are shown in Figure 2.2.1a (Petersen 1984). Although there is only a minor amount of these functional groups in the bitumen, they strongly influence the properties of bitumen and its interaction with other materials, such as stone aggregates. After reaction with atmospheric oxygen, extra functional groups (Figure 2.2.1b) may form, which lead to bitumen's hardening and embrittling. When these functional groups increase to some extent, the intermolecular interaction gets intensive. When subjected to loads, the bitumen molecules or micelles are not sufficiently mobile to flow past one another, and consequently cracking or fracturing would happen. More evidence relating the functional groups to failure of bitumen can be found elsewhere (Petersen 1984; Ding, Repka et al. 2006; Wang, Liu et al. 2006)

Table 2.2.1 Typical elements in bitumen (Plancher, Green et al. 1976)

Elements [wt.%]	Bitumen sources				Average Range
	Mexico	Arkansas-Louisiana	Boscan	California	
Carbon	83.77	85.78	82.9	86.77	82 - 88
Hydrogen	9.91	10.19	10.45	10.94	8-11
Nitrogen	0.28	0.26	0.78	1.1	0 - 1
Sulfur	5.25	3.41	5.43	0.99	0 - 6
Oxygen	0.77	0.36	0.29	0.2	0 - 1.5
Vanadium (mg/kg)	180	7	1.38	4	
Nickel (mg/kg)	22	0.4	109	6	

Research indicated that the addition of hydrated lime to bitumen can reduce the formation of functional groups, such as ketones and carboxylic acids which can increase the viscosity (Plancher, Green et al. 1976; Petersen 1984). The reaction of these functional groups with lime reduced these viscosity-building components and consequently imparted the pavement with tenderness. Other commercial surface-active materials, such as antistripping agents also work in a similar way.

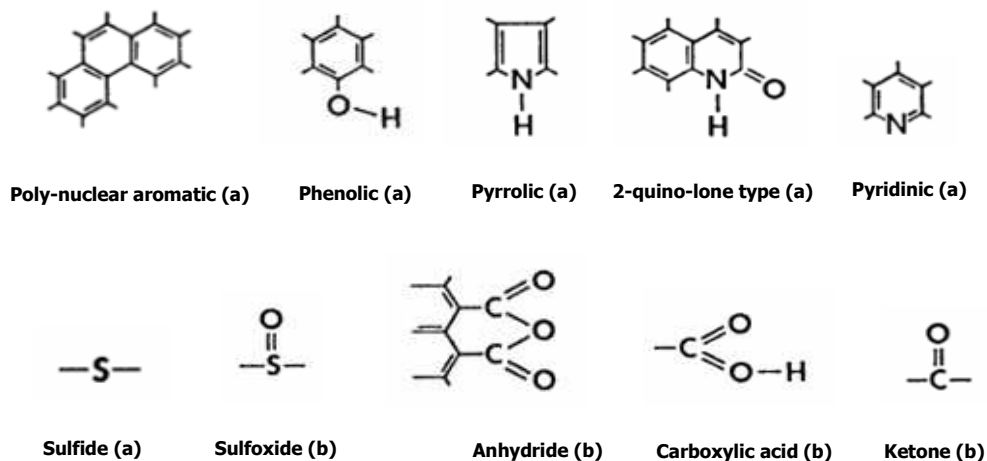


Figure 2.2.1 Functional groups in bitumen molecules: (a) normally present; (b) formed on oxidative ageing (Petersen 1984)

It is impossible to discuss all types of molecular structures which are highly diverse in bitumen and formed under different conditions. However, it is possible to separate bitumen into two chemical groups, asphaltenes and maltenes. The latter can be further subdivided into saturates, aromatics and resins (Halstead 1985; Roberts, Kandhal et al. 1996). Chromatographic methods are most widely used to obtain these four groups. Figure 2.2.2 shows a schematic process of the chromatographic method. Corbett (1969) offered the chemical makeup and physical properties of separate fractions in some typical bitumen (see Table 2.2.2). Although the four groups are not well defined and there is inevitably some overlap between each other, it does enable bitumen's physical properties to be compared with a broad chemical composition. However, the overall properties of the bitumen are determined by the combined effect of these fractions.

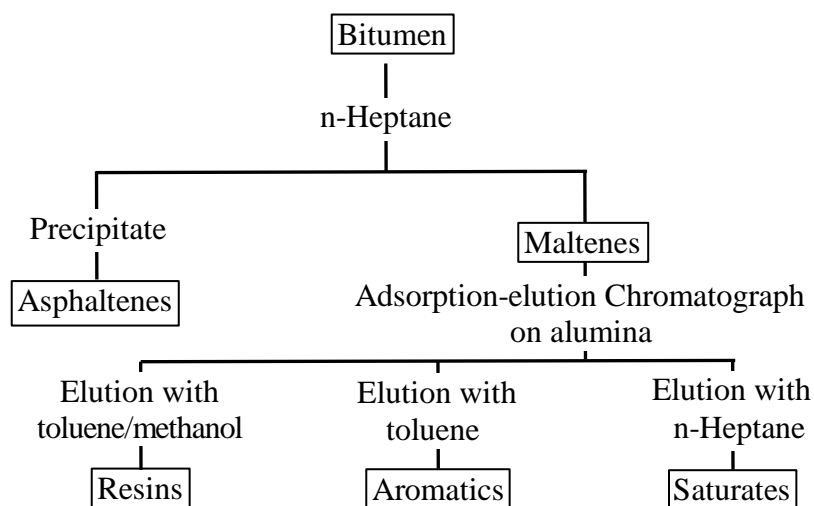


Figure 2.2.2 Schematic process of the chromatographic method to separate bitumen.

The Shell Bitumen Handbook (1990) gives a more detailed description about the characteristics of these four groups. The description given in this handbook is given hereafter:

Asphaltenes are n-heptane insoluble black or brown amorphous solids containing, in addition to carbon and hydrogen, some nitrogen, sulphur and oxygen. Asphaltenes are generally considered as highly polar and complex aromatic materials of fairly high molecular weight. Different methods of determining molecular weights have led to different values ranging widely from 600 to 300000 depending on the separation technique employed. They have a particle size of 5 nm to 30 nm and a hydrogen/carbon (H/C) atomic ratio of about 1.1. The asphaltene content has a large effect on the rheological characteristics of bitumen. Increasing the asphaltene produces harder bitumen with a lower penetration, higher softening point and consequently higher viscosity. Asphaltenes constitute 5% to 25% of the bitumen.

Table 2.2.2 Chemical makeup and physical properties of separate fraction in bitumen (Corbett 1969)

Fractions		Average number of atoms per molecule in the			
		Saturates	Aromatics	Resins	Asphaltenes
Carbon atoms in	Paraffin chains	31	21	24	85
	Naphthene rings	14	17	18	29
	Aromatic rings	0	13	25	115
Other atoms present as	Hydrogen	85	94	105	350
	Sulfur	0	0.5	1	4
	Nitrogen	0	0	1	3
	Oxygen	0	0	1	2.5
Physical properties	Molecular weight	625	730	970	3400
	Softening point(°C)	19	24	77	190
	Relative density (4°C)	0.89	0.99	1.05	1.15
	Color	White	Dark brown	Dark brown	Black
	Physical State	Liquid	Liquid	Solid or semi-solid	Solid

Resins are soluble in n-heptane; like asphaltenes they are largely composed of hydrogen and carbon and contain small amounts of oxygen, sulphur and nitrogen. They are dark brown in colour, solid or semi-solid and very polar in nature. This

particular characteristic makes them strongly adhesive. They are dispersing agents or peptizers for the asphaltenes and the proportion of resins to asphaltenes governs to a degree the sol or the gel type character of the bitumen. Resins separated from bitumen are found to have molecular weights ranging from 500 to 50000, a particle size of 1 nm to 5 nm, and an H/C atomic ratio of 1.3 to 1.4.

Aromatics comprise the lowest molecular weight naphthenic aromatic compounds in the bitumen and represent the major proportion of the dispersion medium for the peptized asphaltenes. They constitute 40% to 65% of the total bitumen and are dark brown viscous liquids. The average molecular weight range is in the region of 300 to 2000, they consist of non-polar carbon chains in which the unsaturated ring systems dominate, and they have a high dissolving ability for other high molecular weight hydrocarbons

Saturates comprise straight and branch-chain aliphatic hydrocarbon, together with alkyl-naphthenes and some alkyl-aromatics. They are non-polar viscous oils which are straw or white in colour. The average molecular weight range is similar to that of aromatics and the components include both waxy and non-waxy saturates. This fraction forms 5% to 20% of the bitumen.

2.2.2 Colloidal nature

The colloidal nature of bitumen was first recognized by Nellensteyn (1928) who considered that asphaltene micelles with high molecular weight were dispersed in an oily medium with much lower molecular weight. These micelles were covered by resins which acted as dispersing agents to keep asphaltenes peptized in the medium (Morgen and Mulder 1995). It means that there is a gradual transition in the colloidal system from central asphaltene clusters to the oily medium.

According to the dispersion degree of micelles, bitumens are classified into three types, “Sol”, “Gel” and “Sol-Gel”. Schematic diagrams of previous two types are shown in Figure 2.2.3.

In general, colloidal nature of bitumen is related to the dispersion state of asphaltenes, temperature and saturates content. In the “Sol” bitumen, the asphaltene micelles are fully peptized and have a good mobility due to sufficient quantities of resins and aromatics. If the resins and aromatics are not sufficient to peptize the asphaltenes micelles, they would associate further, which leads to a “Gel” type of bitumen. “Sol-Gel” type is just intermediate between them. In practice, most bitumens are of intermediate character. The “Gel” character will disappear as the temperature increases. Due to saturates’ non-polarity, a high content of saturates will cause low solvency of maltenes to asphaltenes, and consequently the agglomeration of asphaltenes. The viscosity of bitumen would decrease due to this agglomeration.

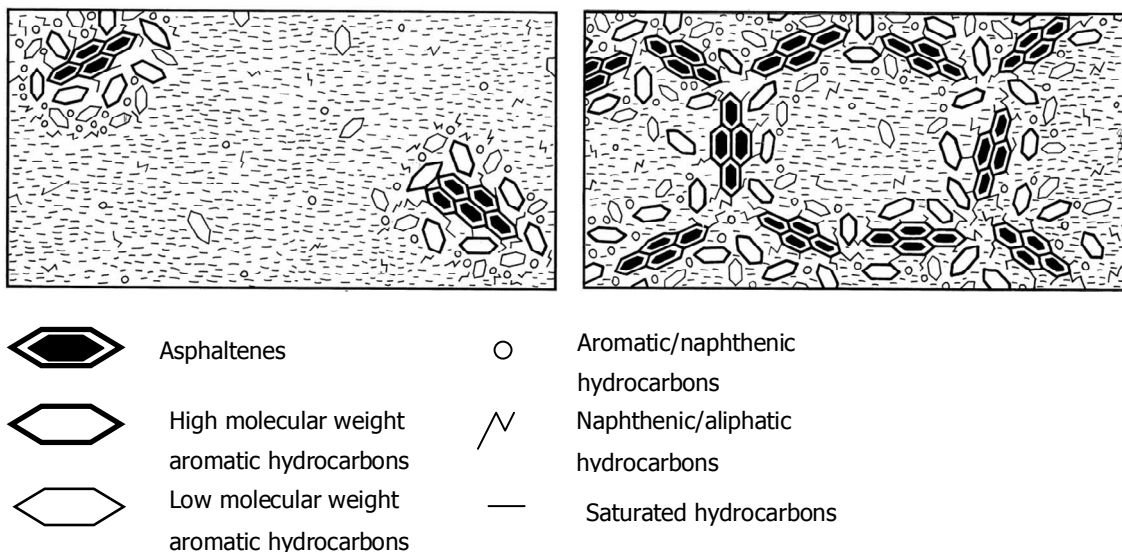


Figure 2.2.3 Schematic diagram of bitumen types: “Sol” (left) and “Gel” (right) (Morgen and Mulder 1995)

2.2.3 Modification to bitumen

To improve the properties of bitumens, modifiers such as some polymers and rubbers are available in the market. Thermoplastic rubbers like styrene-butadiene-styrene (SBS), styrene-butadiene-rubber (SBR) and styrene-isoprene-styrene (SIS) are widely used in modifying bitumen. The former is considered as the most appropriate modifier (Yildirim 2007). It is produced by the polymerization of polystyrene and central segment polybutadiene. After the reaction with a coupling agent, linear or radial type of SBS can be obtained. Due to the inherent incompatibility between styrene blocks and butadiene blocks, it is possible for SBS to form a polymeric network in the bitumen. The polystyrene end-blocks impart the strength to the copolymer while the central blocks endow it with elasticity. Due to these characteristics, SBS could improve the properties of bitumen in terms of low temperature ductility, viscosity and elastic recovery. King et al. (1999) thought that Styrene-butadiene-rubber (SBR) imparted bitumen with better ductility. Meanwhile, Yildirim (2007) considered that SBS gave a higher tensile strength and had a better compatibility with bitumen. To optimize the cost effectiveness of modified bitumens, high quality aggregates are required.

However, some disadvantages can not be ignored in the use of SBS (Polacco, Stastna et al. 2006). SBS is an unsaturated rubber which easily gets aged. Mohammad, Negulescu et al (2003) found that eight-year old SBS modified bitumen recovered from the field had experienced intensive oxidation. Roque, Birgisson et al. (2004) also found that SBS did not have an effect on healing and aging properties of the asphalt mixture.

A saturated polymer, styrene-(ethylene-butylene)-styrene triblock copolymers (SEBS) is obtained by hydrogenation of SBS and has been introduced into bitumen by Ho, Adedeji et al. (1997). Results indicated that less polarity limited its compatibility with bitumen.

Thermoplastic polymers, such as polyethylene (PE), polypropylene (PP), and ethylene vinyl acetate (EVA) are some alternatives used as bitumen modification (Morgen and Mulder 1995). Non polarity of PE and PP leads to a poor compatibility with bitumen. Furthermore, their high crystallization tendency could also disturb the stability of the bitumen system. Vinyl acetate increases the polarity of the ethylene vinyl acetate (EVA) chain, and reduces its crystallization ability (Polacco, Stastna et al. 2006). Therefore, 5 wt.% of EVA in 70 penetration grade bitumen is commonly used in the UK (Morgen and Mulder 1995). However, the same disadvantages, such as high cost and the degradation phenomenon still exist.

Some reactive polymers are also attempted in the bitumen modification. As shown in Figure 2.2.4, terpolymers of ethylene glycidyl methacrylate (GMA) were introduced into bitumen (Yeh, Nien et al. 2005). Polacco, Stastna et al (2004) thought that the epoxy ring in GMA mainly reacted with carboxylic group in asphaltenes and formed an ester link between each other. Meanwhile, the epoxy ring can also be opened by a hydroxyl group and a new hydroxyl group formed on the polymer main chain at the same time reacts with next epoxy ring. In this way, a polymer network involving bitumen molecules could be produced. Due to the polarity and the formation of chemical bond with bitumen molecules, the compatibility between polymers and bitumen is greatly improved, as well as the storage stability. However, it was difficult to determine appropriate dosage of reactive polymers and to control the reaction process.

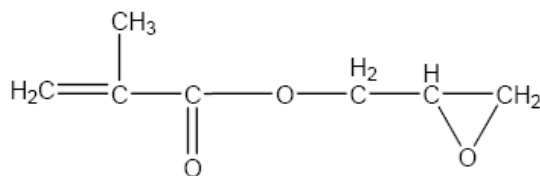


Figure 2.2.4 Structural formula of GMA

2.2.4 Bitumen's natural relation with clays

The natural relation between the clay and the bitumen has been researched by petroleum scientists from Alberta, Canada. The Athabasca oil sand deposits in Alberta typically contain 6-14 wt. % of bitumen and 80-85 wt. % of clay minerals such as quartz, kaolinite, illite, and montmorillonite (Mt). However, these clay minerals could adversely affect bitumen extraction from oil sands. It is considered that bitumen recovery efficiency decreases as these fine particles increase. These

fine particles are normally smaller than 44 micrometers in the oil sands (Hepler and Smith 1994).

Clementz (1976) researched the interaction of Mt with petroleum heavy ends whose main components were the resins and asphaltenes. It was concluded that the basic nitrogen in heavy ends played a role in the adsorption on the surface of Mt; the exchangeable cations on the Mt also caused an increase in the absorption of heavy ends, in the order of $K^+ < Na^+ < Ca^{2+} < Mg^{2+}$. This order is due to different hydration energy of these cations.

2.3 Summary

Based on the literature review, the following summary can be given:

-- Due to the reinforcement from the inorganic layers in two rather than in one dimension (like fiber), the mechanical properties (stiffness and strength) of polymer-clay nanocomposites are superior to those of the pristine or conventionally filled polymers.

-- The dramatic reduction in permeability of the nanocomposites is due to the presence of dispersed large aspect ratio silicate layers which are impermeable to gas molecules. In addition, these layers increase the effective path length for gas diffusion.

-- One important reason for the better thermal stability is that the out-diffusion of the volatile decomposition by-products is hindered as a direct result of the decrease in permeability. Other reasons were suggested, such as the contact with inorganic layers could inactivate polymer molecules or the cross-link between them could prevent the degradation of the matrix.

-- Clay minerals have some natural link with bitumen in the oil sand. For montmorillonite (Mt), basic nitrogen in heavy ends of bitumen played a role in the adsorption on the surface of Mt, and the exchangeable cations (K^+ , Na^+ , Ca^{2+} , Mg^{2+}) on the Mt also influence their interaction

-- Based on the advantages of PCNs, using montmorillonite nanoclay to modify the bitumen with a content as used in the polymer (3~5 wt. %) seems to have potential. Compared with polymer modifiers used in bitumen, nanoclay is an inorganic material and inactive to some ambient factors, like oxygen and humidity.

-- High-shearing mixing method is recommended because it is most accessible to prepare bituminous materials not only in the lab, but also in the factory.

2.4 References

- Alexandre, M. and P. Dubois (2000). "Polymer-layered silicate nanocomposites: preparation, properties and uses of a new class of materials." Materials Science and Engineering: R: Reports 28(1-2): 1-63.
- Alyamac, E. and U. Yilmazer (2007). "Reactive extrusion of poly (ethylene terephthalate)–(ethylene/methyl acrylate/glycidyl methacrylate)–organoclay nanocomposites." Polymer Composites 28(2): 251-258.
- Bergaya, F., B. K. G. Theng, et al. (2006). Handbook of clay science, Elsevier Science.
- Burnside, S. D. and E. P. Giannelis (1995). "Synthesis and properties of new poly (dimethylsiloxane) nanocomposites." Chemistry of materials 7(9): 1597-1600.
- Clementz, D. M. (1976). "Interaction of petroleum heavy ends with montmorillonite." Clays and clay minerals 24(6): 312-317.
- Corbett, L. W. (1969). "Composition of asphalt based on generic fractionation, using solvent deasphalting, elution-adsorption chromatography, and densimetric characterization." Analytical Chemistry 41(4): 576-579.
- Ding, X., C. Repka, et al. (2006). "Effect of illite clay and divalent cations on bitumen recovery." The Canadian Journal of Chemical Engineering 84(6): 643-650.
- Giannelis, E., R. Krishnamoorti, et al. (1999). "Polymer-silicate nanocomposites: model systems for confined polymers and polymer brushes." Polymers in confined environments: 107-147.
- Giannelis, E. P. (1996). "Polymer Layered Silicate Nanocomposites*." Adv. Mater 8: 29-35.
- Giese, R. F. and C. J. Van Oss (2002). Colloid and surface properties of clays and related minerals, CRC.
- Gilman, J. W., C. L. Jackson, et al. (2000). "Flammability properties of polymer-layered-silicate nanocomposites. Polypropylene and polystyrene nanocomposites." Chemistry of materials 12(7): 1866-1873.
- Halstead, W. J. (1985). "Relation of asphalt chemistry to physical properties and specification." Journal of the association of asphalt paving technologist 54 91-117.
- Hepler, L. G. and R. G. Smith (1994). Alberta oil sands: Industrial procedures for extraction and some recent fundamental research. AOSTRA Technical Publication Series #14, Alberta Oil Sands. Technology and Research Authority, Edmonton, AB, Canada.
- Ho, R. M., A. Adedeji, et al. (1997). "Microstructure of triblock copolymers in asphalt oligomers." Journal of Polymer Science Part B: Polymer Physics 35(17): 2857-2877.
- Kawasumi, M., N. Hasegawa, et al. (1997). "Preparation and mechanical properties of polypropylene-clay hybrids." Macromolecules 30(20): 6333-6338.

- Ke, Y. C. and P. Stroeve (2005). Polymer-layered silicate and silica nanocomposites, Elsevier Science.
- King, G., H. King, et al. (1999). "Additives in asphalt." Journal of the Association of Asphalt Paving Technologists 68A: 32-69.
- Kojima, Y., A. Usuki, et al. (1993). "Mechanical properties of nylon 6-clay hybrid." Journal of Materials Research 8(05): 1185-1189.
- Koo, J. H. (2006). Polymer nanocomposites: processing, characterization, and applications, McGraw-Hill Professional.
- Kurokawa, Y., H. Yasuda, et al. (1996). "Preparation of a nanocomposite of polypropylene and smectite." Journal of materials science letters 15(17): 1481-1483.
- Lan, T., P. D. Kaviratna, et al. (1994). "On the nature of polyimide-clay hybrid composites." Chemistry of materials 6(5): 573-575.
- Laus, M., O. Francescangeli, et al. (1997). "New hybrid nanocomposites based on an organophilic clay and poly (styrene-*b*-butadiene) copolymers." Journal of Materials Research 12(11): 3134-3139.
- Liu, L., Z. Qi, et al. (1999). "Studies on nylon 6/clay nanocomposites by melt intercalation process." Journal of applied polymer science 71(7): 1133-1138.
- Messersmith, P. B. and E. P. Giannelis (1995). "Synthesis and barrier properties of poly (ϵ -caprolactone) layered silicate nanocomposites." Journal of Polymer Science Part A: Polymer Chemistry 33(7): 1047-1057.
- Mohammad, L. N., Negulescu, II, et al. (2003). "Investigation of the use of recycled polymer modified asphalt binder in asphalt concrete pavements (with discussion and closure)." Journal of the Association of Asphalt Paving Technologists 72: 551-594.
- Morgen, P. and A. Mulder (1995). The Shell Bitumen Industrial Handbook Shell Bitumen Publications, London.
- Nellensteyn, F. J. (1928). "Relation of the micelle to the medium in asphalt." Journal of the Institute of Petroleum Technologists 14: 134-138.
- Nielsen, L. E. (1967). "Models for the permeability of filled polymer systems." Journal of macromolecular science: part A-Chemistry 1(5).
- Okada, A. and A. Usuki (2006). "Twenty Years of Polymer Clay Nanocomposites." Macromolecular Materials and Engineering 291(12): 1449-1476.
- Okamoto, M., S. Morita, et al. (2000). "Synthesis and structure of smectic clay/poly (methyl methacrylate) and clay/polystyrene nanocomposites via in situ intercalative polymerization." Polymer 41(10): 3887-3890.
- Petersen, J. C. (1984). "Chemical composition of asphalt as related to asphalt durability: state of the art." Transportation Research Record(999).
- Pinnavaia, T. J. and G. W. Beall (2000). Polymer-clay Nanocomposites. Chichester, John Wiley & Sons Ltd.

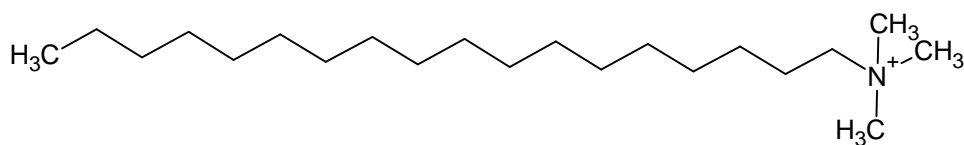
- Plancher, H., E. L. Green, et al. (1976). "Reduction of Oxidative Hardening of Asphalts by Treatment with Hydrated Lime--A Mechanistic Study." Association of asphalt paving technologists (AAPT) 45: 1-24.
- Polacco, G., J. Stastna, et al. (2004). "Rheology of asphalts modified with glycidylmethacrylate functionalized polymers." Journal of colloid and interface science 280(2): 366-373.
- Polacco, G., J. Stastna, et al. (2006). "Relation between polymer architecture and nonlinear viscoelastic behavior of modified asphalts." Current opinion in colloid & interface science 11(4): 230-245.
- Qi, Z. and W. Shang (2002). Theory and Practice in Polymer/Layered Silicate Nanocomposites, Beijing Chemical Industry Press.
- Roberts, F. L., P. S. Kandhal, et al. (1996). Hot Mix Asphalt Materials, Mixture Design, and Construction, National Asphalt Pavement Association Education Foundation. Lanham, MD.
- Roque, R., B. Birgisson, et al. (2004). "Guidelines for the use of modifiers in Superpave mixtures: Executive summary and volume 1 of 3 volumes: Evaluation of SBS modifier." State Job 99052793.
- Shell Bitumen, U. K. (1990). "The Shell Bitumen Handbook." Surrey, UK.
- Su, S., D. D. Jiang, et al. (2004). "Poly (methyl methacrylate), polypropylene and polyethylene nanocomposite formation by melt blending using novel polymerically-modified clays." Polymer degradation and stability 83(2): 321-331.
- Usuki, A., Y. Kojima, et al. (1993). "Synthesis of nylon 6-clay hybrid." Journal of Materials Research 8(05): 1179-1184.
- Wang, S., C. Long, et al. (1998). "Synthesis and properties of silicone rubber/organomontmorillonite hybrid nanocomposites." Journal of applied polymer science 69(8): 1557-1561.
- Wang, Y. P., D. J. Liu, et al. (2006). "Preparation and properties of asphalts modified with SBS/organobentonite blends." Polymers & polymer composites 14(4): 403-411.
- Wang, Z., T. Lan, et al. (1996). "Hybrid organic-inorganic nanocomposites formed from an epoxy polymer and a layered silicic acid (magadiite)." Chemistry of materials 8(9): 2200-2204.
- Wang, Z. and T. J. Pinnavaia (1998). "Hybrid organic-inorganic nanocomposites: exfoliation of magadiite nanolayers in an elastomeric epoxy polymer." Chemistry of materials 10(7): 1820-1826.
- Yasmin, A. (2003). Processing of clay/epoxy nanocomposites with a three-roll mill machine, DTIC Document.
- Yeh, P. H., Y. H. Nien, et al. (2005). "Thermal and rheological properties of maleated polypropylene modified asphalt." Polymer Engineering & Science 45(8): 1152-1158.
- Yildirim, Y. (2007). "Polymer modified asphalt binders." Construction and building materials 21(1): 66-72.

- Zhang, J., E. Manias, et al. (2009). "Tailored Polyethylene Nanocomposite Sealants: Broad-Range Peelable Heat-Seals Through Designed Filler/Polymer Interfaces." Journal of Adhesion Science and Technology 23(5): 709-737.
- Zhang, L., Y. Wang, et al. (2000). "Morphology and mechanical properties of clay/styrene - butadiene rubber nanocomposites." Journal of applied polymer science 78(11): 1873-1878.
- Zheng, X. and C. A. Wilkie (2003). "Nanocomposites based on poly ([epsilon]-caprolactone)(PCL)/clay hybrid: polystyrene, high impact polystyrene, ABS, polypropylene and polyethylene." Polymer degradation and stability 82(3): 441-450.

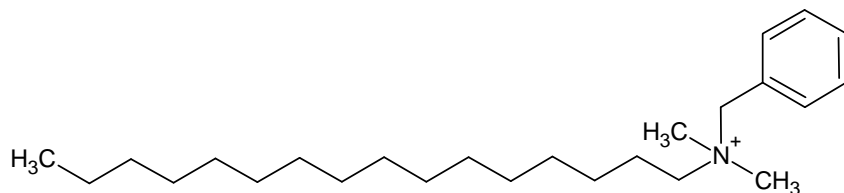
3 PREPARATION OF MONTMORILLONITE MODIFIED BITUMEN

3.1 Introduction

Three types of montmorillonite (Mt) clay, Mt0, Mt1 and Mt2 were used in this study, which were provided by Fenhong Clay Chemical Factory, China. Mt0 is the only inorganic clay, with Na^+ cations residing in the interlayer space of Mt. It has a cation exchange capacity (CEC) of 110 meq/100g. The other two clays, Mt1 and Mt2 were obtained through organically treating Mt0 with octadecyl trimethyl ammonium salt, and benzyl dimethyl hexadecyl ammonium salt, respectively. After the replacement reaction, the surfactant cations (Figure 3.1.1a and b) replaced Na^+ cations and the inorganic Mt became hydrophobic. More information about the characteristics of Mts is given in the following section.



(a) Octadecyl trimethyl ammonium cation



(b) Benzyl dimethyl hexadecyl ammonium cation

Figure 3.1.1 Schematic molecular structure of quaternary ammonium salt cations:
(a) in Mt1 and (b) in Mt2

Three types of base bitumen were involved in this study, with normal paving grades, 40/60 (A), 70/100 (B) and 160/220 (C). All of them were provided by Kuwait Petroleum Research & Technology B.V. Empirical rheological properties of the bitumen are given in Table 3.1.1.

Table 3.1.1 Empirical rheological properties before and after short and long terms ageing

Bitumens	Penetration ^a @ 25°C [0.1mm]			Softening point ^b [°C]		
	Fresh ^c	RTFOT ^d	PAV ^e	Fresh	RTFOT	PAV
A (40/60)	42	27	17	50.0	55.4	61.6
B (70/100)	77	47	28	46.0	51.2	57.2
C (160/220)	171	100	46	38.4	44.2	52.0

^a and ^b were done according to European standards, EN 1426 and EN 1427, respectively. ^c means properties of the virgin bitumen; ^d means properties of the bitumen after aging in the rolling thin film oven test (EN 12607-1); ^e means properties of the bitumen after pressure ageing vessel test at 100 °C (EN 14769). Note that PAV is performed after RTFOT.

3.2 Characteristics of montmorillonites

3.2.1 Thermal stability

Thermogravimetric (TG) and derivative thermogravimetric (DTG) analyses are based on continuously recording relative mass changes of a material sample as a function of a combination of temperature with time and addition of pressure and gas composition. Differential scanning calorimetry (DSC) is used to observe the small energy changes that occur during these physical and chemical processes (Rjeb, Labzour et al. 2005).

To characterize the thermal stability and decomposition of the Mt used in this research, simultaneous DSC-TG analysis was adopted and conducted with a thermal analyzer NETZSCH STA 449 C (Figure 3.2.1) using an atmospheric air stream of 10 ml/min, while heating from room temperature to 800 °C at a linear temperature increase of 10 °C/min.

TG, DTG and DSC curves of the three Mts are shown in Figures 3.2.2, 3.2.3 and 3.2.4. For all of them, thermal decomposition is considered in three regions at the studied temperature range. Initial mass loss is dominated by the volatilization of absorbed water below 200 °C (region I). Subsequently, the decomposition of organic surfactant cations in Mt1 and Mt2 takes place between 200 and 500 °C (region II). Dehydroxylation of the layered silicate occurs between 500 and 800 °C (region III) (Huskic, Brnardic et al. 2008). Due to the absence of surfactants, Mt0 shows no peaks in region II (see Figure 3.2.2).



Figure 3.2.1 Thermal analyzer equipment NETZSCH STA 449 C

In region I of the DTG curve for Mt0 (Figure 3.2.2), a big volatilization peak below 100 °C appears. There is a corresponding endothermic peak on the DSC curve. It was indicated that due to inorganic properties, Mt0 easily absorbed the water when it was exposed to the air. Although Mt1 and Mt2 were organically treated by surfactants, the DTG volatilization peak in this region (Figure 3.2.3 and 4) proved that water absorption still happened. The TG curves indicated that the water contents for Mt0, Mt1 and Mt2 were approximately 5%, 1 % and 2.5 %, respectively. This content not only depends on the type of Mt, but also on environmental conditions, such as relative humidity. It should be noted that the polarity of water would negatively influence the interaction between the Mt and bitumen. Therefore, a certain drying treatment for the Mt is necessary before modification. This treatment is described later on.

As shown from the DTG curves in Figure 3.2.3 and 4, organic substances in Mt1 and Mt2 exhibit different decomposition fashions. There are two DTG peaks for Mt2, and only one for Mt1 in this region. This was due to different molecular structures and consequently different decomposition mechanisms. The corresponding exothermic peak on DSC curves indicated that oxydation reactions of the surfactants took place with some volatile oxydation products, such as CO₂, H₂O and N₂. From the TG curves in this region, it can be calculated that the content of organic matter is 20.1% and 22.9% for Mt1 and Mt2, respectively.

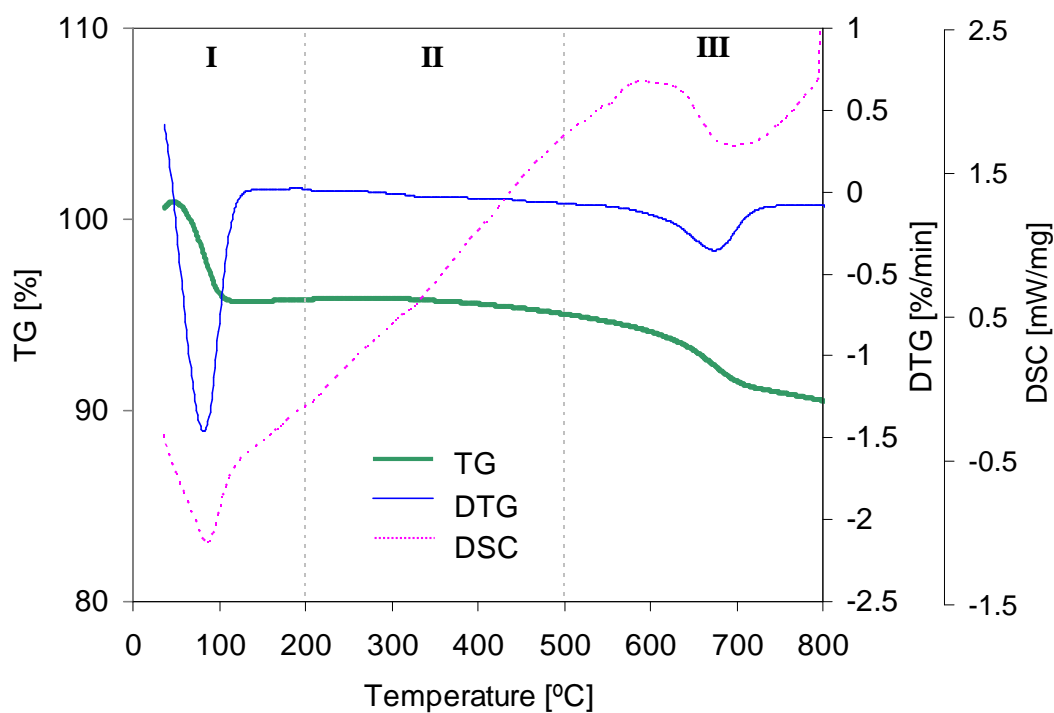


Figure 3.2.2 TG, DTG and DSC curves for Mt0

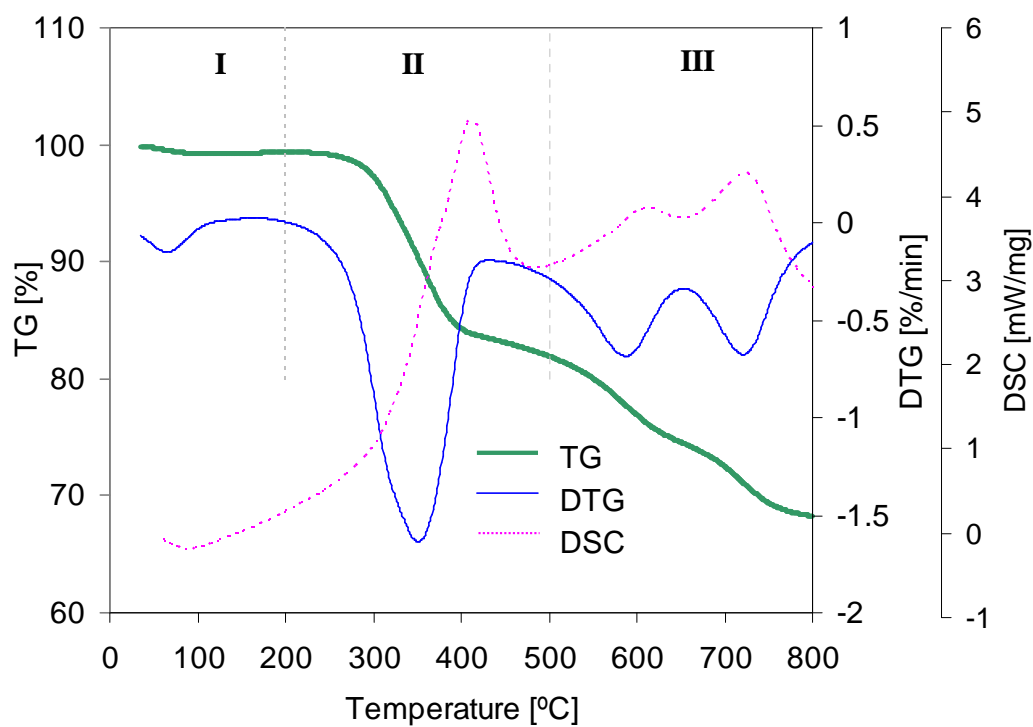


Figure 3.2.3 TG, DTG and DSC curves for Mt1

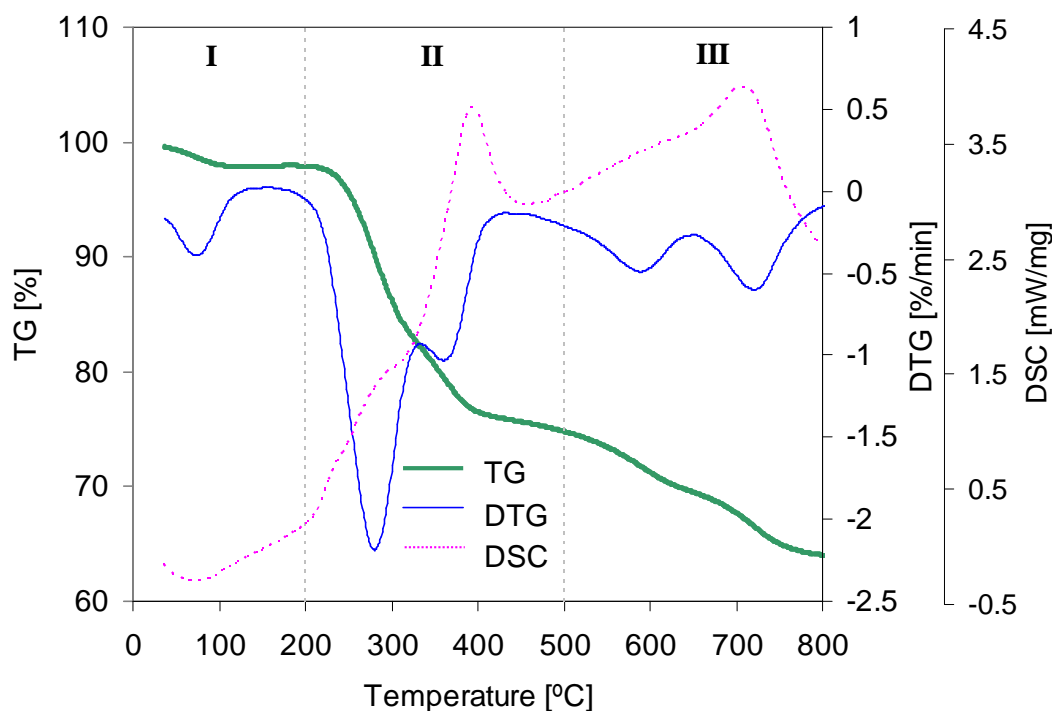


Figure 3.2.4 TG, DTG and DSC curves for Mt2

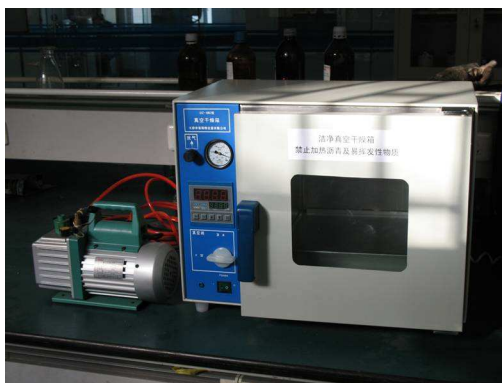


Figure 3.2.5 Vacuum oven used to dry the clay

The thermoanalyses described above indicated that the Mts used in this study have a good thermal stability under 200 °C. Therefore, the temperature at which the bitumen is modified will not influence the properties of Mts because it is normally below 180 °C. To eliminate the effect of the humidity, a vacuum oven (Figure 3.2.5) was used, in which the Mt specimen was kept at 100°C and 0.01 MPa for at least one hour before modification.

3.2.2 Density

The density of Mt was measured to evaluate the volume content of Mt in the bitumen. By combining the TG results described earlier, it is also possible to calculate the relative volume content of surfactants in organo Mt.

The Ultrapycnometer 1000 equipment (Figure 3.2.6a) is specifically designed to measure the volume and true density of solid objects. This is accomplished by employing the Archimedes' principle of fluid displacement and Boyle's law to determine the volume. To assure maximum accuracy, the fluid was replaced by a gas which can penetrate the finest pores. In this test, helium is recommended because its small atomic dimensions assure penetration into crevices and pores approaching one Angstrom (10^{-10} m) in dimension. This size is smaller than the basal spacing between two Mt platelets which is normally larger than 1 nm (10^{-9} m). A few grams of dried Mt powder were needed to fill the specimen cell (Figure 3.2.6b) for the test. The results are given in Table 3.2.1.

Table 3.2.1 True densities of Mts

Clay	True density [g/cm^3]
Mt0	2.7496
Mt1	1.7829
Mt2	1.8336

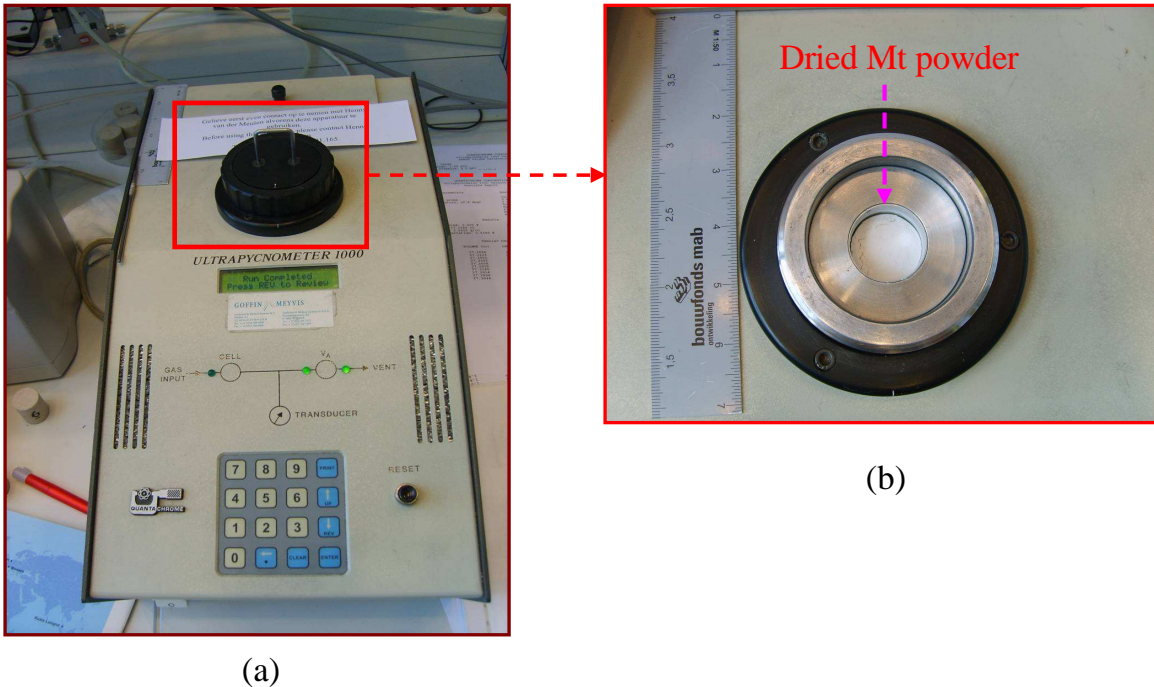


Figure 3.2.6 (a) Ultrapycnometer 1000 equipment for the density measurement and (b) specimen cell

Mt1 and Mt2 were obtained through organically treating Mt0 with different surfactants. The TG results indicated that the surfactant's weight contents of Mt1 and Mt2 were 20.1% and 22.9%, respectively. The molecular weight and volume ($\phi_{\text{surfactants}}$) of the surfactants are much higher than those of Na^+ , which are illustrated in Figure 3.2.7. Therefore, the density of solid platelets of Mt1 and Mt2 can be thought as the same as that of Mt0. Based on the densities of three Mts and surfactants' weight contents in two of them, the surfactant's density and its volume can be evaluated and results are given in Table 3.2.2. As indicated, the density of surfactants in Mt1 and Mt2 is smaller than that of bitumen (about 1.01 g/cm^3). Meanwhile, both the surfactants and solid platelets almost occupied one half of whole volume. These parameters were used to calculate effective the aspect ratio presented in Chapter 6.

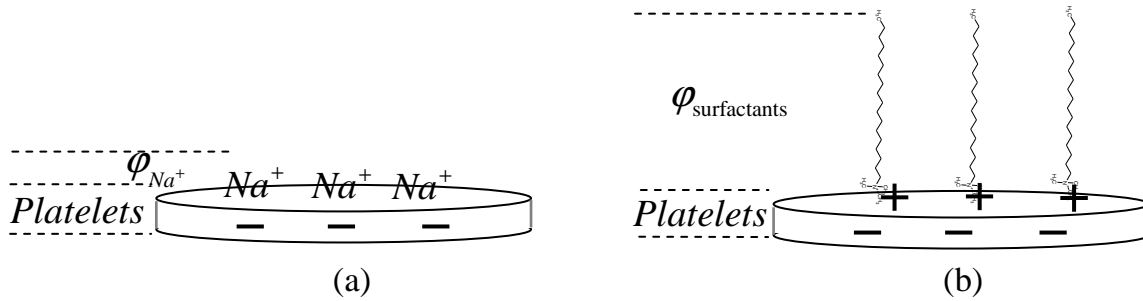


Figure 3.2.7 Schematics of (a) before and (b) after organic treatment to Mt0

Table 3.2.2 Density and volume content of surfactant in the Mt

	Density [g/cm^3]	Volume [%]
Surfactants in Mt1	0.74	51.4
Surfactants in Mt2	0.83	51.3

3.2.3 Basal spacing (d_{001})

In this study, a D/Max-RB diffractometer was adopted to characterize the basal spacing of Mts. The dried clay specimen was densely packed in a plate holder with a smooth flat surface. The X-ray tube in the apparatus produces X-rays with a certain wavelength (λ) and scans the surface of the specimen which contains crystal materials at different incident angles. As illustrated in Figure 3.2.8, the constructive interference of X-ray is recorded by the detector when the lower beam traverses an extra length of $2d\sin\theta$ which is equal to an integer multiple of the wavelength (λ) of the radiation. This phenomenon can be expressed by Bragg's law as follows:

$$2d \sin \theta = n\lambda \quad 3.2.1$$

where,

d = interplanar distance, specifically referring to d_{001} in this study,

n = an integer, and

θ = the angle between the incident ray and the scattering planes.

Further information about XRD can be found elsewhere (Wang and Wiley 2000; Koo 2006).

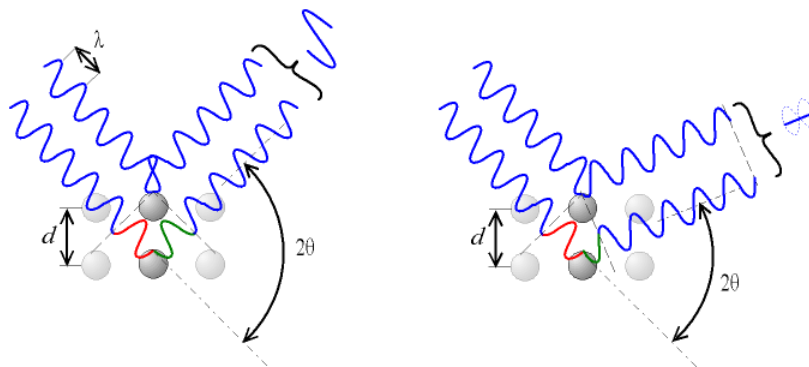


Figure 3.2.8 Bragg diffraction. Two X-ray beams with identical wavelength and phase approach a crystalline solid and are reflected by two different atoms within it. According to the 2θ deviation, the phase shift causes constructive (left figure) or destructive (right figure) interferences (http://en.wikipedia.org/wiki/Bragg's_law)

In this diffractometer, Cu-K α radiation (40kV and 50mA) was used with $\lambda=0.15406$ nm and 2θ ranging from 0.5° to 10° at a speed of $3^\circ/\text{min}$. Through the Bragg's law, the interplanar distance d_{001} , which is also called basal spacing of the Mt, was calculated. The same method is also used in next chapter to characterize the morphology of Mts after adding them to the bitumen.

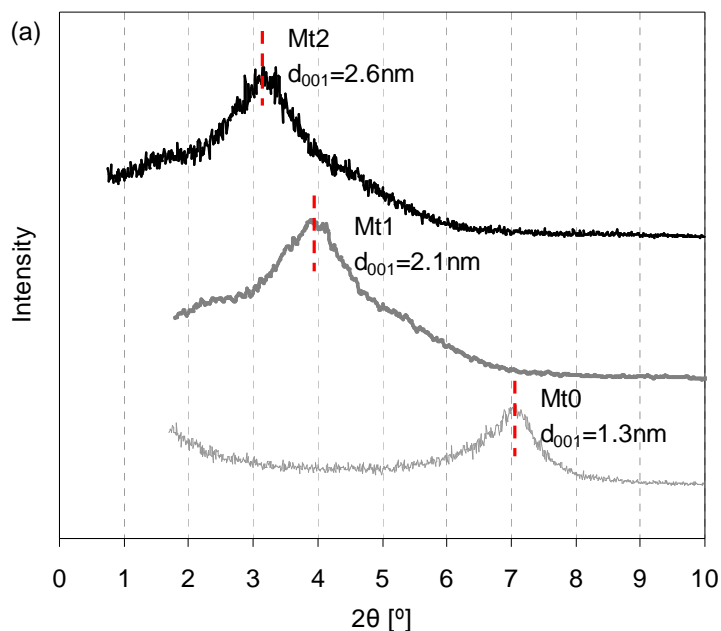


Figure 3.2.9 Change of basal spacing of Mt0 after surfactant treatment

As shown in Figure 3.2.9, the first diffraction peak of the XRD curve for Mt0 was at $d_{001} = 1.3 \text{ nm}$ which was calculated using Bragg's law. After modification by surfactants, the peak was shifted to a lower angle which meant an increase in d_{001} . As indicated, d_{001} increased from 1.3 nm to 2.1 nm and to 2.6 nm for Mt1 and Mt2, respectively. The different change in d_{001} is related to the molecular weight and structure of the surfactants (Dubois 2000). Although d_{001} is changed due to the surfactant, the extent of this change is not a key factor to determine the final modification effect on the matrix.

3.2.4 Particle size

The Mastersizer 2000 laser particle size analyzer was used to characterize the particle size distribution of dried Mt specimens. As shown in Figure 3.2.10, raw Mt0 has a wide particle size distribution. After the surfactant treatment, this distribution for Mt1 and Mt2 becomes close to a log normal distribution and the particle size in the natural state is increased, which could be due to the surfactant modification. It is noted that this method is performed on the assumption that the particles are spherical and non-porous.

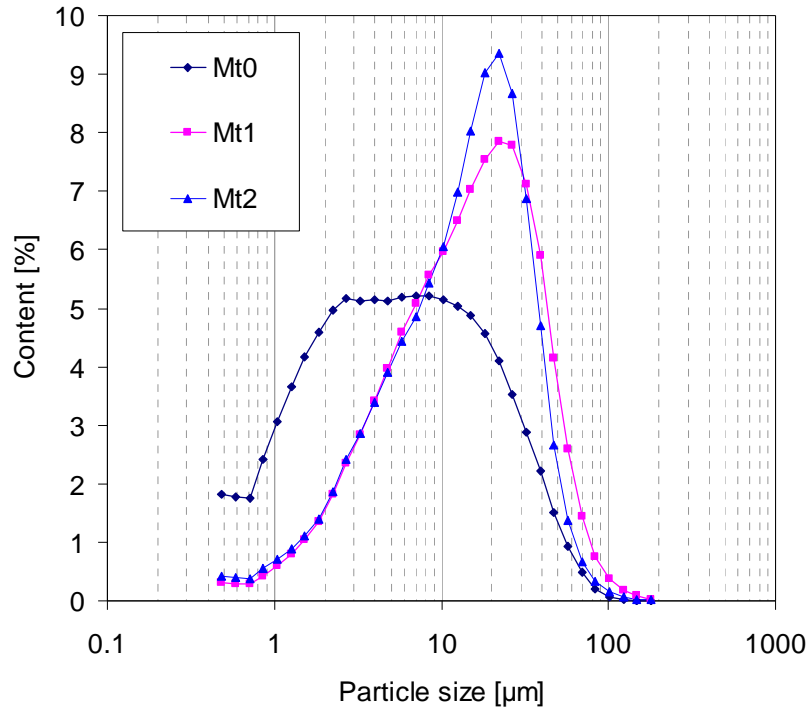


Figure 3.2.10 Particle size distribution for each Mt

Researches indicated that quaternary ammonium surfactants show fluorescent properties. Some of these surfactants were therefore used as fluorescent

brightening agents (FBAs) (Takehi, Maeya et al. 1997; Ju, Long et al. 2006; Liu, Zhang et al. 2010). Therefore, it is possible to use the fluorescence microscope to directly observe the particle size and shape of organo Mt1 and Mt2. The Olympus BH2-RFCA equipment (Figure 3.2.11) was used. A small amount of clay powder was randomly placed on the slide and illuminated with ultraviolet light. Fluorescent images for Mt1 and Mt2 are shown in Figure 3.2.12a and b, respectively. As indicated, the shapes for both particles are irregular with a size at micrometer level. It seems that Mt2 has a stronger fluorescence. The reason could be that benzyl groups on the surfactant in Mt2 promote this property. The fluorescent property implies that it is possible to use this microscope to observe the distribution of organo Mt in the bitumen. Some attempts are described in the Chapter 4.



Figure 3.2.11 Fluorescence microscope Olympus BH2-RFCA

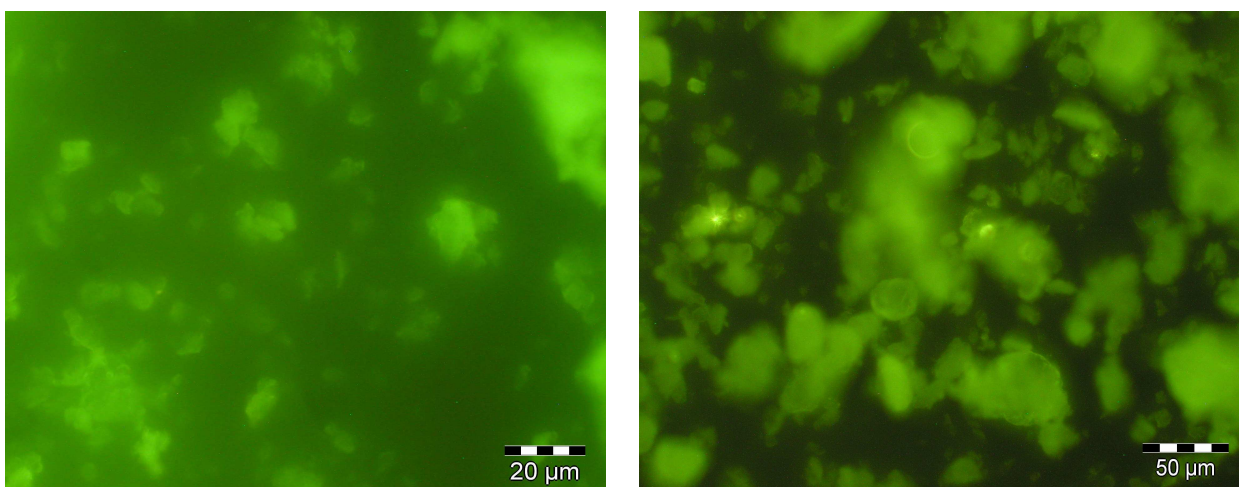


Figure 3.2.12 Fluorescent images: (left) for Mt1 and (right) for Mt2

3.3 Specimen preparation

3.3.1 Equipments

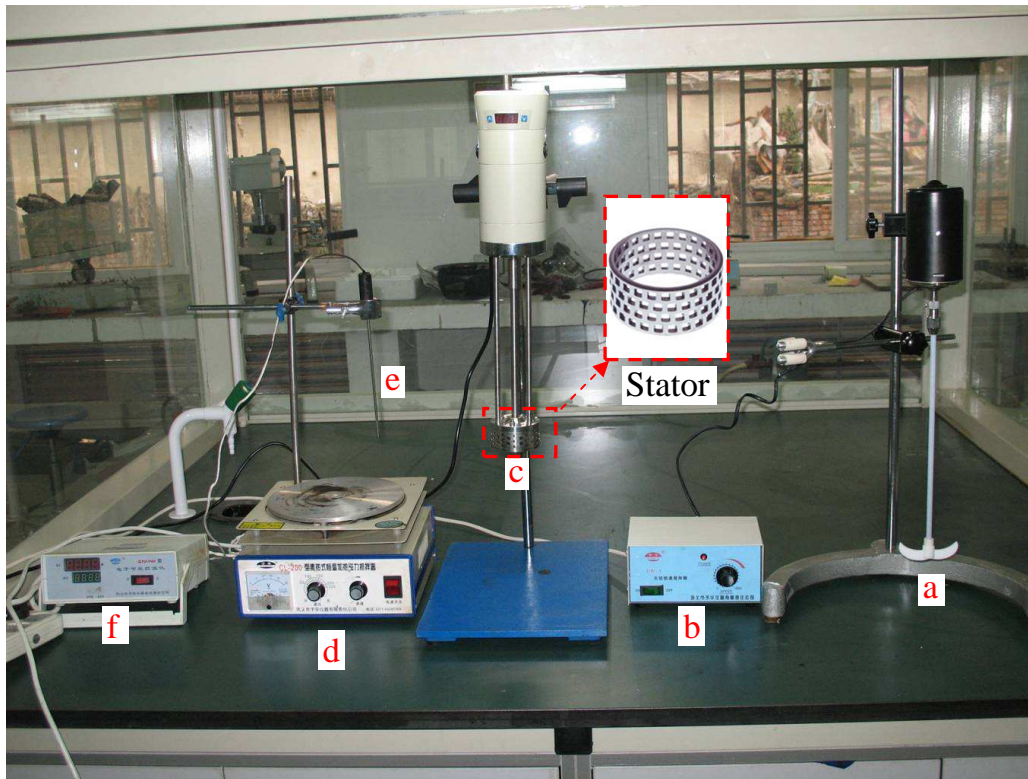


Figure 3.3.1 Equipments used to prepare Mt modified bitumen

The equipment used in preparing Mt modified bitumen is shown in Figure 3.3.1. The function of each of them is as follows:

- a: The low speed mixer to primarily disperse the Mt into the bitumen.
- b: The speed controller of low speed mixer.
- c: High shear mixer (ESR-500).
- d: Heating plate with a fan at the bottom.
- e: Temperature sensor into the bitumen.
- f: Temperature controller of the heating plate.

A square-holed screen stator (see Figure 3.3.1) was chosen in the high shear mixer. Compared with other screens, such as the one with a circular hole, the configuration and fine internal tolerances of this screen provide exceptionally high shear rates which are ideal for the rapid size reduction of soluble and insoluble granular solids.

3.3.2 Preparation protocol

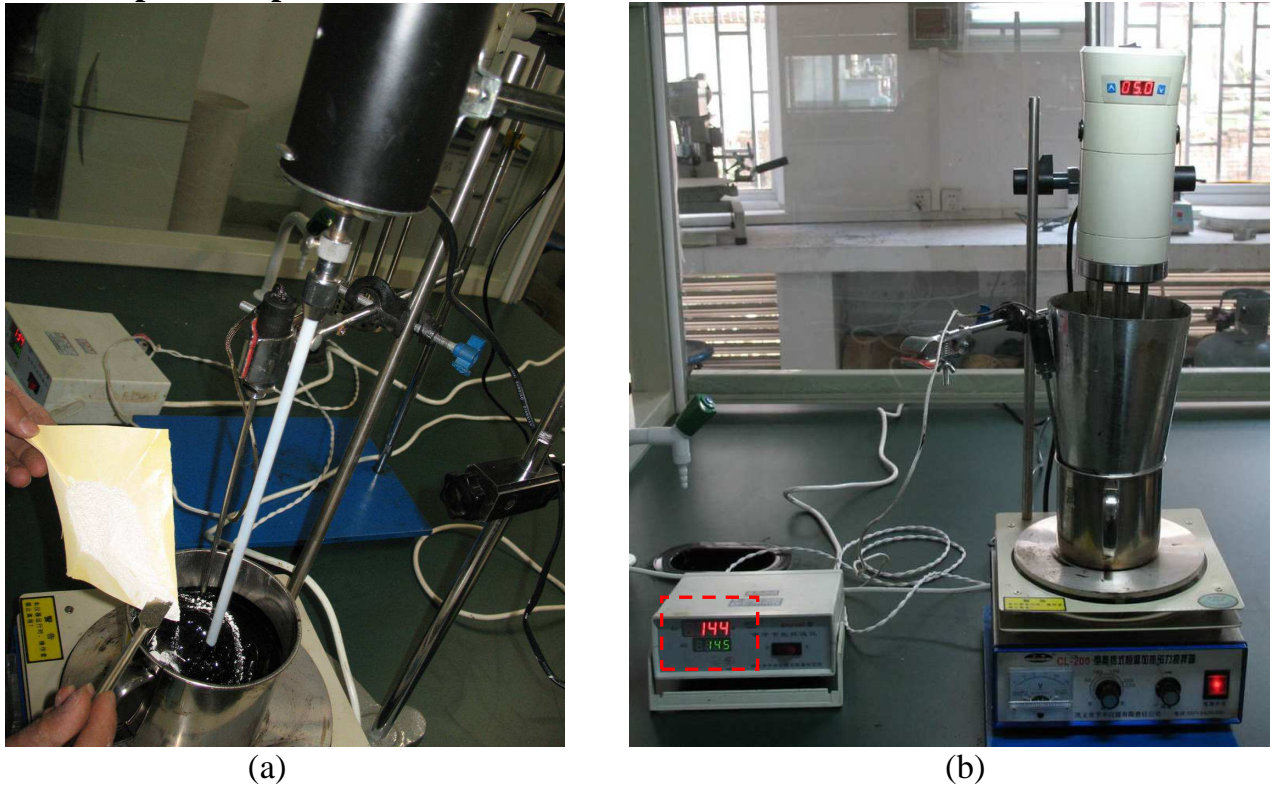


Figure 3.3.2 Two steps for preparing modified bitumen: (a) dispersing the Mt using the low speed mixer; (b) high shearing the mixture

For the preparation of modified bitumen specimens, 450 g of base bitumen was melted and poured into a 1000 ml cylindrical container with a diameter of 10 cm placed on the heating plate. As shown in Figure 3.3.2a, a certain amount of dried Mt was gradually added to the bitumen and meanwhile dispersed with a low speed mixer at 100 rpm for ten minutes. Then, the high shear mixer replaced the low speed mixer to shear the mixture (Figure 3.3.2b). On the screen of the temperature controller in this figure, the red and the green number means the real and the target temperature, respectively. The position of the head of high shear mixer within the container can affect the mixing performance of the machine. The recommended initial position of the head is slightly off centre and approximately 2.0 cm above the bottom of the container. Moving the head off the centre produces a smaller vortex enabling the mixer to operate at higher speeds without splashing or spillage.

The effects of three important factors, high shearing speed, temperature and time are discussed below. Generally, the high shear mixer should run at the highest possible speed without causing excessive aeration, splashing or spillage. High speeds will give faster mixing times and the best end results in terms of particle size reduction. Reducing the speed reduces the shearing efficiency. However, high shearing also produces huge energy into the specimen and consequently increases

its temperature. This effect is dependent on the speed, and should not be ignored for the bitumen specimen, the properties of which can be influenced by the preparation temperature. A preliminary test was performed to check the influence of high shearing speeds on the temperature change of base B (70/100) bitumen.

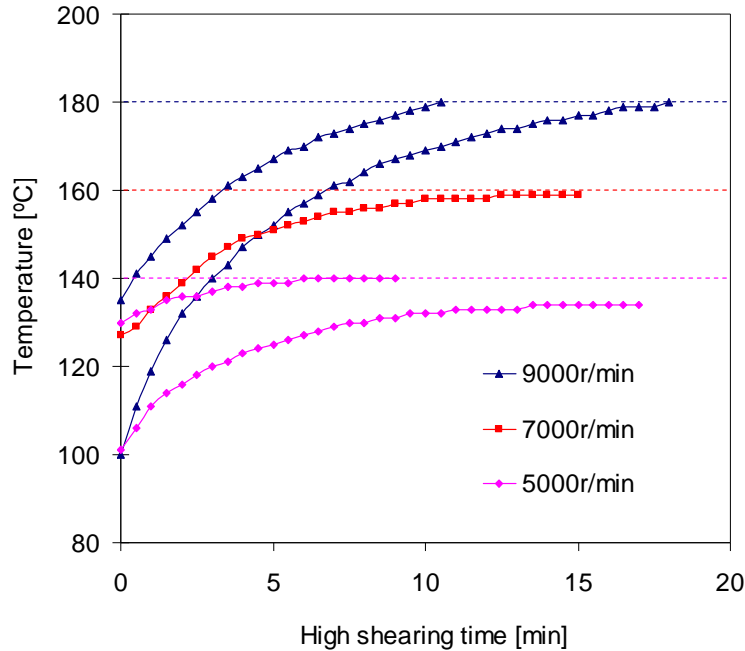


Figure 3.3.3 Influence of high shearing speed on the temperature change of base B (70/100) bitumen

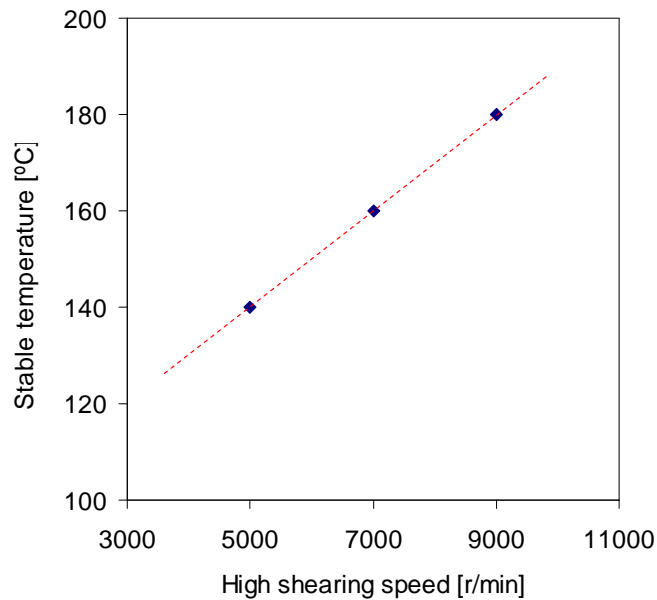


Figure 3.3.4 Relationship between stable temperature and high shearing speed of base B (70/100) bitumen

This base bitumen was prepared at different initial temperatures between 100 °C and 140 °C; three speeds (5000, 7000 and 9000 rpm) were applied. The heating plate did not work during the process of high shearing. As shown in Figure 3.3.3, the specimen's temperature increased and gradually became stable after a few minutes which indicated a balance between the heat dissipation and absorption.

As observed from the curves at 5000 rpm and at 9000 rpm, the finally achieved temperature was independent of the initial temperature of specimen but was related to the speed. The relationship between them is illustrated in Figure 3.3.4. The temperature for preparing bitumen is often below 180°C. Otherwise, the bitumen could get aged due to the volatilization of its oily components. As indicated in this figure, a speed above 9000 rpm is dangerous to this base bitumen. Besides of two fixed factors, environmental temperature (25 °C here) and specimen weight (450g), some other factors could also determine this relationship, such as the penetration grade of the base bitumen and the viscosity change due to the modification. Materials with a higher viscosity need to be mixed at lower speeds in order to keep the temperature stable. A too high speed in that case would result in an increase in temperature. All modified bitumens were prepared at a temperature of 145 ± 5 °C. In this study, the corresponding speed for each modified bitumen can be found between 4000 ± 1500 rpm to keep it within the expected temperature range.

When the temperature and the speed were determined, it was needed to check how the shearing time influences the properties of the base bitumen. Figure 3.3.5 shows the empirically rheological properties of Base B (70/100) as a function of the time. The bitumen was subjected to high shearing at a speed of 5200 rpm and at 145 °C. Within the first one hour, its properties almost did not change. After two hours, the penetration started to decline and softening point increased a little, which is due to ageing. To ensure a complete dispersion of the Mt, the shearing time should be as long as possible but without inducing any ageing effect on the base bitumen. Otherwise, it would be difficult to distinguish the modification effect by Mt. In this study, a shearing time for one hour was used for all bitumens. The same check was performed on other two base bitumens, and the change in these properties also did not happen within one hour. In practice, it is meaningful to decrease the shearing time and increase the efficiency if the same modification effect or the same dispersion state of Mt arrives within a shorter time.

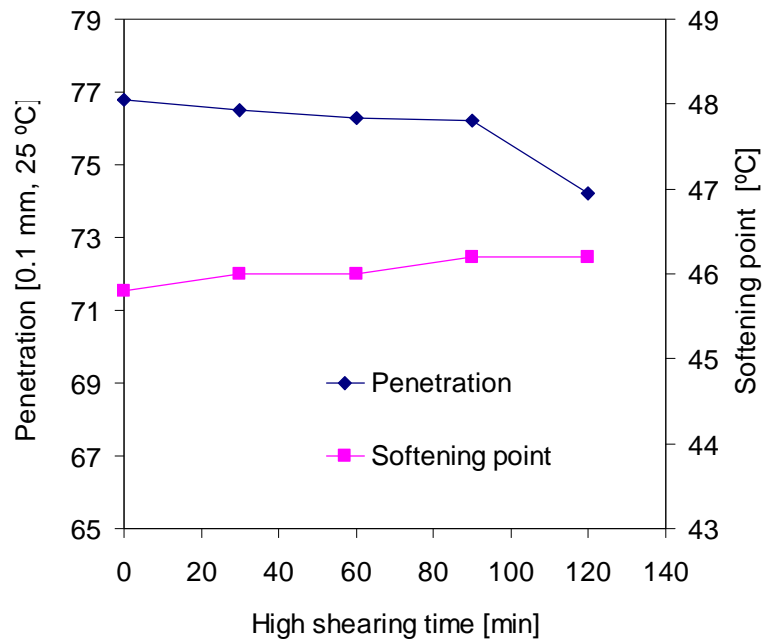


Figure 3.3.5 Penetration and softening point of base B (70/100) bitumen as the function of high shearing time

3.4 Summary and conclusions

Three montmorillonites Mt0, Mt1 and Mt2 were used to modify bitumen. Mt0 is the only inorganic clay and the other two were obtained through organic treatment of Mt0 by different surfactants. The research indicated that this treatment increased the basal spacing and meanwhile decreased the density of Mt0.

The modified bitumens were prepared as follows. 450 g of base bitumen was melted and poured into a 1000 ml cylindrical container placed on the heating plate. A certain amount of dried Mt was gradually added to the bitumen and meanwhile dispersed with a low speed mixer at 100 rpm for ten minutes. Then, the high shear mixer replaced the low speed mixer to shear the mixture. All modified bitumens were prepared at a temperature of 145 ± 5 °C. This temperature didn't influence the properties of the clay modifier. The shearing speed was between 4000 ± 1500 rpm for every bitumen specimen to keep it at the targeted temperature. A shearing time of one hour was used which did not induce any ageing on the base bitumen. After high shearing, 280 g of modified bitumen was divided into eight glass containers to perform rolling thin film oven test (RTFOT). Afterwards, 100 g of short term aged material was poured in two plates for long term aging in the pressure ageing vessel (PAV). All specimens were cooled down and stored for further testing. The same process is preformed on the base bitumen. The whole preparation process is schematically illustrated in Figure 3.4.1.

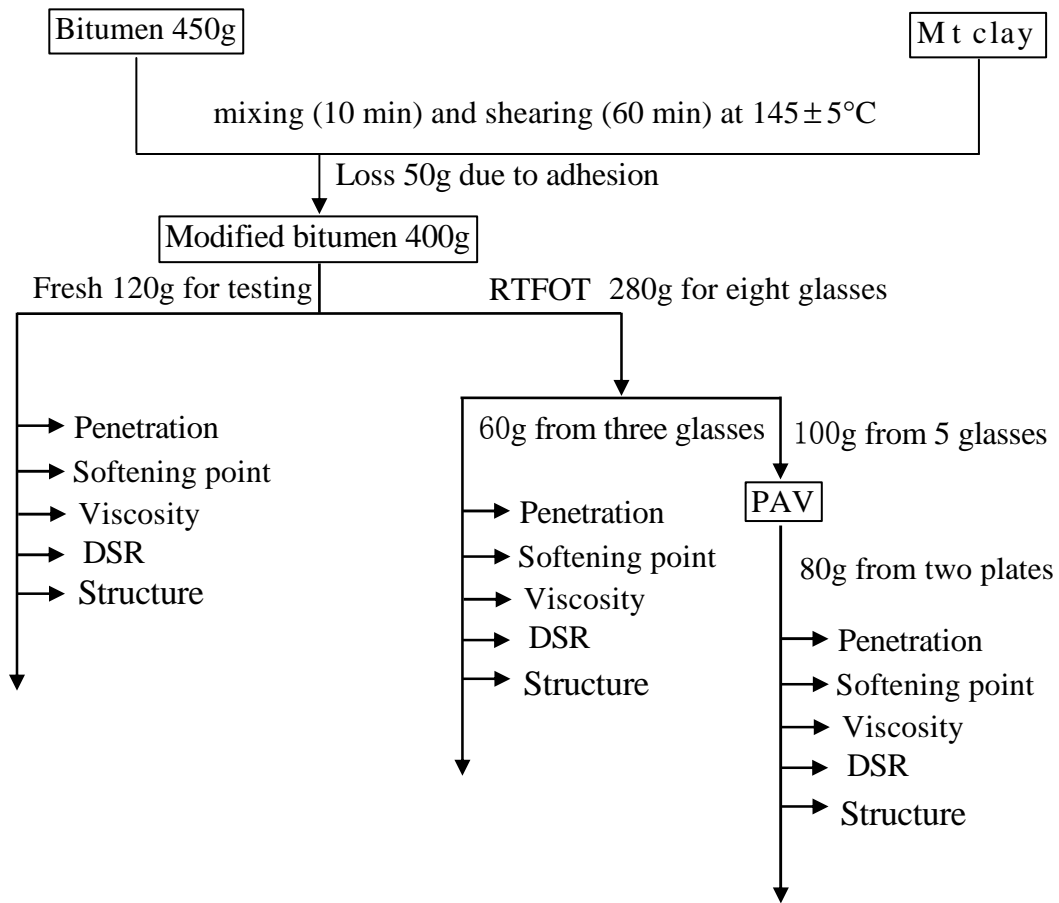


Figure 3.4.1 Schematic illustration for Preparing Mt modified bitumen

Appendix A.1

Preliminary testing to select the montmorillonites

Besides three types of montmorillonites (Mt0, Mt1 and Mt2) in this study, other five types of Mts were also obtained from the market. Basic information for them are given in Table A.1-1. Mt3, Mt4, Mt5 and Mt6 were treated by different organic surfactants. Inorganic Mt7 has the cations Ca^+ living in the interlayer space of nanoclay. However, the surfactant information for parts of organo Mts are not offered by the company. Although some tests had been attempted to characterize these surfactants (see Appendix A.2), these tests did not give a complete insight.

Table A.1-1 Organic modification of nanoclay

Samples	Surfactants	Interlayer spacing (d_{001} nm)
Mt0	Inorganic Na^+ cations, purity > 95 %	1.3
Mt1	Octadecyl trimethyl ammonium	2.1
Mt2	Hexadecyl dimethyl benzyl ammonium	2.6
Mt3	Quarternary ammonium	1.5
Mt4	Quarternary ammonium	3.5
Mt5	unknown	2.1
Mt6	Quarternary ammonium	2.4
Mt7	Inorganic Ca^+ cations, purity > 60 %	--

Preliminary testing was performed in WHUT to select the montmorillonites, using the penetration and the softening point tests. The same Mt content of 4 wt.% was used to modify one base bitumen, AH-90 originating from northern oil field of China. The results are given in Table A.1-2. In comparison, Organo Mt1 and Mt2 influence rheological properties of base bitumen much more. This indicates that a strong interaction exists between the Mt and the bitumen. What is more important is that their surfactant information was offered by the manufacturer. It is helpful to understand the modification results when using these two Mts. To make a comparison between inorganic and organo Mts, Mt0 was also selected, which was offered by the same manufacturer.

Table A.1-2 Empirical rheological properties

Bitumen	^a Penetration at 25 °C [dmm]	^b Softening Point [°C]
Base	77	46.0
+Mt0	73	46.4
+Mt1	67	47.6
+Mt2	65	48.0
+Mt3	70	47.0
+Mt4	73	46.4
+Mt5	73	46.8
+Mt6	69	47.2
+Mt7	76	46.2

^a and ^b were done according to European standards, EN 1426 and EN 1427, respectively.

Appendix A.2

Characterizing organic surfactants on montmorillonite clay using XPS method

1 Introduction

The type of surfactant is a key factor to determine the influence of montmorillonite (Mt) on the matrix. Therefore, it is of fundamental importance to know the composition of the organic surfactant. Sometimes, it is not exactly clear which type of surfactant is used on the Mts available in the market.

In this study, an attempt using the X-ray photoelectron spectrometry (XPS) was made to characterize the organic surfactants on two Mt clays, Mt-A and Mt-B. These two organo Mts were provided by different clay companies and totally different from Mt1 and Mt2. The content of this section has been published elsewhere (Liu, Wu et al. 2010) .

2 Method

X-ray photoelectron spectroscopy (XPS) is a spectroscopy technique that measures the elemental composition, chemical state and electronic state of the elements that exist within a material (Carleya 2001). XPS spectra are obtained by irradiating a material with a beam of X-rays while simultaneously measuring the kinetic energy (KE) and number of electrons that escape from the top 1 to 10 nm of the materials being analyzed.

Because the energy of a particular X-ray wavelength equals a known quantity, the electron binding energy (BE) of each of the emitted electrons can be determined using a following equation:

$$E_{\text{binding}} = E_{\text{photon}} - E_{\text{kinetic}} - \Phi \quad (1)$$

where,

E_{binding} = is the energy of the electron emitted from one electron configuration within the atom

E_{photon} = is the energy of the X-ray photons being used

E_{kinetic} = is the kinetic energy of the emitted electron as measured by the instrument, and

Φ = the work function of the spectrometer (not the material).

Each element produces a characteristic set of XPS peaks at corresponding binding energy values that directly identify the existence of the element on the surface of the material being analyzed. A characteristic peak shift will occur when the chemical state of the element is changed, which is used to speculate about the existence of a related element.

Some details of the XPS equipment used are shown below:

Equipment type:	XSAM800, Kratos Ltd.
Vacuum condition:	2×10^{-7} Pa
Resolution:	0.9 eV/104 CPS
Wide scanning range:	0~1000 eV
Fine scanning range for N1s:	395~415eV
Fine scanning range for C1s:	279~299eV

3 Results and discussion

Figure A.2-1a and b show a wide scan survey spectrum for Mt-A and Mt-B, respectively. The X-axis represents each element's characteristic binding energy of the electron emitted from one electron configuration within an atom and the Y-axis reflects detected photoelectron counts per second (CPS), i.e. intensity. According to the captured surface element signal corresponding to related characteristic peaks, carbon, nitrogen, oxygen, silicon and aluminum were detected for both Mts. This indicates that the elements on the surface of both Mts are similar.

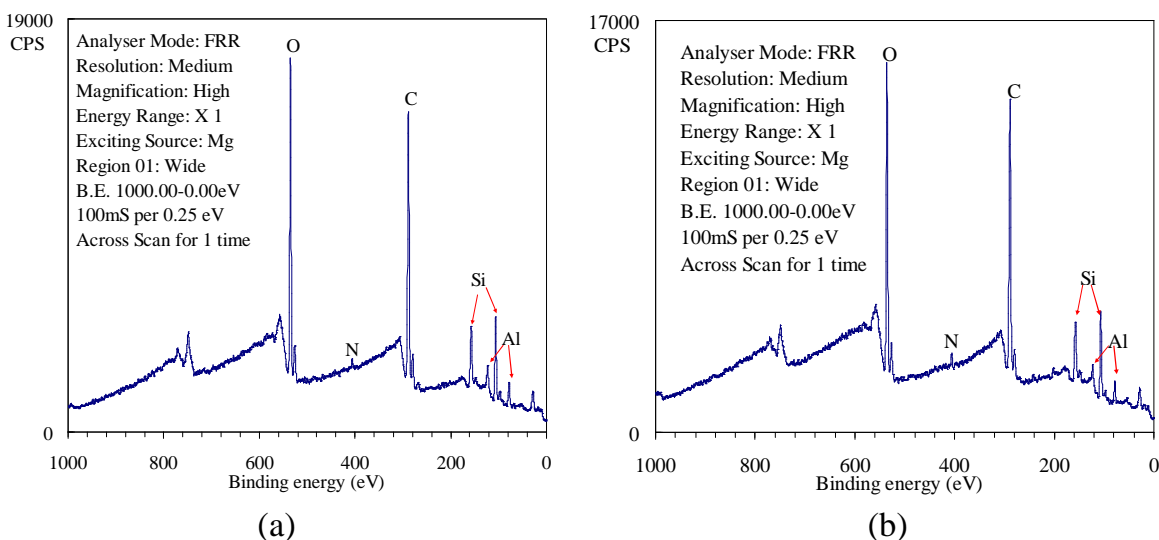


Figure A.2-1 Wide scan survey spectrum for (a) Mt-A and (b) Mt-B

High energy resolution XPS spectra were used to determine the chemical state of the element being detected. An example of the high energy resolution XPS spectrum for carbon is given in Figure A.2-2 (Briggs 1998). In this example, an envelope curve of carbon was obtained. Due to the existence of different functional groups, the characteristic peak of carbon would shift towards a higher binding energy from the typical alkyl carbon peak at around 285 eV. Through professional spectrum analysis software, other characteristic peaks representing

the different chemical state of carbon in the related functional group can also be obtained.

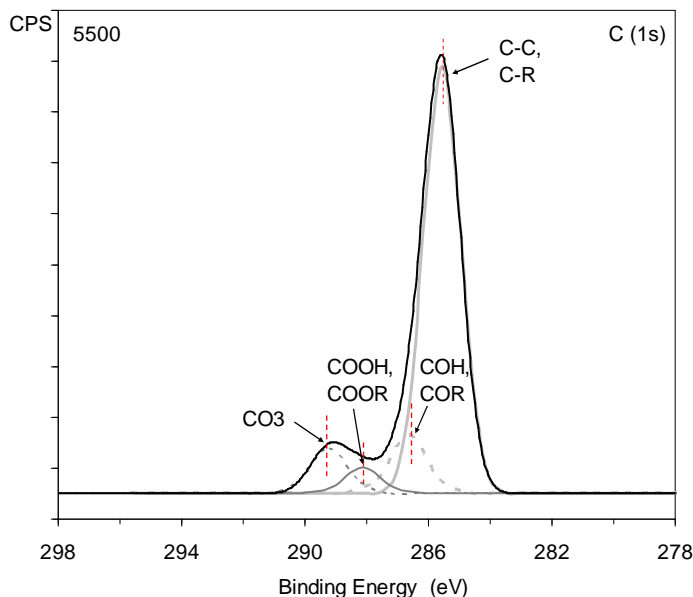


Figure A.2-2 Example of high energy resolution XPS spectrum for carbon at different states (Briggs 1998)

It was expected to observe the difference between organic surfactant cations in both Mts. So the spectrum analysis focused on the elements carbon and nitrogen. High energy resolution XPS spectra of these two elements are shown in Figures A3 and A4, respectively. In Figure A.2-3, it was found that both carbon spectrums are single, symmetrical and similar, with the peaks at 284.8 eV and 285.0 eV respectively. So based on the element analysis results and the example shown in Figure A.2-3, it can be concluded that some organic functional groups, such as carboxylic, hydroxyl, ketone etc., do not exist in the carbon chains of two organic cations in both Mts. The chemical state of carbon in Mt-A and Mt-B mainly exists in the form of C-C. However, because the photoelectron binding energies of carbon in the form of C-C and C=C are very close, it is impossible to decide the existence of C=C through XPS.

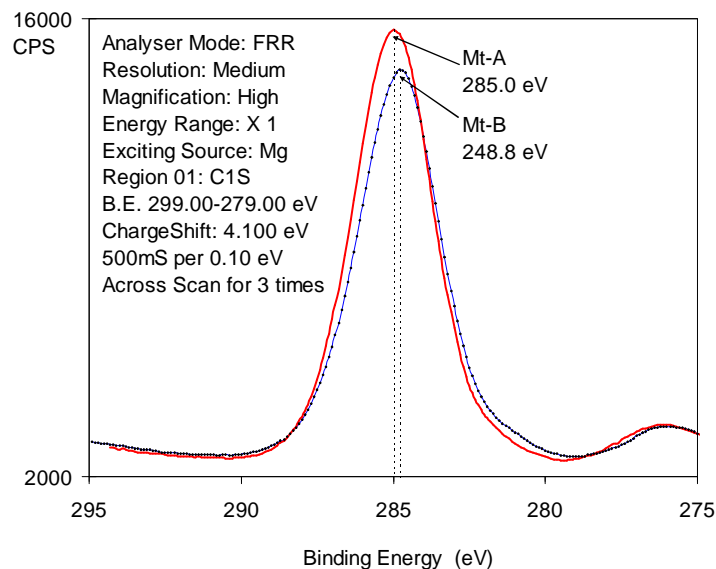


Figure A.2-3 High energy resolution XPS spectrum for carbon in Mt-A and Mt-B

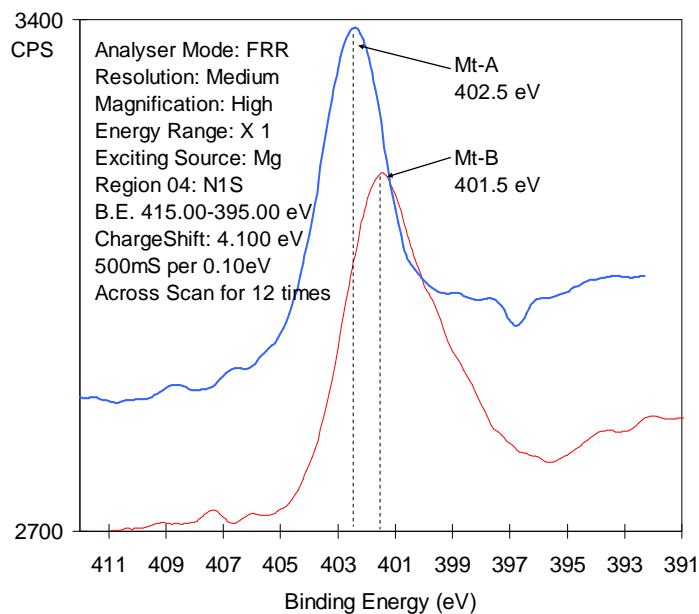


Figure A.2-4 High energy resolution XPS spectrum for nitrogen in Mt-A and Mt-B

As shown in Figure A.2-4, there is a significant difference in the position and configuration of the nitrogen peaks. The nitrogen spectrum for the Mt-A is almost symmetrical with a peak at 402.5 eV, which means that just one chemical state of nitrogen exists. Compared with the spectrum for the Mt-A, the nitrogen spectrum peak for the Mt-B shifts to the position at 401.5 eV and shows a clear asymmetric curve. The photoelectron binding energy of nitrogen in the form of quaternary ammonium is within the range of 401.5 to 402.5 eV (Briggs 1998). It can be concluded that both Mts contain quaternary ammonium cations, the most common surfactants used in the modification of the Mt. However due to the asymmetry of

the nitrogen XPS spectrum for the Mt-B, it is supposed that other chemical states of nitrogen are also possible. Therefore, the nitrogen XPS spectrum may contain other unresolved peaks.

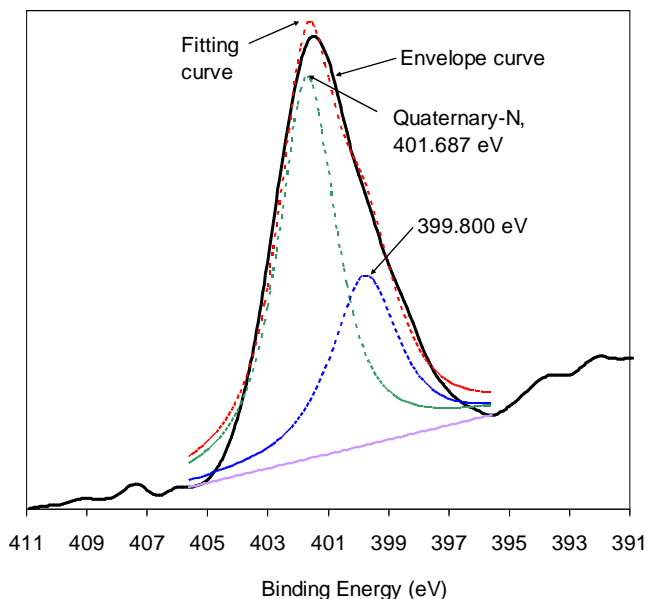


Figure A.2-5 Processing of high energy resolution XPS spectrum for nitrogen in Mt-B

With the professional spectrum analysis software XPSpeak4.1, two peaks were obtained at 401.687 eV and 399.8 eV and their fitting curves are combined close to the envelope as shown in Figure A.2-5. The photoelectron binding energy of nitrogen in the form of amine, amide, nitrile, carbamide etc. is in the range of 399 to 400 eV (Briggs 1998). However the above analysis of the carbon spectrum indicates that the ketone (RCOR') doesn't exist in the carbon chains. Therefore, the existence of amides (RCONH_2) and carbamide ($\text{CO(NH}_2)_2$) is not realistic. In order to detect the accurate molecular structure of the organic surfactant cations, nuclear magnetic resonance (NMR) is necessary in a next study. It could detect the existence of $\text{C}=\text{C}$ bonds and more accurate estimate on the molecular structure of surfactant.

4 Conclusions

The X-ray photoelectron spectroscopy was adopted to characterize the composition of the organic surfactant cations on two montmorillonites from the market. Research indicated that the surfactants were not the same. The surfactant in Mt-A only contained quaternary ammonium surfactants. The other surfactant in Mt-B showed two states of nitrogen: quaternary ammonium and probably amine or nitrile. In general, $\text{C}-\text{C}$ bonds could be detected very well for the two surfactants

and there were no other functional groups, such as carboxylic, hydroxyl, ketone etc. However it was unclear if the surfactants had C=C bonds.

3.5 References

- Briggs, D. (1998). Surface analysis of polymers by XPS and static SIMS, Cambridge Univ Pr.
- Carleya, A. F. (2001). Surface analysis: X-ray photoelectron spectroscopy, Elsevier Ltd., Oxford.
- Dubois, P. (2000). "Polymer-layered silicate nanocomposites: preparation, properties and uses of a new class of materials." Materials Science and Engineering: R: Reports 28(1-2): 1-63.
- Huskic, M., I. Brnardic, et al. (2008). "Modification of montmorillonite by quaternary polyesters." Journal of Non-Crystalline Solids 354(28): 3326-3331.
- Ju, W., P. Long, et al. (2006). "Solvatochromic effect of a fluorescence probe used to study the environmental properties of organic montmorillonite." Colloids and Surfaces A: Physicochemical and Engineering Aspects 279(1-3): 233-237.
- Kakehi, K., Y. K. Maeya, et al. (1997). "Use of a Binary Mixture of Quaternary Ammonium Salts in Fluorometric Determination of Glycosaminoglycans." Analytical biochemistry 252(1): 56-61.
- Koo, J. H. (2006). Polymer nanocomposites: processing, characterization, and applications, McGraw-Hill Professional.
- Liu, G., S. Wu, et al. (2010). "Characterization of Organic Surfactant on Montmorillonite Nanoclay to Be Used in Bitumen." Journal of materials in civil engineering 22: 794.
- Liu, J., G. Zhang, et al. (2010). "Synthesis and optical properties of new amphoteric quaternary ammonium salt fluorescent brighteners." Journal of chemical engineering of Chinese universities 24(5): 53-59.
- Rjeb, M., A. Labzour, et al. (2005). "TG and DSC studies of natural and artificial aging of polypropylene." Physica A: Statistical Mechanics and its Applications 358(1): 212-217.
- Wang, Z. L. and J. Wiley (2000). Characterization of nanophase materials, Wiley Online Library.

4 STRUCTURE OF NANOCCLAY IN MODIFIED BITUMEN

4.1 Introduction

In this chapter, main techniques are introduced, which are often used to characterize the structures of bitumens and nanocomposites. Based on this introduction, some methods were attempted to analyze the structure of Mts in modified bitumen. The obtained results are combined to analyze the properties of modified bitumens in next chapters.

4.1.1 Structures of base and modified bitumens

Base and polymer modified bitumens' structures have been studied using optical, electron and scanning probe microscopy techniques by some researchers (Loeber, Sutton et al. 1996; Wu, Pang et al. 2009). Atomic force microscopy (AFM) has become popular for observation of the surface of a bitumen film with the advantage of no specimen preparation and the ability to operate at ambient temperature. Bitumen is normally described as a colloidal dispersion of asphaltene micelles in the maltenes. The resins as polar components in the maltenes act as the stabilizer for the asphaltene micelles. Figure 4.1.1 shows the “bee” structure of a gel bitumen visualized by AFM with a tapping mode. This structure was believed to be attributed to asphaltene networks (Loeber, Sutton et al. 1996). The AFM method was also used to characterize the ageing behaviour (Wu, Pang et al. 2009). As shown in Figure 4.1.2, a bigger bee-like structure appeared on the surface after PAV aging.

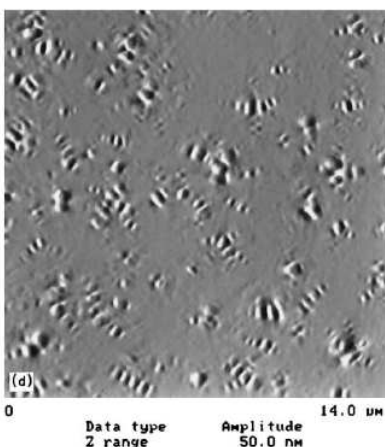


Figure 4.1.1 AFM tapping mode image of a gel bitumen (Loeber, Sutton et al. 1996)

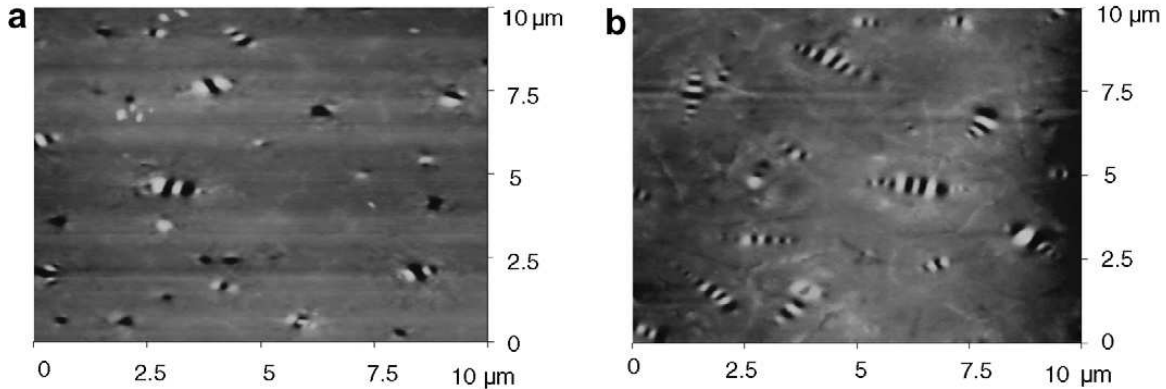


Figure 4.1.2 AFM images of base bitumen (a) before and (b) after PAV ageing (Wu, Pang et al. 2009)

Scanning electron microscopy (SEM) and environmental scanning electron microscopy (ESEM) are also used to observe the surface structure of bitumen (Loeber, Sutton et al. 1996; Rozeveld, Shin et al. 1997). The SEM images of a gel specimen (Figure 4.1.3a) show the same network structure as shown in an AFM images (Figure 4.1.1) but with smaller pores (about 1–2 μm in diameter) and interconnected spherical particles with a diameter of approximately 100 nm. In the SEM image (Figure 4.1.3b), Loeber, Sutton et al. (1996) thought that some polymer threads were adsorbed onto the asphaltene particles. It is noted that extra specimen preparation and the vacuum and low-temperature testing environments in this method can influence the surface structure of bitumen compared with that under ambient conditions.

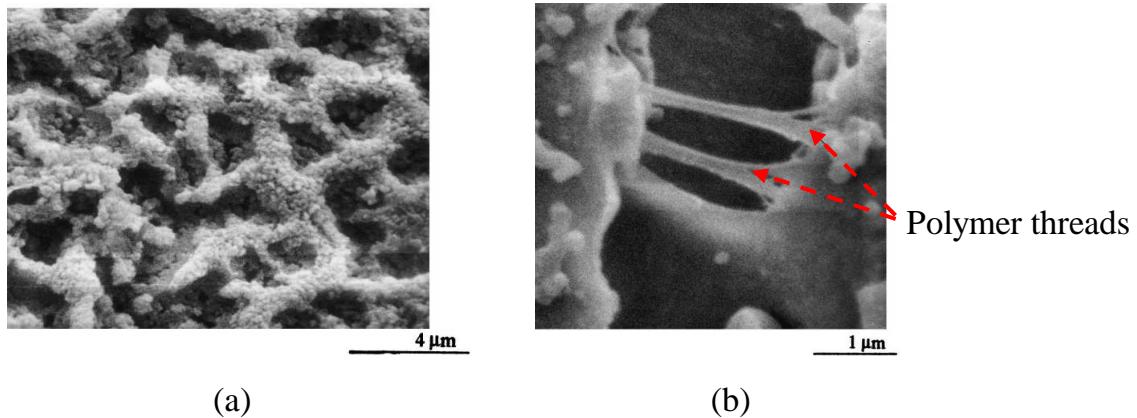


Figure 4.1.3 SEM images of (a) a gel bitumen and (b) polymer modified bitumen (Loeber, Sutton et al. 1996)

With respect to polymer modified bitumens, fluorescence microscopy (FM) is most often used to observe the dispersion of continuous and discontinuous phases. As shown in Figure 4.1.4a, the continuous phase is a bitumen matrix with dispersed polymer particles (appears white here). As the polymer content increases from 3% to 9%, the continuous phase is a polymer matrix with dispersed bitumen

globules (Figure 4.1.4b). The polymer is swollen by absorbing the light aromatic components in the base bitumen, resulting in an increase in volume of added polymer by 4 to 10 times. Lu and Isacsson (1997) pointed out that the SBS polymer network should not be confused with the SBS continuous phase at a high polymer content. Because the network may exist in the polymer-rich phase presenting as discrete particles (Figure 4.1.4a) and the polymer-rich phase as continua (Figure 4.1.4b).

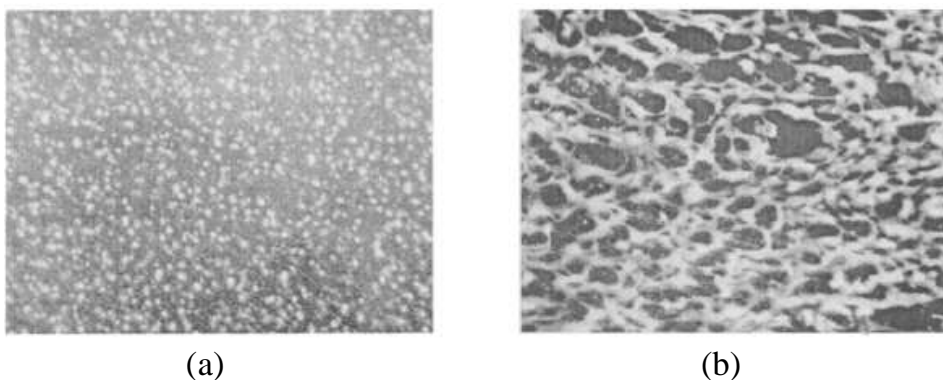


Figure 4.1.4 Fluorescence images of polymer modified bitumens with (a) 3% and (b) 9% Kraton linear SBS D-1101 (Lu and Isacsson 1997)

It is noted that SEM, AFM and FM only reveal surface features which can not represent the internal structure of materials. Bearsley and Forbes (2004) adopted confocal laser-scanning microscope (CLSM) to examine the asphaltene network structures in situ. They considered that the light coloured flecks in Figure 4.1.5 were asphaltene aggregates with a typically size of 2-7 μm dispersed in a darker maltene matrix. By comparing the CLSM images of non-waxy and waxy bitumens, Lu, Langton et al. (2005) proved that the features observed with CLSM (Figure 4.1.6) were actually wax crystals. Waxy bitumens from different crude origins displayed a large variation of structures, varying from tiny needles to elongated needles, flakes and even crescent shaped structures.

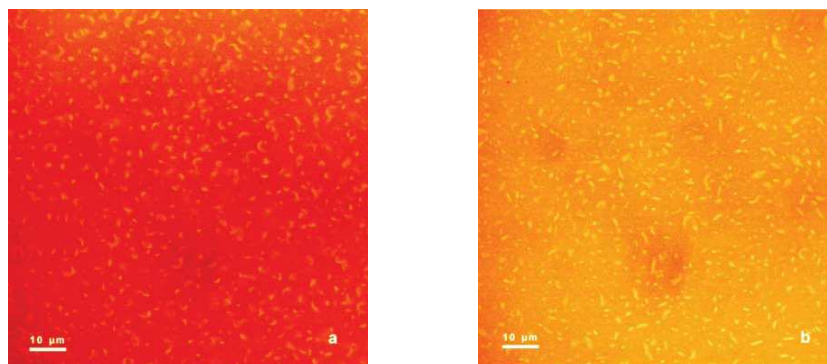


Figure 4.1.5 CLSM image of (a) 180/200 and (b) 80/100 bitumen (Bearsley and Forbes 2004)

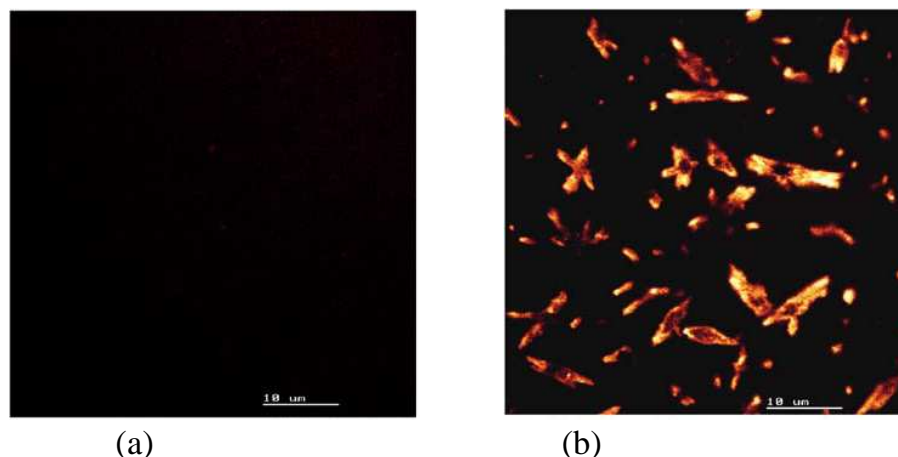


Figure 4.1.6 Comparison of CLSM images for bitumen (a) without and (b) with 6.2 wt. % waxy (scale: 10 μ m) (Lu, Langton et al. 2005)

4.1.2 Structures of clay in the polymer

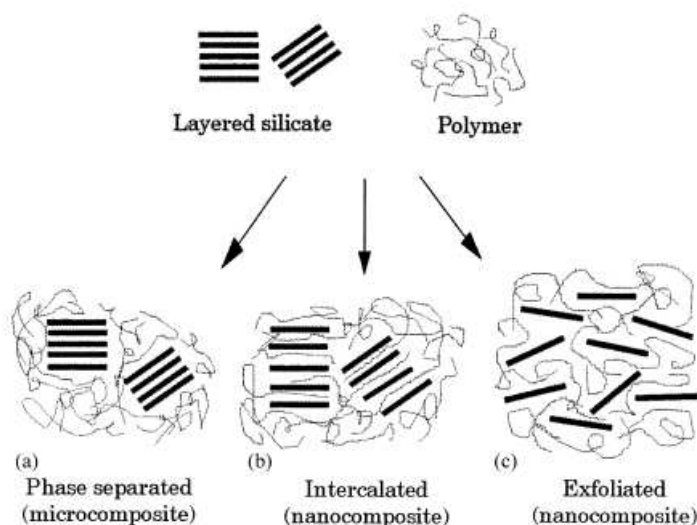


Figure 4.1.7 Scheme of different types of composite arising from the interaction of layered silicates and polymers: (a) phase separated microcomposite; (b) intercalated nanocomposite; (c) exfoliated nanocomposite (Alexandre and Dubois 2000)

As summarized by Alexandre and Dubois (2000), three main types of composites (Figure 4.1.7) may be obtained when a layered clay is associated with a polymer, depending on the nature of the components used (layered silicate, organic cation and polymer matrix) and the method of preparation. When the polymer is unable to intercalate between the silicate layers, a phase separated composite (Figure 4.1.7a) is obtained, whose properties stay in the same range as traditional microcomposites. Beyond this classical family of composites, two types of

nanocomposites can be observed. Intercalated structure (Figure 4.1.7b) in which a single (and sometimes more than one) extended polymer chain is intercalated between the silicate layers resulting in a well ordered multilayer morphology built up with alternating polymeric and inorganic layers. When the silicate layers are completely and uniformly dispersed in a continuous polymer matrix, an exfoliated or delaminated structure is obtained (Figure 4.1.7c).

The structure of the nanocomposites has traditionally been characterized using X-ray diffraction (XRD) and transmission electron microscopy (TEM) (Koo 2006). Due to the periodic arrangement of the silicate layers both in the pristine and the intercalated states, with periodicity of 1-4 nm and the presence of high atomic number species in the layers, the choice of X-ray diffraction in determining the interlayer spacing is obvious (Alexandre and Dubois 2000). Typical XRD patterns for the three structures illustrated in Figure 4.1.7 are shown in Figure 4.1.8. Curve (a) represents an “immiscible” system (here polyethylene/organo-silicate), and is identical with the XRD curve of the neat organo-silicate. For the intercalated case of curve b, the basal spacing shifts to a higher value as the gallery (interlayer space) expands to accommodate the intercalating polymer. Curve c means a typical exfoliated or delaminated structure or a disordered system (Vaia, Vasudevan et al. 1995).

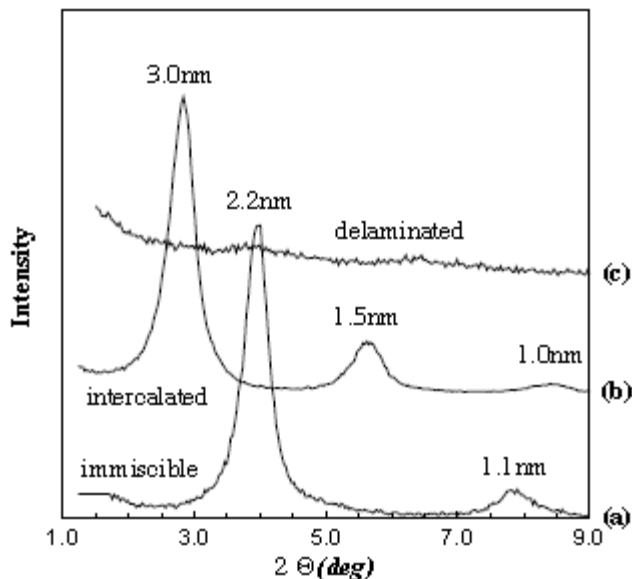


Figure 4.1.8 Typical XRD patterns from polymer/silicate hybrids (Vaia, Vasudevan et al. 1995)

XRD can not provide definite information regarding the structure of an exfoliated or a delaminated nanocomposite. This is because a large spacing exists between the layers (i.e. exceeding 8 nm in the case of ordered exfoliated structure) or

because the nanocomposite does not present ordering anymore (i.e. destroyed crystal structure). In this case, TEM has proven to be an extremely useful technique to characterize the nanocomposite morphology. Figure 4.1.9 shows the TEM micrographs obtained for nanocomposites (Ammala, Hill et al. 2007). Besides these two well defined structures (intercalated and an exfoliated), other intermediate organizations can exist presenting both intercalation and exfoliation. In this case, a broadening of the XRD diffraction peak could be observed and one must rely on TEM observation to define the overall structure.

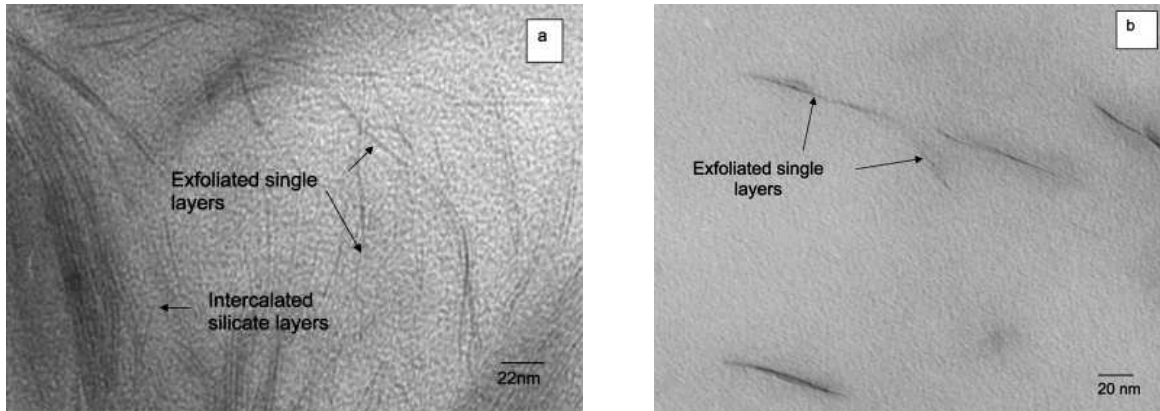


Figure 4.1.9 High-resolution TEM micrographs of (a) the nylon 6-kaolinite nanocomposite and (b) the nylon 6-montmorillonite Cloisite 30B nanocomposite (Ammala, Hill et al. 2007)

4.1.3 Summary

For the bituminous materials, the characterization of the structure focuses on the surface area using SEM, AFM and FM at micrometer level. With respect to nanocomposites, more internal structures are characterized using XRD and TEM at a nanometer level. In this study, both groups of the equipments were used to characterize Mt structures in bitumen.

4.2 Methods

4.2.1 XRD

The same diffractometer introduced in Chapter 3 was adopted to characterize the basal spacing (d_{001}) of Mts in the bitumen. More information about the theory can be found in Chapter 3 or elsewhere (Wang and Wiley 2000; Koo 2006). In this test, Cu-K α radiation (40kV and 50mA) was used with $\lambda=0.15406$ nm and 2θ ranging from 0.5° to 10° at a speed of $3^\circ/\text{min}$. To make the specimen, hot liquid bitumen was poured on an aluminum holder (Figure 4.2.1 right) lying on silicone paper. After cooling down to the room temperature, a specimen with a clear and smooth surface (Figure 4.2.1 left) was obtained. This surface was exposed to the X-ray radiation during the test.

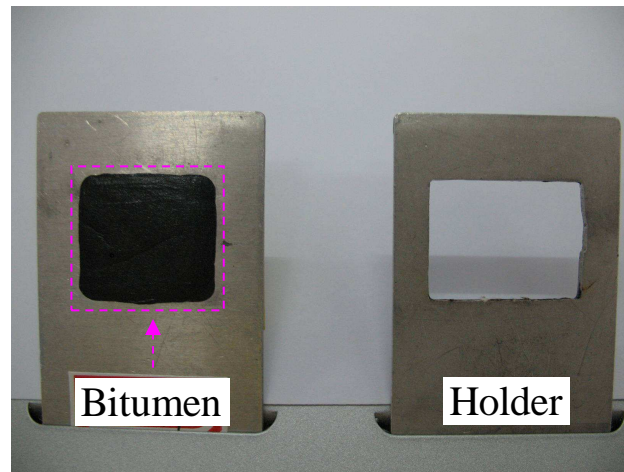


Figure 4.2.1 Bitumen specimen used for XRD test

4.2.2 X-ray computed tomography (CT) scanning

The X-ray computed tomography (CT) scanning has been used in the field of pavement research to analyze the aggregate particles, as well as voids in bituminous mastics and mixtures in three dimensions (Nielsen 2007). In this study, the Nanotom CT scanner (Figure 4.2.2a) from Phoenix|x-ray Systems+Services Inc. was used to directly observe the Mt's structure in the bitumen. It can provide a non-destructive three-dimensional visualization and characterization of objects with a highest resolution of about 1 micron achieved on samples with a maximum size of about 2 mm. As illustrated in Figure 4.2.2b, a high power nanofocus X-ray tube emits a series of x-rays at different angles for each time after a small rotation of the sample core. The strength of the rays is measured by the detector after they have passed through the core. Then, a series of two-dimensional images are taken in a cross section of the core. Contrast in an image depends on differences in X-ray absorption which is closely related to the components' densities in the core. With the program datos|x-reconstruction, a 3D volume model is constructed by integrating the recorded images of the core and all necessary geometrical information is saved. The X-ray tube in this equipment has a high voltage up to 180kV, power up to 15 W and a minimal focal spot size smaller than 0.9 μ m.

The specimen core in this test is a plastic pipe with a diameter of 3mm into which the bitumen in liquid state is sucked. A Focal model was used for testing.

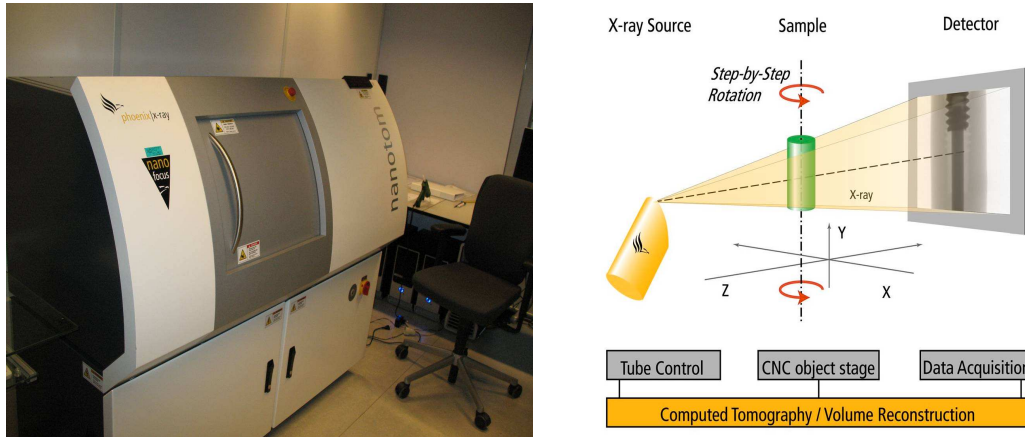


Figure 4.2.2 (a) Nanotom CT scanner and (b) its schematically mechanism

4.2.3 Fluorescence microscope and other methods

The same Olympus BH2-RFCA fluorescence microscope (FM) as introduced in Chapter 3 was used to observe the Mts in the bitumen. To make a specimen (Figure 4.2.3), a bead of bitumen was dropped onto a microscope slide and placed on a heating plate at 100 °C to melt for one minute. When the bitumen becomes liquid, it spreads out to form a round film with a diameter of about 8 mm. At that moment, the heating is stopped and the slide is kept undisturbed with a cover. The test was performed after its cooling down to room temperature for two hours.

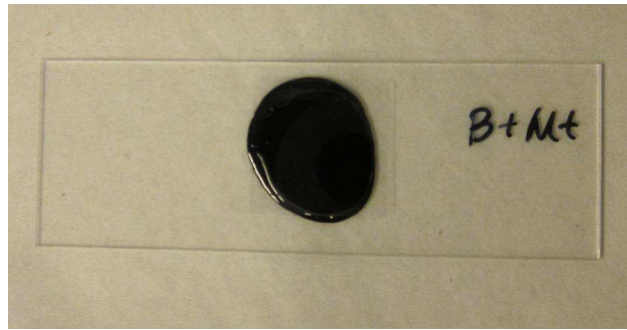


Figure 4.2.3 Bitumen specimen under the fluorescence microscope

The DI Nanoscope IV atomic force microscope (AFM) was used to observe the surface feature of Mt modified bitumen. A tapping mode was adopted because this mode is suitable to test soft materials while preventing the tip from sticking to the surface in ambient conditions. At this mode, the triangular silicon cantilever with a constant force of about 0.57 N/m and the fundamental resonance frequency near 73 kHz were adopted. The same preparation method for the FM test was used.

4.3 Results and analyses

4.3.1 XRD

As shown in Figures 4.3.1, 2, 3 and 4, the basal spacing (d_{001}) of Mts before and after mixing with bitumen were characterized using XRD. After mixing with bitumen, the first diffraction peak in most curves is shifted towards a lower angle which means an increase in d_{001} . According to Bragg's law, d_{001} and its increase rate before and after mixing were calculated and the results are given in Table 4.3.1. In base A and B (see Table 3.1.1), Mt1 and Mt2 had increased in d_{001} with almost a factor 2. However, they exhibited a relatively small change (46.0% and 37.3%, respectively) in softer base C. According to Figure 4.1.7 and the examples in Figure 4.1.8, it can be concluded that for Mt1 and Mt2, intercalated structures have formed in the three base bitumens. Another important characteristic is that intercalated structures commonly have more, even up to 13 order peaks or reflections in the XRD curve compared with the pure Mt (Vaia, Vasudevan et al. 1995). The only inorganic Mt0 shows little change in d_{001} which means that it owns an immiscible or a phase separated structure in base B.

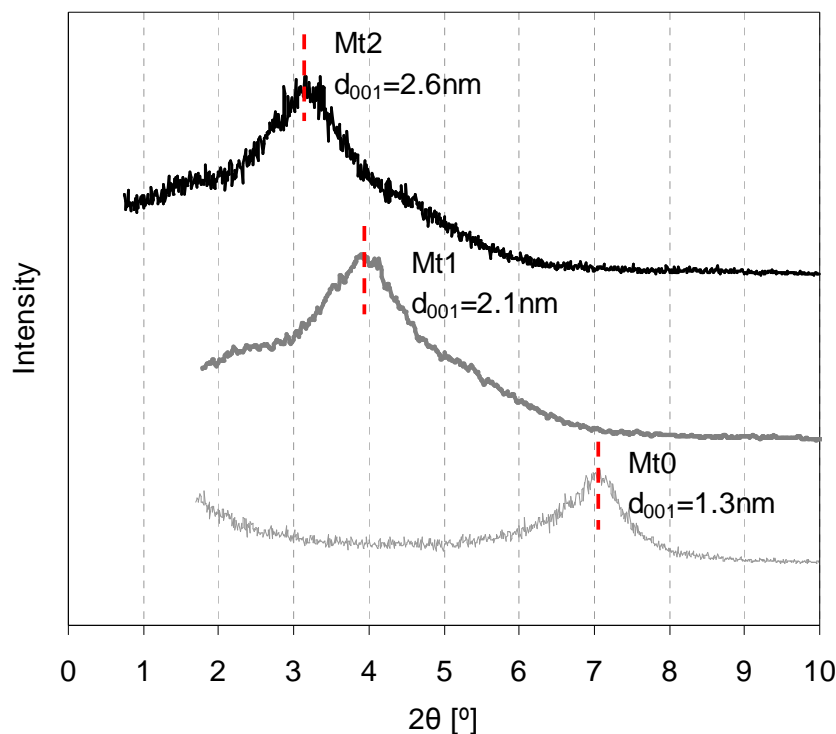


Figure 4.3.1 XRD curves of Mts before mixing with bitumens

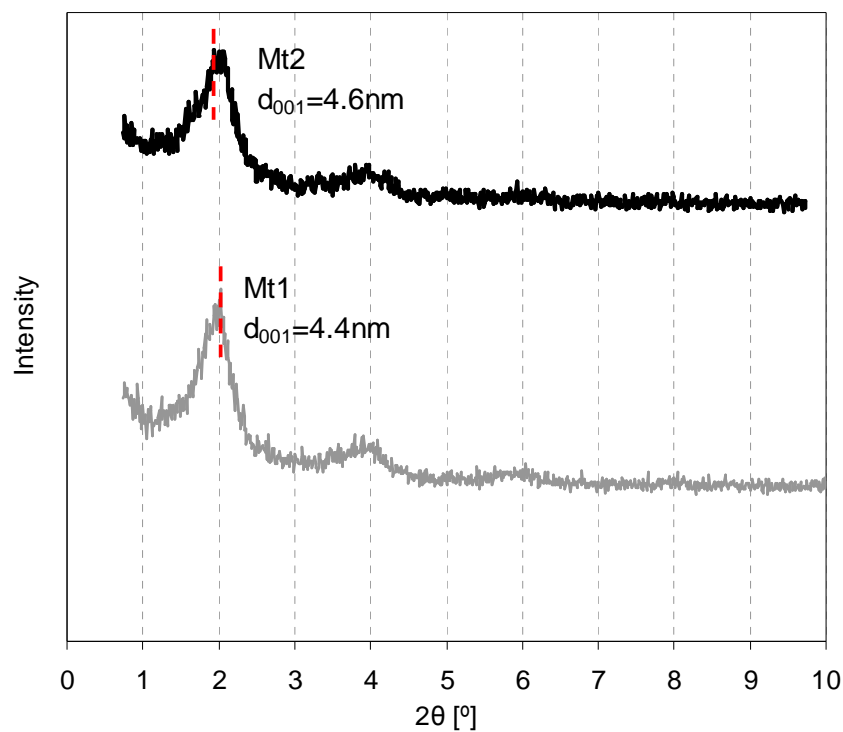


Figure 4.3.2 XRD curves of 4 wt.% Mts in base A

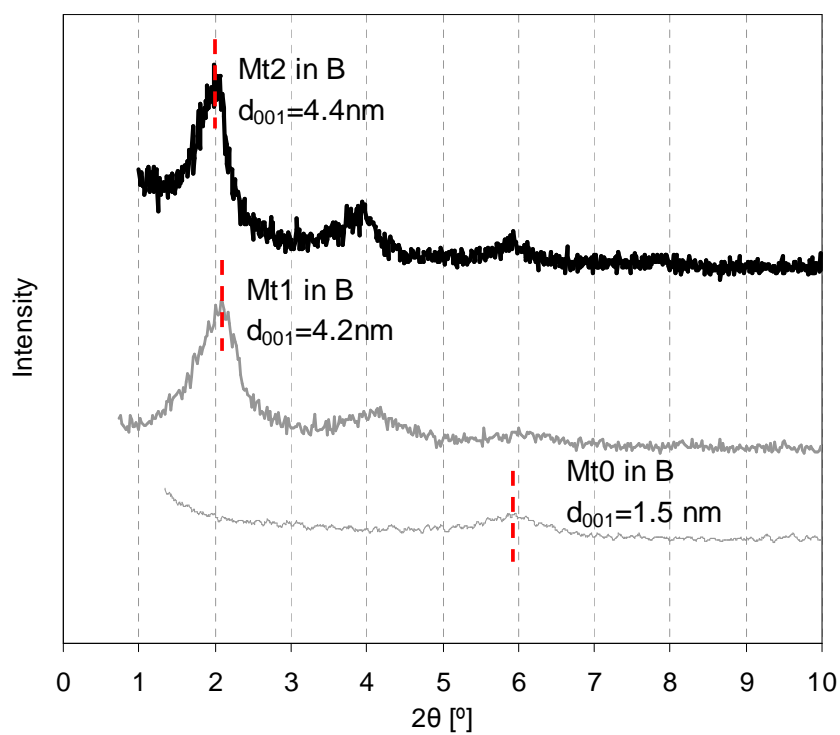


Figure 4.3.3 XRD curves of 4 wt.% Mts in base B

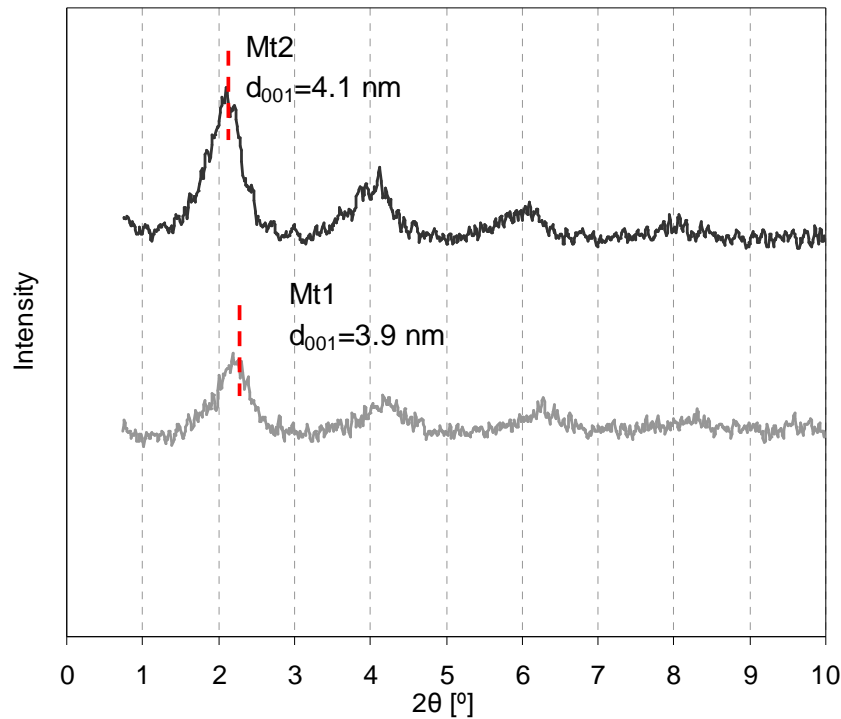


Figure 4.3.4 XRD curves of 4 wt.% Mts in base C

Table 4.3.1 Basal spacing (d_{001}) of Mts after mixing with bitumen at 4 wt.%

Specimens	2θ [°]	* Basal spacing d_{001} [nm]	# Increase rate in d_{001} [%]
A+4%Mt1	2.01	4.4	52.2
A+4%Mt2	1.94	4.6	42.9
B+4%Mt0	5.90	1.5	13.1
B+4%Mt1	2.11	4.2	50.0
B+4%Mt2	2.02	4.4	40.5
C+4%Mt1	2.27	3.9	46.0
C+4%Mt2	2.13	4.1	37.3

*: calculated using Bragg's law, $2d_{001}\sin\theta=\lambda$ (here, $\lambda=0.15406$).

#: equal to $(d_{\text{after}} - d_{\text{before}})/d_{\text{before}} \times 100$. Here, d_{before} and d_{after} mean the basal spacing of Mt before and after mixing with bitumen, respectively.

It was mentioned above that the structures of Mt in the matrix depend on the nature of the components used and the method of preparation. Different bitumens and Mts have been used in this study and two structures were formed, the intercalated for organo Mt and the phase separated for inorganic Mt, using the same preparation method. It was indicated that the high-shear mixing method could not result in an exfoliated structure of Mts in the bituminous matrix. The

reason could be that the exfoliated structure of Mt with a specific surface area (BET) normally bigger than $100 \text{ m}^2/\text{g}$ is not stable in the liquid bitumen because of its huge surface energy. The Mt layers would automatically gather together to reduce this energy, and consequently stabilize the whole system. This can easily occur when the viscosity of the matrix is low. The smaller d_{001} change of Mt1 and Mt2 in the softer base C also reflects the influence of the viscosity or the state of the matrix on the Mt structures.

As introduced in Chapter 2, synthesis methods for nanocomposites mainly include solution intercalation, melt intercalation, roll milling, in-situ polymerization and high-shear mixing (Koo 2006). High-shearing mixing is most accessible to prepare bituminous materials not only in the lab, but also in the factory. To achieve an exfoliated state of organo Mt, two other physical methods, melt intercalation and roll milling are recommended for future research. The matrixes in these methods are close to solid, and the silicate layers can easily get exfoliated and stay stable.

Recently, an exfoliated structure of Mt in bitumen observed by XRD has also been published (Galooyak, Dabir et al. 2010). The authors scanned the specimen with 2θ from 1.5° to 15° . The beginning 2θ (1.5°) is much high and hard to reflect the first diffraction peak. Therefore, the intercalated state could be mistaken for the exfoliated.

4.3.2 Micro-CT Scanning

Figure 4.3.5a and b present CT scanning images of B+4%Mt0 at the maximum resolution (around $1 \mu\text{m}$) in 3D and 2D, respectively. Clay particles observed are at micrometer level. To make a comparison also, CT scanning on a mortar containing normal filler was performed. The mortar consisted of bitumen and Wigro 60k filler with the ratio of 1:1 by weight. The size and components of Wigro 60k filler can be found in Table 7.2.3, Chapter 7. The mortar CT images show a dense particle distribution (Figure 4.3.6) due to higher filler content, but similar shape and size as Mt0 (Figure 4.3.5). This means that the structure of Mt0 in the bitumen is just like that of conventional filler. This structure also corresponds to the tiny change of its basal spacing before and after mixing with bitumen as observed from the XRD curves. It may be due to the fact that the hydrophilic surface of natural Mt0 exhibits poor compatibility with the bitumen, which makes it difficult for the bitumen molecules to enter the interlayer space of Mt0. However, it was not possible to observe Mt1 and Mt2 from Figure 4.3.7a and b. This means that a high dispersion for Mt1 and Mt2 exists in the bitumen, which is out of the resolution of CT scanning at micrometer level.

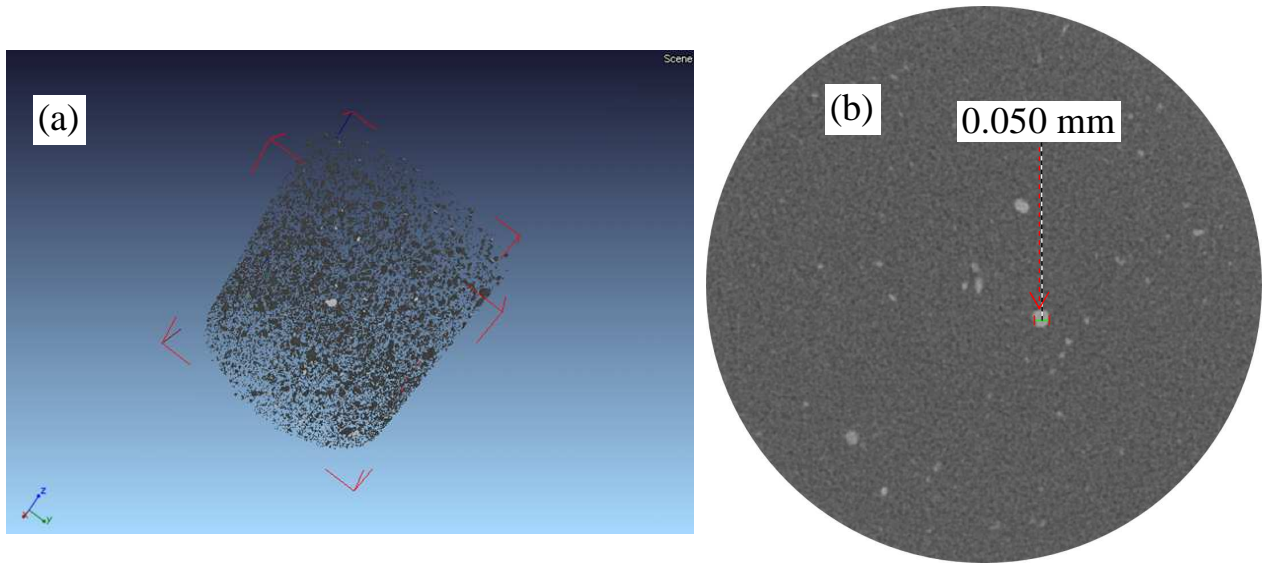


Figure 4.3.5 CT scanning (a) 3D and (b) 2D cross-section images of Mt0 particles with 4 wt.% in base B bitumen

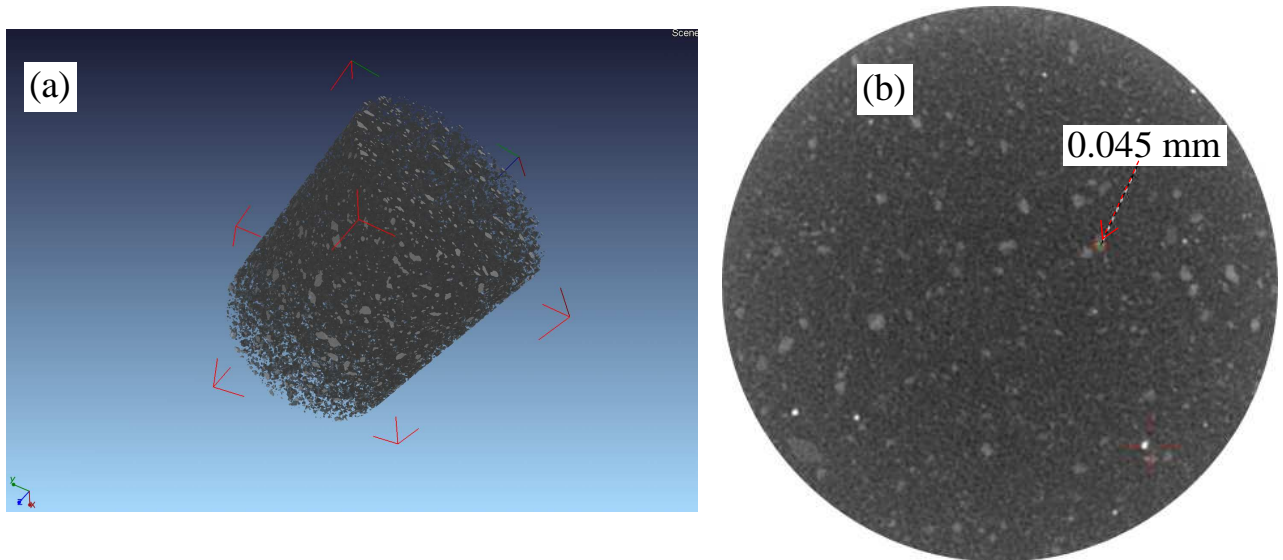


Figure 4.3.6 CT scanning (a) 3D and (b) 2D cross-section images of mortar (base B bitumen:Wigro 60k filler = 1:1 by weight)

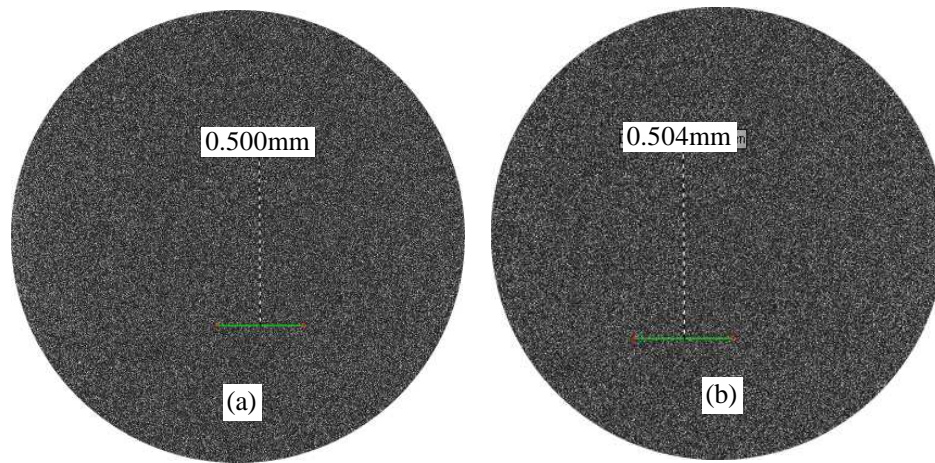


Figure 4.3.7 CT scanning 2D images of (a) Mt1 and (b) Mt2 with 4 weight% in base B bitumen

4.3.3 Fluorescence image

As introduced in Chapter 3, Mt1 and Mt2 are fluorescent due to the presence of quaternary ammonium surfactants on the surface of layered silicate, which makes it possible to observe them in bitumen using the fluorescence microscope. Figures 4.3.8a and b show the fluorescence images of B+4%Mt1 and B+4%Mt2, respectively. A few Mt1 particles could be distinguished at a micrometer level. Due to higher fluorescence, it was easier to observe Mt2 particles under the same conditions. Compared with SBS modified bitumen (Figure 4.3.9), both B+4%Mt1 and B+4%Mt2 show lower fluorescence.

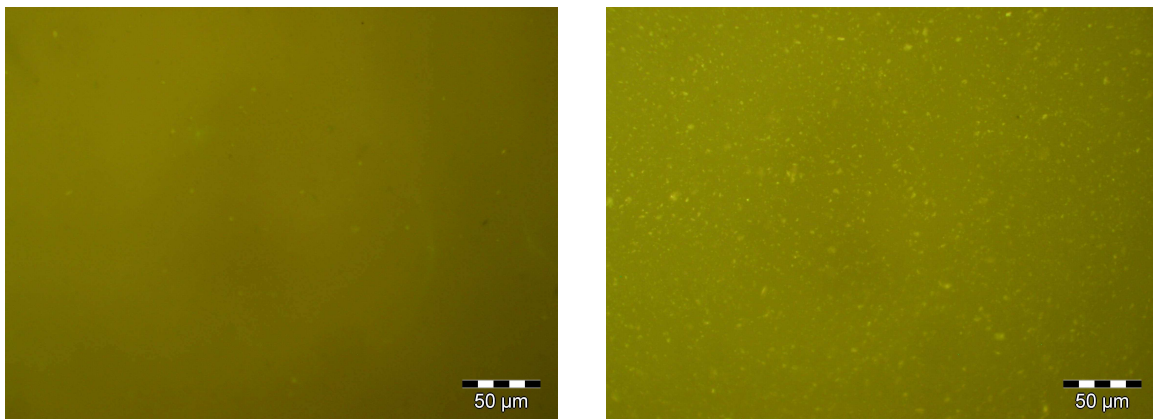


Figure 4.3.8 Fluorescence images of (a) B+4%Mt1 and (b) B+4%Mt2

XRD results indicated that the organo Mts swell due to the intercalation of bitumen molecules. Therefore, the particles observed in fluorescence images are not pure clay and can be called as clay-rich phases. These phases should have a similar density as bitumen. Otherwise, it is possible to observe them using the CT scanning based on the density difference.

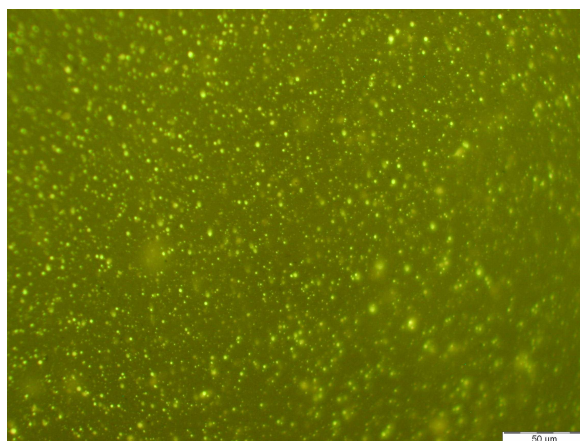


Figure 4.3.9 Fluorescence images of 5% D1101SBS modified bitumen

4.3.4 Other methods

AFM was used to scan an area of $15 \times 15 \mu\text{m}^2$ repeatedly. A 2D image was preserved and shown in Figure 4.3.10. Typical “bee” structures can easily be observed and one of them was particularly scanned at a higher magnification and presented in a 3D perspective view. According to this 3D image, a major pleat can be found, which enables the formation of a “bee” structure in the 2D image. A similar “bee” structure had been reported earlier (Masson 2006) and was believed to be attributed to the asphaltenes in bitumen. However, it is hard to catch the existence of the Mt on the surface of the bitumen film by using this method.

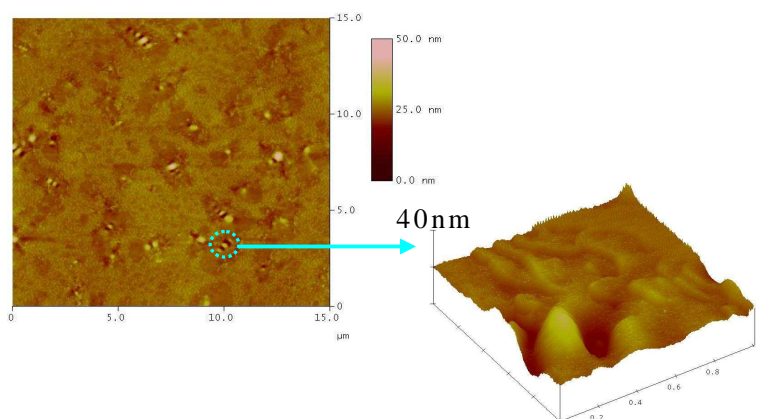


Figure 4.3.10 AFM image of B+4%Mt1

The transmission electron microscope (TEM) method was tried but failed because some small bitumen molecules easily evaporated due to the vacuum environment at ambient temperature. An environmental TEM method is recommended in the future.

4.4 Summary and conclusions

Different methods have been used to observe the structures of inorganic and organo Mts in the base bitumen. XRD results indicated that an intercalated structure for organo Mts was formed in the three base bitumens used. A phase separated structure was found when natural Mt was used in one base bitumen. Micro-CT images further proved that natural Mt acted like the conventional filler at a micrometer level, probably due to its hydrophilic surface causing poor compatibility with the bitumen. Due to the high dispersion, it was hard to find organo Mts in the bitumen with the CT scanner. However, it was possible to observe them using the fluorescence microscope due to the fluorescent properties of the surfactants on the Mt. Because the bitumen molecules had entered the interlayer space of organo Mt, the observed particles are not pure clay and can be called as clay-rich phases. Meanwhile, these phases should have a similar density as bitumen. Otherwise, the CT scanning could find them at a micrometer level. It was not possible to catch the existence of Mt on the surface of the bitumen film using the AFM method. An environmental TEM method is recommended in the future.

A high-shearing mixing method is the most accessible one to prepare bituminous materials not only in the lab, but also in the factory. The results indicated that this preparation method did not result in an exfoliated structure for Mts in the bituminous matrix; just intercalated and phase separated structure were formed, depending on the type of Mt. The reason could be that the exfoliated structure normally has a high specific surface area (normally larger than $100 \text{ m}^2/\text{g}$) and is not stable in the liquid bitumen. The smaller structure change of organo Mt in the soft base bitumen observed using XRD reflects this influence (the state of matrix or its viscosity) on the final structure of Mt. To achieve an exfoliated state of organo Mt, two other physical methods, melt intercalation and roll milling are recommended for future research

4.5 Reference

- Alexandre, M. and P. Dubois (2000). "Polymer-layered silicate nanocomposites: preparation, properties and uses of a new class of materials." Materials Science and Engineering: R: Reports 28(1-2): 1-63.
- Ammala, A., A. J. Hill, et al. (2007). "Poly (m xylene adipamide)kaolinite and poly (m xylene adipamide)montmorillonite nanocomposites." Journal of Applied Polymer Science 104(3): 1377-1381.
- Bearsley, S. and A. Forbes (2004). "Direct observation of the asphaltene structure in paving grade bitumen using confocal laser scanning microscopy." Journal of Microscopy 215(2): 149-155.
- Galooyak, S. S., B. Dabir, et al. (2010). "Rheological properties and storage stability of bitumen/SBS/montmorillonite composites." Construction and building materials 24(3): 300-307.
- Koo, J. H. (2006). Polymer nanocomposites: processing, characterization, and applications, McGraw-Hill Professional.
- Loeber, L., O. Sutton, et al. (1996). "New direct observations of asphalts and asphalt binders by scanning electron microscopy and atomic force microscopy." Journal of Microscopy 182(1): 32-39.
- Lu, X. and U. Isacson (1997). "Compatibility and storage stability of styrene-butadiene-styrene copolymer modified bitumens." Materials and Structures 30(10): 618-626.
- Lu, X., M. Langton, et al. (2005). "Wax morphology in bitumen." Journal of materials science 40(8): 1893-1900.
- Masson, J. (2006). "Bitumen morphologies by phase detection atomic force microscopy." Journal of Microscopy 221(1): 17-29.
- Nielsen, C. B. (2007). Microstructure of porous pavements-- Experimental procedures, Road Directorate, Danish Road Institute.
- Rozeveld, S. J., E. E. Shin, et al. (1997). "Network morphology of straight and polymer modified asphalt cements." Microscopy research and technique 38(5): 529-543.
- Vaia, R. A., S. Vasudevan, et al. (1995). "New polymer electrolyte nanocomposites: Melt intercalation of poly (ethylene oxide) in mica type silicates." Advanced materials 7(2): 154-156.
- Vaia, R. A., S. Vasudevan, et al. (1995). "New polymer electrolyte nanocomposites: Melt intercalation of poly(ethylene oxide) in mica-type silicates." Advanced materials 7(2): 154-156.
- Wang, Z. L. and J. Wiley (2000). Characterization of nanophase materials, Wiley Online Library.
- Wu, S., L. Pang, et al. (2009). "Influence of aging on the evolution of structure, morphology and rheology of base and SBS modified bitumen." Construction and building materials 23(2): 1005-1010.

5 AGEING PROPERTIES

5.1 Introduction

Bitumen ageing is one of the main reasons for asphalt pavement failure. In this chapter, the influence of montmorillonites (Mts) on the ageing properties of base bitumen is evaluated. Firstly, some background about the ageing of bitumen will be given.

5.1.1 Ageing effect

Normally, ageing effects on bitumen are classified into two stages: short term and long term (Morgen and Mulder 1995; Roberts, Kandhal et al. 1996). Short term ageing takes place during mixing, storage, transportation, laying and compaction of the mixture. In the first period of mixing, thin bitumen films, with a thickness of several micrometers on the aggregates, easily get aged when they are exposed to air at temperatures ranging from 135 °C to 180 °C. At that moment, oxidation and volatilization of oily components are the main reason for the ageing. For the next periods, ageing continues but at a slower rate.

Long term ageing refers to the hardening of bitumen during the service life of the asphalt mixture. Compared with short term ageing, the ageing rate is less and longer time periods are needed to obtain equivalent ageing. The type of mixture has a big influence on the ageing rate. For example, porous asphalt concrete, which is widely used in the Netherlands, has a higher air void content, which is leading to a much quicker ageing than dense asphalt due to the easier entry of air.

Figure 5.1.1 illustrates how bitumen ageing is developing as indicated by means of the viscosity ratio from the mixing to the service stage.

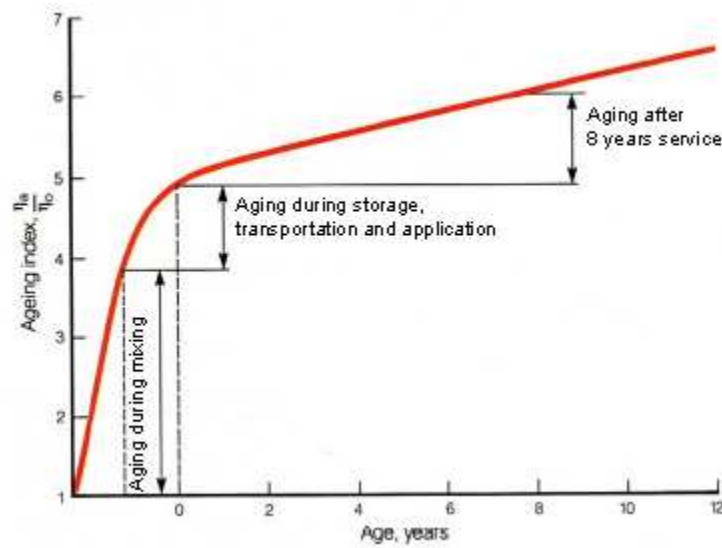


Figure 5.1.1 Effect of short and long term ageing of the bitumen as indicated by means of the viscosity ratio (Morgen and Mulder 1995)

Apart from oxidation and volatilization as mentioned above, also some other factors contributing to ageing of bitumen have been reported. All of them are summarized and defined as follows (Roberts, Kandhal et al. 1996):

-- Oxidation: Oxidation is the reaction of oxygen with bitumen, the rate depending on the character of the bitumen and the temperature. This reaction is easier to take place with the presence of ultraviolet (UV) light.

-- Volatilization: Volatilization is the evaporation of the lighter fractions from the bitumen and is primarily a function of temperature. Usually, it is not a significant factor contributing to long term aging in the pavement.

-- Thixotropy: Thixotropy (steric hardening) is a progressive hardening due to the formation of a structure within the bitumen over a period of time. This hardening can be destroyed to a degree by reheating and working the material. It is generally associated with pavements which have little or no traffic and its magnitude is a function of the bitumen content. It is a physical hardening which may be attributed to molecular structuring, i.e. the reorganization of asphalt molecules to approach an optimum thermodynamic state under the specific set of conditions (Petersen 1984).

-- Polymerization: Polymerization is a combination of similar molecules to form larger molecules, resulting in a progressive hardening. At low temperatures, the rate of association is considered slow as a result of higher viscosity of the binder.

-- Syneresis: Syneresis is an exudation reaction in which the thin oily liquids are excluded to the surface of the bitumen film. With the elimination of these oily constituents, the bitumen becomes harder.

-- Separation: Separation is the removal of the oily constituents, resins, or asphaltenes from the bitumen caused by absorption into some porous aggregates.

Some other factors, like humidity, light, microbiological deterioration, and the interaction with mineral aggregates have also been considered (Anderson, Christensen et al. 1994; Roberts, Kandhal et al. 1996). Based on these factors, it is concluded that the ageing process in the field contains extremely complicated chemical and physical reactions. Among these factors, oxidation and volatilization are two fundamental and irreversible effects on the ageing of bitumen (Petersen 1984)

The change of physical properties of bitumen due to ageing is a function of the chemical change of each component. As shown in Figure 5.1.2, oxidation causes the transformation of naphthene aromatics (non-polar component) to polar aromatics (resins), and further to polar asphaltenes, while another non-polar component saturates had no reaction (Domke, Davison et al. 1999).

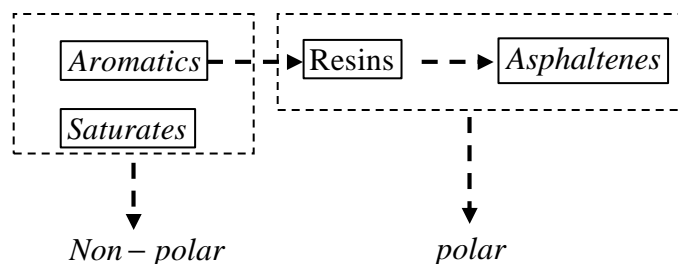


Figure 5.1.2 Schematic diagram of bitumen components moving towards polar fractions due to ageing

Component transformation involves several events including oxidation at the molecular level and structuring at intermolecular level. Some oxidation products are formed, such as carbonyl, sulfoxide, carboxylic anhydrides and small amounts of other highly oxidized species (Bell, Sosnovske et al. 1994; Petersen and Harnsberger 1998; Wu, Pang et al. 2009). Carbonyl (C=O) and sulfoxide (S=O) are most representative and often used to characterize the ageing degree of bitumen in the lab and the field (Lamontagne, Dumas et al. 2001; Hagos 2008; Wu, Pang et al. 2009).

It is proposed in literature that the formation of carbonyl and sulfoxide is the result of free radical reaction (Kelemen, George et al. 1990; Ouyang, Wang et al. 2006). Although some mechanisms are argued in academia, the consensus reached is that ageing makes bitumen hard and brittle, and finally leads to the failure of the pavement.

5.1.2 Improvement of bitumen ageing

Polymer modifiers have been adopted to improve the rheological properties of bitumen. In practice, styrene-butadiene-styrene (SBS), styrene-ethylene-butylene-styrene (SEBS), ethylene vinyl acetate (EVA) etc. are used for different purposes and applications (Lu, Isacson et al. 1999). Research indicated that the ageing behaviour of some modified bitumen gets improved due to the breakdown of the polymer. Although the breakdown of the polymer reduces the number of large polymer molecules, and consequently the effectiveness of the polymer, this change is believed to produce a reduction in viscosity which partially balances the hardening of the base bitumen thus enhancing resistance to ageing (Isaccson 1999; Hagos 2008).

Based on the known thermo-oxidative mechanism of SBS copolymer degradation and the present experimental evidence, Cortizo et al. (2004) suggested that the initial polymeric free radicals would react with some asphalt components with C=C double bond producing a link between them, and increasing in the polarity and the molecular size of modified asphalt components. Based on this theory, Ouyang et al. (2006) considered that the SBS copolymer seemed to protect the asphalt fraction trapped in the polymeric network against oxidation.

Two antioxidants, zinc dialkyldithiophosphate (ZDDP) and zinc dibutyl dithiocarbamate (ZDBC) with 1 wt % were added to polymer modified bitumen by Ouyang et al. (2006). Research indicated that antioxidants could delay the oxidation of the PMA by the inhibition of peroxides and radical scavenging, to further prevent propagation of the free radical chain or to prevent the formation of the peroxy radicals. Due to the complexity of the bitumen system, the proper mechanisms need further investigation.

The mechanisms for ageing improvement introduced above are always accompanied by a series of chemical reactions. As the reactions continue, the effectiveness of the modifier in improving this behaviour of bitumen will be reduced. In this chapter, Mt nanoclay used to modify the bitumen has good physicochemical stability. It was expected that the scale effect and barrier properties of Mt platelets could prevent the penetration of oxygen and consequently improve the ageing resistance. Therefore, this is a kind of physical method which could effectively retard the oxidation of bitumen in the long term ageing

5.2 Characterization methods

5.2.1 Simulation in the lab

The rolling thin film oven test (RTFOT) (EN 12607-1) and the pressure ageing vessel (PAV) (EN 14769) were used to simulate the short term and long term ageing of bitumen, respectively. For RTFOT, eight cylindrical bottles with an opening as shown in Figure 5.2.1 are placed in an oven at 163 °C. In each bottle, 50 g of bitumen is placed. The bottles rotate in a carousel, and hot and fresh air is periodically injected into the bottles at a rate of 4000 ± 200 ml/min for 75 min.

After ageing, some tests were performed, such as penetration, softening point and dynamic viscosity, to determine the ageing properties of the bitumen. The weight change of the specimen is recorded. According to Zupanick and Baselice (1997), losing weight and gaining weight can take place simultaneously due to the volatilization of oily components and oxidation of bitumen itself. Therefore, it became difficult to evaluate the ageing effect in terms of weight change of specimen. Parmeggiani (2000) proposed the nitrogen rolling thin film oven test (NRTFOT) in which nitrogen instead of air was injected into the bottle. In this case, the extent of volatilization of bitumen can be accessed. On the other hand, the effect of the loss of oily components on properties of the remainder can also be evaluated.

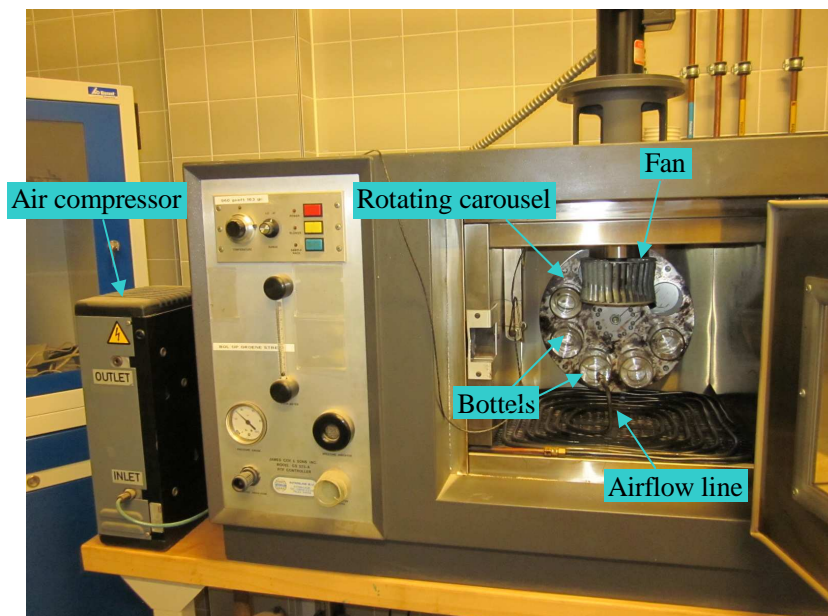


Figure 5.2.1 Rolling thin film oven test (RTFOT) equipment (left) and the bottle for holding the specimen (right)

The thin film oven test (TFOT) (EN 12607-2) is also used to simulate short term ageing of base bitumen. In comparison, RTFOT produces a more severe ageing of the bitumen because the rolling effect exposes more fresh bitumen surface to the

hot airflow, and more volatilization happens. However, the rolling effect on the bitumen has something to do with its viscosity at the test temperature (normally 163 °C). Bitumen with a high viscosity will flow slower in a rolling bottle under the influence of gravity than a low viscosity bitumen. It means that the RTFOT procedure does not provide equivalent oxidation conditions for materials with viscosity (or consistency) differences, such as base bitumen and polymer modified bitumen (PMB) (Hagos 2008). A steel rod with the same length as the bottle was placed into the rolling bottle to reduce the influence of viscosity on the exposure of bitumen (Bahia, Hislop et al. 1998). The rod worked as a roller and rotated due to its gravity in the bottle. In this way, the rod was expected to uniformly expose a bitumen film. However, results did not show the improved ageing effect on modified bitumen which has a higher viscosity.

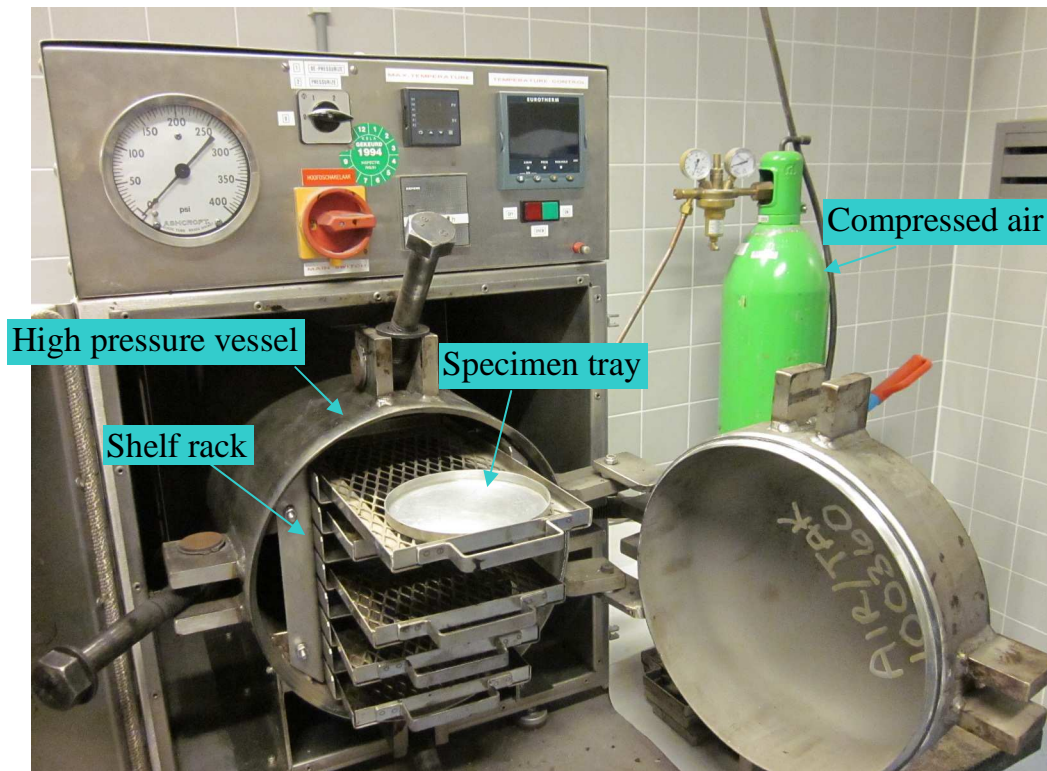


Figure 5.2.2 Pressure ageing vessel equipment

According to the norm EN 14769, the pressure ageing vessel (PAV) (Figure 5.2.2) is usually adopted to simulate the oxidation process that takes place during the service life of the pavement. The bitumen firstly suffers the short term ageing using the RTFOT method. 50 ± 0.5 g of specimen is poured in a pan with a diameter of 140 mm. The thickness of the film is about 3.2mm. Then, the pan is placed on a shelf rack. The number of pans depends on the amount of bitumen required for the subsequent tests. Typical testing temperatures used in PAV are 85

°C, 90 °C, 100 °C and 110 °C. 100 °C was used in this study. The higher temperatures may make this ageing procedure unsuitable for evaluation of bitumen containing some polymers as they could exhibit segregation that does not occur during the service life. The applied air pressure is 2.1 ± 0.1 MPa for 20 hours.

Compared to the RTFOT method, it seems that the PAV method is a static test because the specimen container is not moved. However, some foam could be observed on the surface after the test. This is probably due to the high air pressure during the test. An example for the base bitumen 70/100 is shown in Figure 5.2.3. It means that the air easily penetrates into the bitumen under the high pressure and the applied temperature. The extent of foam is dependent on the viscosity of the bitumen and the testing temperature. The foam indicates some dynamic interaction between the bitumen and air during the test procedure. Therefore, the PAV ageing procedure could also be considered as a dynamic ageing test.



Figure 5.2.3 the surface foam after PAV ageing for the base bitumen 70/100

In Europe, there are also other methods to simulate bitumen ageing. All of them are summarized by Hagos (2008) and listed in Table 5.2.1. It is observed that RTFOT and PAV used shorter testing times than other similar tests.

Table 5.2.1 Summary of bitumen ageing methods (Hagos, 2008)

Test method	Temperature (°C)	Duration (min / hr)	Sample size (g)	Film thickness (mm)	Other features	Standard
<i>Short-term aging</i>						
1. Thin Film Oven Test (TFOT)	163	5 hr	50	3.2	--	EN 12607-2
2. Rolling Thin Film Oven Test (RTFOT)	163	75 min	35 x 8 bottles	1.25	15 rpm, air flow 4 l/min	EN 12607-1
3. Rotating Cylinder Aging Test (RCAT)	163	235 min	500 - 550	--	5 rpm, air flow 4 l/min	NEN-EN 15323 (Draft)
4. German Rotating Flask Test (MGRFT)	165	150 min	100	--	flask rotation 20 rpm	DIN 52016
Modified* German Rotating Flask Test	165	210 min	200	--	flask rotation 20 rpm	DIN 52016
<i>Long-term aging</i>						
1. Pressure Aging Vessel Test (PAV), [POV]	90	20 hr			2.1 MPa pressure	EN-14769 (SHRP B-005)
2. High Pressure Aging Test (HiPAT)	85	65 hr	50	3.2	2.1 MPa pressure	
3. Rotating Cylinder Aging Test (RCAT)	85 / 90	240 / 144 hr	500 - 550	2.0	1 rpm, 4.5 l/hr Oxygen	BRRC method
4. Modified German Rotating Flask Test	85	65 hr	200	--	flask rotation 20 rpm	DIN 52016
5. Weatherometer aging *	60	1000 hr	PA mixture	4.5% bitumen	Temp. +UV +humidity (refer to section 4.3.3)	New method - Simulation of field conditions

5.2.2 Ageing evaluation

After artificial ageing in the laboratory, some bitumen properties are changed. Ageing is normally evaluated by measuring some rheological property (e.g. penetration, softening point and viscosity) before and after ageing (Lu and Isacsson 1998), as well as some chemical properties. The tests used in this study are introduced below.

5.2.2.1 Rheological methods

The empirical rheological properties, penetration (EN1426) and softening point (EN 1427) are used to evaluate the hardening of bitumen due to ageing (Morgen and Mulder 1995), as follows:

$$\text{Retained penetration} = \frac{\text{Penetration after ageing}}{\text{Penetration before ageing}} \quad 5.2.1$$

$$\text{Change in softening point} = T_2 - T_1 \quad 5.2.2$$

where,

T_1, T_2 = the softening point before and after ageing, respectively.

In general, ageing characterized by means of the ageing index (AI) in this chapter is defined as:

$$AI = \frac{|I_{aged}^*|}{|I_{fresh}^*|} \quad 5.2.3$$

where,

$|I_{fresh}^*|, |I_{aged}^*|$ = the rheological parameters of the bitumen (such as complex modulus or viscosity) before and after ageing, respectively.

The AI value is used by Lu and Isacsson (1998) to evaluate the ageing properties of polymer modified bitumen (PMB). The rheological parameter used in that study was the complex modulus. A high value of the AI means a high degree of bitumen ageing. As shown in Figure 5.2.4, ageing indices of PMB can be higher or lower than the index of one. This was believed to be due to degradation of the polymer and oxidation of the bitumen. Therefore, Lu and Isacsson thought that the AI used here was not a suitable parameter in case of PMBs. Meanwhile, it did not seem to be possible to apply a certain value of the ageing index in characterizing PMB ageing properties. Ageing analyses of modified bitumen should also take into account the effect of ageing on the modifier itself, e.g. what is the effect of ageing on the polymer in polymer modified bitumen.

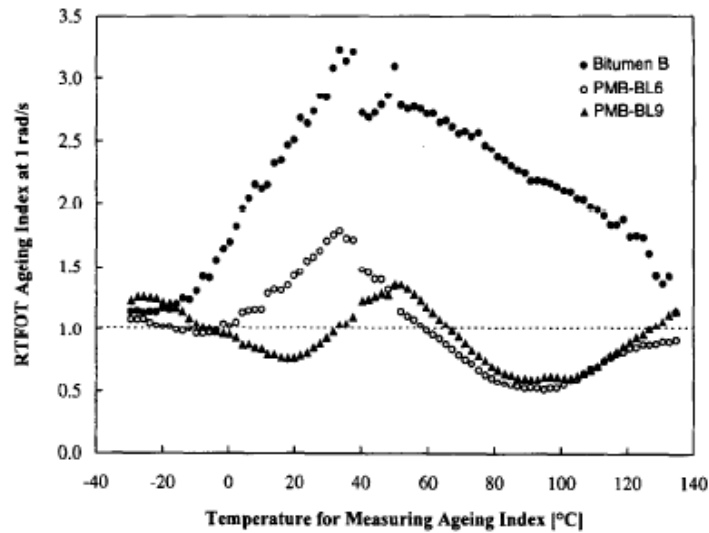


Figure 5.2.4 Temperature dependence of the RTFOT ageing index ($|G_{aged}^*|/|G_{fresh}^*|$) at 1 rad/s (Lu and Isacsson 1998)

5.2.2.2 Chemical characterization on ageing

Many researches adopted the Fourier transform infrared (FTIR) spectroscopy to characterize the ageing behaviour (Bell and Sosnovske 1994; Lamontagne, Dumas et al. 2001; Hagos 2008; Wu, Pang et al. 2009). Bitumen ageing is a complex series of chemical reactions involving oxidation at molecular level and structuring at intermolecular level (Bell and Sosnovske 1994). Due to oxidation, there are two major products, ketones (C=O) and sulfoxides (S=O). As shown in Figure 5.2.5a, characteristic peaks of C=O and S=O after ageing are located at 1700 cm^{-1} due to the stretch vibration of carbonyl group and around 1030 cm^{-1} due to the stretch vibration of sulphoxide group, respectively (Wu, Pang et al. 2009). The increase in the area under these two peaks is usually used to describe the ageing degree. With respect to SBS modified bitumen in Figure 5.2.6b, the peak at around 968 cm^{-1} was caused by the stretch vibration of chain segments of butadiene and was becoming lower due to the degradation of SBS.

Besides of the functional group method, there are other chemical methods. The gel permeation chromatography technique (GPC) is generally used to record the molecular weight distribution of bitumen before and after ageing (Hagos 2008). The Gaestel index (IC) was used to characterize the change in the chemical composition before and after ageing and defined as follows:

$$IC = \frac{\text{Asphaltenes} + \text{Saturates}}{\text{Aromatics} + \text{Resins}} \quad 5.2.4$$

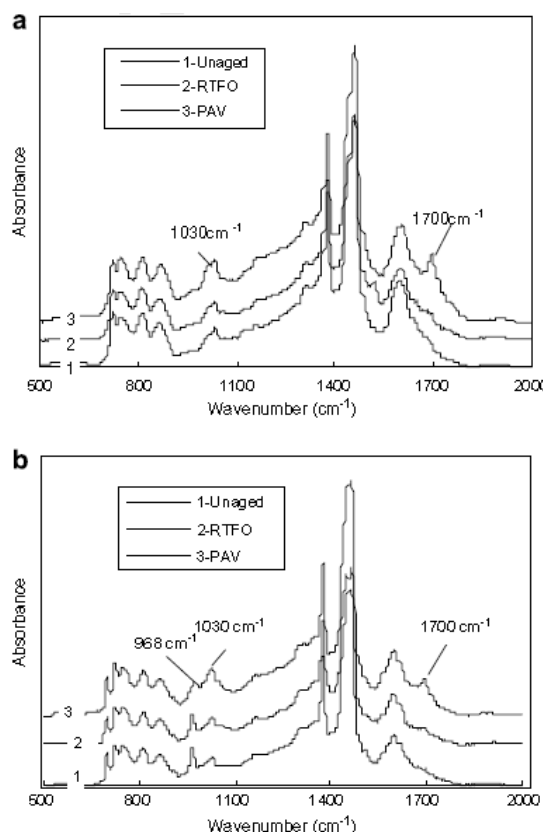


Figure 5.2.5 FTIR spectrum of bitumen before and after ageing: (a) base bitumen; (b) SBS modified bitumen, at the mode of absorbance (Wu, Pang et al. 2009)

In this chapter, FTIR spectra of base and modified bitumens were recorded using a Thermo Nicolet Model Nexus FTIR – Raman spectrophotometer. The version of analysis software was Omnic 6.2. The specimen preparation followed the experience of Wu, Pang et al. (2009). 5 % bitumen by weight was dissolved in carbon disulfide. Then, a certain amount of solution was dropped onto the KBr stage and dried by the infrared lamp to form a film specimen.

5.2.2.3 Summary

Accelerating ageing in the laboratory is based on some mechanisms in terms of increasing the temperature, the size of surface area exposed to air or oxygen, environmental pressure, and decreasing the specimen's film thickness. Therefore, the ageing analysis should be performed using the different artificial mechanism as produced by the different types of the equipments.

Due to the complex ageing behaviour of bitumen, a unique ageing indicator is not enough in some cases to characterize the ageing behaviour. Ageing analyses of modified bitumen should also take into account the effect of ageing on the modifier itself, e.g. what is the effect of ageing on the polymer in the case of polymer modified bitumen.

5.3 Ageing results and analyses

5.3.1 Empirical rheological properties

Tables 5.3.1 and 5.3.2 give the penetration and softening point values of all bitumens before and after ageing, which were performed according to European standards, EN 1426 and EN 1427, respectively. The addition of Mts at the same weight content of 4% changes these values of the base bitumens to different degrees. In general, the organio Mts, especially Mt2, can strongly influence these rheological properties. The only inorganic Mt0 contributed a little bit to the change of empirical rheological properties of base B. This may be due to a weak interaction with the matrix. In the previous chapter, it has been shown that CT scanning images also indicated that the Mt0 existed in the bitumen as normal filler particles at micrometer level. It was speculated that 4 weight % of filler hardly changes the properties of bitumen. The change of these properties also depends on the type of base bitumen. For example, the same amount of Mt2 made a decrease of 13% and 14% in the penetration of base B and C, larger than that of 9.5% in the case of harder base bitumen A.

Table 5.3.1 Penetrations at 25°C (0.1mm) before and after short and long terms ageing

Bitumens	Test values									Mean value			Standard deviation		
	Fresh ^a			RTFOT ^b			PAV ^c			Fresh	RTFOT	PAV	Fresh	RTFOT	PAV
A (40/60)	41	42	42	27	26	28	19	16	17	42	27	17	0,6	1,0	1,6
A+4%Mt1	39	40	38	28	26	30	15	19	17	39	28	17	1,0	2,0	2,0
A+4%Mt2	38	38	37	27	27	26	15	16	13	38	27	15	0,5	0,5	1,5
B (70/100)	73	77	80	49	47	46	29	26	28	77	47	28	3,5	1,5	1,5
B+4%Mt1	70	67	72	52	54	51	29	31	28	70	52	29	2,5	1,6	1,5
B+4%Mt2	66	67	69	44	46	45	26	27	29	67	45	27	1,6	1,0	1,6
B+4%Mt0	71	73	75	46	48	50	30	29	29	73	48	29	2,0	2,0	0,8
C (160/220)	174	171	169	97	100	102	46	47	46	171	100	46	2,5	2,5	0,8
C+4%Mt1	160	163	158	102	103	100	43	45	42	160	102	43	2,6	1,5	1,5
C+4%Mt2	146	148	147	89	94	91	44	45	45	147	91	45	1,0	2,5	0,5

^a means properties of the virgin bitumen; ^b means properties of the bitumen after aging in the rolling thin film oven test (EN 12607-1); ^c means properties of the bitumen after pressure ageing vessel test (EN 14769 at 100 °C).

Table 5.3.2 Softening points (°C) before and after short and long terms ageing

Bitumens	Test values						Mean values		
	Fresh		RTFOT		PAV		Fresh	RTFOT	PAV
A (40/60)	49,5	50,4	55,1	55,6	61,9	61,4	50,0	55,4	61,6
A+4%Mt1	51,4	51,1	56,0	56,1	62,4	62,1	51,2	56,0	62,2
A+4%Mt2	52,3	52,8	57,5	57,3	64,2	64,3	52,6	57,4	64,2
B (70/100)	45,9	46,2	51,3	51,0	57,1	57,3	46,0	51,2	57,2
B+4%Mt1	46,1	46,6	50,4	50,0	57,2	57,5	46,4	50,2	57,4
B+4%Mt2	48,0	48,1	52,7	52,4	58,7	58,9	48,0	52,6	58,8
B+4%Mt0	46,1	46,3	51,3	51,6	57,0	57,4	46,2	51,4	57,2
C (160/220)	38,3	38,4	44,1	44,3	52,3	51,8	38,4	44,2	52,0
C+4%Mt1	40,3	41,2	45,1	45,4	53,6	53,2	40,8	45,2	53,4
C+4%Mt2	42,3	42,8	47,4	47,7	55,3	55,6	42,6	47,6	55,4

Ageing properties of bitumens are normally evaluated by measuring rheological properties (e.g. penetration, softening point and viscosity) before and after artificial ageing in the laboratory. Retained penetration and increment in softening point are very important indices to characterize the ageing properties of bitumen. Higher retained penetration and lower increment in softening point means better ageing resistance.

Figure 5.3.1a shows the retained penetration values for the base and modified bitumens after RTFOT ageing. For the three base bitumens, this value decreased with increasing penetration grade, which means that base bitumens themselves show different ageing resistance. They also show a different increase in retained penetration due to the addition of organo Mt1 an Mt2. There was an increase between 6% and 7% for base A, between 7% and 13% for base B, and between 3% and 5% for base C. This means that organo Mts improves the short term ageing resistance for base bitumens, especially for base B. In comparison, Mt1 leads to a better improvement in ageing resistance than Mt2. Due to inorganic characteristic, Mt0 contributed less to the ageing resistance for base B.

After further ageing by PAV, the retained penetration value for all bitumens decreased to a lower level shown in Figure 5.3.1b. Although the modified bitumens still show higher values than that of the base ones, the difference between them is rather small. This indicates that the Mt modification gives a less effective improvement in terms of PAV results than in RTFOT results.

As shown in Figure 5.3.2a, RTFOT ageing causes an increase in softening point. In general, a lower increment in softening point results in a higher retained

penetration. After the RTFOT ageing, PAV ageing resulted in a significant increase in softening point for all bitumens (see Figure 5.3.2b). Meanwhile, the softening point values of the base and modified bitumens became more comparable. Therefore, it is hard to distinguish the ageing properties of these bitumens in terms of increment in softening point after PAV ageing.

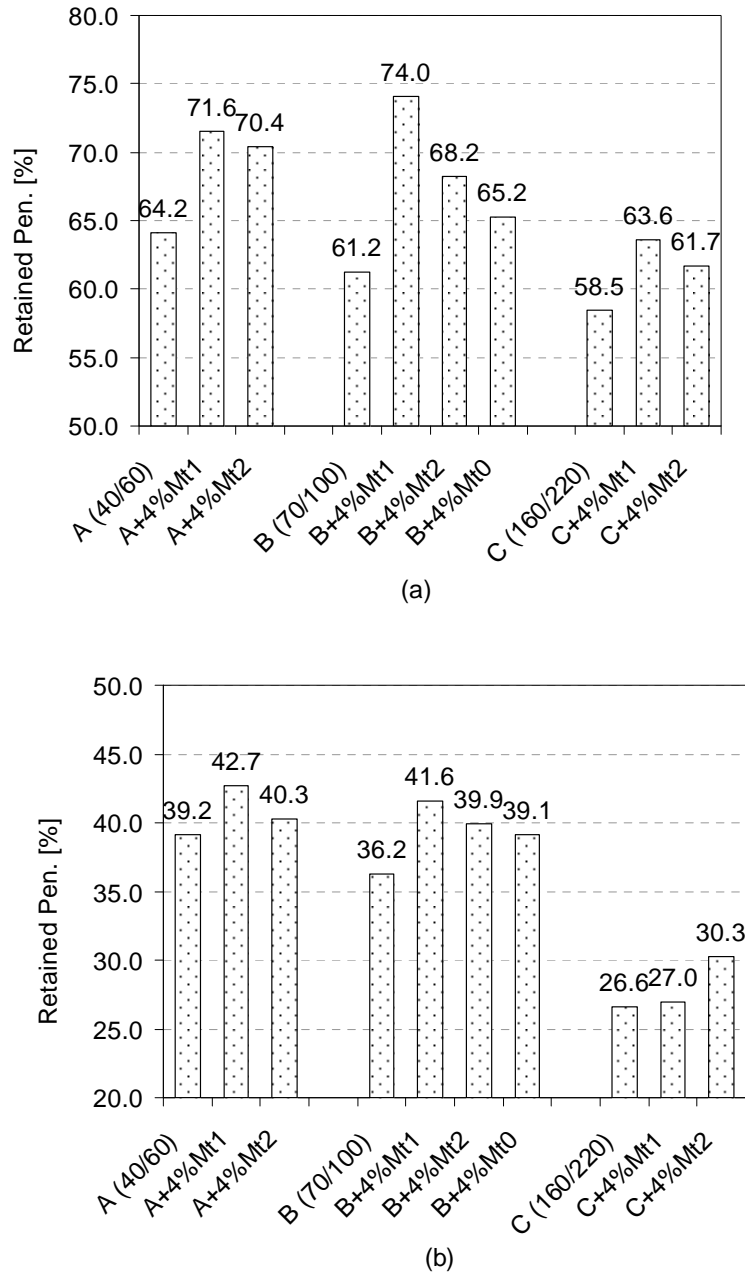


Figure 5.3.1 Retained penetration for all bitumens after (a) RTFOT ageing and (b) PAV ageing, respectively

During the RTFOT procedure, the viscosity of the material has to be taken into account because it will influence the ageing efficiency. For example, a material with a high viscosity will flow slowly in the rolling bottle under the effect of gravity whereas the one with low viscosity will flow quickly. Different flow speed could result in a variation of exposure of fresh material to air. In other words, the increase of viscosity could decrease the ageing effect on the specimen. Therefore, it becomes complicated to evaluate the ageing resistance of materials with different viscosities using the RTFOT method.

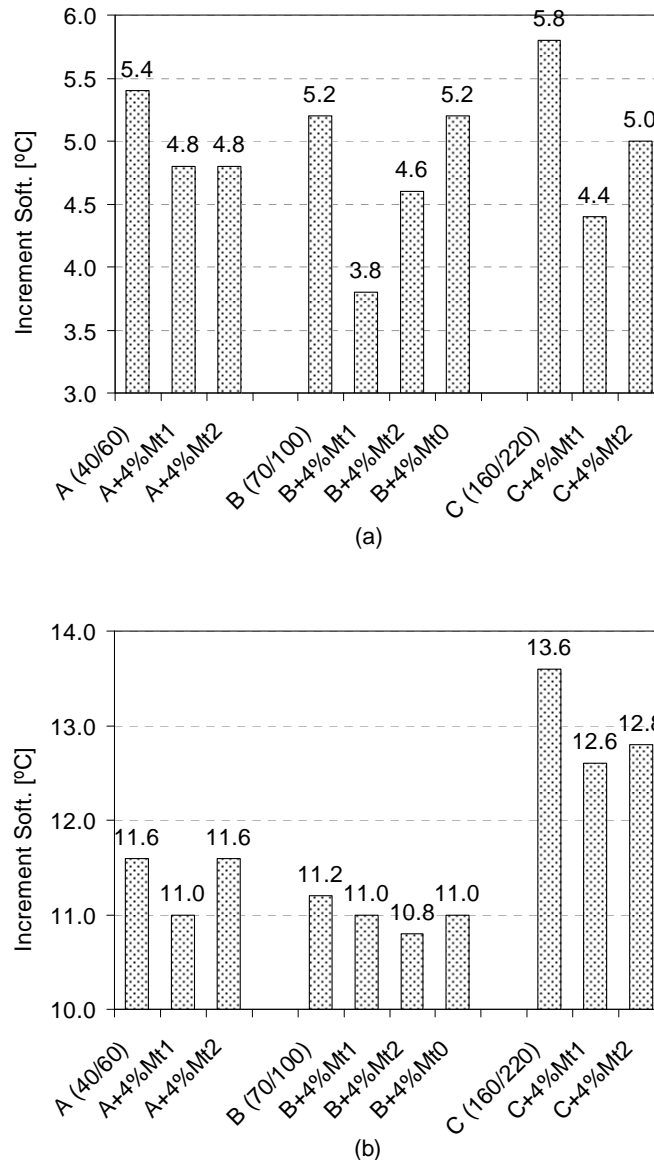


Figure 5.3.2 Increment in softening point for all bitumens after (a) RTFOT ageing and (b) PAV ageing, respectively

Figure 5.3.3 shows the retained penetration versus the viscosity values for the base and modified bitumens. The viscosity at 150 °C which was obtained based on EN 13702-1 is used in this figure. Although it should be more reasonable to adopt the viscosity at the testing temperature of 163 °C, it was regarded that the viscosities at these two temperatures were very close and the difference between them would not influence the trend of test results.

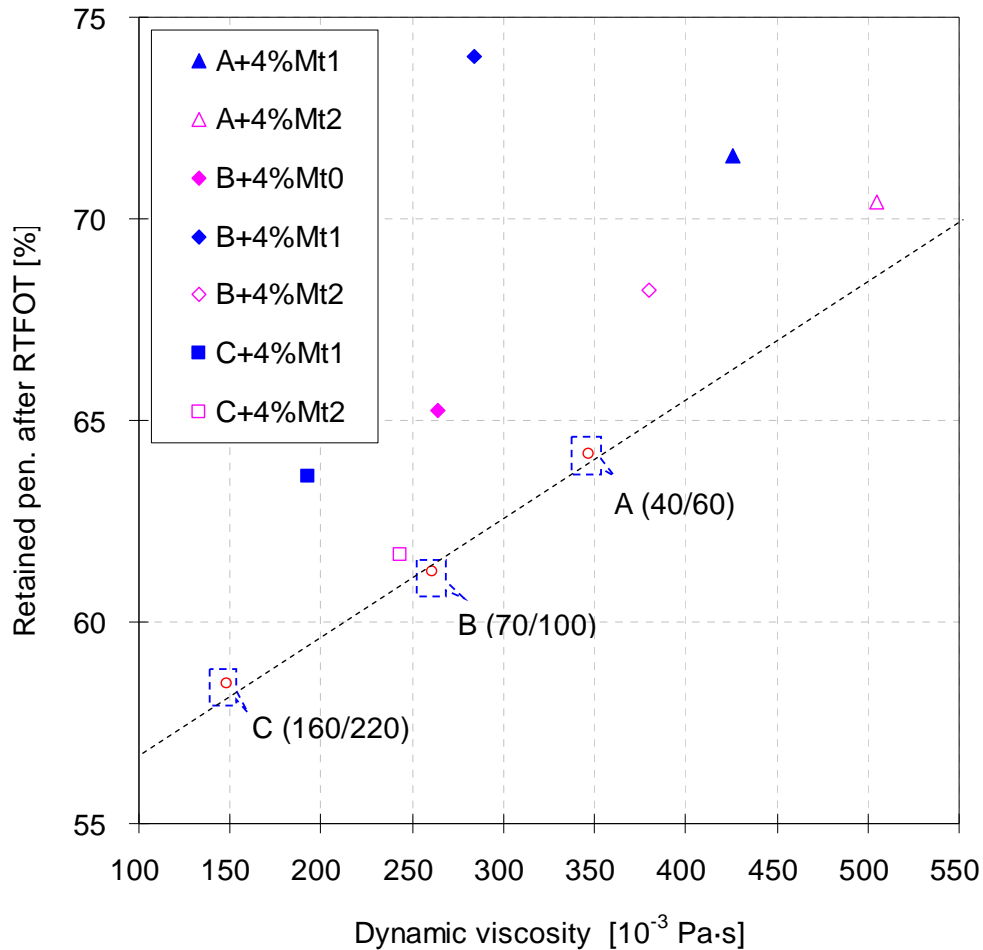


Figure 5.3.3 Retained penetration versus dynamic viscosity at 150 °C for base and modified bitumens

For base bitumens, soft C shows a low retained penetration, hard A has a high retained penetration, and B is just in the middle. The relationship between retained penetration and viscosity at 150 °C shows a linear trend. This proves that the viscosity of bitumen can influence the ageing effect of RTFOT.

With respect to the modified bitumens, their retained penetration increases with increasing viscosity. However, these data points in this figure were not on the trend line of base bitumens; they are located above this line. This means that the

improvement of ageing resistance was not only due to the increase of viscosity, but also due to the enhancement of Mt particles in the ageing behaviour of bitumen. Especially, Mt1 contributed a little to the change of the viscosity of base B, but a relatively high increase in its retained penetration.

5.3.2 Fundamental rheological properties

Although the measurement of empirical rheological properties did reflect the ageing properties of base and modified bitumens, it was not possible to apply a certain factor in comprehensively characterizing the ageing behaviour. A fundamental method was recommended in which the ageing was characterized by the ageing index (AI) defined as:

$$AI = \frac{|G_{aged}^*|}{|G_{fresh}^*|} \quad 5.3.1$$

where,

$|G_{fresh}^*|$ and $|G_{aged}^*|$ = the complex modulus of the bitumen before and after artificial ageing, respectively.

Figures 5.3.4 and 5.3.5 show the AI curves of base A and B as a function of temperature at four frequencies after RTFOT ageing and PAV ageing, respectively. At a high frequency, such as 100 rad/s or 10 rad/s, the AI values for both base bitumens increased with increasing test temperature. After 40 °C, it gradually reached a plateau at which the AI became almost stable. With respect to a low frequency, such as 1 rad/s or 0.1 rad/s, there was a peak on the curve between 20 °C and 40 °C, which was more obvious at 0.1 rad/s. The AI values at different frequencies became closer at the extreme temperatures of -10 °C and 60 °C. This is because bitumen at these extreme temperatures almost reached its glassy or fluid state which reduces the sensitivity of the ageing index on the temperature and frequency. The change in trend of these curves indicates that the AI of the base bitumens A and B is more sensitive at a low frequency and at non-extreme temperatures. Therefore, the frequency of 0.1 rad/s was adopted to characterize the ageing properties of modified bitumens.

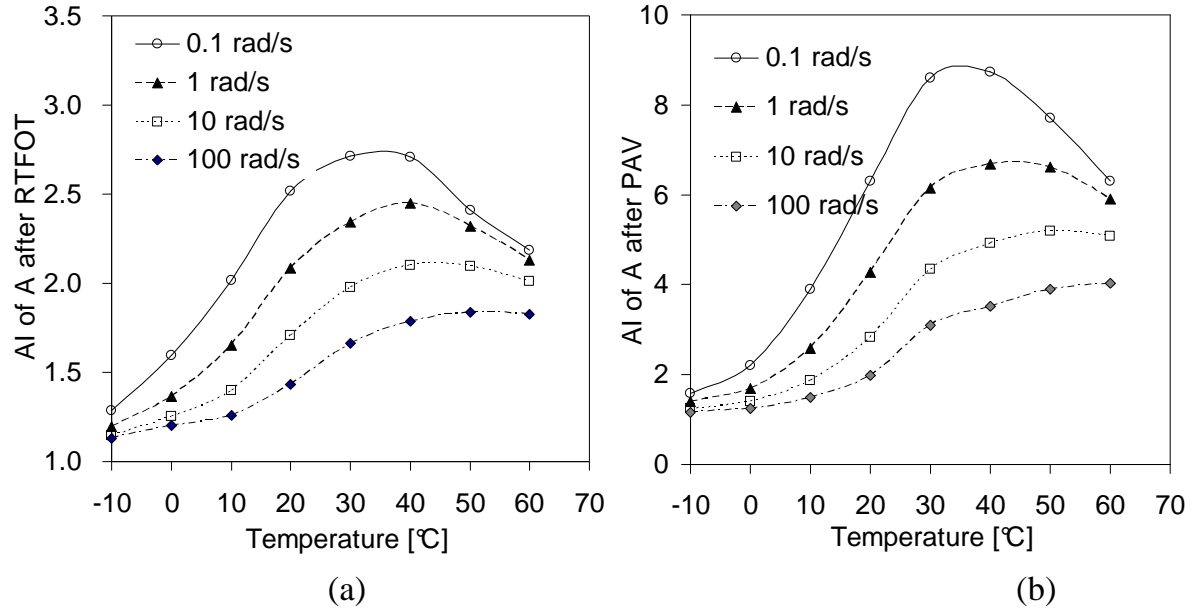


Figure 5.3.4 Ageing indices for base A as a function of temperature at four frequencies after (a) RTFOT and (b) PAV ageing, respectively

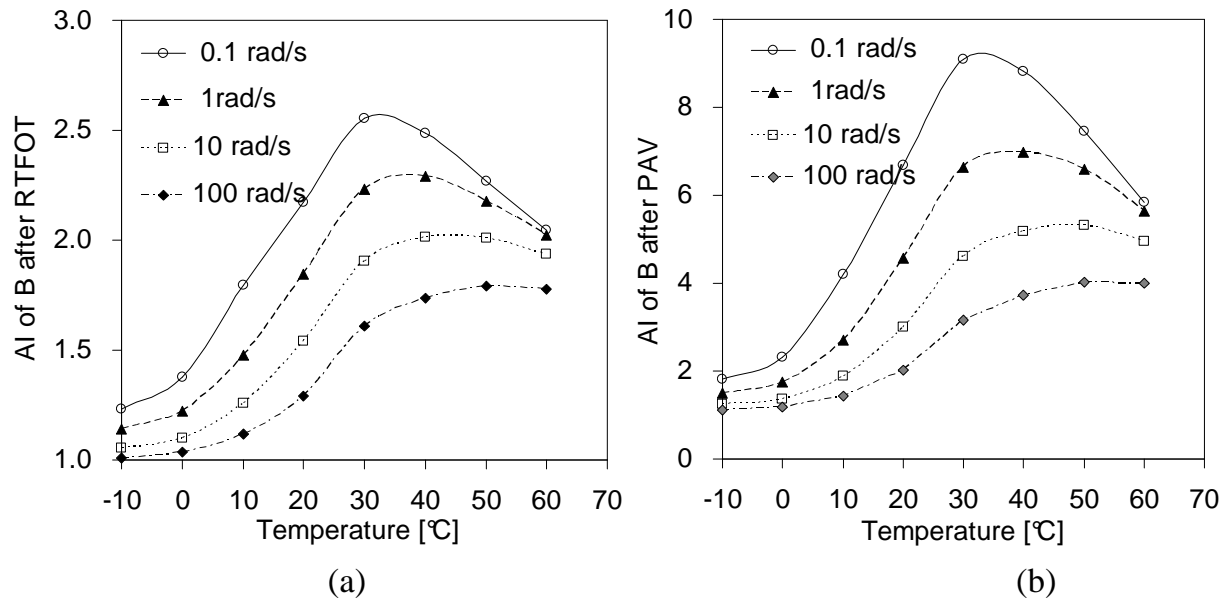


Figure 5.3.5 Ageing indices for base B as a function of temperature at four frequencies after (a) RTFOT and (b) PAV ageing, respectively. Original data are given in Table 1 of Appendix B

As shown in Figures 5.3.6a and b, all *AI* curves of the base and corresponding modified bitumens show a similar trend. A high *AI* value means a high degree of bitumen ageing. The curve of base A was located at the top of the clusters in Figure 5.3.6a and was followed by the curves of A+4%Mt2 and A+4%Mt1, respectively. This implies that base A has a relatively poor ageing resistance and

the addition of Mts could change this behaviour. In comparison, Mt1 gave more improvement of the ageing behaviour of base A more than Mt2.

As indicated in Figure 5.3.6b, the curve of B+4%Mt0 is very close to that of the base. This indicates comparable ageing properties between them. Generally, the curves of B+4%Mt1 and B+4%Mt2 were located at the bottom of the graph, which implies improved ageing behaviour. However, it is difficult to compare the behaviour of B+4%Mt1 with B+4%Mt2 because their curves crossed between 20 °C and 30 °C. This may be due to different temperature susceptibility of the modified bitumens.

As shown in Figures 5.3.7a and b, the curves for all modified bitumens after PAV ageing became closer to those of base A and B. This implies a less effective improvement in the long term ageing resistance, which was also concluded from the empirical rheological properties discussed in the previous section. The reason for this could be because the oxygen under high pressure of 2.1 MPa and at the temperature of 100 °C weakens the barrier effect of Mt and it becomes easier for the oxygen to penetrate the bitumen film.

The improvement of the short term ageing behaviour of the modified bitumen could be due to the high surface area of Mt and consequently its barrier property. This property not only hinders the penetration of the oxygen molecules, but also increases their average path length (Osman, Mittal et al. 2007). This interpretation is illustrated in Figure 5.3.8. For bituminous materials, another reason could be that the volatilization of the oily components decreases due to this barrier property. Although less effective ageing improvement was observed from the PAV results, it is believed that the long term ageing behaviour can be enhanced in the field because the temperature and the air pressure are low, compared to the test conditions. The function of Mt could work well during the service life due to its stable physicochemical properties.

Original data of the complex modulus (G^*) of base and modified bitumens before and after ageing are given in Tables 1 and 2 of Appendix B.

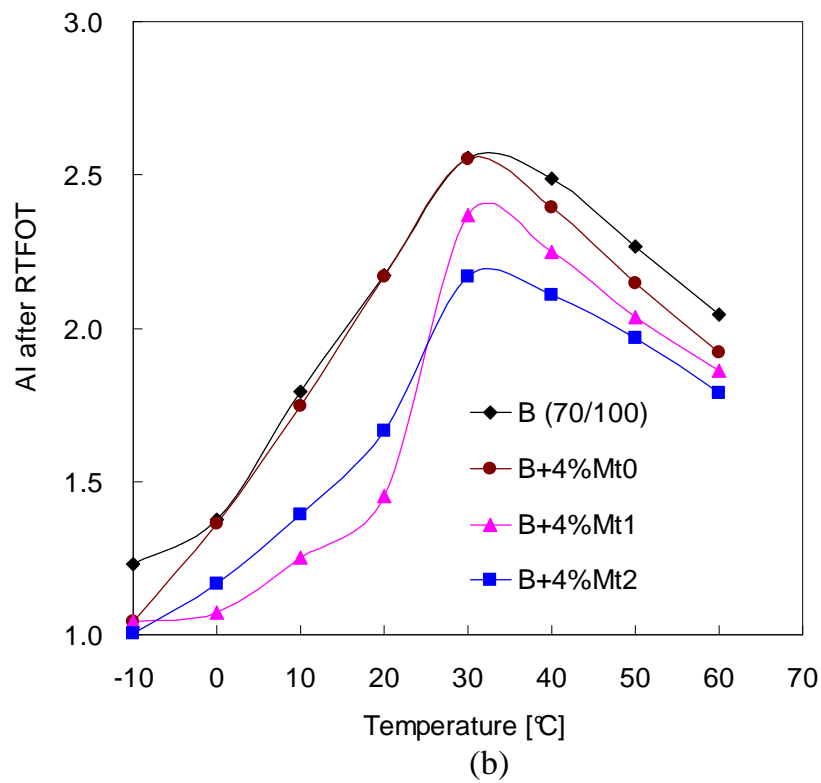
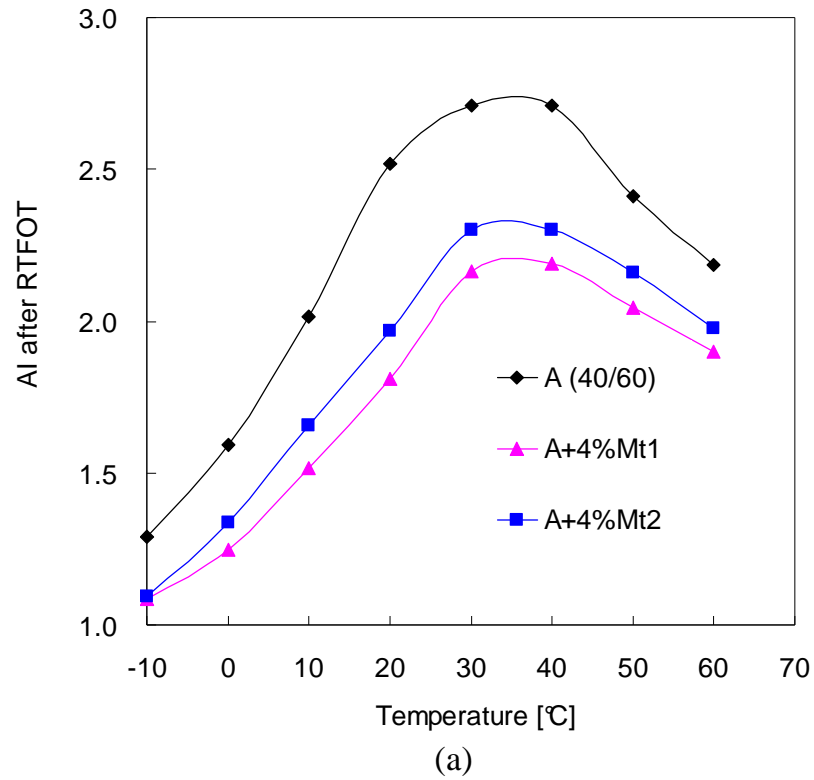


Figure 5.3.6 RTFOT ageing curves for (a) base A and its modified bitumens and (b) base B and its modified bitumens

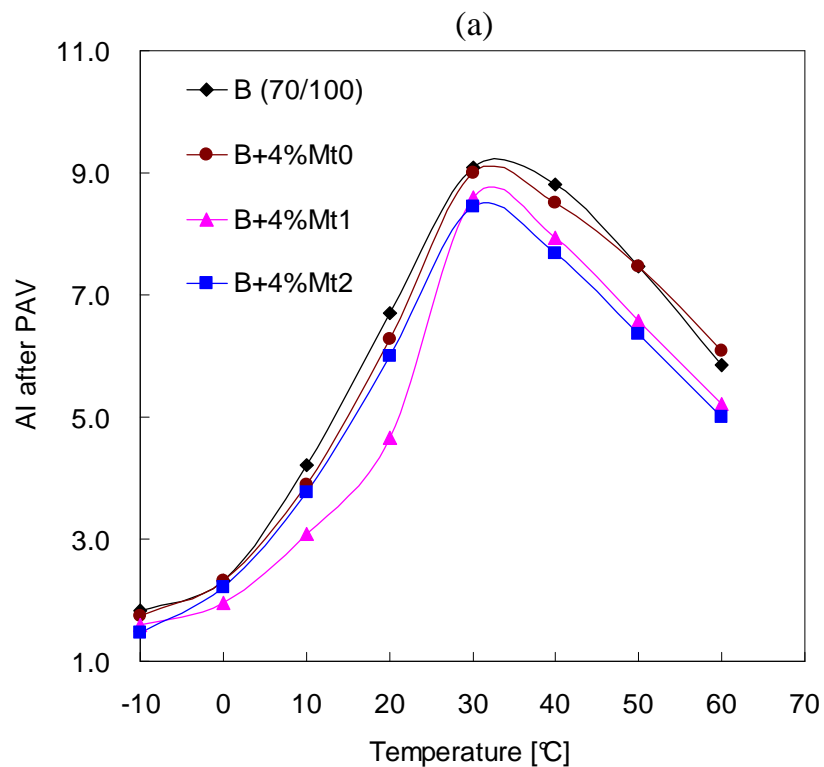
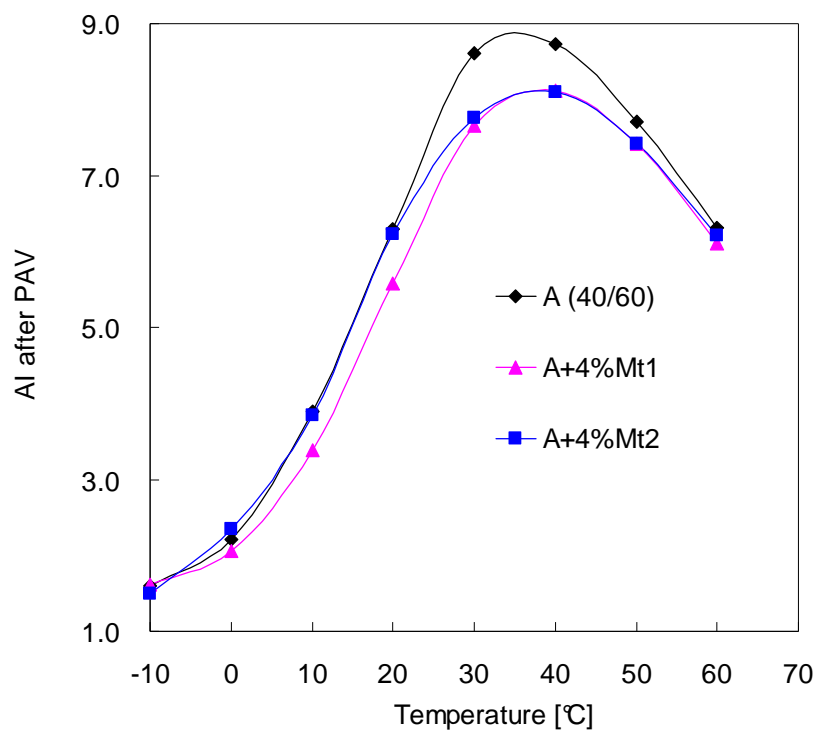


Figure 5.3.7 PAV ageing curves for (a) base A and its modified bitumens and (b) base B and its modified bitumens

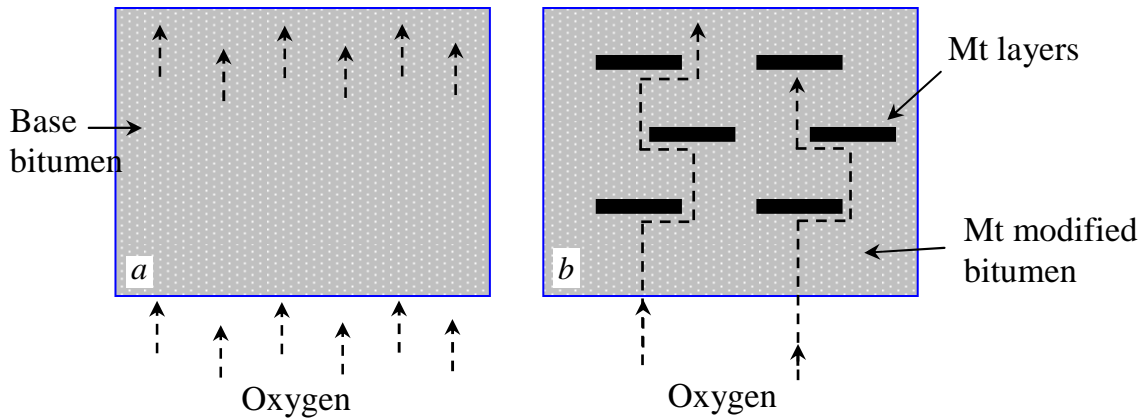


Figure 5.3.8 Schematic of the penetration of oxygen in (a) the base and (b) Mt modified bitumen

As observed from the ageing curves in this section, the AI value of base and modified bitumens is more sensitivity at a temperature range between 20 °C and 40 °C. The ageing values at this range are given in Table 5.3.3. To build a relationship with the retained penetration at the same temperature, a median AI value at 25 °C was obtained based on the values at 20 °C and 30 °C. As shown in Figure 5.3.9, there is a linear relationship between the two evaluation methods for RTFOT and PAV, respectively. It is logical that the trendlines have a negative slope because a low AI value and a high retained penetration both mean good ageing resistance. As observed, the trendline for the PAV was steeper than that for the RTFOT. It was shown that the PAV ageing reduced the bitumen's sensitivity to the penetration. Therefore, it is more suitable to characterize ageing after PAV with the AI (the ratio of $|G_{aged}^*|/|G_{fresh}^*|$) instead of retained penetration.

Table 5.3.3 AI values (the ratio of $|G_{aged}^*|/|G_{fresh}^*|$) at key temperatures after RTFOT and PAV test

Bitumen	AI after RTFOT			AI after PAV		
	at 20°C	at 30°C	at 40°C	at 20°C	at 30°C	at 40°C
A (40/60)	2.5	2.7	2.7	6.3	8.6	8.7
A+4%Mt1	1.8	2.2	2.2	5.6	7.7	8.1
A+4%Mt2	2.0	2.3	2.3	6.2	7.8	8.1
B (70/100)	2.2	2.6	2.5	6.7	9.1	8.8
B+4%Mt0	2.2	2.6	2.4	6.3	9.0	8.5
B+4%Mt1	1.5	2.4	2.3	4.7	8.6	7.9
B+4%Mt2	1.7	2.2	2.1	6.0	8.5	7.7

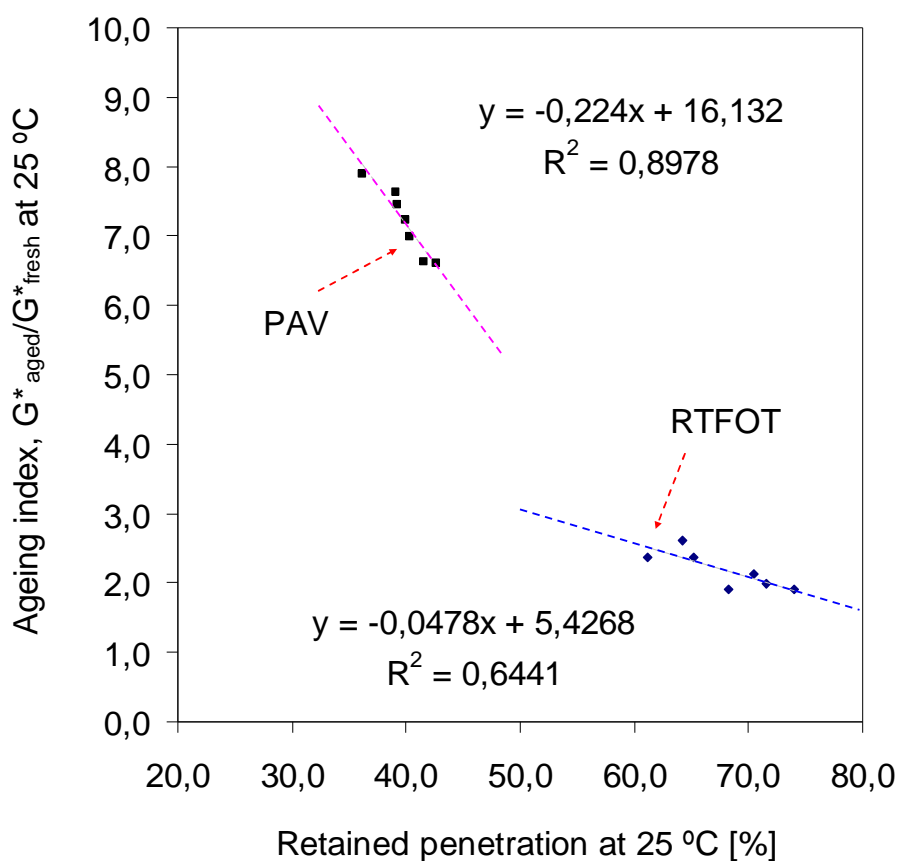


Figure 5.3.9 Relationship between ageing index (the ratio of $|G^*_{aged}|/|G^*_{fresh}|$) and retained penetration at 25 °C after RTFOT and PAV ageing, respectively

5.3.3 FTIR method

FTIR was used to evaluate the ageing behaviour of Mt modified bitumen. First, the FTIR tests on two pure Mts, inorganic Mt0 and organo Mt2 were performed; their full spectra ranging from 4000 cm^{-1} to 600 cm^{-1} are illustrated in Figure 5.3.10. For the inorganic Mt0, the asymmetric stretching vibration and the symmetric stretching vibration of the hydroxyl ($-\text{OH}$) groups are observed at 3608 cm^{-1} and 3403 cm^{-1} , respectively; in-plane bending vibration of the $-\text{OH}$ groups is characterized at 1627 cm^{-1} ; The broad band with the maximum at 980 cm^{-1} and the small peak appearing at 909 cm^{-1} belong to out-plane and in-plane stretching vibrations of Si-O bonds of the tetrahedral silica layers; the peaks at 791 and 615 cm^{-1} imply the Si-O and Al-O bending vibrations of the octahedral and tetrahedral silica-alumina layers (Sarier, Onder et al.; Onal and SarIkaya 2008). Due to the modification, Mt2 has more characteristic peaks: the asymmetric and symmetric stretching vibrations of the $-\text{CH}_3$, $-\text{CH}_2$ and $-\text{CH}$ groups are observed at 2918 and 2848 cm^{-1} , respectively; the peak of scissoring vibrations of $-\text{CH}_2$ is revealed at 1464 cm^{-1} ; some distinctive peaks are also observed at 743 cm^{-1} and 651 cm^{-1} ,

indicating the presence of the surfactant. Compared with Mt0, a slight shift of some local peaks on the spectra of Mt2 could take place due to the modification.

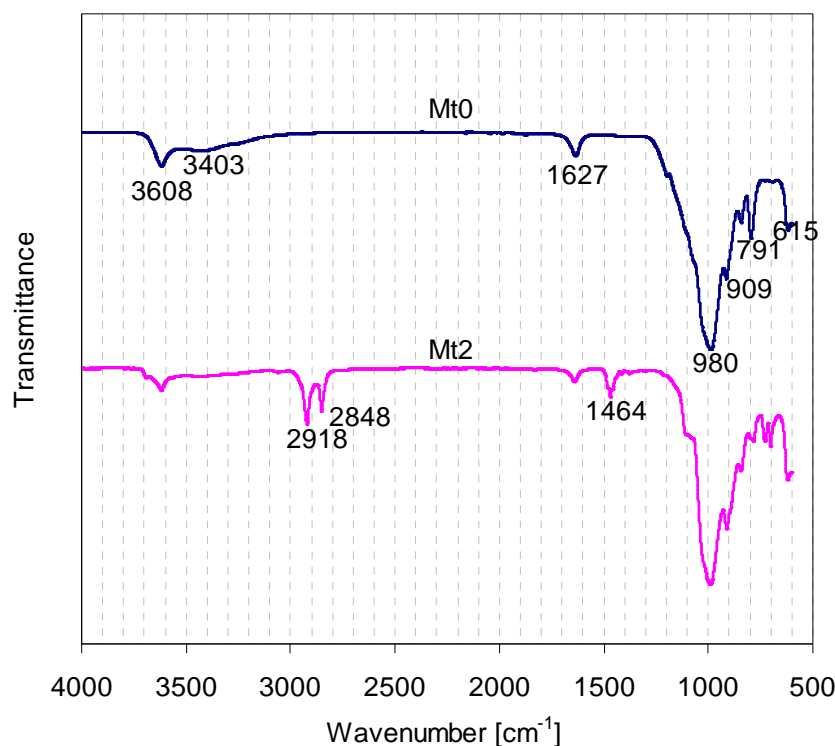


Figure 5.3.10 Full spectra for two pure Mts, inorganic Mt0 and organo Mt2 at the range from 4000 cm^{-1} to 600 cm^{-1}

FTIR is also adopted by many researchers to observe the evolution of chemical structures of bitumen as a result of ageing (Lamontagne, Dumas et al. 2001; Wu, Pang et al. 2009). According to previous researchers' experience, two important functional groups on the base B are characterized in the FTIR spectra shown in Figure 5.3.11. One is the carbonyl group at 1700 cm^{-1} and another is the sulphoxide group at 1030 cm^{-1} . Both of them belong to the stretching vibration and are formed due to the oxidation, dehydrogenation and crosslinking reactions taking place at the same time (Siddiqui and Ali 1999). The more severe the oxidation reaction is carried out, the more carbonyl and sulphoxide groups are formed. Therefore, the relative content of these two groups was used to represent the ageing degree of bitumen (Lamontagne, Dumas et al. 2001; Hagos 2008). As observed in Figure 5.3.11, the sulphoxide group is more sensitive to the ageing, and its band becomes broader as the ageing proceeds from RTFOT to PAV (see right part of this figure). With respect to the carbonyl group, it seems that the RTFOT ageing did not produce this group. However, the carbonyl group is

affected by PAV ageing. The sulphoxide group shows a clearer evolution of ageing than the carbonyl group.

In terms of B+4%Mt2, some characteristic peaks due to the addition of Mt2 are observed in Figure 5.3.12, such as the -OH groups at 3608 cm^{-1} . Especially, there are two peaks 1100 and 1040 cm^{-1} which should be strongly related to the Si-O peaks on Mt2 (see Figure 5.3.10). Unfortunately, the sulphoxide peak at 1030 cm^{-1} was covered by the peak at 1040 cm^{-1} which seriously interrupted the observation of the evolution of ageing. As was the case for the base bitumen, the carbonyl group was only observed on the PAV spectra of modified bitumen.

Due to the interference of the Si-O in the Mt with the characteristic peak of the bitumen, it was hard to characterize the evolution of modified bitumen before and after ageing. As mentioned above, the FTIR peak for the carbonyl group in the modified bitumen was not influenced by the addition of the Mt and only appeared after PAV ageing. Therefore, this functional group could be used to characterize the ageing evolution of the Mt modified bitumen by designing different ageing protocols which should at least generate a higher ageing effect than the standard RTFOT, e.g. simply increasing the test time of RTFOT.

Compared with the chemical method described in this section, the rheological methods discussed in the previous two sections are more useful to characterize the ageing properties of Mt modified bitumens.

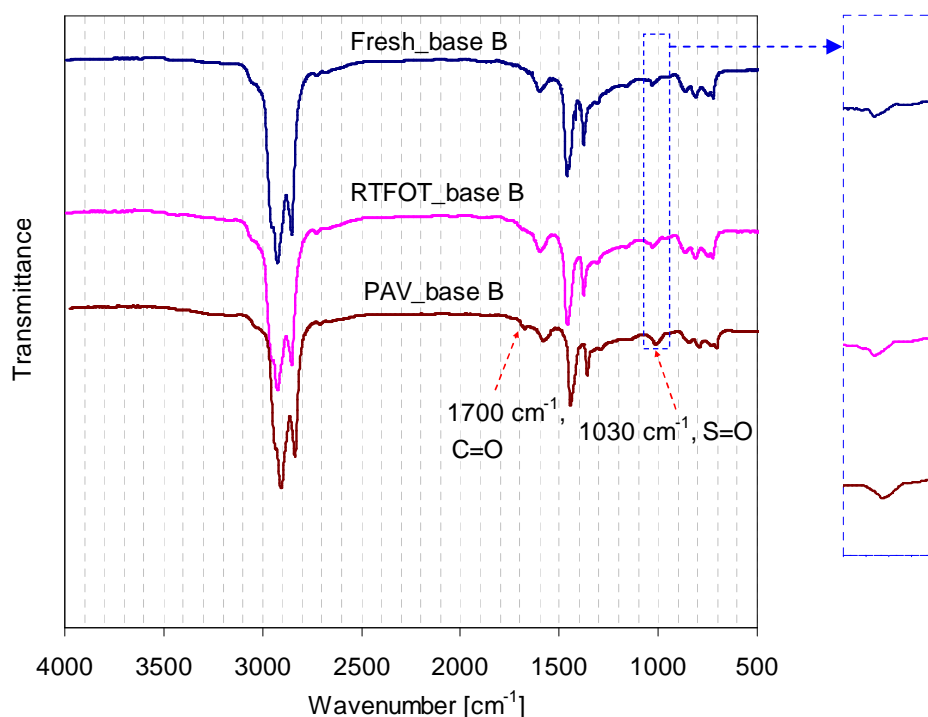


Figure 5.3.11 Ageing evolution of base B (70/100) bitumen characterized by the FTIR from fresh to the PAV aged state

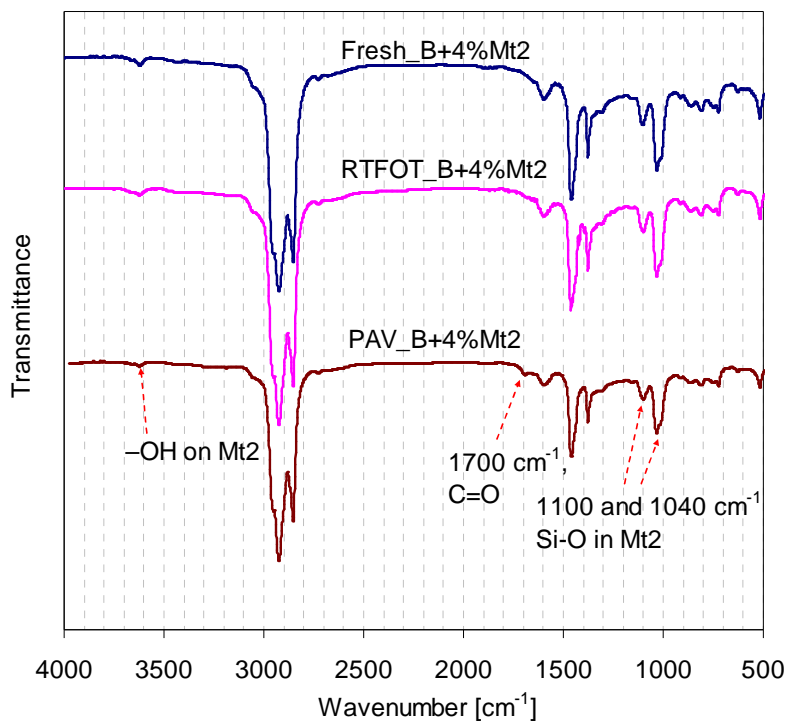


Figure 5.3.12 Ageing evolution of Mt2 modified bitumen characterized by the FTIR from fresh to the PAV aged state

5.3.4 Morphology change after ageing

XRD was performed to observe the change of Mts' morphology due to ageing. As shown in Figure 5.3.13, the XRD peak for B+4%Mt1 after RTFOT was the same as that for the fresh. However, it moved a little towards a higher 2θ value after PAV ageing. As given in Table 5.3.4, basal spacing d_{001} shrank from 4.24 to 4.11 nm, which means a decrease in d_{001} by 6.6% from RTFOT to PAV. With respect to B+4%Mt2 (Figure 5.3.14), its peak began to shift earlier after RTFOT, and its peak band after PAV even becomes smaller. As indicated in Table 5.3.4, d_{001} of B+4%Mt2 after RTFOT and PAV ageing reduced by 4.4% and by 9.4%, respectively.

Because the Mt is highly dispersed into the bitumen after high shear mixing, its surface area becomes very large. Therefore, the Mt layers would automatically accumulate to reduce the surface energy in the bitumen at a liquid state. Especially during the PAV test with a high air pressure (2.1 MPa), this activity takes place easier. Therefore, there is always a certain degree of shrinkage of d_{001} after PAV ageing. The accumulation of Mt would reduce its scale effect and negatively influence its contribution to ageing resistance of bitumen. This could be one of the reasons that we see a less effective improvement in the PAV ageing resistance of modified bitumen.

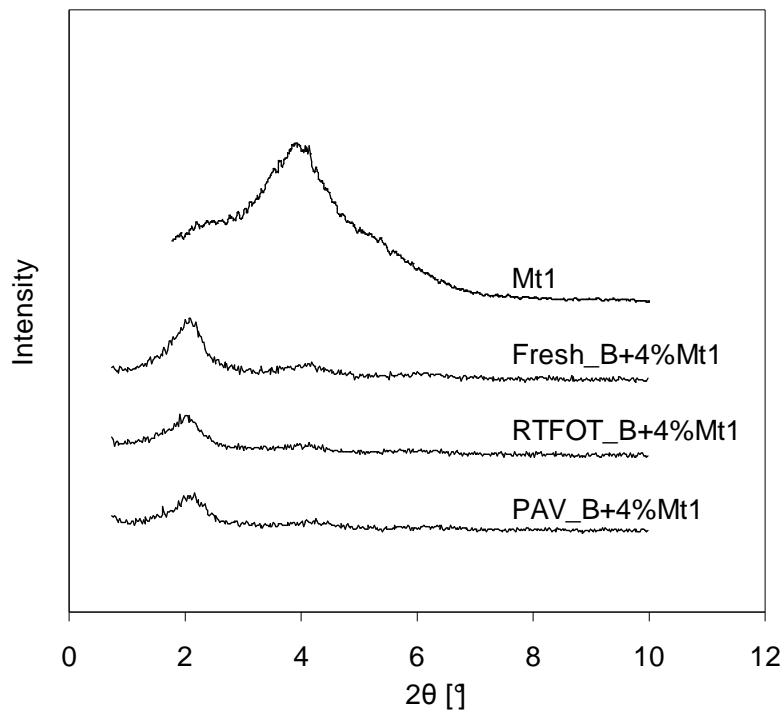


Figure 5.3.13 XRD curves for Mt1 and B+4%Mt1 before and after ageing

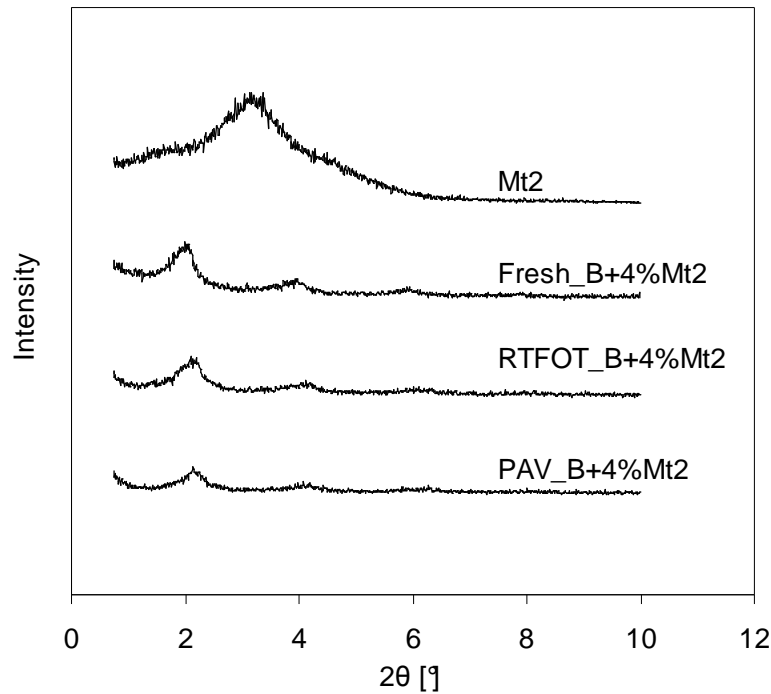


Figure 5.3.14 XRD curves for Mt2 and B+4% Mt2 before and after ageing

Table 5.3.4 Basal spacing (d_{001}) of Mt in the bitumen and its change due to ageing

Materials	2θ [°]	Basal spacing (d_{001})	*Increment Rate in d_{001}
		[nm]	[%]
Mt1	4.20	2.10	-
Fresh_B+4%Mt1	2.08	4.24	101.9
RTFOT_B+4%Mt1	2.08	4.24	101.9
PAV_B+4%Mt1	2.15	4.11	95.3
Mt2	3.14	2.81	-
Fresh_B+4%Mt2	2.02	4.37	55.4
RTFOT_B+4%Mt2	2.08	4.24	51.0
PAV_B+4%Mt2	2.15	4.11	46.0

*increment rate here is based on d_{001} of the pure Mt clay

5.4 Summary and conclusions

In this chapter, RTFOT and PAV methods were adopted to simulate the short term and long term ageing of base and Mt modified bitumens. Empirical rheological tests (i.e. penetration and softening point) and DSR test were performed to characterize the ageing properties. The results show that organo Mts improve the short term ageing resistance of base bitumen. The barrier properties of Mt particles hindering the penetration of oxygen is the main reason for this improvement. Meanwhile, the reduction of volatilization of the oily components of bitumen due

to these barrier properties could be another reason. Less effective ageing improvement was observed after PAV results. This could be because the oxygen under a high pressure of 2.1 MPa and at a temperature of 100 °C weakens the barrier effect of Mt and it becomes easier for the oxygen to penetrate the bitumen film. A certain degree of shrinkage of basal spacing under PAV conditions is another reason. It is believed that the long term ageing behaviour of bitumen can be enhanced in the field during the service life due to barrier function and stable physicochemical properties of Mt.

Besides rheological tests, FTIR tests were performed to evaluate the ageing effect on the chemical change of modified bitumens. Since the presence of Si-O on the Mt results in a peak on the FTIR spectra of bitumen which is very close to the sulfoxide peak, it is very difficult to use the sulfoxide peaks as an ageing indication. Although the carbonyl peak on the FTIR spectra was not influenced by the addition of the Mt, it only appeared after PAV ageing. In comparison, rheological methods such as DSR method are more effective to characterize the ageing properties of Mt modified bitumens.

Appendix BTable B1 Complex modulus, G^* of base A (40/60) and B (70/100) before and after ageing at different temperatures and frequencies

Tem. [°C]	Fre. [rad/s]	G^* [Pa] for base A			G^* [Pa] for base B		
		Fresh	RTFOT	PAV	Fresh	RTFOT	PAV
-10	0,1	89880000	115840485	143109903	53200000	65492424	97130303
	1	142400000	170609727	201015421	118200000	134673868	176270383
	10	233700000	267900000	290700000	208300000	219964800	261624800
	100	317200000	358471375	369084015	306900000	309580349	344424891
0	0,1	13800000	21984828	30360000	9812000	13510105	22783991
	1	39140000	53525585	65856086	33200000	40564364	57828364
	10	93720000	117386667	130640000	82110000	90365625	112678125
	100	177500000	213377660	220930851	159800000	165946154	188482051
10	0,1	1290000	2601148	5026066	901900	1618534	3796938
	1	6600000	10883392	17024735	4565000	6749539	12343133
	10	23140000	32411582	43163502	17650000	22204839	33117473
	100	69330000	87213088	103070013	50850000	56890691	72848936
20	0,1	106000	266755	667589	50860	110565	340383
	1	716300	1493530	3061365	344300	634730	1569259
	10	3998000	6821984	11343532	2059000	3168306	6184981
	100	16560000	23738719	32956847	9626000	12410380	19490661
30	0,1	11330	30722	97503	6744	17237	61248
	1	89030	208368	548220	51450	114941	340915
	10	609700	1206000	2646500	372200	709459	1716678
	100	3297000	5484632	10212406	2203000	3546969	6941528
40	0,1	1432	3880	12492	924	2297	8146
	1	13370	32730	89419	7931	18175	55427
	10	105400	221670	517941	64000	129007	332225
	100	735300	1314563	2586375	463400	805433	1723958
50	0,1	214	516	1648	148	337	1108
	1	2181	5062	14403	1449	3155	9541
	10	19680	41244	101959	13060	26241	69523
	100	157600	289815	615592	107000	191489	431216
60	0,1	43	93	268	29	59	169
	1	431	917	2542	285	577	1607
	10	4066	8171	20626	2737	5296	13589
	100	36260	66109	146242	24300	43215	97200

Table B2 Complex modulus, G^* of base and modified bitumens before and after ageing at different temperatures and at a frequency of 0.1 rad/s

Bitumens	G^* [Pa]							
	-10 °C	0 °C	10 °C	20 °C	30 °C	40 °C	50 °C	60 °C
A (40/60)	Fresh	8,99E+07	1,38E+07	1,29E+06	1,06E+05	1,13E+04	1,43E+03	214 43
	RTFOT	1,16E+08	2,20E+07	2,60E+06	2,67E+05	3,07E+04	3,88E+03	516 93
	PAV	1,43E+08	3,04E+07	5,03E+06	6,68E+05	9,75E+04	1,25E+04	1648 268
A+4%Mt1	Fresh	1,04E+08	1,39E+07	1,65E+06	1,35E+05	1,01E+04	1,40E+03	230 47
	RTFOT	1,12E+08	1,73E+07	2,50E+06	2,44E+05	2,18E+04	3,07E+03	471 89
	PAV	1,66E+08	2,84E+07	5,60E+06	7,51E+05	7,72E+04	1,14E+04	1710 286
A+4%Mt2	Fresh	2,41E+08	1,62E+07	1,86E+06	1,54E+05	1,42E+04	2,01E+03	306 61
	RTFOT	2,63E+08	2,16E+07	3,08E+06	3,04E+05	3,27E+04	4,62E+03	659 121
	PAV	3,58E+08	3,79E+07	7,16E+06	9,58E+05	1,10E+05	1,63E+04	2266 378
B (70/100)	Fresh	5,32E+07	9,81E+06	9,02E+05	5,09E+04	6,74E+03	9,24E+02	148 29
	RTFOT	6,55E+07	1,35E+07	1,62E+06	1,11E+05	1,72E+04	2,30E+03	337 59
	PAV	9,71E+07	2,28E+07	3,80E+06	3,40E+05	6,12E+04	8,15E+03	1108 169
B+4%Mt0	Fresh	5,88E+07	1,13E+07	1,11E+06	5,09E+04	8,72E+03	1,05E+03	168 37
	RTFOT	6,12E+07	1,54E+07	1,95E+06	1,10E+05	2,23E+04	2,50E+03	362 71
	PAV	1,03E+08	2,61E+07	4,35E+06	3,19E+05	7,84E+04	8,89E+03	1258 225
B+4%Mt1	Fresh	5,01E+07	1,11E+07	1,21E+06	9,03E+04	9,87E+03	1,22E+03	197 42
	RTFOT	5,23E+07	1,19E+07	1,52E+06	1,31E+05	2,34E+04	2,74E+03	401 78
	PAV	7,97E+07	2,16E+07	3,75E+06	4,20E+05	8,49E+04	9,67E+03	1296 218
B+4%Mt2	Fresh	2,16E+08	1,37E+07	1,27E+06	9,03E+04	1,00E+04	1,48E+03	253 54
	RTFOT	2,17E+08	1,59E+07	1,76E+06	1,50E+05	2,17E+04	3,12E+03	498 97
	PAV	3,16E+08	3,02E+07	4,78E+06	5,42E+05	8,45E+04	1,14E+04	1604 270

5.5 Reference

- Anderson, D. A., D. W. Christensen, et al. (1994). Binder Characterization and Evaluation. Volume 3: Physical Characterization. SHRP-A-369.
- Bahia, H. U., W. P. Hislop, et al. (1998). "Classification of asphalt binders into simple and complex binders." Journal of the Association of Asphalt Paving Technologists 67: 1-24.
- Bell, C. A. and D. Sosnovske (1994). Aging: Binder Validation, National Research Council, Washington DC. Rep. No. SHRP-A-384.
- Bell, C. A., D. Sosnovske, et al. (1994). Aging: binder validation, Strategic Highway Research Program, National Research Council.
- Cortizo, M. S., D. O. Larsen, et al. (2004). "Effect of the thermal degradation of SBS copolymers during the ageing of modified asphalts." Polymer Degradation and Stability 86(2): 275-282.
- Domke, C. H., R. R. Davison, et al. (1999). "Effect of oxidation pressure on asphalt hardening susceptibility." Transportation Research Record: Journal of the Transportation Research Board 1661(-1): 114-121.
- Hagos, E. T. (2008). The effect of aging on binder properties of porous asphalt concrete. Delft University of Technology. PhD thesis.
- Isaccson, U., Lu, X (1999). "Laboratory investigation of polymer modified bitumen." Association of Asphalt Paving Technologists (AAPT) 68: 35-63.
- Kelemen, S. R., G. N. George, et al. (1990). "Direct determination and quantification of sulphur forms in heavy petroleum and coals:: 1. The X-ray photoelectron spectroscopy (XPS) approach." Fuel 69(8): 939-944.
- Lamontagne, J., P. Dumas, et al. (2001). "Comparison by Fourier transform infrared (FTIR) spectroscopy of different ageing techniques: application to road bitumens." Fuel 80(4): 483-488.
- Lu, X. and U. Isacsson (1998). "Chemical and rheological evaluation of ageing properties of SBS polymer modified bitumens." Fuel 77(9-10): 961-972.
- Lu, X., U. Isacsson, et al. (1999). "Rheological properties of SEBS, EVA and EBA polymer modified bitumens." Materials and Structures 32(2): 131-139.
- Morgen, P. and A. Mulder (1995). The Shell Bitumen Industrial Handbook Shell Bitumen Publications, London.
- Onal, M. and Y. Sarıkaya (2008). "Some physicochemical properties of methylammonium and ethylenediammonium smectites." Colloids and Surfaces A: Physicochemical and Engineering Aspects 312(1): 56-61.
- Osman, M. A., V. Mittal, et al. (2007). "Poly (propylene) Layered Silicate Nanocomposites: Gas Permeation Properties and Clay Exfoliation." Macromolecular Chemistry and Physics 208(1): 68-75.
- Ouyang, C., S. Wang, et al. (2006). "Improving the aging resistance of styrene-butadiene-styrene tri-block copolymer modified asphalt by addition of antioxidants." Polymer Degradation and Stability 91(4): 795-804.
- Parmeggiani, G. (2000). Nitrogen Rolling Thin Film Oven Test Laboratory Testing Proposals. Euroasphalt and Eurobitume Congress. Barcelona.

- Petersen, J. C. (1984). "Chemical composition of asphalt as related to asphalt durability: state of the art." Transportation Research Record(999).
- Petersen, J. C. and P. M. Harnsberger (1998). "Asphalt aging: Dual oxidation mechanism and its interrelationships with asphalt composition and oxidative age hardening." Transportation Research Record: Journal of the Transportation Research Board 1638(-1): 47-55.
- Roberts, F. L., P. S. Kandhal, et al. (1996). Hot Mix Asphalt Materials, Mixture Design, and Construction, National Asphalt Pavement Association Education Foundation. Lanham, MD.
- Sarier, N., E. Onder, et al. "The Modification of Na-Montmorillonite by Salts of Fatty Acids: An Easy Intercalation Process." Colloids and Surfaces A: Physicochemical and Engineering Aspects.
- Siddiqui, M. N. and M. F. Ali (1999). "Investigation of chemical transformations by NMR and GPC during the laboratory aging of Arabian asphalt." Fuel 78(12): 1407-1416.
- Wu, S., L. Pang, et al. (2009). "Influence of aging on the evolution of structure, morphology and rheology of base and SBS modified bitumen." Construction and building materials 23(2): 1005-1010.
- Zupanick, M., Baselice, V. (1997). "Characterizing Asphalt Volatility." Transportation Research Board, TRB 1586: 1-9.

6 RHEOLOGICAL PROPERTIES

6.1 Introduction

Rheology is the science dealing with the flow of matter, mainly liquids, and in some cases solids and soft solids as well (Morrison 2001). Rheological properties of bitumen significantly influence the performance of asphalt mixture during its manufacture, transportation, construction, and service life. Bitumen is a viscoelastic material, and it exhibits either elastic or viscous behaviour, or a combination of these, depending on the temperature and loading time (Lu, Isacsson et al. 1999). At a sufficient low temperature or high loading frequency, bitumen behaves as an elastic solid, and at a high temperature or low loading frequency, it can even become a Newtonian liquid which behaviour is independent of the shear rate. Between these two extremes, bitumen behaves as a viscoelastic material.

Dynamic viscoelastic properties generally refer to the responses of a material to periodically varying strains or stresses (Ferry 1980). Within the linear viscoelastic range, the relationship between strain and stress is linear, and uniformly influenced by frequency and temperature. The dynamic response of bitumen within this range is related to properties of asphalt pavements, such as deformation and cracking resistance.

Montmorillonite (Mt) modification may change the rheological properties of bitumen due to the Mt platelets reinforcement and Mt-bitumen interactions. The rheological effect of this modification can be described with a dynamic mechanical analysis. The major objectives of this chapter are to characterize the rheological behaviour of bitumens with modification of Mts, and investigate the effect of the Mt type, as well as the bitumen grade, on the viscoelastic properties of modified bitumens using a dynamic mechanical analysis.

6.2 Methods

6.2.1 Materials

The Base and modified bitumens involved in this research are given in Table 6.2.1.

Table 6.2.1 Codes of base and modified bitumens

Codes	Nanoclay type	Clay content [mass %]
Base A (40/60)	-	0
A+4%Mt1	Mt1	4
A+4%Mt2	Mt2	4
Base B (70/100)	-	0
B+4%Mt0	Mt0	4
B+4%Mt1	Mt1	4
B+8%Mt1	Mt1	8
B+12%Mt1	Mt1	12
B+4%Mt2	Mt2	4
B+6%Mt2	Mt2	6
B+8%Mt2	Mt2	8

6.2.2 Cone and plate rheometer

The cone and plate rheometer was used to measure the dynamic viscosity and shear rate dependency of the viscosity. These tests were done at the Wuhan University of Technology. An MCR 101 rheometer (see Figure 6.2.1) from Anton Paar Instruments was used for this purpose; its configuration with 50 μm gap between the cone and the plate is shown in Figure 6.2.2.



Figure 6.2.1 Image of MCR 101 rheometer from Anton Paar Instruments used to measure the dynamic viscosity and shear rate dependency of the viscosity

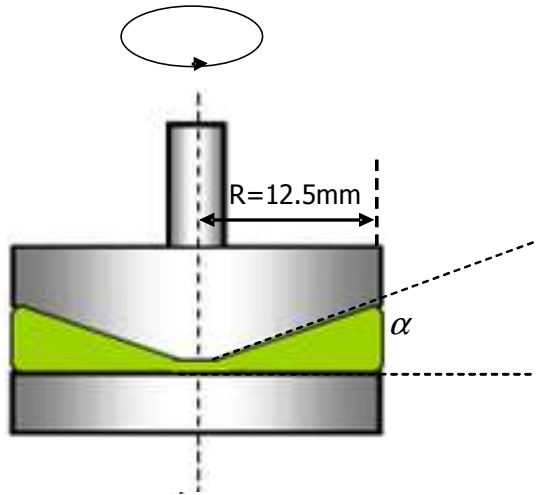


Figure 6.2.2 Configuration of cone and plate device in the rheometer

The shear stress and the shear rate in this method can be calculated from Equations 6.2.1 and 6.2.2.

$$\tau = \frac{3T}{2\pi R^3} \quad 6.2.1$$

$$\dot{\gamma} = \frac{\Omega}{\alpha} \quad 6.2.2$$

where,

T = the torque,

R = the radius of the cone,

$\dot{\gamma}$ = shear rate,

Ω = rotation speed of the cone spindle, and

α = cone angle, here 0.997° .

The viscosity is then calculated by

$$\eta = \frac{\tau}{\dot{\gamma}} = \frac{3\alpha T}{2\pi R^3 \Omega} \quad 6.2.3$$

In this study, the dynamic viscosity was measured according to EN 13702-1, and the following steps were taken:

(1) Input the diameter and angle of cone into the window of the software at the selected shear rate.

(2) Place the sample on the stage and press the selected cone onto the sample. Remove any surplus material of the sample and bring the system to the test temperature.

(3) Commence the first measurement at the lowest temperature:

Temperature: $60\text{ }^{\circ}\text{C} \pm 0.5\text{ }^{\circ}\text{C}$;

Shear rate: 0.05 s^{-1} .

Check the reading after a delay of 15 min when reaching the temperature, note the temperature, cone size, speed and reading.

(4) Repeat the test and calculate the result as an average of two tests. Replace the specimen and increase the temperature to the next test temperature. Commence the second measurement:

Temperature: $100\text{ }^{\circ}\text{C} \pm 0.5\text{ }^{\circ}\text{C}$;

Shear rate: 500 s^{-1} .

(5) Replace the specimen and increase the temperature to the next test temperature.

Commence the third measurement:

Temperature: $150\text{ }^{\circ}\text{C} \pm 1.0\text{ }^{\circ}\text{C}$;

Shear rate: 500 s^{-1} .

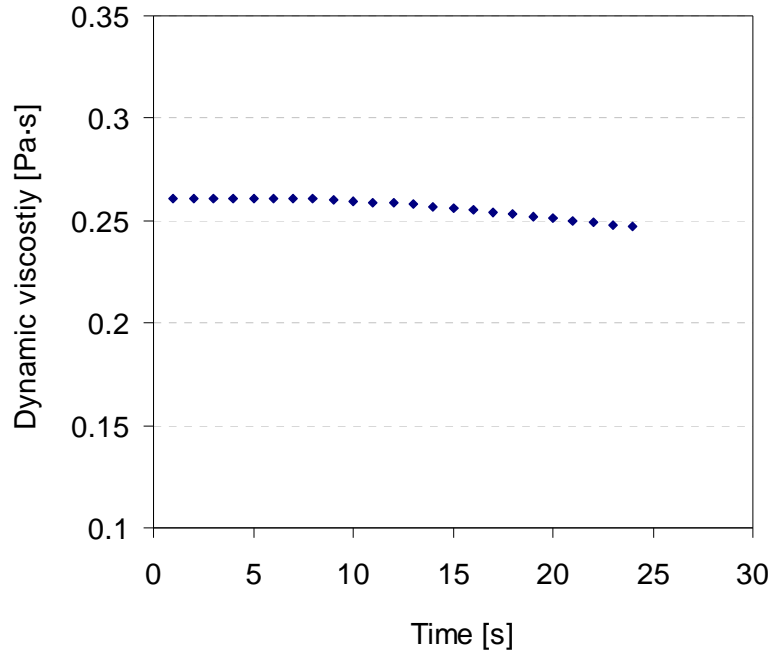


Figure 6.2.3 Example of the dynamic viscosity of B (70/100) at a shear rate of 500 s^{-1} and a temperature of 150°C .

Figure 6.2.3 gives an example of the dynamic viscosity of B (70/100) at a shear rate of 500 s^{-1} and a temperature of 150°C . As can be seen, the viscosity value kept stable at first, and gradually decreased after several seconds. The main reason for the decline was that part of the bitumen stuff flew over due to the rotation of cone. Therefore, an average value taken over the first few seconds was obtained.

6.2.3 Dynamic shear rheometer

Dynamic shear rheometer (DSR) AR 2000ex (see Figure 6.2.4) was adopted to evaluate the dynamic viscoelastic properties of the materials as a function of temperature and frequency.

Figure 6.2.5 shows the parallel-plates configuration used. The input parameters of the DSR test are given in Table 6.2.2. For temperatures from -10°C to 20°C , parallel plates with the 8 mm diameter and a 2 mm gap between them were chosen; for temperatures above 20°C , 25 mm diameter parallel plates and a 1 mm gap between the plates were chosen. The frequency ranged from 0.1 rad/s to 400 rad/s which means 0.016 Hz to 64 Hz. First of all, a strain amplitude sweep was necessary to determine the linear viscoelastic range of bitumen at each testing temperature. The chosen strain for the frequency sweep tests must be within the linear viscoelastic range. Otherwise, it can not really reflect the material's essential properties.



Figure 6.2.4 Image of dynamic shear rheometer (DSR) AR 2000ex (<http://www.tainstruments.com/>)

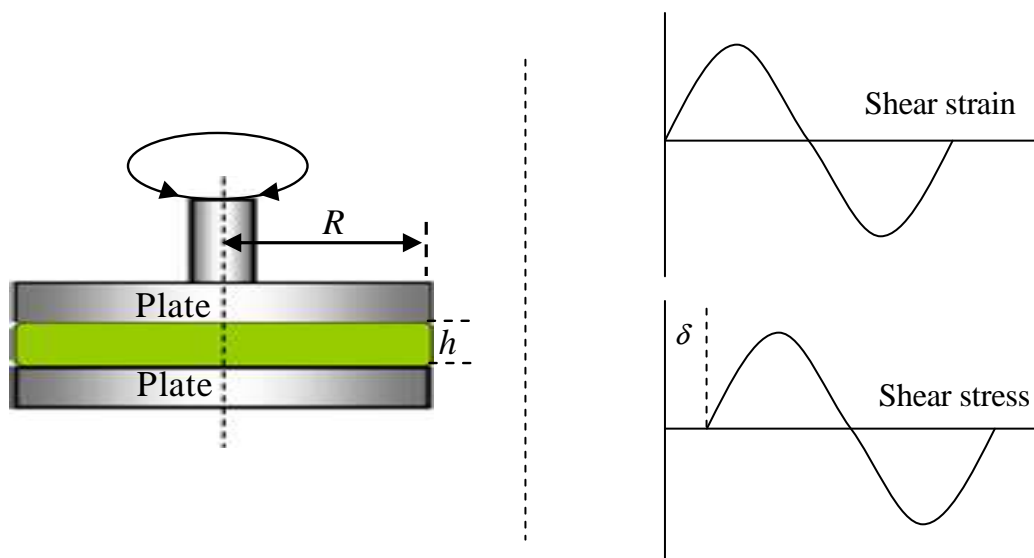


Figure 6.2.5 Configuration of DSR parallel plates device loaded with sinusoidally varying shear strain

Table 6.2.2 Configuration and input parameters in DSR

Device	Diameter, R [mm]	Temperature [°C]	Gap, h [mm]	Frequency [rad/s]
DSR	25	30, 40, 50, 60	1	0.1 ~ 400
	8	-10, 0, 10, 20	2	

In the parallel plates method, the applied peak shear strain (γ_0) should be within the linear viscoelastic range at the corresponding temperature. The dynamic oscillating shear strain (γ^*) and stress (τ^*) are respectively defined as:

$$\gamma^* = \gamma_0 \sin(\omega t) \quad 6.2.4$$

and

$$\tau^* = \tau_0 \sin(\omega t + \delta) \quad 6.2.5$$

where:

ω = angular frequency,

t = the time,

τ_0 = peak shear stress, and

δ = phase angle.

It is convenient to express the oscillating strain and stress as complex quantities following:

$$\gamma^* = \gamma_0 e^{i\omega t} \quad 6.2.6$$

and

$$\tau^* = \tau_0 e^{i(\omega t + \delta)} \quad 6.2.7$$

The complex shear modulus G^* is then calculated following:

$$G^* = \tau^* / \gamma^* = (\tau_0 / \gamma_0) e^{i\delta} = (\tau_0 / \gamma_0) (\cos \delta + i \sin \delta) = G' + iG'' \quad 6.2.8$$

where:

G' = storage modulus, or elastic modulus, and

G'' = loss modulus, or viscous modulus.

The storage modulus G' describes the amount of energy stored and released elastically in each oscillation and is thus called the elastic modulus; G'' describes the average energy dissipation rate associated with the viscous effects and is thus called the viscous modulus (Lu and Isacsson 1997). The phase angle is the phase difference between the stress and strain, and reflects the viscoelastic characteristic of the material. Purely viscous liquids and ideal elastic solids have phase angles of 90° and 0° , respectively.

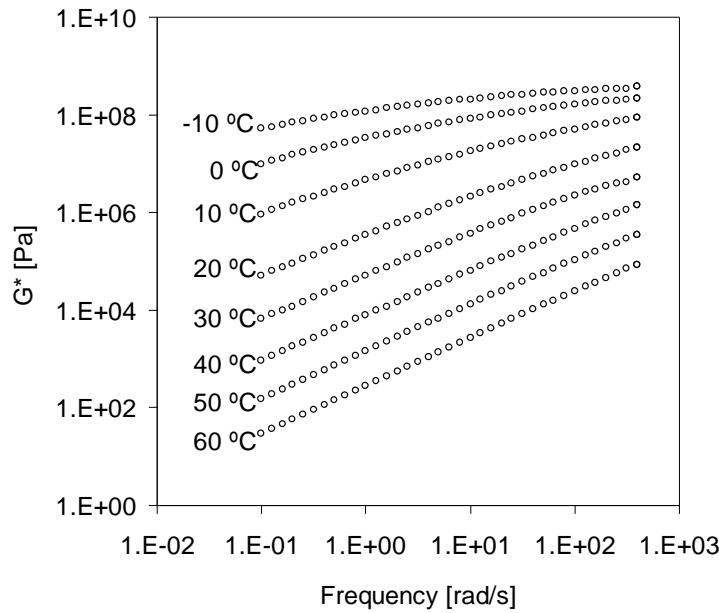


Figure 6.2.6 Complex modulus as a function of frequency and temperature

Figure 6.2.6 gives a typical example of frequency-sweep results at several temperatures as conducted on bitumen B (70/100). It is known that the rheological properties of bituminous materials can be well described by a master curve using the time-temperature superposition principle. This principle allows to shift the data as shown in Figure 6.2.6 to a reference temperature as a function of the reduced frequency. The shifting factor is obtained using the Williams-Landel-Ferry (WLF) model as follows:

$$\log a_T(T) = \frac{C_1(T - T_R)}{C_2 + T - T_R} \quad 6.2.9$$

where,

a_T = shift factor at a temperature of T ,

T_R = reference temperature [°C],

C_1 and C_2 = constants [-].

a_T was also obtained using the Arrhenius equation:

$$\log(a_T) = \frac{\Delta E_a}{2.303R} \left(\frac{1}{T} - \frac{1}{T_0} \right) \quad 6.2.10$$

where,

ΔE_a = apparent activation energy [J/mol], and

R = universal gas constant, 8.314 J/(K·mol)

The reduced frequency is determined by multiplying the test frequency by a shift factor a_T . To construct the complex modulus and phase angle master curve, a reference temperature of 20 °C is chosen. The data of complex modulus G^* and phase angle δ were fitted into the following S-curve model:

$$G^* = G_{\min}^* + (G_{\max}^* - G_{\min}^*) \times (1 - e^{-(\frac{f_r}{\beta})^\gamma}) \quad 6.2.11$$

$$\delta = \delta_{\min} + (\delta_{\max} - \delta_{\min}) \times e^{-(\frac{f_r}{\beta})^\gamma} \quad 6.2.12$$

where,

G^* = complex modulus [Pa],

f_r = reduced frequency [rad/s],

G_{\min}^* , G_{\max}^* = complex modulus when f_r is 0 or infinite [Pa],

δ = phase angle [°],

δ_{\min} , δ_{\max} = phase angle when f_r was infinite or 0 [°],

β = location parameter [rad/s], and

γ = shape parameters [-].

All the model parameters can be obtained by using the Solver function in the Excel spreadsheet through minimizing the mean relative error.

6.3 Results and analyses

6.3.1 Properties characterized by the cone and plate rheometer

6.3.1.1 Dynamic viscosity

Table 6.3.1 gives the dynamic viscosity results at the three selected temperatures, 60 °C, 100 °C, and 150 °C (European norm EN 13702-1). It was observed that the addition of the Mts increased the viscosity of both base bitumens to a different degree which depended on the type of Mt, as well as the testing temperature.

Table 6.3.1 Dynamic viscosity at three standard temperatures

Binder	Dynamic viscosity [Pa.s]		
	60 °C ($\dot{\gamma}=0.05 \text{ s}^{-1}$) *	100 °C ($\dot{\gamma}=500 \text{ s}^{-1}$)	150 °C ($\dot{\gamma}=500 \text{ s}^{-1}$)
A (40/60)	438.0	6.19	0.347
A+4%Mt0	487.0	6.68	0.379
A+4%Mt1	523.5	7.53	0.426
A+4%Mt2	651.0	8.81	0.505
B (70/100)	195.5	3.63	0.261
B+4%Mt0	210.5	3.94	0.264
B+4%Mt1	265.5	4.57	0.284
B+4%Mt2	297.0	5.29	0.380

*: The choice of shear rate $\dot{\gamma}$ at each temperature is according to EN 13702-1 which is introduced in the section of 6.2.2.

Figure 6.3.1 shows the increment ratio (k) of the viscosity for the modified bitumens at three temperatures. This ratio was calculated using the following equation:

$$k = \frac{\eta_m - \eta_{base}}{\eta_{base}} \times 100 \quad 6.3.1$$

where,

η_{base} = dynamic viscosity of the base bitumen [Pa.s], and

η_m = dynamic viscosity of the modified bitumen [Pa.s].

As indicated in Figure 6.3.1, the increment ratios of A+4%Mt2 and B+4%Mt2 were more than 40% at each testing temperature, which indicated that Mt2 strongly influences the viscosity of bitumen. The only inorganic Mt0 showed a low influence on the viscosity, and most increment ratios were lower than 10% at each testing temperature. The increment ratios of A+4%Mt1 were around 20%, and those of B+4%Mt1 were between 8% and 36%.

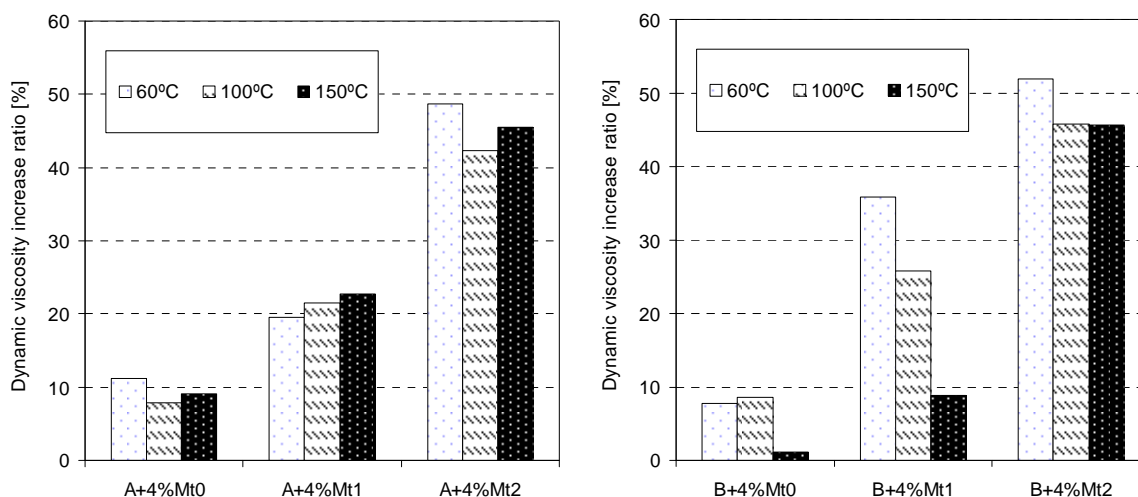


Figure 6.3.1 Dynamic viscosity increment ratio for modified bitumens at three standard temperatures

The increase of viscosity might be mainly attributed to two reasons: one is that the Mt platelets limit the flow of bitumen; another is that part of the bitumen molecules are confined to the two dimensional galleries of the Mt clay. The change of viscosity could also reflect the strength of the interfacial bond between bitumen and the Mt. Therefore, the results could imply that inorganic Mt0 has a weak interfacial bond with the base bitumen, and Mt2 a stronger interfacial bond.

6.3.1.2 Shear rate sweeps

Figure 6.3.2 shows the relationship between shear stress and shear rate for the B bitumen series at 135 °C. B+4%Mt1 and B+4%Mt2 behaved similarly and like a Bingham liquid. This means that they act as a rigid body at low stresses but flow as a viscous fluid at high stresses. The reason for this behaviour is that the Mt particles limit the flow of the bitumen. Until a shear rate of 1.1 s^{-1} , the shear stress for both modified bitumens is almost the same (1.05 Pa). After that, the shear stress proportionally increases with increasing shear rate. The base bitumen behaved more like a Newtonian liquid as its shear stress was proportional to the shear rate almost from the beginning. As discussed before, the inorganic Mt0 particles are present in the bitumen as conventional particles. Some of these particles were present in the gap between the cone tip and the plate. The distance of the gap was 50 μm , and equaled to the maximum size of these particles. Therefore, some noise occurred between shear stress and shear rate for B+4%Mt0 at low shear stress levels. As shear stress increased above 1.2 Pa, the Newtonian behaviour recovered due to the escape of the particles from the gap.

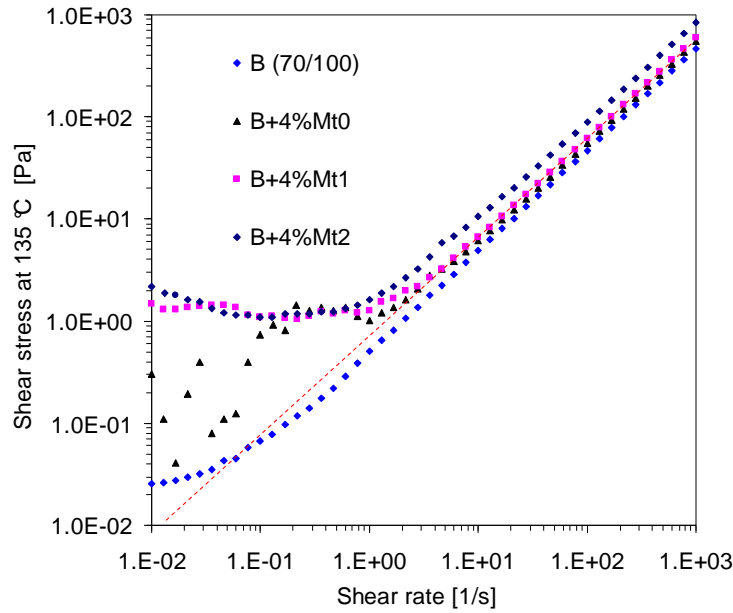


Figure 6.3.2 Shear stress vs. shear rate of the bitumens at 135 °C

Figure 6.3.3 shows the shear rate dependency of the viscosity at 135 °C. With the addition of Mt1 and Mt2, the degree of shear thinning of the bitumen was enhanced, and the viscosity increased remarkably at low shear rates. A Newtonian plateau was reached above a shear rate of 10 s^{-1} . B+4%Mt2 had a higher viscosity than B+4%Mt1 at the same shear rate. Some noise in the viscosity curve of the bitumen with Mt0 was observed before it reached the Newtonian plateau. The viscosity of all bitumens remains below $3 \text{ Pa}\cdot\text{s}$ in this region which is important for the workability of bitumen during mixing and laying of asphalt mixture.

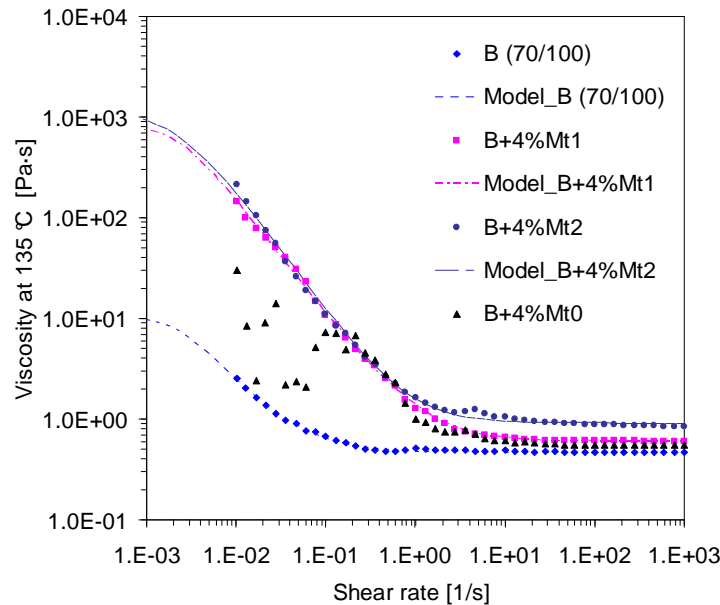


Figure 6.3.3 Shear rate dependency of viscosity of the bitumens at 135 °C.

A shear thinning fluid displays decreasing viscosity with increasing shear rate. Shear thinning often happens in some macromolecule materials, and it is explained by the fact that macromolecule chains usually exist in a state of random orientation and high entanglement, and will get disentangled and become oriented at high shear rates (Chen, Yang et al. 2005). With respect to pure bitumen, shear thinning means that the imposed shear stress reaches a critical value which can alter the colloidal equilibrium, thus orienting or disrupting asphaltene micelles or the micelles aggregates (Polacco, Berlincioni et al. 2005). The reinforcement of this behaviour is also believed to be related to the orientation effect of the Mt particles existing as dispersed intercalated platelets observed by XRD tests and maybe as a few single platelets in the bitumen (see the 2D model in Figure 6.3.4). By imposing a shear stress on the modified bitumen, these platelets orient themselves which strengthen the shear thinning behaviour.

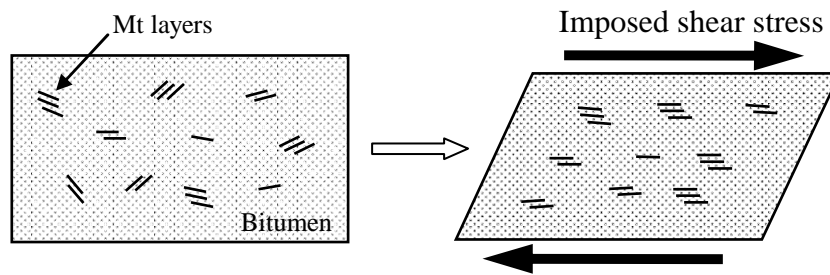


Figure 6.3.4 2D Model of shear thinning behaviour of Mt modified bitumen

The Carreau model (Hsu, Shie et al. 2005) was adopted to describe this shear thinning behaviour:

$$\eta = \eta_{\infty} + \frac{\eta_0 - \eta_{\infty}}{(1 + (\frac{\dot{\gamma}}{\dot{\gamma}_c})^2)^s} \quad 6.3.2$$

where,

η_0 = zero shear viscosity [Pa·s],

η_{∞} = infinite shear viscosity [Pa·s],

s = a parameter related to the slope of the shear thinning region, and

$\dot{\gamma}_c$ = a critical shear rate for the onset of the shear thinning region.

In this model, a zero shear Newtonian plateau is assumed at the beginning until a $\dot{\gamma}_c$ value at which shear thinning starts (see Figure 6.3.5). With the increase of the shear rate, the viscosity gradually reaches an infinite shear Newtonian plateau. The shear thinning region is between these two plateaus. The models that were fitted to the data are shown in Figure 6.3.3, and related parameters are listed in Table 6.3.2.

The addition of Mt1 and Mt2 to the base bitumen increased η_0 by almost two orders of magnitude. A high η_0 at high temperatures implies a good drainage resistance of the asphalt mix during transportation, and will keep an average bitumen film on the surface of aggregates to improve the durability of the asphalt mix.

Table 6.3.2 Parameters in the Carreau Model for bitumen at 135°C

Code	η_0 [Pa·s]	η_∞ [Pa·s]	$\dot{\gamma}_c$ [s ⁻¹]	s	R ² [%]
B (70/100)	10.8	0.47	0.002	1.12	99.7
B+4%Mt1	827.4	0.60	0.002	1.17	99.6
B+4%Mt2	1280.9	0.92	0.002	1.23	99.0

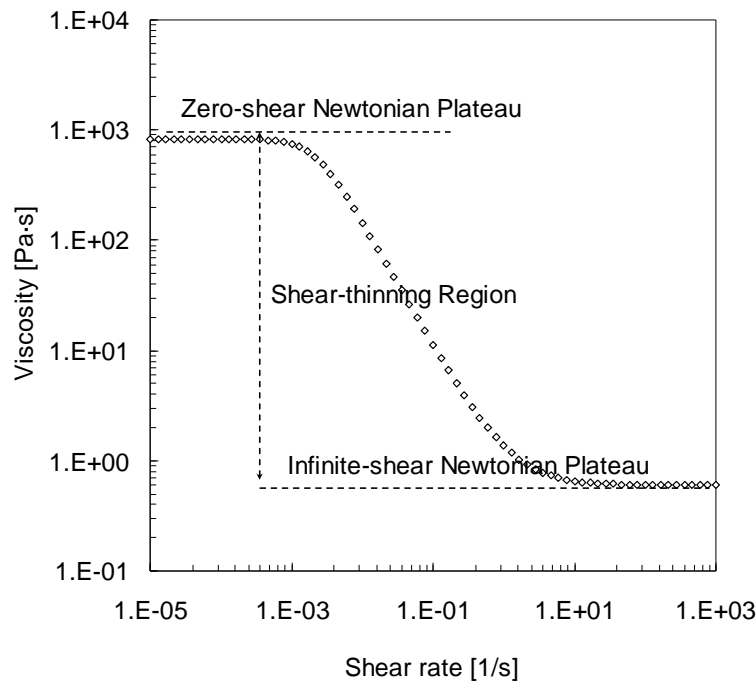


Figure 6.3.5 Relationship between viscosity and shear rate in the Carreau model

6.3.2 Master curves by DSR

Compared with empirically rheological properties, i.e. penetration and softening point, master curves reflect a rheological spectrum over a wide frequency or temperature range. Therefore, the use of master curve is becoming more and more popular in characterizing bitumen's rheological properties. As shown in Figure 6.3.6, the complex modulus and phase angle master curves of base bitumens are constructed using the WLF shifting method at a reference temperature of 20 °C. As indicated, base A (40/60) exhibited a higher complex modulus G^* and a lower phase angle δ than base B (70/100) over a frequency range from 10^{-5} rad/s to 10^5 rad/s. Since different compositions of bitumens result in different rheological properties, they also influence the interaction of bitumen with the Mts.

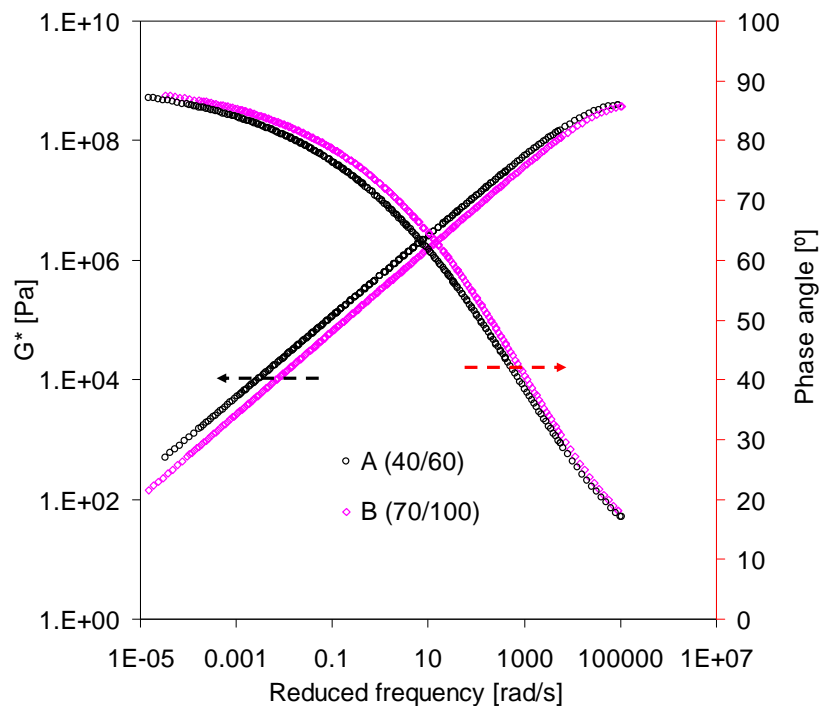


Figure 6.3.6 Complex modulus and phase angle master curves of base bitumens at a reference temperature of 20 °C

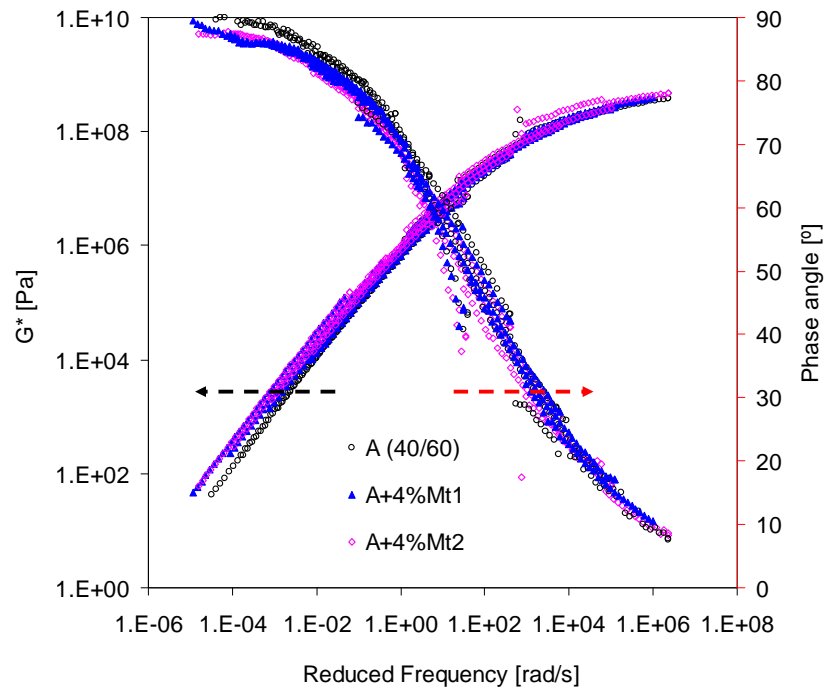
In this section, base A and B were modified with Mt0, Mt1 and Mt2 at 4 mass%. In total, seven master curves of bitumens were constructed. Tables 6.3.3 and 6.3.4 give their shifting factors and the fitted model parameters. As shown in Figure 6.3.7, 4 mass% of Mt1 and Mt2 can influence the rheological properties of base A and B. The increase in complex modulus due to the modification was accompanied by a decrease in the phase angle, which was more evident at the low frequency range. The curves of B+4%Mt0 almost overlapped with these of base B, which means the inorganic Mt0 hardly changes the properties of base B.

Table 6.3.3 Shift factors and model parameters used in the master curve construction of bitumen A series

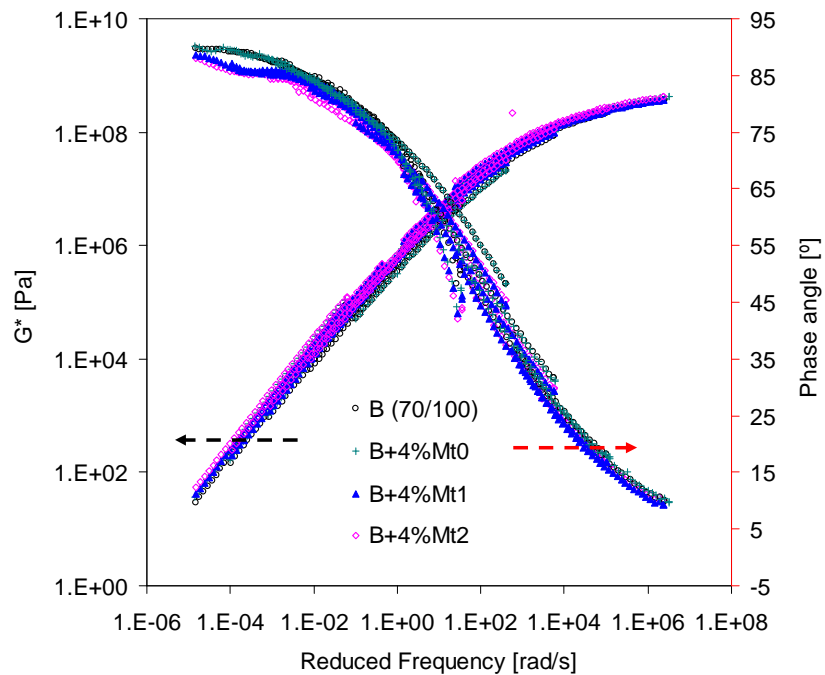
	Parameter	A	A+4%Mt1	A+4%Mt2
Shift factor	C_1	27.8	27.6	27.6
	C_2	250.0	250.5	251.0
Complex modulus	G_{\max}	4.2E+08	4.3E+08	4.4E+08
	G_{\min}	0.0	0.0	0.0
	β	30725.8	22203.4	22200.4
	γ	0.7	0.7	0.7
Phase angle	δ_{\max}	90.0	87.1	87.1
	δ_{\min}	10.1	8.9	8.9
	β	859.8	853.3	854.3
	γ	0.186	0.185	0.201

Table 6.3.4 Shift factors and model parameters used in the master curve construction of B bitumen series

	Parameter	B	B+4%Mt0	B+4%Mt1	B+4%Mt2
Shift factor	C_1	27.8	26.0	27.6	27.6
	C_2	250	230	250	250
Complex modulus	G_{\max}	4.15E+08	4.15E+08	4.22E+08	4.25E+08
	G_{\min}	0	0	0	0
	β	30725.8	22452.5	22203.4	22203.4
	γ	0.694	0.696	0.677	0.677
Phase angle	δ_{\max}	90.0	90.0	87.1	87.1
	δ_{\min}	10.06	9.03	8.89	8.89
	β	859.8	1500.0	853.3	853.3
	γ	0.186	0.200	0.185	0.185



(a)



(b)

Figure 6.3.7 Complex modulus and phase angle master curves of (a) base A and its modified bitumens, and (b) base B and its modified bitumens at a reference temperature of 20 °C

Figures 6.3.8 and Figure 6.3.9 show the frequency sweep curves of bitumens at 60 °C and 20 °C. In general, Figure 6.3.8b shows that the modified bitumens exhibit a higher G^* and lower phase angle, except B+4%Mt0. There is a plateau on the phase angle curve at 60 °C for A+4%Mt1, B+4%Mt1, and B+4%Mt2, which mainly occurred at the frequency range between 1.0 rad/s and 10 rad/s. For A+4%Mt2, it took place over the range from 0.1 rad/s to 1.0 rad/s.

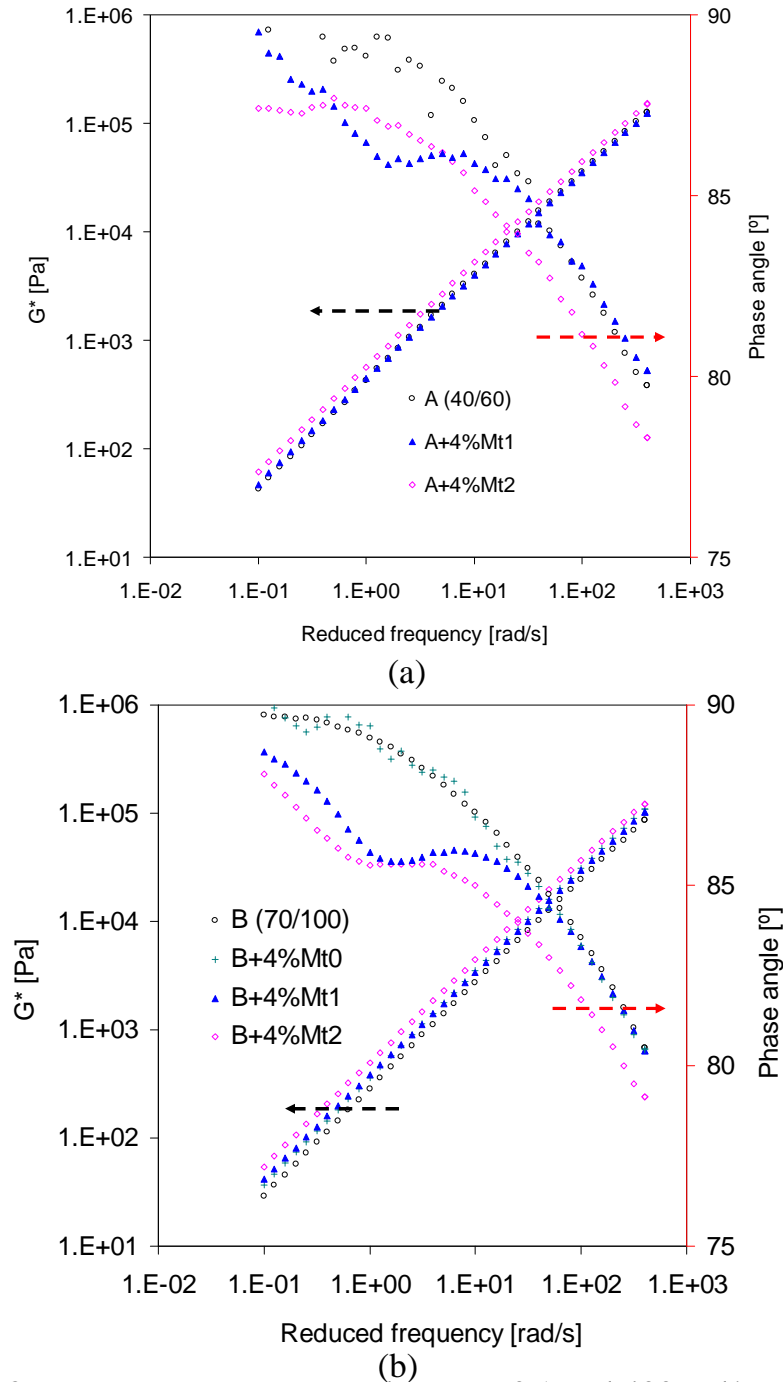
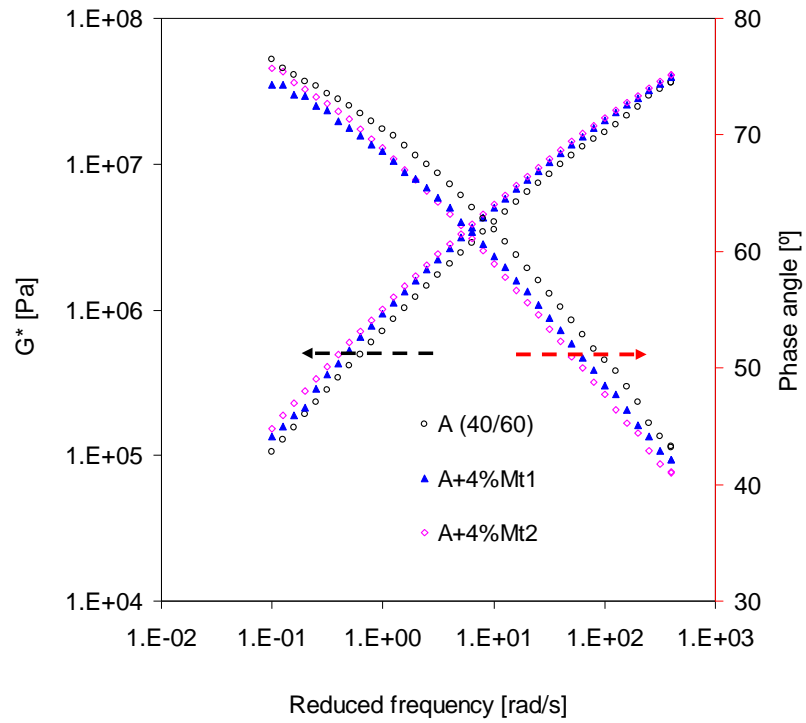
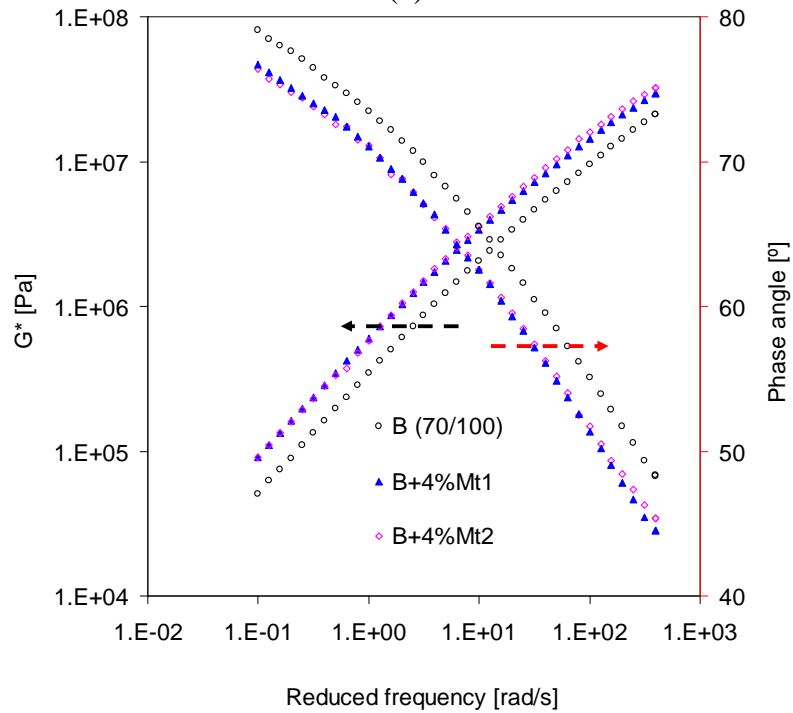


Figure 6.3.8 Frequency sweep curves between 0.1 and 400 rad/s on (a) Bitumen A Series and (b) B series at 60 °C



(a)



(b)

Figure 6.3.9 Frequency sweep curves between 0.1 rand and 400 rad/s on (a) base A and its modified bitumens, and (b) base B and its modified bitumens at a temperature of 20 °C

In fact, the test temperature also influenced the range of phase angle plateau. As indicated in Figure 6.3.10, the plateau for B+4%Mt1 which is taking place between 1.0 rad/s and 10 rad/s at 60 °C moves backwards to the range between 0.4 rad/s and 1.1 rad/s at 50 °C, and next between 0.1 rad/s and 0.3 rad/s at 40 °C. Eventually, it disappeared at 30 °C. The reason for this behaviour is that the bitumen molecules are intercalated in the modified clays, implying that there will be an interaction between the surfactant of the clay and the bitumen. This interaction has an effect on the deformation characteristics of the modified bitumen which is visible at certain frequencies and temperature conditions. It appears that the observed plateaus are shifting to the lower frequency range at lower temperature. It would therefore also have been measured at 30 °C if the equipment would be capable to measure at lower frequencies.

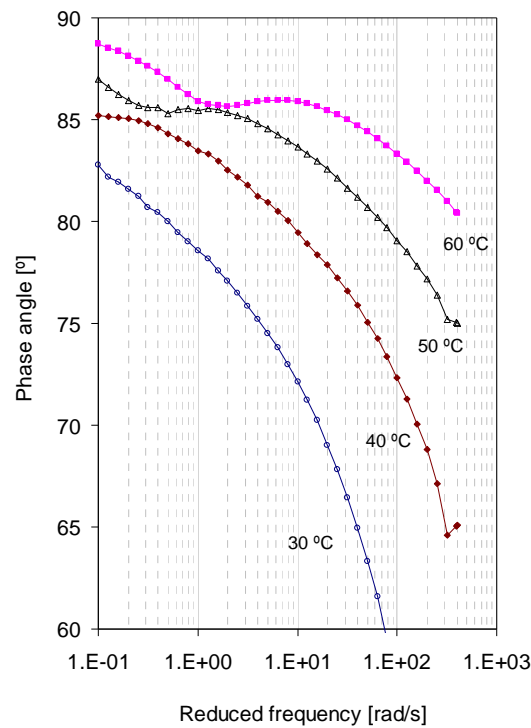


Figure 6.3.10 Frequency sweep curves between 0.1 rand and 400 rad/s on B+4%Mt1 at temperatures of 30, 40, 50, and 60 °C

Figure 6.3.11 shows the storage modulus (G') ratio and loss modulus (G'') ratio of the modified bitumen to the base bitumen at 60 °C and 20 °C. As indicated, G' ratios corresponding to base A and base B in Figure 6.3.11 a and b were influenced by the frequency, and changed from 1.5 to 10 and from 1.5 to 15, respectively. At a same frequency, bitumens modified by Mt2 had a higher G' ratio than these modified by Mt1. However, the Mts contributed less to the change of G'' at this temperature. When the temperature decreased to 20 °C, the storage

modulus ratios also decreased to a range between 1.1 and 1.6 for the A series , and between 1.5 and 2.5 for the B series.

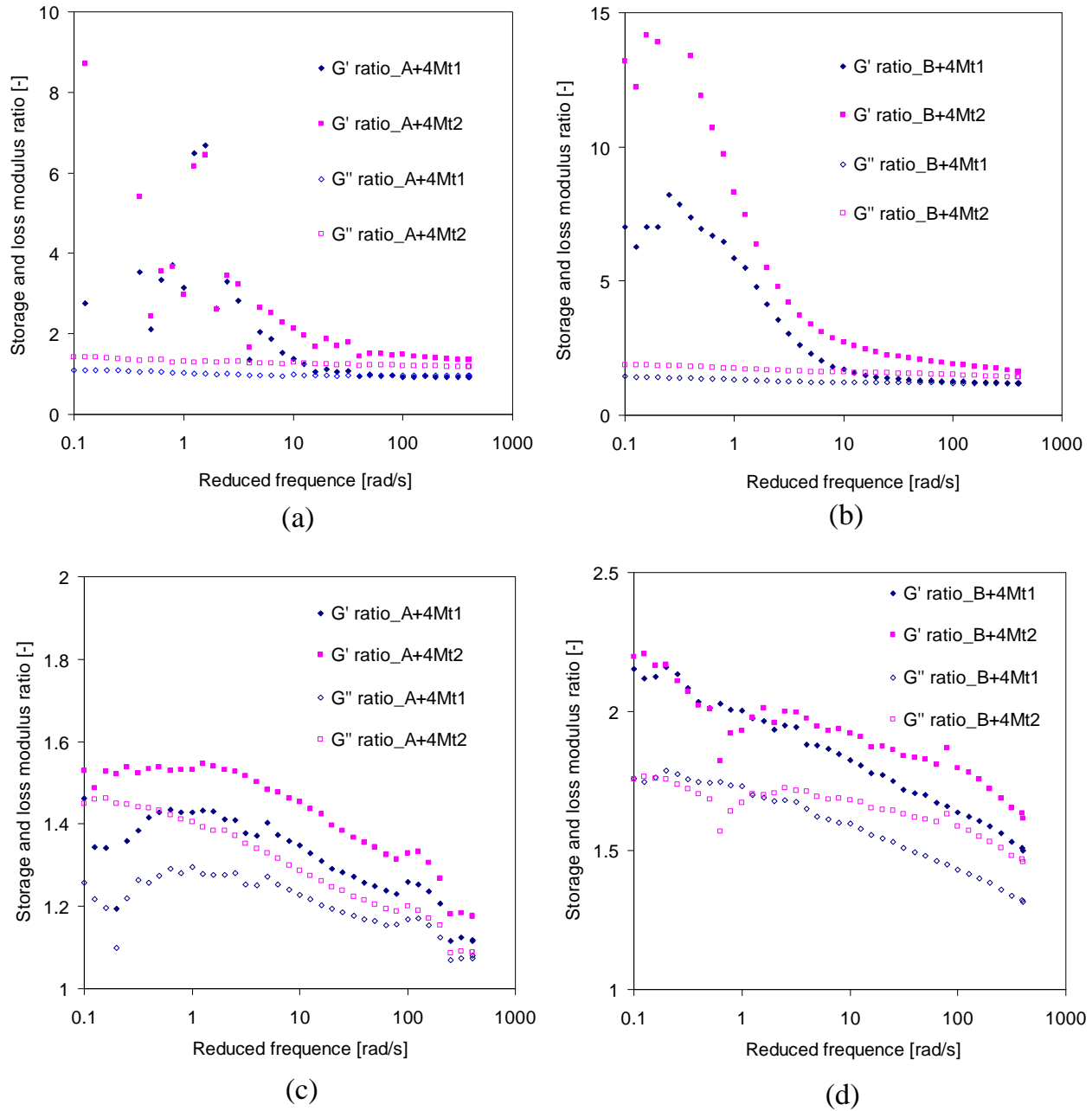


Figure 6.3.11 the storage modulus (G') ratio and loss modulus (G'') ratio of the modified bitumen to the base bitumen at 60 °C for (a) and (b), and at 20 °C for (c) and (d)

The Young's modulus of clay platelets was considered to be within of range 178-265 GPa. This assumption is based on values taken from literature for layered structure clay minerals (Kornmann, Berglund et al. 1998; Feng, Gong et al. 2004; Zhu and Narh 2004; Chen and Evans 2006). Therefore, it is logical that the Mt modification changes the rheological properties of bitumen in terms of storage modulus. The surfactant on the Mt also influences the rheological properties due to the compatibility between the Mt and bitumen. It seemed that bitumen itself also influenced the modification effect, such as the G' ratio for base B being higher than that for base A when modified with the same Mt. The reason could be that the base B bitumen has a smaller average molecular weight than base A, and therefore the Mt can swell more easily in the base B bitumen in which the clay platelets contributed more to the change of modulus.

6.3.3 Composite model

As introduced above, low concentrations of the Mt changed the rheological properties of bitumen. In related fields of nanocomposites, some reasons are discussed. The reduced mobility of constrained matrix molecules was considered to be responsible to the increase of modulus; a strong interaction between the matrix and the Mt could also be a reason for the increase of the modulus (Kojima, Usuki et al. 1993; Okada and Usuki 2006). Some composite models, such as the Halpin-Tsai model and Simha model, were developed to explain the reinforcement mechanism in nanocomposites (Simha 1940; Halpin and Kardos 1976; Vlasveld, De Jong et al. 2005). In these models, the property change of the matrix itself and the interaction between the matrix and the Mt were ignored; the property improvement was considered to be related to the Mt's modulus, its concentration, shape, size and orientation. These models were encouraging to be used to predict the properties of nanocomposites (Kuelmann, Osman et al. 2005; Vlasveld, De Jong et al. 2005).

In this section, the Simha model is introduced to further describe the influence of Mt on the rheological properties of base bitumen.

6.3.3.1 Theory

When a material is tested under a sinusoidally oscillating load, as is done to the bitumen in this chapter, the complex viscosity η^* is defined as:

$$\eta^* = G^* / \omega = G' / \omega - iG'' / \omega = \eta' + i\eta'' \quad 6.3.3$$

where,

η' = the real or in phase component of η^* [Pa·s], and also called dynamic viscosity, and

η'' = the imaginary or out-of-phase component of η^* [Pa·s], which is only important in a mathematical sense.

The dynamic viscosity η' can be expressed using the following equation (Utracki and Lyngaae-Jorgensen 2002):

$$\eta' = \eta_0 (1 + G''/G_\eta)^{-m} \quad 6.3.4$$

where,

η_0 = zero shear viscosity, [Pa·s],

G_η = characteristic modulus [Pa], and

m = shape factor [-].

Equation 6.3.4 was derived from linear viscoelastic and pseudoplastic materials, and hence it was unable to describe the yield stress.

Through fitting of Equation 6.3.4, η_0 of base and modified bitumens is obtained and applied to Equations 6.3.5 and 6.3.6 to calculate viscosities defined as:

$$\eta_{relative} = \frac{\eta_c}{\eta_m} \quad 6.3.5$$

$$\eta_{reduced} = \frac{\eta_c - \eta_m}{\eta_m \phi} \quad 6.3.6$$

where,

$\eta_{relative}$ = the relative viscosity [-],

$\eta_{reduced}$ = the reduced viscosity [-],

η_m = the viscosity of matrix [Pa·s],

η_c = the viscosity of nanocomposite [Pa·s], and

ϕ = volume fraction of Mt platelets which is extremely low.

The intrinsic viscosity refers to the inherent viscosity and is defined as:

$$[\eta] = \lim_{\phi \rightarrow 0} \frac{\eta_c - \eta_m}{\eta_m \phi} \quad 6.3.7$$

Here, $[\eta]$ is dimensionless as a result of viscosity ratio. According to Einstein's viscosity equation, $[\eta]$ of a Newtonian liquid with a low volume fraction of spheres is constant and equal to 2.5. For the particle with fiber shape and disk shape at low concentrations, some linear models were assumed by Simha (1940). These models are shown below:

$$[\eta] = \frac{(a/b)^2}{15[\log 2(a/b) - \frac{3}{2}]} + \frac{(a/b)^2}{5[\log 2(a/b) - \frac{1}{2}]} + \frac{14}{15} \quad (\text{fiber shape}) \quad 6.3.8$$

$$[\eta] = \frac{16}{15} \frac{(a/b)}{\tan^{-1}(a/b)} \quad (\text{disk shape}) \quad 6.3.9$$

where,

a/b = aspect ratio.

The equation for $[\eta]$ for platelets was approximated by a linear function for all aspect ratios:

$$[\eta] = 0.679(a/b) + 0.454 \quad 6.3.10$$

Another simplified model by Luciani, Leterrier et al. (1999) also showed a good fit with experimental measurements:

$$[\eta] = \frac{4}{9} + \frac{4}{3\pi}(a/b) \quad 6.3.11$$

A different form of a relation between the intrinsic viscosity and the aspect ratio of disk-shaped particles was given by Utracki and Lyngaae-Jorgensen (2002):

$$[\eta] = 2.5 + 0.025[1 + (a/b)^{1.47}] \quad 6.3.12$$

Besides the models introduced above, the semi-empirical Halpin-Tsai model is most often used, which takes into account the shape and the aspect ratio of the reinforcing particles. Equation 6.3.13 shows the traditional forms of the Halpin-Tsai equation.

$$\frac{E_c}{E_m} = \frac{1 + \zeta k \varphi_f}{1 - k \varphi_f} \quad 6.3.13$$

in which,

$$k = \frac{\left(\frac{E_f}{E_m} - 1\right)}{\left(\frac{E_f}{E_m} + \zeta\right)} \quad 6.3.14$$

where,

E_c = composite Young's modulus,

E_f = particle modulus,

E_m = matrix modulus,

ζ = shape factor, depending on the geometry, orientation and aspect ratio of the particles, and

φ_f = volume fraction particle.

Using models from Equation 6.3.8 to 6.3.14, Vlasveld, De Jong et al. (2005) calculated the aspect ratios of particles in nanocomposites and microcomposites with different amounts and types. Results indicated that the Simha model (Equation 6.3.10) predicted reasonable aspect ratios which were comparable with those based on TEM observations and Halpin-Tsai model.

6.3.3.2 Volume fraction

As introduced in Chapter 3, the densities of Mts were determined using an Ultrapycometer. This value for Mt1 is 1.78 g/cm³, 1.83 g/cm³ for Mt2, and 2.75 g/cm³ for pure Mt0 (without surfactant). The simultaneous thermogravimetric (TG) analysis indicated that the surfactant contents of Mt1 and Mt2 were 20.1% and 22.9% by weight, respectively.

To clearly understand each fraction in bitumen, a simplified composite model is shown in Figure 6.3.12. Based on the data above, the volume contents of each fraction were obtained and given in Table 6.3.5. The densities of surfactants on Mt1 and Mt2 were calculated to be 0.74 g/cm³ and 0.83 g/cm³ (Table 3.2.2). As indicated in Table 6.3.5, the value of $\phi_{\text{surfactants}}$ was comparable to that of $\phi_{\text{platelets}}$. In this study, the surfactants were regarded as part of the matrix and were assumed to have the same modulus as bitumen, i.e. $G_{\text{matrix}}^* = G_{\text{bitumen}}^*$. Although some assumptions and simplifications are made in this section, this could not significantly influence the overall conclusions and change the trend of the results.

Table 6.3.5 Volume contents of fractions in the Mt modified bitumen						
Volume	B+4%Mt1	B+8%Mt1	B+12%Mt1	B+4%Mt2	B+6%Mt2	B+8%Mt2
$\phi_{\text{platelets}}$ [%]	1.15	2.25	3.30	1.11	1.64	2.17
$\phi_{\text{surfactants}}$ [%]	1.07	2.09	3.07	1.05	1.56	2.06
ϕ_{bitumen} [%]	97.78	95.66	93.63	97.84	96.80	95.77

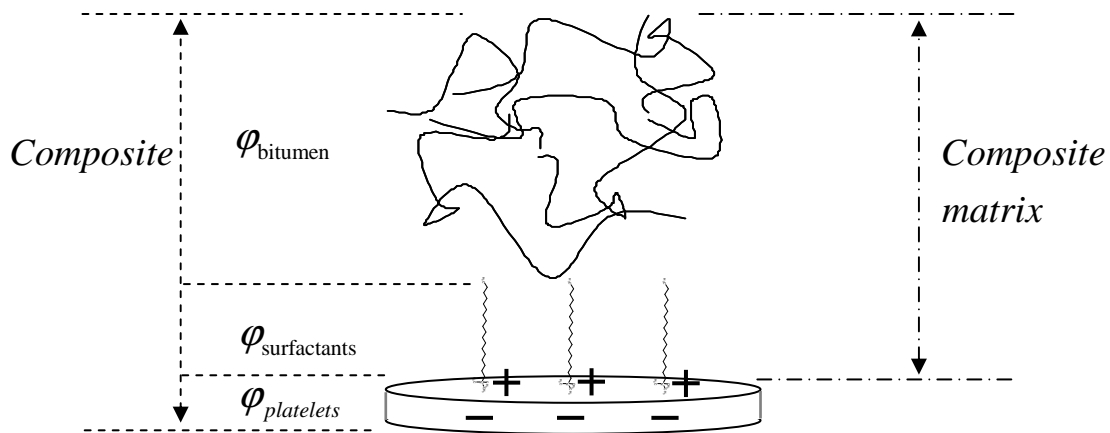


Figure 6.3.12 Composite fractions of Mt modified bitumen

6.3.3.3 Results and analysis

Figure 6.3.13 shows an example of the dynamic viscosity η' of base B as function of frequency at different temperatures. A zero shear plateau was clearly observed at a temperature of 60 °C within the low frequency range. As the temperature decreases, shear thinning takes place due to breaking of the structure. The model represented by Equation 6.3.4 can not describe this behaviour precisely because it is derived from linear viscoelastic and pseudoplastic materials, without taking the yield stress into account. Related parameters are given in Table 6.3.6.

Table 6.3.6 Parameters in the model represented by Equation 6.3.4 for base bitumen at different temperatures

Factors	10 °C	20 °C	30 °C	40 °C	50 °C	60 °C
η_0	5.0E+06	3.2E+05	4.5E+04	9.3E+03	1.5E+03	2.9E+02
G_η	2.2E+07	4.3E+06	2.5E+06	1.3E+04	7.7E+03	4.9E+03
m	3.37	1.34	1.55	0.22	0.14	0.10
R^2	0.9956	0.9758	0.9610	0.9870	0.9950	0.9978

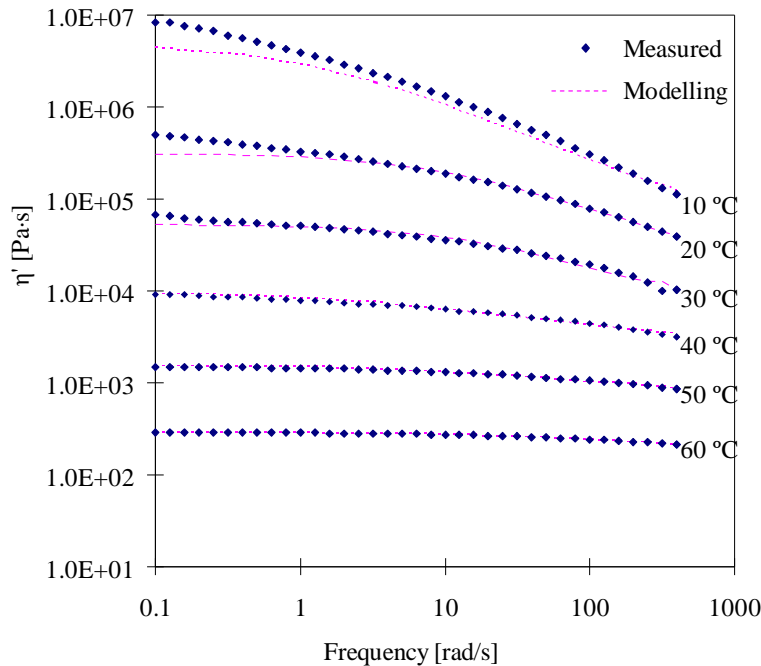


Figure 6.3.13 Dynamic viscosity η' of base B as function of frequency at different temperatures

After fitting the measured data into Equation 6.3.4, η_0 and other parameters for all bitumens were obtained and listed in Table 6.3.7. It is shown that the correlation coefficients are very high. Mt2 gives a higher η_0 than Mt1. Figure 6.3.14 shows the dynamic viscosity η' of the base and modified bitumens as function of the frequency at 60 °C. The curves for the bitumen with 8% Mt2 and 12% Mt1 almost overlapped. For most curves, a zero shear plateau could be observed.

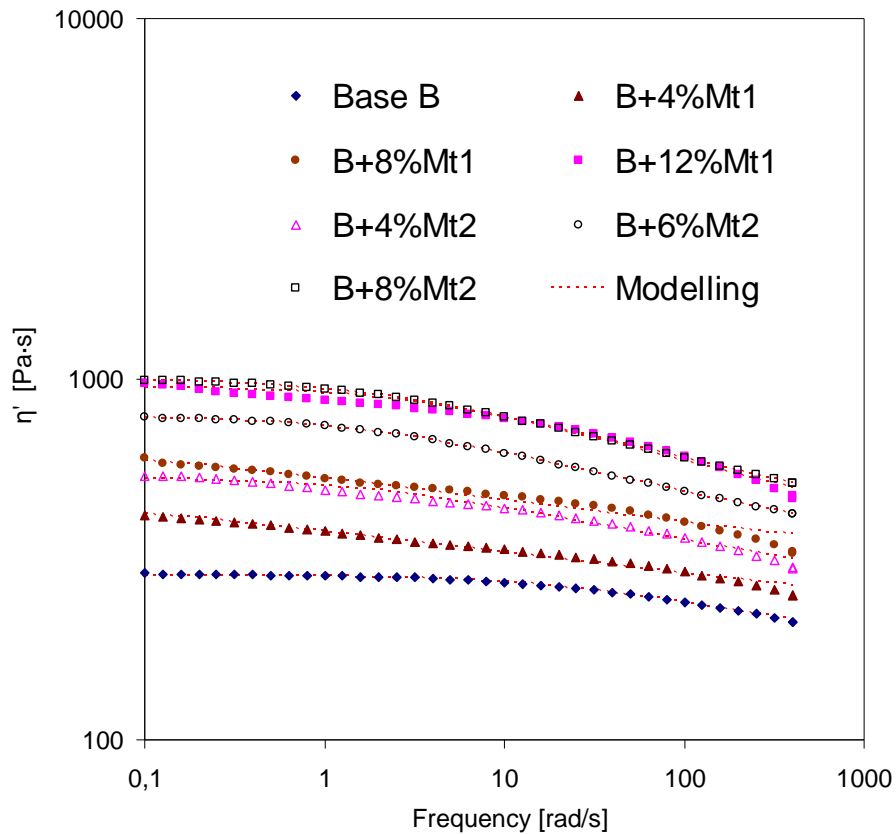


Figure 6.3.14 Dynamic viscosity η' of base and modified bitumens as function of frequency at 60 °C

Table 6.3.7 Parameters in Equation 6.3.4 for modified bitumens

Factors	η_0	G_η	m	R^2
B+4%Mt1	446.7	28.4	0.06	0.98
B+8%Mt1	626.6	47.6	0.07	0.96
B+12%Mt1	955.0	3016.0	0.16	0.98
B+4%Mt2	532.7	770.1	0.10	0.98
B+6%Mt2	789.5	1630.7	0.13	0.94
B+8%Mt2	1002.3	2824.1	0.15	0.99

It was found that the difference of η_0 between the base and modified bitumens in Table 6.3.2 was bigger than that in Table 6.3.7. The reason could be due to the state of bitumen and the testing mode. At a high temperature of 135 °C, the bitumen became liquid, and the Mt platelets' structure was completely broken as a function of the shear rate sweep in the rotation mode. Therefore, the platelets contributed more to η_0 than that obtained within the range of linear viscoelasticity in the oscillation mode. The η_0 value obtained within the range of linear viscoelasticity was preferred to be used in the composite model because it could reflect the real situation of bitumen in a solid state.

$\eta_{relative}$ (see Equation 6.3.5) as a function of volume content was calculated based on η_0 ; the results are shown in Figure 6.3.15. As indicated, the viscosity of base bitumen increased by several times due to adding a small part of Mt platelets.

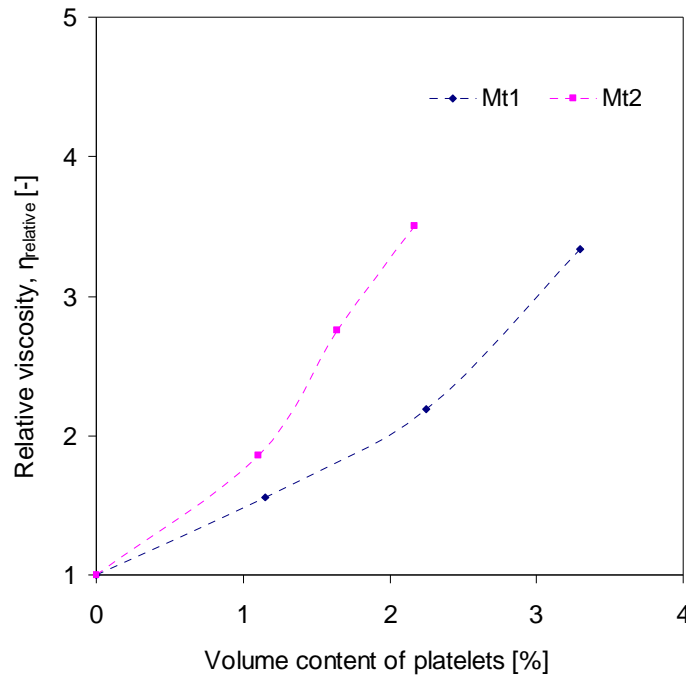


Figure 6.3.15 Relative viscosity, $\eta_{relative}$ vs. the volume contents of Mt1 and Mt2 platelet

Considering the low clay concentration, the data were fitted to the second-order Einstein-type equation (Utracki and Lyngaae-Jorgensen 2002):

$$\eta_{relative} = 1 + [\eta]\phi + k([\eta]\phi)^2 \quad 6.3.15$$

where,

k = interaction constant.

The least-squares fit gave values of intrinsic viscosity (see Equation 6.3.7): for bitumen with Mt1, $[\eta] = 25.1$ and $k = 0.50$ with $R^2 = 0.99$; for bitumen with Mt2, $[\eta] = 51.5$ and $k = 1.15$ with $R^2 = 0.9953$. As calculated using Equation 6.3.10, the aspect ratio (a/b) value was 36.3 and 75.2 for Mt1 and Mt2, respectively.

$\eta_{reduced}$ (see Equation 6.3.6) was also obtained and plotted as function of the platelets volume content (Figure 6.3.16). For bitumens modified with the Mt, $\eta_{reduced}$ increases with increasing volume content. As shown, the intrinsic viscosity $[\eta]$ can also be estimated at zero concentration through a linear fit, and appeared to be equal to 34.66 and 41.665 for bitumens modified with Mt1 and Mt2, respectively. As calculated using Equation 6.3.10, the aspect ratio (a/b) value was 50.4 and 60.7 for Mt1 and Mt2, respectively.

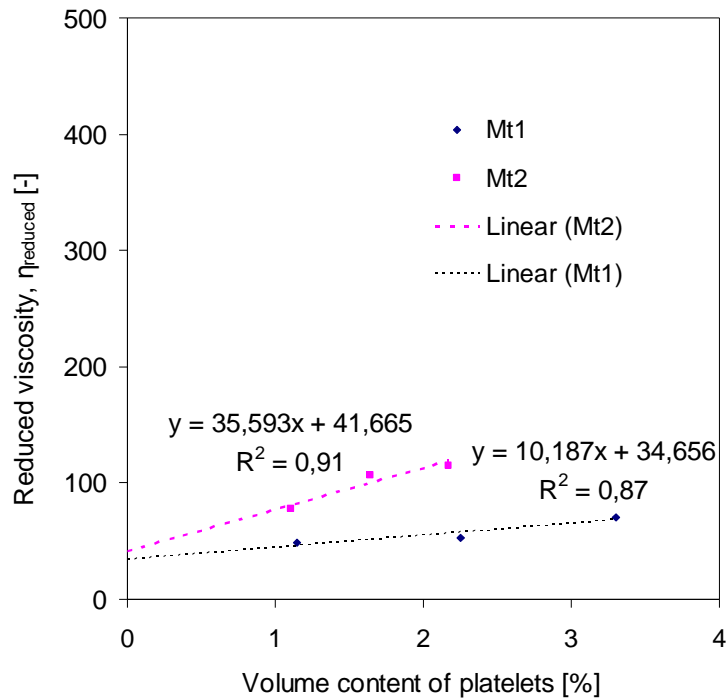


Figure 6.3.16 Reduced viscosity, $\eta_{reduced}$ vs. the volume contents of Mt1 and Mt2 platelets

It is thought that the calculated value could represent the real situation of Mt at the lowest concentration (4 mass% in this study). To validate the calculated value of a/b , a transmission electron microscope (TEM) was tried, but it failed due to some small bitumen molecules easily evaporating at the vacuum environment and room temperature. An environmental TEM method is recommended for the future. For one piece of platelet, a/b value was approximately estimated as 100 (length : thickness = 100 nm : 1 nm). The calculated a/b corresponds to the intercalated

morphology of Mt at 4 mass% detected by XRD which means that the platelets are not completely exfoliated and are still stacked together to some extent.

6.4 Summary and conclusions

In this chapter, DSR equipment was adopted to characterize the rheological properties of bitumen modified by the Mts in terms of viscosity and dynamic response. The change of viscosity might be mainly attributed to two reasons: one was that the Mt platelets limit the flow of bitumen; another was that part of the bitumen molecules were confined to the two dimensional galleries of Mt clay. The change of viscosity could also reflect the strength of the interfacial bond between bitumen and the Mts. According to the extent of change, it was indicated that inorganic Mt had a weaker interfacial bond with the base bitumen than the Mts with surfactants. When imposing a shear stress on the bitumen at a liquid state, the Mt platelets oriented themselves resulting in the reinforcement of shear thinning, as well as a higher zero shear viscosity. This implies a good drainage resistance of the asphalt mix during transportation, and would keep an average bitumen film on the surface of aggregates to improve the durability of asphalt.

Complex modulus and phase angle master curves of base bitumens were constructed using the WLF shifting method at a reference temperature of 20 °C. It was observed that the increase in complex modulus due to the modification, except by natural inorganic Mt, was accompanied by a decrease in the phase angle, which was more evident at a low frequency range. A phase angle plateau was found for organo Mt modified bitumen at high temperature within the low frequency range. The reason for the interaction between the surfactant of the clay and the bitumen has an effect on the deformation characteristics of the modified bitumen which is visible at certain frequencies and temperature conditions.

The Simha model was used to calculate the aspect ratio (a/b) value of the Mt in the bitumen. The calculated a/b corresponds to the intercalated morphology of Mt1 and Mt2 at 4 mass% detected by XRD. This means that the platelets are not completely exfoliated and are still stacked together to some extent. To validate this aspect ratio, an environmental TEM method is recommended for the future.

Appendix C

Table C1 Frequency sweep results of Bitumen A series

Tep. [°C]	Freq. [rad/s]	Base A (40/60)		A+4%Mt1		A+4%Mt2	
		Complex modulus [Pa]	Phase angle [°]	Complex modulus [Pa]	Phase angle [°]	Complex modulus [Pa]	Phase angle [°]
-10	1	142400000	21,16	166000000	23,24	219400000	24,2
-10	10	233700000	15,67	271200000	16,42	359400000	19,5
-10	100	317200000	10,08	379600000	10,91	408600000	10,41
-10	400	387500000	7,555			476200000	8,307
0	0,1	13800000	57,43	13850000	56,98	16150000	43,88
0	1	39140000	39,94	44890000	38,61	47750000	36,95
0	10	93720000	29,35	105500000	28,66	107800000	27,49
0	100	177500000	20,84	197400000	20,49	196100000	19,78
0	400	240100000	17,19	266200000	17,16	260300000	16,14
10	0,1	1290000	66,1	1651000	65,32	1863000	64,68
10	1	6600000	56,92	8595000	54,43	8914000	53,64
10	10	23140000	45,73	29330000	43,52	30410000	42,43
10	100	69330000	33,6	77410000	33,33	78670000	32,32
10	400	110000000	28,38	123500000	27,88	124300000	26,99
20	0,1	106000	76,45	134500	74,33	154100	75,73
20	1	716300	70,5	938900	68,66	1017000	68,89
20	10	3998000	61,89	5021000	59,64	5301000	58,92
20	100	16560000	50,67	19960000	48,54	20770000	47,78
20	400	36240000	43,19	39870000	42,19	41170000	41,03
30	0,1	11330	83,95	10090	82,27	14190	81,23
30	1	89030	78,22	79720	78,23	109200	76,65
30	10	609700	71,52	554600	71,51	723500	69,33
30	100	3297000	55,39	3049000	56,37	3639000	52,46
30	400	7247000	43,05	6854000	43,87	7664000	39,51
40	0,1	1432	87,57	1401	85,81	2008	85,57
40	1	13370	83,47	12300	82,8	17280	81,85
40	10	105400	79,4	97660	78,86	132100	77
40	100	735300	71,07	689000	71,73	878000	69,29
40	400	2125000	65	2019000	64,7	2475000	61,1
50	0,1	213,8	89,43	230,3	87,43	305,5	87,41
50	1	2181	87,39	2091	85,75	2811	85,78
50	10	19680	83,37	18550	83,39	24330	82,01
50	100	157600	78,38	148900	78,92	187500	77,1
50	400	516900	74,8	492300	75,26	600300	73,42
60	0,1	42,51	90,09	46,9	89,52	60,98	87,41
60	1	430,6	88,85	443,7	86,48	566,8	87,41
60	10	4066	87,08	3996	85,9	5230	85,13
60	100	36260	82,72	35030	83,05	44320	81,17
60	400	127700	79,74	124100	80,16	151700	78,3

Table C2 Frequency sweep results of Bitumen B series

Tep.	Freq.	Base B (70/100)		B+4%Mt0		B+4%Mt1		B+4%Mt2	
		Complex modulus [Pa]	Phase angle [°]	Complex modulus [Pa]	Phase angle [°]	Complex modulus [Pa]	Phase angle [°]	Complex modulus [Pa]	Phase angle [°]
[°C]	[rad/s]								
-10	0,1	53200000	39,25	58770000	36,97	50130000	36,49	2,16E+08	35,88
-10	1	118200000	26,65	142000000	25,84	129200000	25,21	140900000	25,9
-10	10	208300000	18,62	247200000	18,32	220900000	17,36	244800000	17,99
-10	100	306900000	12,53	359200000	12,24	315800000	11,62	356800000	12,01
-10	400	368500000	10,03	430900000	9,736	375700000	9,285	426400000	9,783
0	0,1	9812000	52,65	11310000	54,29	11070000	53,22	13660000	57,19
0	1	33200000	41,04	40070000	40,43	38970000	39,61	41880000	40,1
0	10	82110000	30,57	99360000	30,56	93380000	29,13	101200000	29,82
0	100	159800000	22,29	191900000	21,74	175000000	20,65	193200000	21,4
0	400	218800000	18,19	260800000	17,84	236500000	16,78	2,61E+08	17,64
10	0,1	901900	69,01	1114000	69,02	1213000	67,63	1,27E+06	67,35
10	1	4565000	59,24	5832000	58,49	6211000	57,11	6,09E+06	58,07
10	10	17650000	47,66	21950000	46,94	22540000	45,5	23210000	46,69
10	100	50850000	37,31	62520000	36,64	61160000	34,97	67440000	35,51
10	400	84960000	31,59	104200000	31,23	98790000	29,36	111700000	29,86
20	0,1	50860	79,05	50860	79,05	90310	76,68	90280	76,4
20	1	344300	73,48	323593,657	73,48	604000	71,04	583500	71,09
20	10	2059000	65,55	2059000	65,55	3375000	62,55	3552000	62,54
20	100	9626000	55,08	9626000	55,08	14460000	51,36	15970000	51,7
20	400	21210000	48,3	21210000	48,3	29700000	44,51	32480000	45,39
30	0,1	6744	84,63	8721	84,17	9870	82,77	9998	81,08
30	1	51450	80,09	72240	79,57	76460	78,56	77140	76,62
30	10	372200	73,91	519300	72,67	532500	72,15	517500	70,66
30	100	2203000	61,24	2880000	58,5	2957000	57,47	2816000	56,18
30	400	5325000	49,76	6720000	47,21	6695000	45,67	6298000	43,68
40	0,1	923,8	87,75	1045	88,01	1219	85,2	1478	84,46
40	1	7931	84,5	10040	84,36	10480	83,49	12410	81,62
40	10	64000	79,57	83200	80,26	84570	79,46	96210	77,55
40	100	463400	73,61	611900	72,92	602000	72,35	655900	70,74
40	400	1386000	67,05	1825000	67,08	1752000	65,08	1882000	63,29
50	0,1	148,4	89,26	168,4	89,58	196,9	86,99	252,6	86,03
50	1	1449	87,36	1704	87,77	1881	85,45	2256	84,94
50	10	13060	84,09	15590	84,17	16980	83,65	19230	82,21
50	100	107000	79,59	127200	79,49	138700	79,07	147900	77,76
50	400	355100	75,72	423500	76,02	457500	75,02	470200	74,11
60	0,1	28,96	89,73	36,98	90,1	41,81	88,69	54,02	88,09
60	1	285	89,07	361,2	89,41	379,5	85,91	494,9	85,55
60	10	2737	87,02	3492	86,9	3376	85,89	4405	84,99
60	100	24300	83,56	30910	83,34	29450	83,31	36760	81,84
60	400	86020	80,49	109800	80,45	101800	80,42	122000	79,14

6.5 Reference

- Chen, B. and J. R. G. Evans (2006). "Elastic moduli of clay platelets." Scripta Materialia 54(9): 1581-1585.
- Chen, D., Yang H., et al. (2005). "Rheological and extrusion behavior of intercalated high-impact polystyrene/organomontmorillonite nanocomposites." Composites Science and Technology 65(10): 1593-1600.
- Feng, M., F. Gong, et al. (2004). "Effect of clay on the morphology of blends of poly (propylene) and polyamide 6/clay nanocomposites." Polymer International 53(10): 1529-1537.
- Ferry, J. D. (1980). Viscoelastic properties of polymers, John Wiley & Sons Inc.
- Halpin, J. C. and J. L. Kardos (1976). "The Halpin-Tsai equations: a review." Polym. Eng. Sci 16(5): 344-352.
- Hsu, J. P., C. F. Shie, et al. (2005). "Sedimentation of a cylindrical particle in a Carreau fluid." Journal of colloid and interface science 286(1): 392-399.
- Jager, A., R. Lackner, et al. (2007). "Identification of viscoelastic properties by means of nanoindentation taking the real tip geometry into account." Meccanica 42(3): 293-306.
- Kojima, Y., A. Usuki, et al. (1993). "Mechanical properties of nylon 6-clay hybrid." Journal of Materials Research(USA) 8(5): 1185-1189.
- Kornmann, X., L. A. Berglund, et al. (1998). "Nanocomposites based on montmorillonite and unsaturated polyester." Polymer Engineering & Science 38(8): 1351-1358.
- Kuelppmann, A., M. A. Osman, et al. (2005). "Influence of platelet aspect ratio and orientation on the storage and loss moduli of HDPE-mica composites." Polymer 46(2): 523-530.
- Kunert, M. (2000). Mechanical properties on nanometer scale and their relations to composition and microstructure. A nanoindentation study on carbon implanted Ti-6Al-4V. Max Planck Institute. Stuttgart.
- Liu, G., M. v. d. Ven, et al. (2010). "A nanoindentation study on the rheological behaviour of bituminous binders." Journal of Wuhan University of Technology 32 (17): 47-50.
- Lu, H., G. Huang, et al. (2006). "Characterization of the linear viscoelastic behavior of single-wall carbon nanotube/polyelectrolyte multilayer nanocomposite film using nanoindentation." Thin Solid Films 500(1-2): 197-202.
- Lu, X. and U. Isacsson (1997). "Rheological characterization of styrene-butadiene-styrene copolymer modified bitumens." Construction and building materials 11(1): 23-32.
- Lu, X., U. Isacsson, et al. (1999). "Rheological properties of SEBS, EVA and EBA polymer modified bitumens." Materials and Structures 32(2): 131-139.
- Luciani, A., Y. Leterrier, et al. (1999). "Rheological behaviour of dilute suspensions of platelet particles." Rheologica Acta 38(5): 437-442.
- Morrison, F. A. (2001). Understanding rheology, Oxford University Press, USA.

- Okada, A. and A. Usuki (2006). "Twenty Years of Polymer Clay Nanocomposites." Macromolecular Materials and Engineering 291(12): 1449-1476.
- Oliver, W. C. and G. M. Pharr (1992). "Improved technique for determining hardness and elastic modulus using load and displacement sensing indentation experiments." Journal of materials research 7(6): 1564-1583.
- Polacco, G., S. Berlincioni, et al. (2005). "Asphalt modification with different polyethylene-based polymers." European Polymer Journal 41(12): 2831-2844.
- Sadr, A., Y. Shimada, et al. (2009). "The viscoelastic behavior of dental adhesives: A nanoindentation study." dental materials 25(1): 13-19.
- Simha, R. (1940). "The Influence of Brownian Movement on the Viscosity of Solutions." The Journal of Physical Chemistry 44(1): 25-34.
- Sneddon, I. N. (1965). "The relation between load and penetration in the axisymmetric Boussinesq problem for a punch of arbitrary profile." International Journal of Engineering Science 3(1): 47-57.
- Stangl, K., A. Jager, et al. (2006). "Microstructure-based identification of bitumen performance." Int J Road Mater Pavement 7: 111-142.
- Tweedie, C. A. and K. J. V. Vliet (2006). "Contact creep compliance of viscoelastic materials via nanoindentation." Journal of materials research 21(6): 1576-1589.
- Utracki, L. A. and J. Lyngaae-Jorgensen (2002). "Dynamic melt flow of nanocomposites based on poly- ϵ -caprolactam." Rheologica Acta 41(5): 394-407.
- Vlasveld, D. P. N., M. De Jong, et al. (2005). "The relation between rheological and mechanical properties of PA6 nano-and micro-composites." Polymer 46(23): 10279-10289.
- Zhu, L. and K. A. Narh (2004). "Numerical simulation of the tensile modulus of nanoclay filled polymer composites." Journal of Polymer Science Part B: Polymer Physics 42(12): 2391-2406.

7

FATIGUE-----FROM BINDER TO MIXTURE

7.1 Introduction

Fatigue is a common phenomenon in most materials, and refers to the changes in properties resulting from the applied cyclic loads. Usually, fatigue results in a reduction in stiffness and strength, and ends with fracture.

7.1.1 Fatigue in asphalt mixtures

7.1.1.1 Fatigue phenomenon

In many countries all over the world, traffic loads are increasing not only in number, but also in magnitude. As a result, these increasing vehicle loads accelerate the deterioration of asphalt pavement, and lead to fatigue cracking of which examples are shown in Figure 7.1.1.

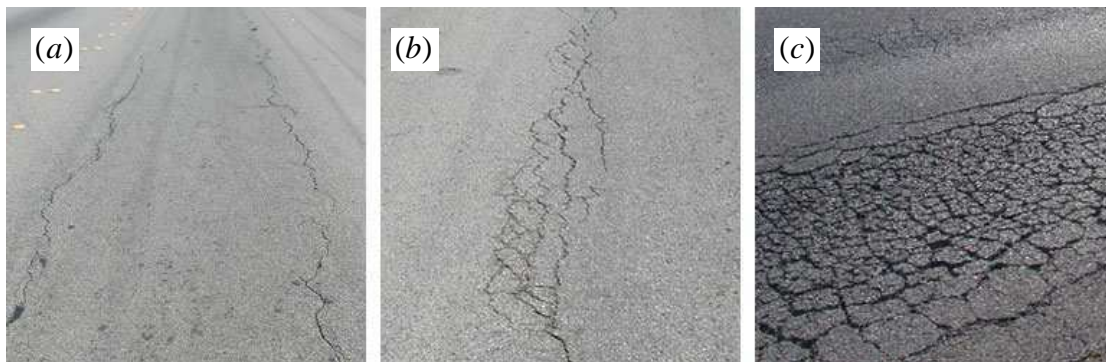


Figure 7.1.1 (a) Low-severity fatigue crack, (b) medium-severity fatigue crack, and (c) high severity fatigue crack (alligator crack) (Martin 2006)

The cracking can result in moisture penetration which could weaken the soil foundation. The combined effect of loads, cracks, weakened foundation etc. will lead to rapid failure of pavement structures. Therefore, it is meaningful to further understand the fatigue mechanism in relation to asphalt pavement performance.

7.1.1.2 Fatigue failure mechanism

Most fatigue cracks can be observed at the asphalt surface. According to the formation mechanism, two types of fatigue cracking are defined, being “bottom-up” and “top-down”.

Figure 7.1.2 shows the development of the stresses due to a moving wheel applied to an element in the pavement and how they change with time. Traditionally, it is believed that bottom-up cracking which propagates upward is due to the tensile stress at the bottom of the asphalt layer. Gradually, it becomes visible at the pavement surface as some longitudinal or transverse cracks in the wheel tracks, forming even a cracking pattern like the alligator skin in a serious situation (Molenaar 2007). The accelerated pavement testing device, Lintrack of the Delft University of Technology proved the presence of these cracks and growth at the bottom of the asphalt layer (Medani and Molenaar 2000).

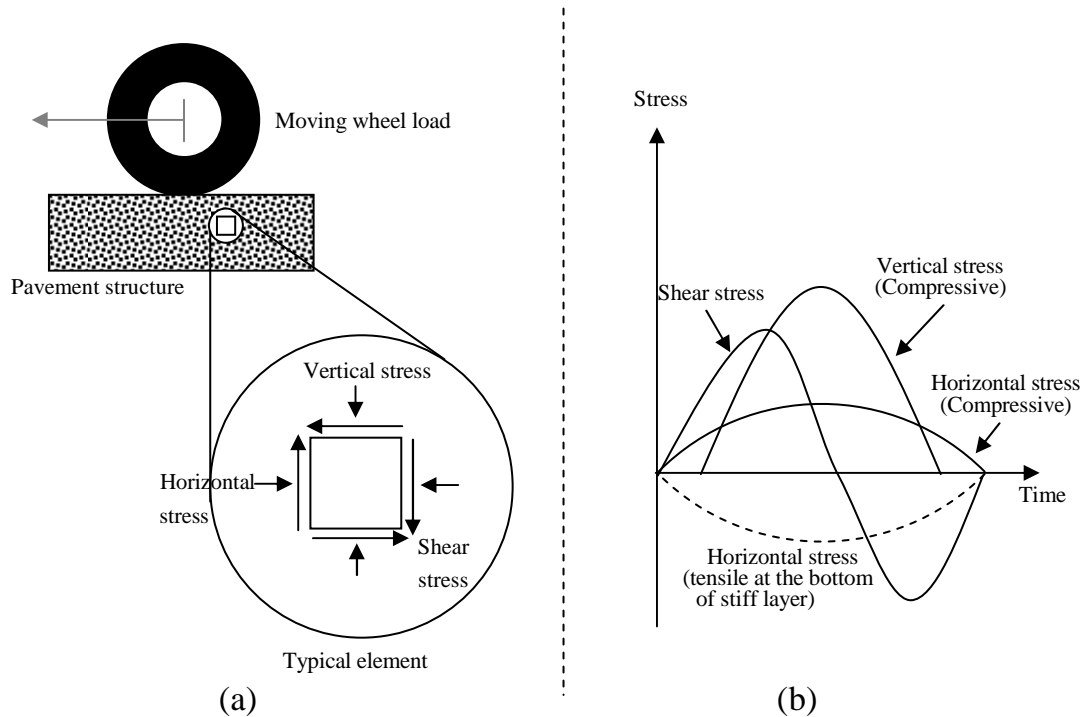


Figure 7.1.2 (a) an element in a pavement and (b) stresses on the element

With respect to the top-down cracking, some researches indicate that these cracks initiate at the surface, and are mostly due to the horizontal shear stresses under the tire in the wheel track (Molenaar 1983; Gerritsen 1988). These shear stresses result in local high tensile strains nearby the tyre edge, and are responsible for the premature longitudinal surface cracking. Severe bitumen hardening occurring at the surface also contributes to the early top-down cracking (Rolt 2000). The

occurrence of this cracking has little to do with the structural strength of the pavement.

7.1.1.3 Laboratory methods and criteria

Methods

In the laboratory, the parallel-plates (P-P) device in the dynamic shear rheometer (DSR) is normally used to evaluate the fatigue properties of bitumen and mortar. Figure 7.1.3 shows some phenomena taking place during the fatigue testing in the DSR (Bodin, Soenen et al. 2004).

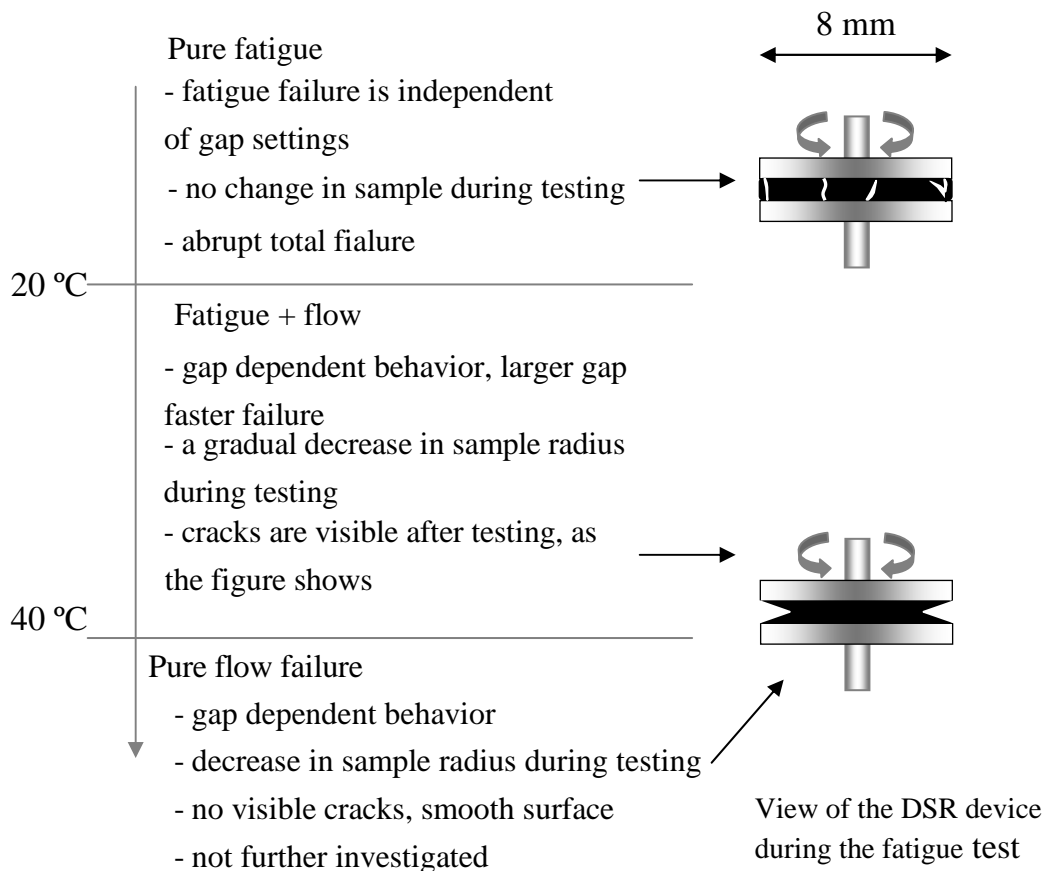


Figure 7.1.3 Schematic representation of the different phenomena taking place in the DSR during binder fatigue testing (Bodin, Soenen et al. 2004)

With respect to asphalt mixtures, Figure 7.1.4 gives a summary of several fatigue testing methods. Different countries in Europe prefer different methods. For example, the four-point bending beam test is normally used in the Netherlands, the indirect tensile test in Sweden, and the two-point bending test in France. The fatigue result is related to the method, the size of specimen, loading mode, etc. Whatever test is used, the results only reflect the fatigue properties of specimen, and not the properties of the material. In order to relate laboratory fatigue to field

fatigue, shift factors are needed, which vary hugely due to different testing conditions and the field environment.

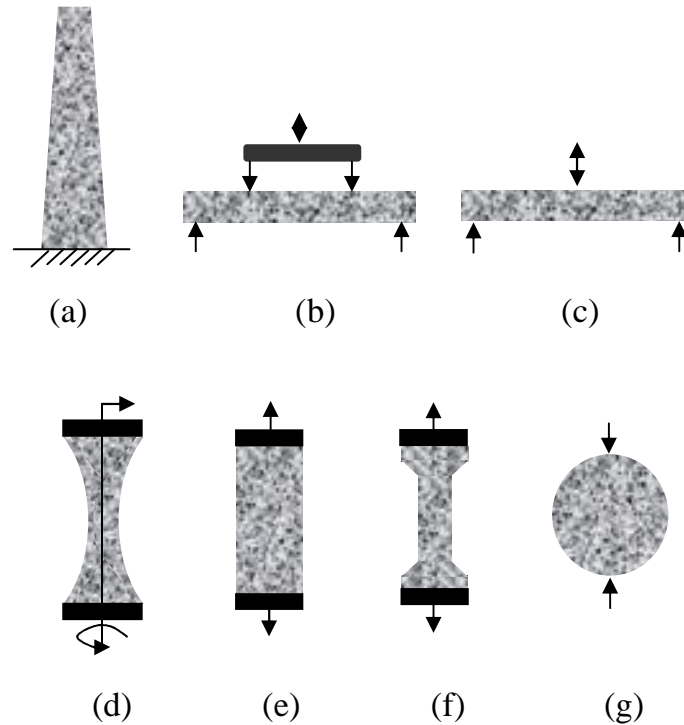


Figure 7.1.4 Schematic summary of several fatigue test methods: (a) two point bending; (b) four point bending; (c) three point bending; (d) rotating bending; (e) direct axial loading; (f) direct axial loading (necked specimen); (g) the indirect tensile test

Traditional fatigue criteria

Fatigue tests in the laboratory are normally performed in two loading modes: the strain controlled and the stress controlled mode. In the strain controlled mode, fatigue failure is defined when a 50% reduction of the initial stiffness modulus is reached. In the stress controlled mode, fatigue failure is traditionally considered to occur when the modulus is at 10% of its original value. These definitions are somewhat arbitrary and do not represent the internal state of the material.

The dissipated energy criteria

An estimate of the fatigue life based on dissipated energy was reported by van Dijk et al. (1972) and Chomton et al. (1972). Due to the viscoelastic behaviour of asphalt mixtures at ambient temperatures, energy is dissipated during loading and unloading periods, as demonstrated in Figure 7.1.5 in which the comparison

between a linear elastic material and a viscoelastic one is given. Within an elastic material (Figure 7.1.5b), all the energy is stored in the material during the loading period and will be recovered during the unloading period. For a viscoelastic material, there is a hysteresis loop during the loading and unloading periods (Figure 7.1.5c). The dissipated energy is equivalent to the area within the loop. The sustained hysteresis was stated as a necessary condition for fatigue, and was related to the rate of damage accumulation (Erber, Guralnick et al. 1993). It is commonly believed that a large part of the dissipated energy is translated into heat, and just a small part contributes to damage during the fatigue test.

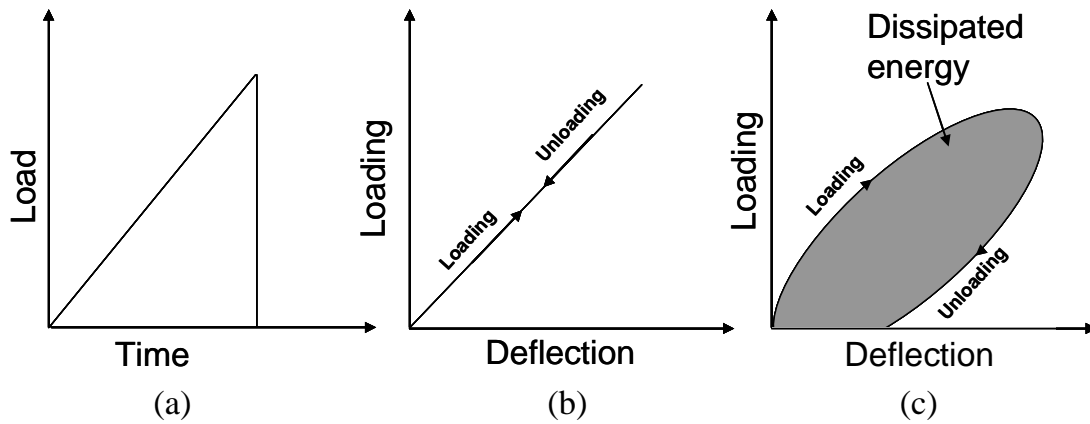


Figure 7.1.5 (a) Load versus time applied on specimen, (b) a linear elastic behaviour, and (c) a viscoelastic behaviour (Rowe 1996)

When a viscoelastic material is sinusoidally loaded, and the load and deflection relationship are expressed using stress and strain, the dissipated energy per loading cycle is obtained as follows:

$$w_i = \pi \sigma_i \varepsilon_i \sin \phi_i \quad 7.1.1$$

where,

- w_i =dissipated energy at cycle i ,
- σ_i =stress amplitude at cycle i ,
- ε_i =strain amplitude at cycle i , and
- ϕ_i =phase lag at cycle i .

Hopman et al. (1989) proposed a ratio of energy dissipation, and the following researchers (Pronk 1995; Anderson, Hir et al. 2001) named it as dissipated energy ratio (DER) which was defined as follows:

$$DER = \frac{\sum_{i=1}^n w_i}{w_n} \quad 7.1.2$$

where,

$\sum_{i=1}^n w_i$ = the total sum of dissipated energy up to cycle n, and
 w_n = the dissipated energy at cycle n.

Bahia et al. (2001) applied the DER concept to analyze the fatigue behavior of binders under strain and stress control modes, as shown in Figure 7.1.6. The intersection of the two asymptotes determines the fatigue life (N_p).

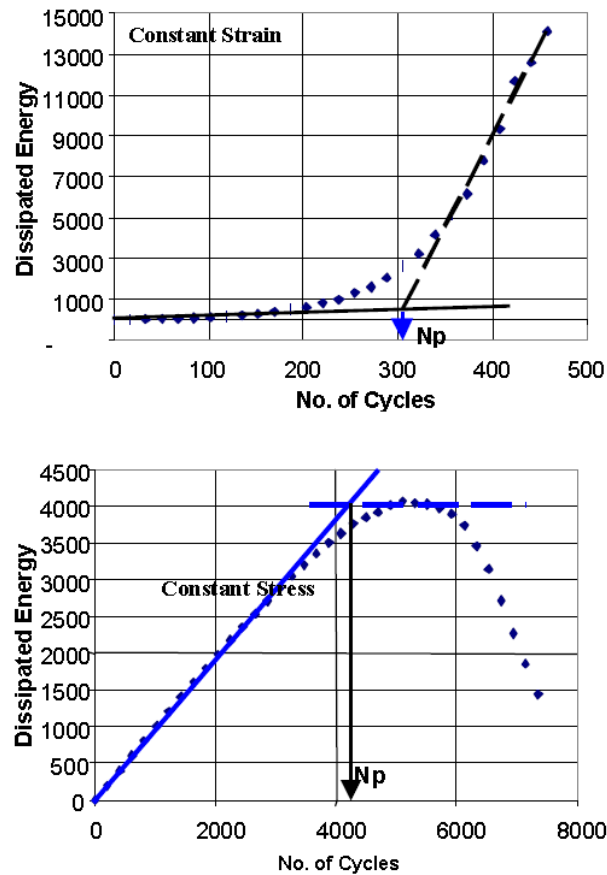


Figure 7.1.6 Fatigue life criterion under the strain and stress control modes (Bahia, Zhai et al. 2001)

Ghuzlan and Carpenter (2000) proposed a fatigue criterion based on dissipated energy for asphalt mixtures, named as a ratio of dissipated energy change (RDEC). This criterion was defined as the change in dissipated energy (ΔDE) between

cycles n and $n+1$ divided by the total dissipated energy (DE) at load cycle n , following:

$$\frac{\Delta DE}{DE} = \frac{\left| \sum_i^n w_i - \sum_i^{n+1} w_i \right|}{\sum_i^n w_i} \quad 7.1.3$$

where,

$\sum_i^n w_i$ = the total sum of dissipated energy up to cycle n , and

$\sum_i^{n+1} w_i$ = the total sum of dissipated energy up to cycle $n+1$.

Bahia et al. (2001) stated that the $\frac{\Delta DE}{DE}$ approach was more useful in the stress controlled mode than in the strain controlled test. The scattered points shown in Figure 7.1.7 made it impossible to clearly define the N_p value from the strain controlled test.

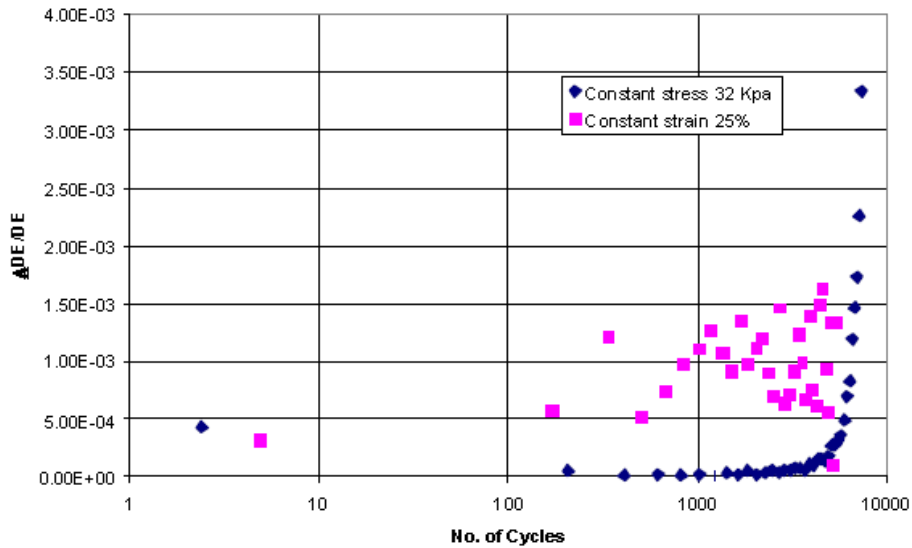


Figure 7.1.7 Ratio of dissipated energy change (RDEC) under the strain and stress control modes (Bahia, Zhai et al. 2001)

Fatigue models based on the dissipated Energy

Several models had been made to build the relationship between fatigue life and the dissipated energy. Van Dijk (1975) proposed a unique relationship between the number of load applications to fatigue life (N_f) and the total dissipated energy per unit volume to the fatigue point, characterized by

$$W_{tot} = AN_f^z \quad 7.1.4$$

where,

W_{tot} = total cumulative dissipated energy to fatigue failure, and

A and z = factors related to the properties of material.

Function 7.14 can also be transformed to the following equation,

$$\bar{W} = \frac{W_{tot}}{N_f} = AN_f^{z-1} \quad 7.1.5$$

where,

\bar{W} = the mean energy dissipated per cycle.

An important parameter ψ was introduced by Dijk (1975) and defined as follows,

$$\psi = \frac{W_{initial}}{W_{tot}}, \quad \text{with } W_{initial} = N_f \cdot \pi \cdot \sigma_0 \cdot \varepsilon_0 \cdot \sin \phi_0 \quad 7.1.6$$

where,

σ_0 = the initial stress,

ε_0 = the initial strain, and

ϕ_0 = the initial phase angle.

As indicated in Figure 7.1.8, this parameter proved to be related to the loading mode and the mix stiffness (van Dijk 1975). For a strain control mode, ψ was between 1 and 1.5, and for a stress control mode, it was between 0.5 and 1. It was almost close to 1 for both control modes as the stiffness increased in magnitude. This meant that at a high mixture stiffness, ψ would be independent of loading mode.

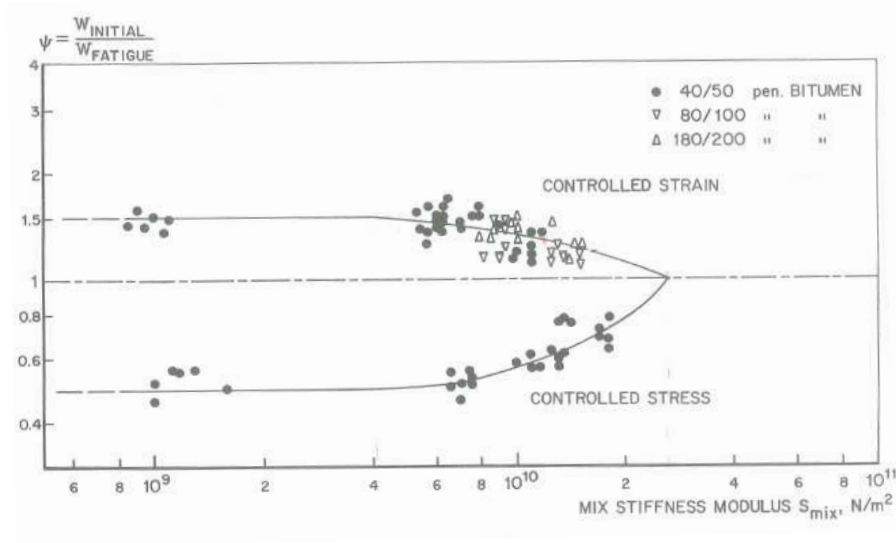


Figure 7.1.8 Relation of ψ and mixture stiffness modulus for the asphalt concrete (van Dijk 1975)

Combining the functions 7.1.5 and 7.1.6, van Dijk (1975) devised the following fatigue life relation:

$$N_f = \left[\frac{\pi \cdot S_{initial} \cdot \sin \phi_0}{A\psi} \right]^{\frac{1}{z-1}} \cdot \epsilon_0^{\frac{2}{z-1}} \quad 7.1.7$$

where,

$$S_{initial} = \sigma_0 / \epsilon_0, \text{ the initial fatigue stiffness modulus.}$$

A simple fatigue model for the mortar was developed by Mo (2010), as follows,

$$N_f = \left(\frac{w_{initial}}{W_0} \right)^{-b} \quad 7.1.8$$

where,

$$w_{initial} = \pi \cdot \sigma_0 \cdot \epsilon_0 \cdot \sin \phi_0, \text{ the initial dissipated energy,}$$

$$W_0 = \text{the energy limit that will lead to failure within one cycle, and}$$

$$b = \text{model constant.}$$

Although Mo's relationship between the initial dissipated energy per cycle and the number of cycles to failure may not be well explained by a simple power law describe above, this model showed a good fit with the test data (Mo 2010).

The fracture mechanics approach

In the mechanistic approach, fatigue behavior of asphalt concrete was considered as a damage process, and fracture mechanics principles were used in order to take into account the detrimental effect of stress concentrations around the crack tip of asphalt mixtures (Paris and Erdogan 1963; Molenaar 1983; Molenaar 1984; Si, Little et al. 2002). Fatigue life, under a given state of stress, was defined as the number of loading cycles during which damage increased according to a crack propagation law from an initial state to a critical level (Si, Little et al. 2002).

This approach was based on the fracture mechanics theory, and Paris's crack growth law (Paris and Erdogan 1963) was used, which is as follows:

$$\frac{dc}{dN} = AK^n \quad 7.1.9$$

where,

- K = stress intensity factor,
- c = crack length, and
- N = number of loading cycle.

The stress intensity factor K depends on the structure and the type of loading. Three loading types are summarized in Figure 7.1.9:

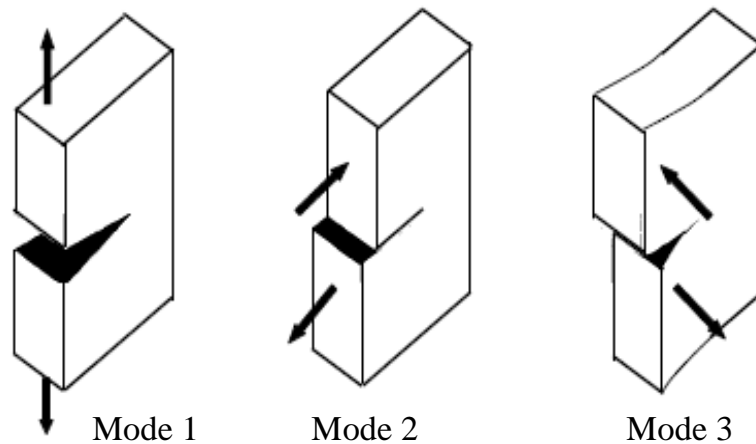


Figure 7.1.9 Three modes of loading to describe the crack growth phenomenon (Broek 1991)

The first is the opening mode with tensile or bending stresses; the second is the sliding or shearing mode with shear stresses; and the last one is the tearing mode with torsional stresses. The first two modes are very important to the initiation of asphalt's cracking. Bending stress in mode 1 at the bottom of layers could lead to the bottom-up cracking in the asphalt. Shear stress in mode 2 and loading

conditions following mode 3 could take place at the contact area between tire and road, and results in the top-down cracking.

Given A and n are known, the fatigue life of the material can be calculated using following equation:

$$N_f = \int_{c_0}^{c_f} \frac{dc}{AK^n} \quad 7.1.10$$

where,

c_0 = the initial crack length, and

c_f = final crack length.

Molenaar (1984) gave the A -value between 5×10^{-3} and 5×10^{-9} N/mm^{1.5}, and n -value between 2 and 5 using uniaxial tensile tests on various Dutch mixtures, tested at frequencies between 1 and 10 Hz, and temperatures between 5 and 25 °C.

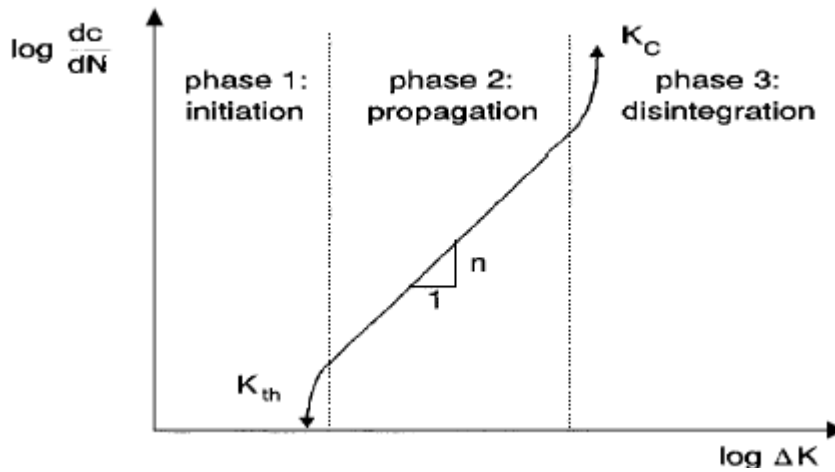


Figure 7.1.10 Fatigue crack growth (Ewalds and Wanhill 1986)

As shown in Figure 7.1.10, there are three distinctive stages in fatigue: initiation, propagation, and failure (Ewalds and Wanhill 1986). ΔK in this figure was the difference between maximum and minimum stress intensity factor K during dynamic loading. The three phases are defined as follows:

- The initiation phase: the development of microcracks.
- The propagation phase: the development of macro cracks out of microcracks. In this phase, a stable crack growth occurs.
- The disintegration phase leading to collapse and final failure of the material. In this phase, an unstable crack growth can be observed.

7.1.2 Fatigue in polymer-clay nanocomposites (PCN)

An interesting fatigue phenomenon of one nanocomposite has been reported by Jin et al (2006). In this research, polyurethane used as damping material, was modified by 3 wt.% of an organic nanoclay, and an intercalated nanocomposite was synthesized. The clay layers showed reversible deformation behaviour during the uniaxial tension fatigue test, and this behaviour was recorded through the change of the basal spacing of clay layers measured by XRD. Figure 7.1.11 gives a schematic diagram for this reversible behaviour.

Based on this behaviour, it was assumed that each unit composed of two clay layers and intercalated polymer chains behaved like a nanospring. On this assumption, these nanospring systems could play an important role in reducing the concentrated stress in the material, and prevent the development of fatigue cracks. Therefore, the fatigue resistance of composite was improved, which had been proved by the experiment

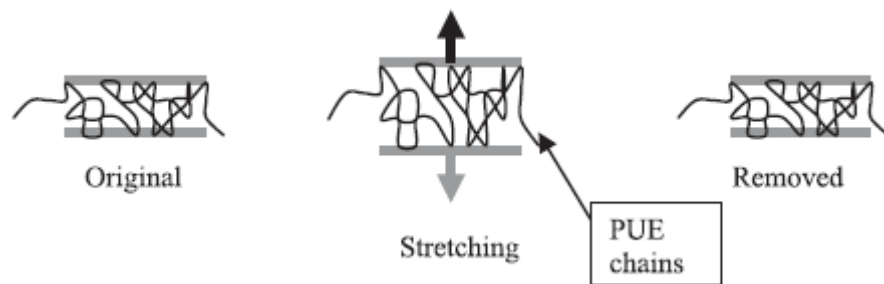


Figure 7.1.11 Schematic diagram of the basal spacing on a nanoscale change during the uniaxial tension fatigue test (Jin, Chen et al. 2006)

7.1.3 Conclusion

Although fatigue of asphalt mixtures is a complicated phenomenon, the methods and theories introduced above give possibilities to evaluate fatigue properties in the laboratory. It should be realized that the results obtained in the laboratory only reflect the fatigue properties of specimen itself, not the properties of material. However, they are still useful and meaningful for pavement design and determining effect of mixture modification.

It is arbitrary to define the fatigue failure of bitumen or asphalt mixture specimens as the number of load repetition at which the stiffness modulus reduces to a 50% of the initial stiffness modulus in the strain controlled mode or to 10% of the initial stiffness modulus in the stress controlled mode. Although the fracture mechanics approach gives a fundamental description of fatigue, it is more complicated and beyond the scope of this study. By comparison, the dissipated energy ratio (DER) gives a clearer definition of fatigue failure, especially in the stress controlled mode.

Therefore, this method is used in evaluating the fatigue properties of bitumen and motar in this research.

Polymer materials normally benefit from the addition of nanoclay in the terms of mechanical properties, thermal stability and barrier properties. The main reasons for these improvements are the strong interfacial interactions between the matrix and the nanoclay, and the size effect of the nanoclay (Ray, Bousmina et al. 2005). However, weak interfacial interactions could even worsen these properties. Unfortunately, only a limited amount of literature can be found about the contribution of nanoclay to the fatigue properties of polymer. The reason could be that fatigue was not the main research focus in most PCN materials, when comparing with other properties. However, fatigue as one of main damage forms of asphalt has to be taken into account when modifying asphalt mixture with nanoclay.

7.2 Experimental program

7.2.1 Raw materials

The materials used in this study include bitumen, montmorillonite nanoclay (Mt), filler, fine sand, and stones.

7.2.1.1 Bitumens

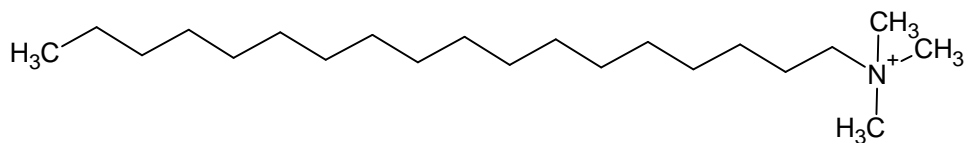
Bitumens with normal paving grades, 40/60 (A) and 70/100 (B) were provided by Kuwait Petroleum Research & Technology B.V., and were used as base material for the modification. Their empirical rheological properties are listed in Table 7.2.1. More detailed information about the rheological properties of base and modified bitumens can be found in Chapter 3.

Table 7.2.1 Empirical rheological properties of base bitumens

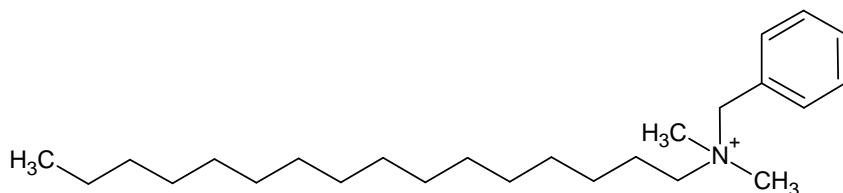
Bitumens	Penetration @ 25°C [0.1mm]			Softening point [°C]		
	Fresh	RTFOT	PAV	Fresh	RTFOT	PAV
A (40/60)	42	27	17	50.0	55.4	61.6
B (70/100)	77	47	28	46.0	51.2	57.2

7.2.1.2 Montmorillonite nanoclay (Mt)

Two organo montmorillonites, the Mt1 and the Mt2 were used to modify the bitumen. They were provided by the Fenhong Clay Chemical Factory, China. The Mt1 had been organically treated by octadecyl trimethyl ammonium salt, and the Mt2 by benzyl dimethyl hexadecyl ammonium salt. The molecule structures of these two cations contained in the nanoclays are shown in Figure 7.2.1. The Mt1 has an apparent density of 1.78 g/cm³, and the Mt2 of 1.83 g/cm³. More detailed information about the nanoclay can also be found in Chapter 3.



(a) Octadecyl trimethyl ammonium cation



(b) Benzyl dimethyl hexadecyl ammonium cation

Figure 7.2.1 Schematic molecular structure of ammonium salt cations: (a) in the Mt1 and (b) in the Mt2

7.2.1.3 Filler and sand

In this study, fine sand and filler were blended with bitumen for the preparation of the mortar. The sand used was crushed sand with a nominal maximum aggregate size of 2 mm. The gradation is shown in Table 7.2.2. The density of the fine sand is 2.675kg/m³

Table 7.2.2 Grading of fine sand

Sieve size [mm]	4.0	2.0	0.5	0.18	0.063
Passing percentage [%]	100.0	93.6	34.1	11.0	1.8

The applied filler was a Wigro 60k limestone filler with 25-35 wt. % hydrated lime. Its characteristics are listed in Table 7.2.3

Table 7.2.3 Characteristics of Wigro 60K

Density kg/cm ³	Limestone powder wt. %	Hydrate d lime wt. %	Bitumen number ml/100g	Cumulative retained on the sieve %	Solvabilit y in HCl wt. %	Voids vol. %
2475-2675	65-75	25-35	56-62	2mm : 0 0.09mm : 0-15 0.063mm: 5-25	68-88	44-50

7.2.1.4 Stones

Crushed Norwegian granite was used in the asphalt mixture. Through sieving by hand, the granite was divided into seven piles of stones with different sizes.

Apparent particle densities of the stones are listed in Table 7.2.4, and the particle size distribution of each fraction is shown in Table 7.2.5.

Table 7.2.4 Apparent particle density of stones

Size of stones [mm]	11.2-16	8-11.2	5.6-8	4-5.6	2-6	1-2	0-1
Apparent particle density [kg/m ³]	2711.4	2706.9	2629.9	2700.7	2702.6	2682.7	2647.8

Table 7.2.5 Passing percentage for each type of stones [%]

Sieve size [mm]	Size of stones [mm]						
	11.2-16	8-11.2	5.6-8	4-5.6	2-6	1-2	0-1
0.063	0.0	0.0	0.0	0.30	0.2	0.0	7.0
0.18	0.0	0.0	0.0	2.6	1.3	0.0	28.7
0.5	0.0	0.0	0.0	4.60	1.7	0.0	66.2
1	0.0	0.0	0.0	6.90	2.7	2.0	100.0
2	0.0	0.0	0.0	13.9	13.8	74.3	100.0
2.8	0.0	0.0	0.0	30.0	30.0	98.0	100.0
4	0.0	0.0	0.0	51.2	71.9	99.9	100.0
5.6	0	0	2.0	100.0	96.7	100.0	100.0
8	0	18.8	87.6	100.0	100.0	100.0	100.0
11.2	4.6	88.7	100	100.0	100.0	100.0	100.0
16	86.3	100	100	100.0	100.0	100.0	100.0

7.2.1.5 Specimen preparation

Bitumen

With respect to bitumen, fatigue testing was conducted on the base bitumen 70/100 (B) and bitumens modified by two organic nanoclays Mt1 and Mt2. The preparation of modified bitumen has been discussed in detail in Chapter 3. Fatigue tests were done on the virgin bitumens. Ageing was only taken into account in the fatigue test performed on the mortar. Table 7.2.6 gives the codes of bitumen in the fatigue test.

Table 7.2.6 Codes of base and modified bitumens used in the fatigue test

Codes	Nanoclay type	Clay content [mass %]
70/100 (B)	-	0
B+4%Mt1	Mt1	4
B+4%Mt2	Mt2	4

Mortar

The mortar consisting of bitumen, filler, and sand is the real glue that binds the aggregate particles together in the asphalt mixture. According to Muraya's

research (2007), aggregate skeletons of porous asphalt (PAC), stone matrix asphalt (SMA), and dense asphalt mixtures are composed of aggregates larger than 0.5 mm, 2mm, and 0.063mm, respectively. The aggregates less than 0.5mm and 2mm for PAC and SMA specimens were observed to segregate during mixing. Based on the observation, he concluded that particles less than 0.5 mm and 2mm for PAC and SMA were not part of the aggregate skeleton. Therefore, the fine sand was sieved by hand in this research and the part smaller than 0.5 mm was only used in the mortar's preparation.

It is well known that the ageing and fatigue of the mortar used in porous asphalt concrete could result in raveling. This was the reason why fatigue properties of mortar were investigated in this study. The following mass ratio for the mortar was adopted in this study, 0.34:0.30:0.36 (bitumen : filler : fine sand). Two types of bitumens, base 70/100 (B) and one modified by Mt2 were used in the mortar's preparation. The filler and fine sand were uniformly blended with bitumen at a temperature of 175°C.

In addition, the mortar was subjected to a short ageing protocol to simulate the ageing that occurred during mixing, laying and compaction of the asphalt mixture in the field. The process of the ageing was as follows: first, the mortar was heated to 185 °C and then poured over a flat silicone paper on the tray to form a film with a thickness of 2 mm; next, the tray was kept in an oven for 1.5 hours at a temperature of 175 °C; finally, the mortar on the tray was taken out for the specimen preparation.

A special mould made of silicone plastic was designed for preparing the mortar specimen. After mixing and ageing, the mortar was heated to 175 °C, and agitated until it was flowable. Then, the mortar was carefully poured into the mould. After casting, the mould was placed in an oven with a temperature of 175 °C for a few minutes to remove air voids in the specimen. After that, the mould was first cooled down at room temperature, and then stored at -10 °C for 2hours till the specimens could be removed from the mould. The whole process and the size of the specimen are shown in Figure 7.2.2. More information on the specimen preparation can be found elsewhere (Khedoe and Moraal 2007; Mo 2010).

Long term ageing of the mortar could not be neglected, and had been performed by Khedoe and Moraal (2007) using a weatherometer. The data about the long term ageing presented by Mo (2010) however showed the complexity of the weatherometer method. To better qualify the effect of the nanoclay on the properties of the mortar, it was therefore decided to do the fatigue tests only on the fresh and short term aged mortars.

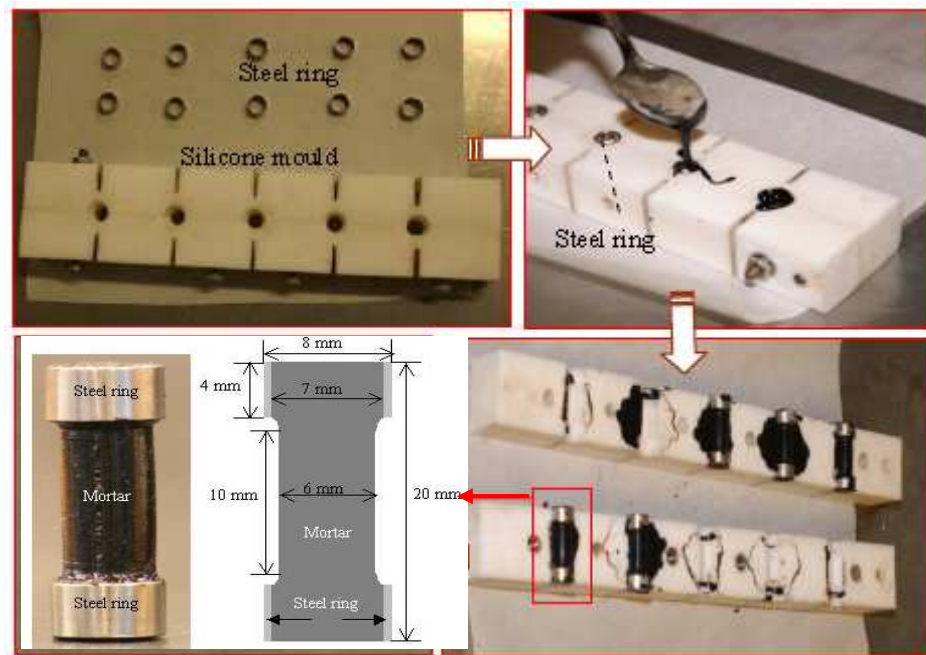


Figure 7.2.2 Preparation of the mortar specimens (upper left: steel rings and silicone mould; upper-right: casting hot mortar into the mould; bottom-right: opening the mould to remove the specimens; bottom-left: the obtained specimen and its geometry) (Khedoe and Moraal 2007; Mo 2010)

Mixture

Two mixtures, one with the base bitumen (A 40/60) and another with the modified bitumen (A+4%Mt2) were prepared for the fatigue test. The mass content of each component in the mixture is given in Table 7.2.7. The gradation (0/16) of the dense mixture is shown in Figure 7.2.3.

Table 7.2.7 Mixture components for dense mixture 0/16 design

Component type	% [mass/(total mass of aggregates)]
22.4 - 16	0
16-11.2	14.0
11.2-8	14.0
8-5.6	15.0
5.6-4	12.0
6-2	11.0
2-1	13.0
1-0	15.0
Wigro 60k filler	6.0
bitumen content *	6.0

*: Bitumen content on 100% aggregates by mass

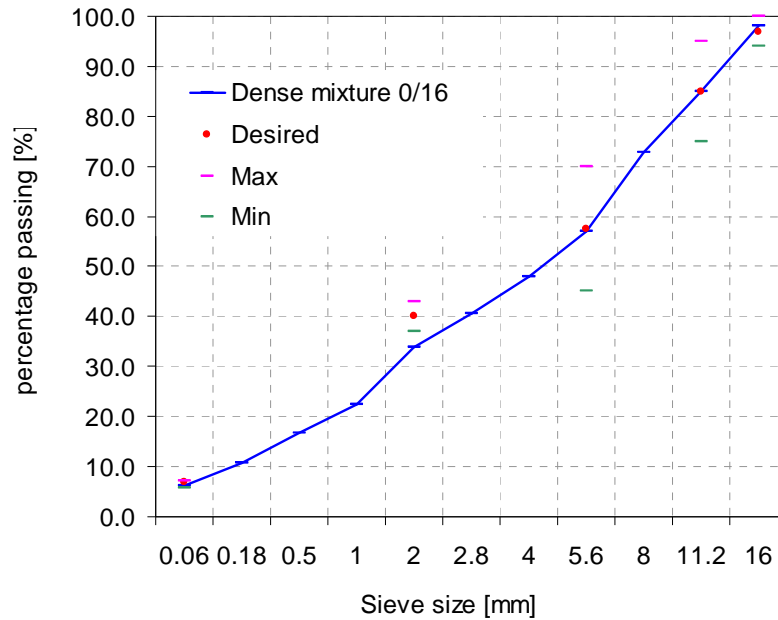


Figure 7.2.3 Gradation of dense mixture 0/16.

Marshall specimens were prepared by compacting each side of specimen with 75 blows. To reach the same air void, the mixing temperatures were 170 °C and 175 °C for the base and modified bitumen, respectively. For each mixture, five Marshall specimens with a thickness of 35 mm were prepared for testing. Their volumetric properties are presented in Table 7.2.8.

Table 7.2.8 Codes and fatigue test conditions for the mixture

Specimen*	Air voids [%]	Stress [MPa]	Specimen*	Air voids [%]	Stress [MPa]
SM-1	3.0	1.92	MM-1	2.8	1.92
SM-2	3.1	1.61	MM-2	3.0	1.62
SM-3	2.5	1.20	MM-3	2.3	1.19
SM-4	2.5	0.89	MM-4	2.8	0.89
SM-5	3.0	0.50	MM-5	3.3	0.50

*:Note that SM is the standard mixture specimen, and MM is the modified mixture specimen. All of them are with a height of 35 mm and a diameter of 101.5 mm.

7.2.2 Test description and interpretation

7.2.2.1 Testing of the bitumen

Test description

The cone and plate (C-P) device was used in the DSR AR 2000ex to perform the bitumen fatigue test. As shown in Figure 7.2.4, the diameter of cone and plate was 8 mm, the angle of cone was 26.6°, and the thickness of edge film was 2 mm. The tip of cone was cut off over a height of 0.065 mm, and a gap of this magnitude (0.065 mm) was kept during the test to avoid blocking by some fine particles from bitumen.



Figure 7.2.4 Image of the C-P device used in the fatigue test

Table 7.2.9 gives the testing parameters. The tests were performed in the stress controlled model and at a temperature of 10 °C. Three shear stress levels were chosen in order to limit the fatigue time between 1 and 3 hours and assure an adequate development of fatigue damage in the samples.

Table 7.2.9 Parameters in the bitumen fatigue test

Items	Value
Applied shear stress [MPa]	0.4, 0.5, and 0.6
Frequency [Hz]	10
Temperature [°C]	10
Duration [hours]	1-3

Test interpretation

As introduced in section of 7.1.1.3, the parallel-plates (P-P) device in the DSR instrument was used for the fatigue test on bitumen. The following paragraphs discuss why in this study the C-P device was preferred over the P-P device.

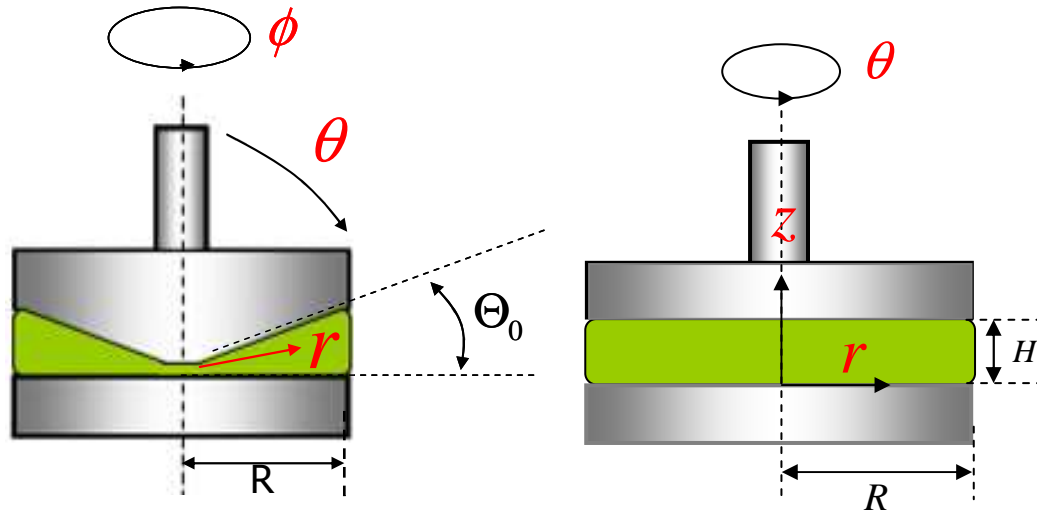


Figure 7.2.5 Schematics of (a) a C-P device in the spherical coordinate system r, θ, ϕ , and (b) a P-P device in the cylindrical coordinate system r, θ, z .

Figure 7.2.5 gives the schematics of both devices in different coordinate systems. Using the spherical coordinate system r, θ, ϕ for a C-P device, the Newtonian constitutive equation for the flow in the space is as follows:

$$\underline{\underline{\tau}} = \begin{pmatrix} 0 & 0 & 0 \\ 0 & 0 & \eta \left(\frac{\Omega}{\Theta_0} + \frac{\Omega}{\Theta_0} \left(\frac{\pi}{2} - \theta \right) \cot \theta \right) \\ 0 & \eta \left(\frac{\Omega}{\Theta_0} + \frac{\Omega}{\Theta_0} \left(\frac{\pi}{2} - \theta \right) \cot \theta \right) & 0 \end{pmatrix}_{r\theta\phi} \quad 7.2.1$$

where,

- $\underline{\underline{\tau}}$ = shear stress tensor,
- η = viscosity of flow,
- Ω = angular velocity of the cone, and
- Θ_0 = cone angle.

Then, this constitutive equation can be transformed to one simple scalar equation:

$$\tau = \eta \frac{\Omega}{\Theta_0} \left[1 + \left(\frac{\pi}{2} - \theta \right) \cot \theta \right] \quad \left(\frac{\pi}{2} - \Theta_0 \leq \theta \leq \frac{\pi}{2} \right) \quad 7.2.2$$

where,

τ = the stress scalar.

Equation 7.2.2 indicates that τ is only related to θ , when other parameters can be regarded as constants.

If the cone angle Θ_0 is extremely small, and θ is close to $\frac{\pi}{2}$, we obtain

$$\tau_{\frac{\pi}{2}-\Theta_0} = \tau_{\frac{\pi}{2}} = \eta \frac{\Omega}{\Theta_0} \quad 7.2.3$$

Equation 7.2.3 indicates that the shear stress is constant and uniform in the C-P device when an extremely small cone angle is used. However, the cone angle Θ_0 used in this study was equal to 0.464 rad (around 26.6°), and could not be regarded as extremely small. After substituting θ equal respectively to $\frac{\pi}{2} - \Theta_0$ and $\frac{\pi}{2}$ into

Equation 7.2.2, we obtain a ratio as follows:

$$\tau_{\frac{\pi}{2}-\Theta_0} : \tau_{\frac{\pi}{2}} = 1.2 : 1 \quad 7.2.4$$

The ratio means that the shear stress distribution does not vary too much, and can still be regarded as almost constant and uniform in the C-P device.

Similarly, we obtain the shear stress tensor $\underline{\underline{\tau}}$ and scalar τ in the cylindrical coordinate system r, θ, z for the P-P device, as follow:

$$\underline{\underline{\tau}} = \begin{pmatrix} 0 & 0 & 0 \\ 0 & 0 & \eta \frac{r\Omega}{H} \\ 0 & \eta \frac{r\Omega}{H} & 0 \end{pmatrix}_{r\theta\phi} \quad 7.2.5$$

and

$$\tau = \eta \frac{R\Omega}{H} \quad (0 \leq r \leq R) \quad 7.2.6$$

where,

Ω = angular velocity of the plate, and

H = the gap distance between the two plates.

Equation 7.2.6 indicates that the shear stress τ in the middle of plate is equal to 0, and reaches the maximum of $\eta \frac{R\Omega}{H}$ at the edge. Therefore, the shear stress distribution in the P-P device is not uniform, which means that the fatigue cracks as shown in Figure 7.1.3 can not occur at the same time. More mathematical background about this can be found in the book by Morrison (2001).

The fatigue failure in the C-P device (Figure 7.2.6) was annular, and visible from the edge to the centre which is due to the uniform shear stress, and the simultaneous fatigue occurrence on the whole cross section.



Figure 7.2.6 Typical fatigue failure impressions on the cross section in the C-P device

Figure 7.2.7 shows the comparison between fatigue curves (the dissipated energy ratio versus the number of loading cycles) using both devices on the base 70/100 bitumen. Fatigue life hereafter was defined as the number of cycles corresponding to the peak point of curve. As indicated, the fatigue life determined by the C-P device was shorter than that determined by the P-P device at the same shear stress level, which meant that the C-P device can save lots of time to complete the fatigue test. A shift factor of around 1.5 was observed for the fatigue life determined by the C-P device to the one determined by the P-P device. This shift is related to the internal shear stress and the material volume in each device.

Because of the advantage of the uniform shear stress distribution and the shorter time needed for a fatigue test, the C-P device was preferred to evaluate the fatigue properties of bitumen.

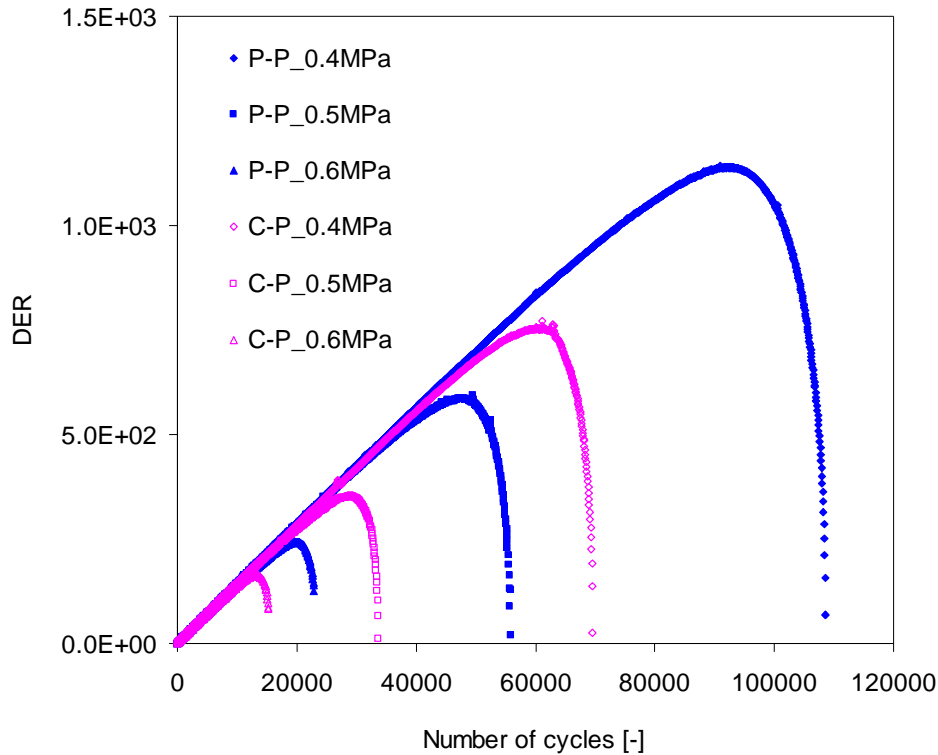


Figure 7.2.7 Comparison between fatigue curves when using the C-P device and the P-P device at three shear stresses.

7.2.2.2 Testing of the mortar

Test description

Figure 7.2.8 shows the setup for the mortar fatigue tests as performed by means of the DSR AR 2000ex. The installation process was as follows: first, fixing the top steel ring of specimen by the clamp and adjusting it to be vertical, then lowering the specimen to touch the bottom plate, and covering the bottom ring with the epoxy glue. The mortar specimen was protected by the rings, and there was no deformation or creep due to fixing. After hardening of the glue, the test can be performed. The adhesion between the mortar and steel ring was found to be strong enough, and no failure between them was observed during testing. The applied torque time signal was a pure sinusoidal wave under torque controlled mode. Table 7.2.10 gives the parameters used in the mortar fatigue test.

In addition, a frequency sweep on the mortar specimen was performed to obtain the rheological properties at temperatures of 0 °C, 10 °C, 20 °C, and 30 °C. The applied shear strain stayed within the linear viscoelastic range.

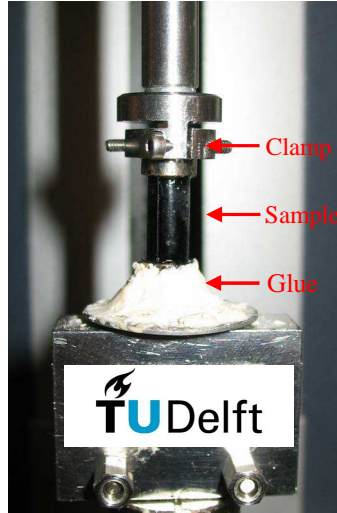


Figure 7.2.8 Device for the mortar fatigue test in DSR AR 2000ex

Table 7.2.10 Parameters used in the mortar fatigue test

Items	Value
Temperature [°C]	10
Frequency [Hz]	10
Time [hours]	0.5-3
Shear stress level [MPa]	1.0-1.3

Test interpretation

Shear stress and strain at the outer edge of the mortar column can be calculated using the following standard equations:

$$\tau = \frac{2 \times T}{\pi \times r^3} \quad 7.2.7$$

and

$$\gamma = \frac{r \times \theta}{h} \quad 7.2.8$$

where,

- T = torque, N·mm,
- r = specimen radius, 3mm here,
- γ = shear strain,
- θ = deflection angle, rad, and
- h = specimen height, mm.

Figure 7.2.9 gives two fatigue failure modes for the specimens. The upper one failed at the conjunction part between the mortar and the ring, which was due to the effect of stress concentration. The bottom one failed in the middle part of the

specimen. When observing the failed specimens, we found that the second case mainly happened when there was a surface defect due to the specimen preparation. Results indicated that most specimens failed following the first mode and just few specimens following the second one. Only the data obtained from specimens that failed following the first mode were used.

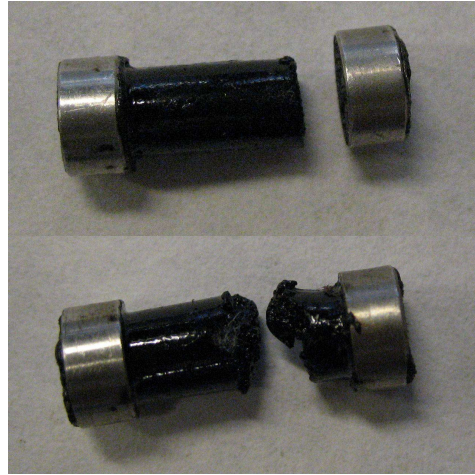


Figure 7.2.9 Two fatigue failure modes for the mortar specimen

Through a finite element simulation, Mo (2010) recommended a calibration factor $k=1.1$ to the standard stress in Equation 7.2.7, (i.e. $\tau = k \cdot (2 \times T) / (\pi \times r^3)$) and an effective height $h=12.742$ mm in Equations 7.2.8, respectively. Note that these calibrations were suitable to the first fatigue failure mode shown in Figure 7.2.9. These two calibration parameters were used in this study.

7.2.2.3 Testing of the mixture

Test description

The universal testing machine capable of generating a maximum loading of 25 kN (UTM-25) was used in the mixture fatigue test and the resilient modulus test. The latter test was finished in the Wuhan University of Technology who owned the same machine as TUDelft. Figure 7.2.10 shows the specimen loading apparatus and deformation sensor mounting system in the UTM-25. The load with a resolution of 1 N was applied over the specimen through the upper strip with a width of 12.5 mm. The lower strip with the same width was fixed firmly to the base plate. Two horizontal sensors were recording horizontal deformations within the range of ± 0.5 μm . The vertical sensor was capable of recording the vertical deformation within a range of ± 1.0 μm . The test was performed in a temperature-controlled cabinet which can control the temperature within ± 0.1 $^{\circ}\text{C}$.

Detailed testing conditions are given in Tables 7.2.11 and 7.2.12. More information about these two tests were presented elsewhere (Poot, Ven et al. 2008)



Figure 7.2.10 Indirect tensile testing device for the fatigue test and resilient modulus test

Table 7.2.11 Detailed parameters used in the mixture fatigue test

Temperature [°C]	5
Frequency [Hz]	10
Time [hour]	0.5-20
Stress level [MPa]	0.5-2.0
Waveform	Haversine
Recorded data	Vertical displacement

Table 7.2.12 Input parameters used in the resilient modulus test

Parameters	Values/Description
Loading mode	Dynamic indirect tensile test
Waveform	A haversine plus a rest period
Pulse width [ms]	63, 125, 200, 300
Ratio of the total pulse period to the pulse width (T_t / T_p)	10
Assumed Poisson's ratio	0.35
Recorded data	Resilient horizontal displacement
Test temperature [°C]	5, 12.5 20, 35
Loading amplitude	2 kN at 5°C; 1.2 kN at 12.5°C; 0.6 kN at 20°C; 0.1 kN at 35°C
Recorded Pulse cycles	Last 5

Test interpretation

Figure 7.2.11 shows 2D stress distribution in the specimen. This uniform tensile stress over most of the height of the specimen mainly contributed to the fatigue damage of the specimen. However, some factors could influence the test and especially the presence of rather high compressive strength near the load strips can not be neglected, especially at higher temperatures. For example, testing at high temperatures could lead to plastic deformation. It could also decrease the difference between the tensile strength and the compression strength (Molenaar 2002). As a result of this, wedging or compressive failure might occur at the loading strips. In order to avoid these failure types, a temperature of 5 °C was chosen for the fatigue tests, and the applied tensile stress was taken much lower than the tensile strength.

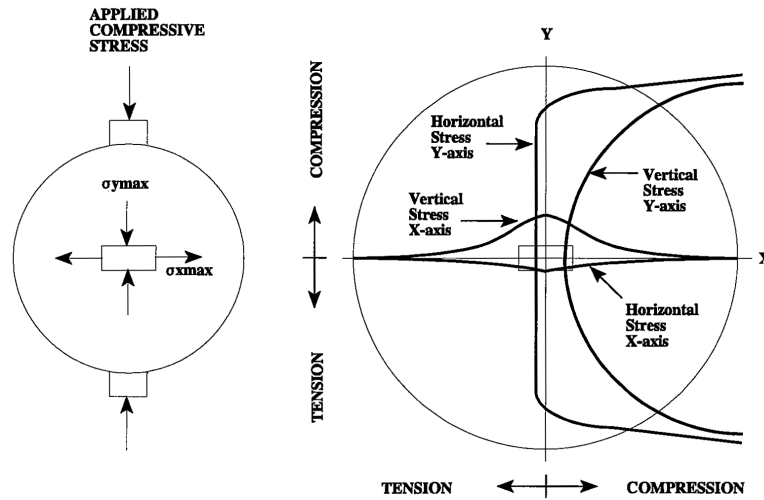


Figure 7.2.11 2D stress distributions for the indirect tensile fatigue test

With respect to the resilient modulus test, less than 10% of the indirect tensile strength at the testing temperature was selected as the load amplitude, and 10% of the load amplitude was used as the contact load to maintain a positive contact between the loading strips and the specimen during the test. The resilient modulus was calculated for each cycle using the following equation:

$$E_r = \frac{F_{peak}}{\Delta H_t t} (0.27 + \nu) \quad 7.2.9$$

where,

E_r = resilient modulus, MPa,

F_{peak} = peak force, kN,

ν = Poisson ratio, 0.35,

t = thickness, mm, and

ΔH_r = total recoverable horizontal deformation, μm

The resilient modulus was obtained by calculating an average of the values of the last 5 pulses.

7.3 Fatigue results and analyses

7.3.1 Binder fatigue

Figure 7.3.1 presents a typical fatigue curve obtained by the cone and plate device using the dissipated energy ratio (DER) method. As indicated, the development of the fatigue curve was divided into three stages: first, the relation between N and DER can be represented with a straight line, which meant that the energy per cycle was dissipated in linear viscoelastic damping, and damage was negligible. Next, the curve deviated from the straight line, indicating that the fatigue crack initiated by consuming extra energy beyond viscoelastic damping. Finally, the crack started to propagate, and ended with the final failure due to accumulation of damage. A graphical method was proposed to define the number of load repetitions at which crack propagation starts. This number was determined by the intersection of the straight line and of the horizontal line passing through the peak of the curve (Santagata, Baglieri et al. 2008). The fatigue curve can reflect the development of fatigue undergoing the transition from initiation to failure. The peak of fatigue curve defines clearly the fatigue life N_f in the stress control mode.

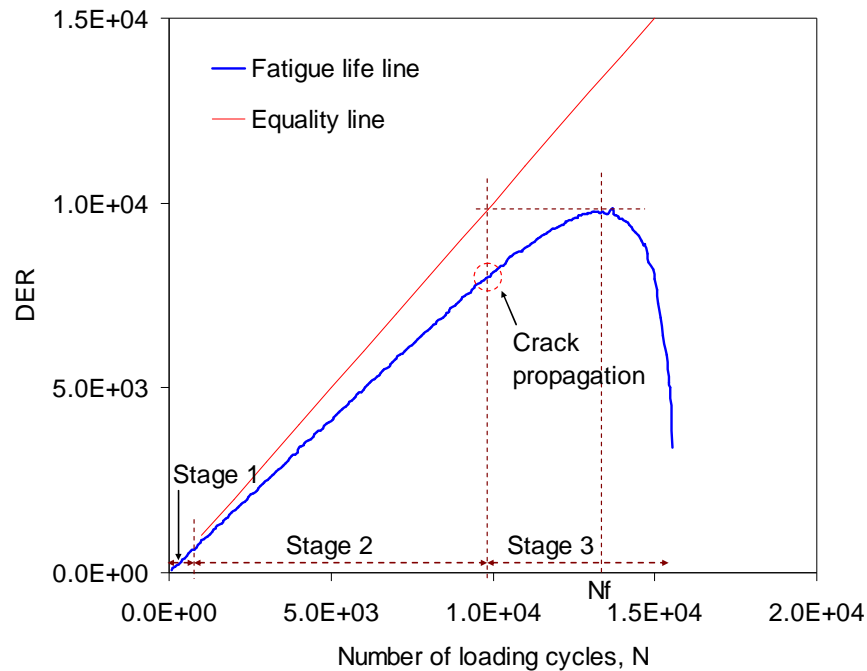


Figure 7.3.1 Typical fatigue curve represented by the dissipated energy ratio

Figures 7.3.2a, b and c show the fatigue curves for bitumens at different loading levels. It appears that the cluster of curves in each figure deviate from the equality line at the same point, meaning that bitumens owned the same first stage. With respect to the next two stages, the curves showed an obvious difference. The modification with 4wt. % of nanoclay can improve the fatigue life of base bitumen. Compared with the nanoclay Mt1, the Mt2 contributed more to the change of fatigue properties in the last two stages. The change in complex modulus and phase angle as observed during the test pictured in Figure 7.3.2a are shown in Figure 7.3.3.

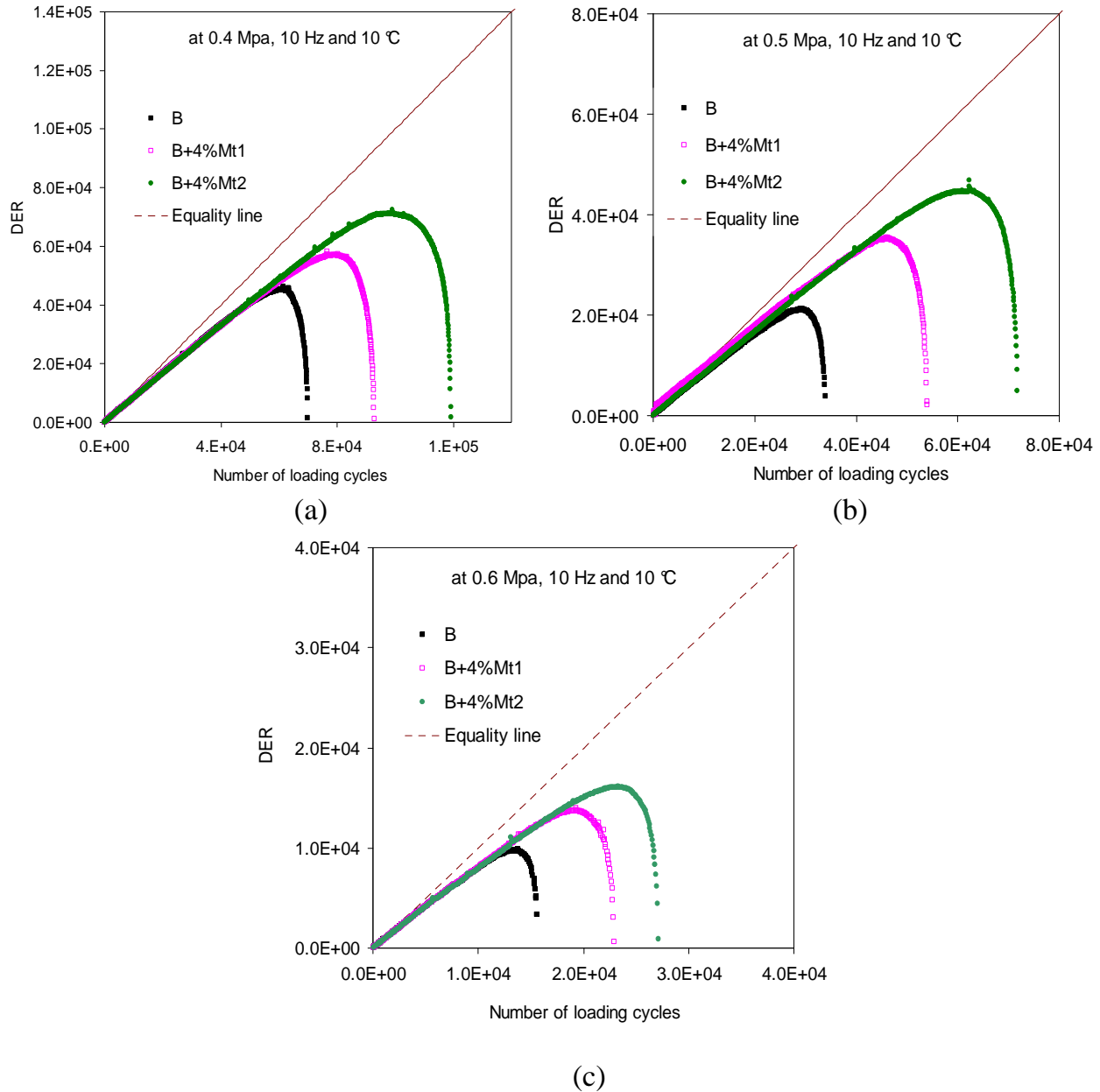


Figure 7.3.2 Fatigue curves for all bitumens at three stress levels: (a) 0.4 MPa; (b) 0.5 MPa; (c) 0.6 MPa

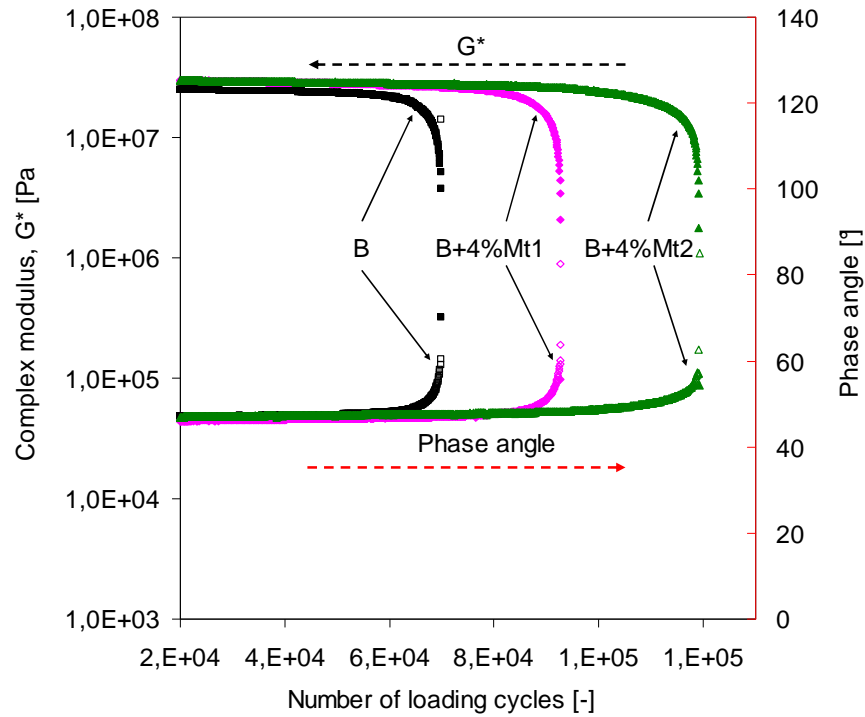


Figure 7.3.3 Change in complex modulus and phase angle during fatigue test at 0.4 MPa

Table 7.3.1 gives fatigue results as a function of shear stress, which are plotted in Figure 7.3.4 using classic power law function.

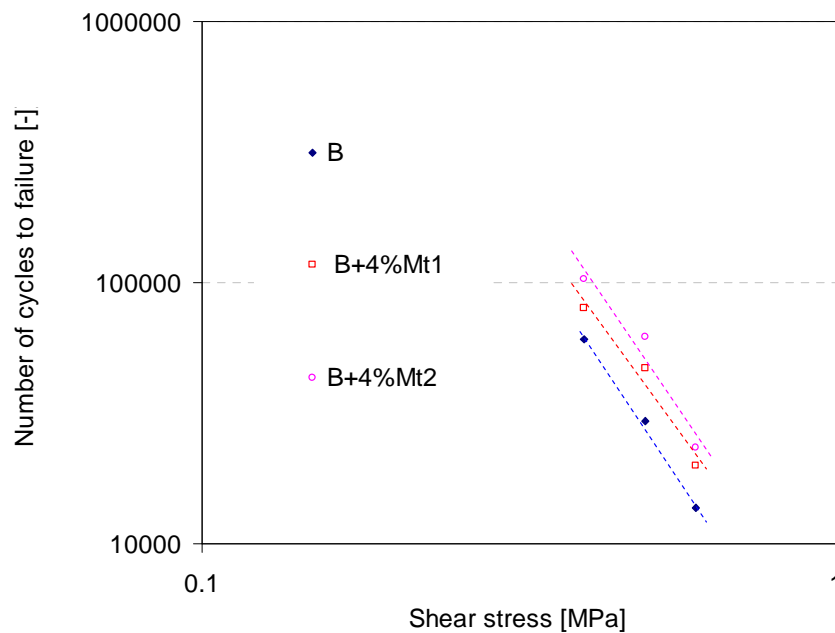


Figure 7.3.4 Fatigue life versus shear stress for base and modified bitumens

Table 7.3.1 Fatigue results as a function of shear stress

Codes	Shear stress [MPa]	N_f	N_f as a function of shear stress
B	0.4	60540	$y = 2195.2x^{-3.6521}$ $R^2 = 0.9942$
	0.5	29460	
	0.6	13680	
B+4%Mt1	0.4	80280	$y = 3816.1x^{-3.3996}$ $R^2 = 0.9644$
	0.5	46920	
	0.6	19920	
B+4%Mt2	0.4	103020	$y = 4179.8x^{-3.5982}$ $R^2 = 0.9439$
	0.5	62160	
	0.6	23460	

Figure 7.3.5 gives a comparison of the initial dissipated energy per cycle ($w_{initial}$) for the base and modified bitumens at three loading levels. It is obvious that an increase of stress level resulted in an increase of $w_{initial}$. At the same loading level, $w_{initial}$ of the modified bitumens was smaller than that of the base bitumen by an average of 18%. This decrease is due to an increase in stiffness and a decrease of the phase angle. According to the energy theory, a small $w_{initial}$ implies less damage happening at the beginning. Therefore, the modified bitumen exhibits a better fatigue resistance. It is necessary to note that $w_{initial}$ for both modified bitumens are comparable. However, Mt2 contributes more to the improvement of fatigue life, by an increase from 70% to 110% as shown in Figure 7.3.6. Therefore, it is concluded that the $w_{initial}$ is not the only factor that determines the fatigue life.

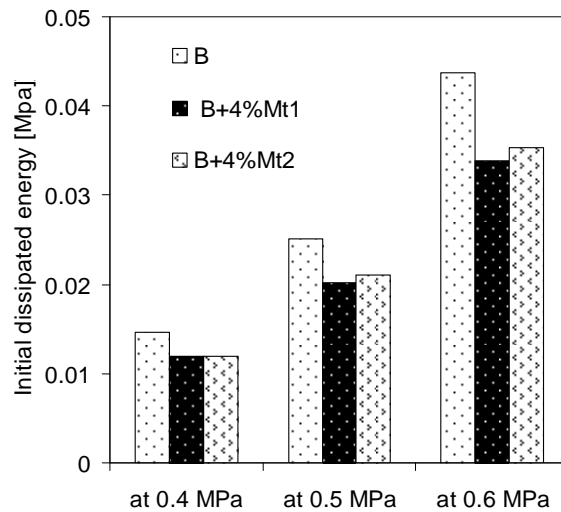


Figure 7.3.5 Comparison of the initial dissipated energy per cycle for the base and modified bitumens at the same loading condition

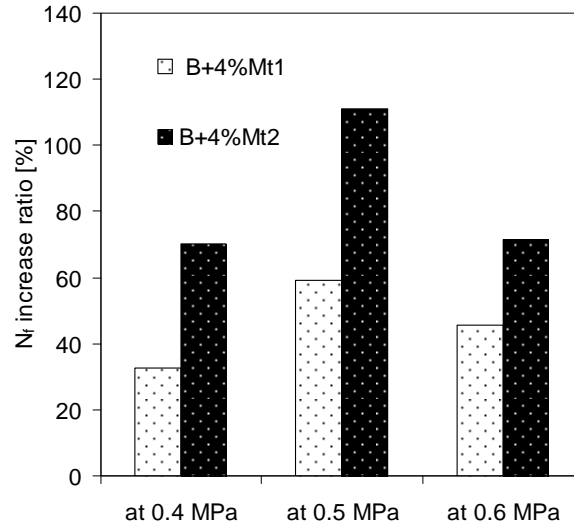


Figure 7.3.6 Fatigue life increase ratio for both modified bitumens at the same loading condition

It is believed that the interfacial interactions between the surfactants on the nanoclay and bitumen molecules play a key role in the improvement of the fatigue life. The surfactants on the nanoclay Mt1 contain straight carbon chains, and the surfactants on the nanoclay Mt2 own a straight carbon chain plus a phenyl (see Figure 7.2.1). The reason for more improvement in fatigue properties by the Mt2 could be that the surfactants on the Mt2 have a stronger interaction with bitumen which consists of all kinds of hydrocarbons in terms of straight and branched chains, saturated rings and aromatic rings.

The model introduced by Mo (2010) was used to characterize the fatigue life (see Equation 7.1.8). After fitting, related parameters in this model are given in Table 7.3.2. One can observe that W_0 increases due to the modification. It is interesting to note that values of obtained W_0 are higher than those of the mortar tested by Mo (2010). This difference is caused by different means and specimen's geometry. The specimen in the cone-plate device has a bigger cross section. It appears that W_0 is not a material parameter. Nevertheless, the parameters obtained from the cone-plate device reflect the influence of nanoclay on the fatigue properties and therefore still make sense.

Table 7.3.2 Model parameters based on initial dissipated energy

Bitumens	W_0 [MPa]	b [-]	R^2
B	46.9	1.3653	0.9999
B+4% Mt1	56.5	1.3418	0.9823
B+4% Mt2	59.9	1.3653	0.9595

On the basis of this model, Figure 7.3.7 was devised, which shows the relation between $w_{initial}$ and the number of cycles to failure. One will observe that the same fatigue line ranking is obtained as the one shown in Figure 7.3.4. What is different is that the fatigue line for B+4%Mt1 is closer to that for base B.

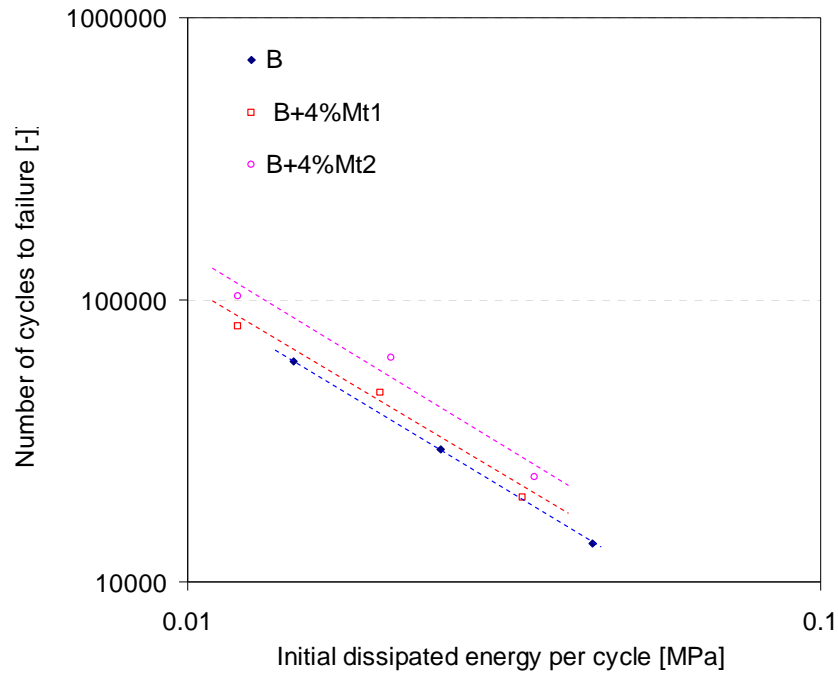


Figure 7.3.7 Relation between Fatigue life and initial dissipated energy per cycle for the base and modified bitumens

A parameter ψ is introduced by van Dirk (1975) which is the ratio between the artificial total dissipated energy, based on the initial values of stress, strain and phase angle, and the real total dissipated energy (see Equation 7.1.6). ψ mainly depends on the type of test and the material stiffness. Figure 7.3.8 shows the relation between complex modulus of bitumens at the fatigue test conditions (10 Hz, 10 °C) and the parameter ψ . In stress controlled mode, ψ is normally less than 1. At three stress levels, base B shows an average value of 0.95, B+4%Mt1 of 0.92 and B+4%Mt2 of 0.92. The nanoclay modification increases the modulus of base bitumen, but does not influence ψ too much.

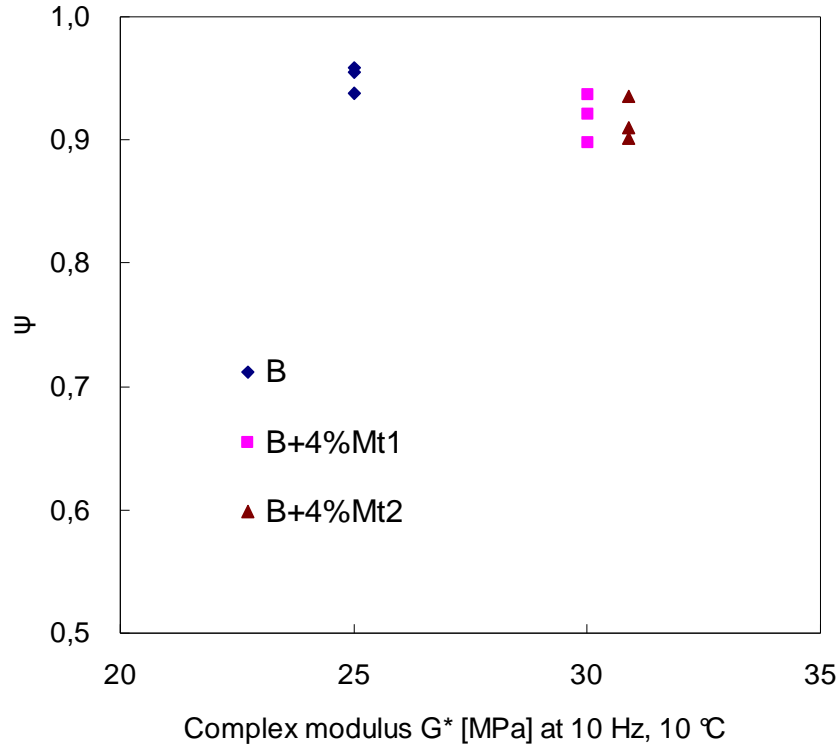


Figure 7.3.8 Relation between the complex modulus of bitumens at fatigue testing conditions and the parameter ψ

7.3.2 Mortar fatigue

To better understand the fatigue behaviour of the mortar, it was necessary to firstly describe its rheological properties and how they are affected by ageing and modification. Figure 7.3.9 shows the master curves of the mortars with the WLF shifting at a reference temperature of 20 °C. This shifting procedure was the same as the one used for the bituminous materials described in previous chapter. Since four testing temperatures (0 °C, 10 °C, 20 °C, and 30 °C) were involved, and the fitted curve was very smooth.

As indicated, ageing resulted in an increase in the complex modulus of the standard and modified mortars which was accompanied by a decrease in phase angle, especially in the low frequency range. The high frequency part of this figure was magnified, and shown on the top. By comparison, the effect of ageing and modification was determined. It appears that the master curves of fresh modified mortar and aged standard mortar almost overlap each other. This indicates that the ageing effect on rheological properties of the standard mortar was similar to that induced by the modification with the nanoclay.

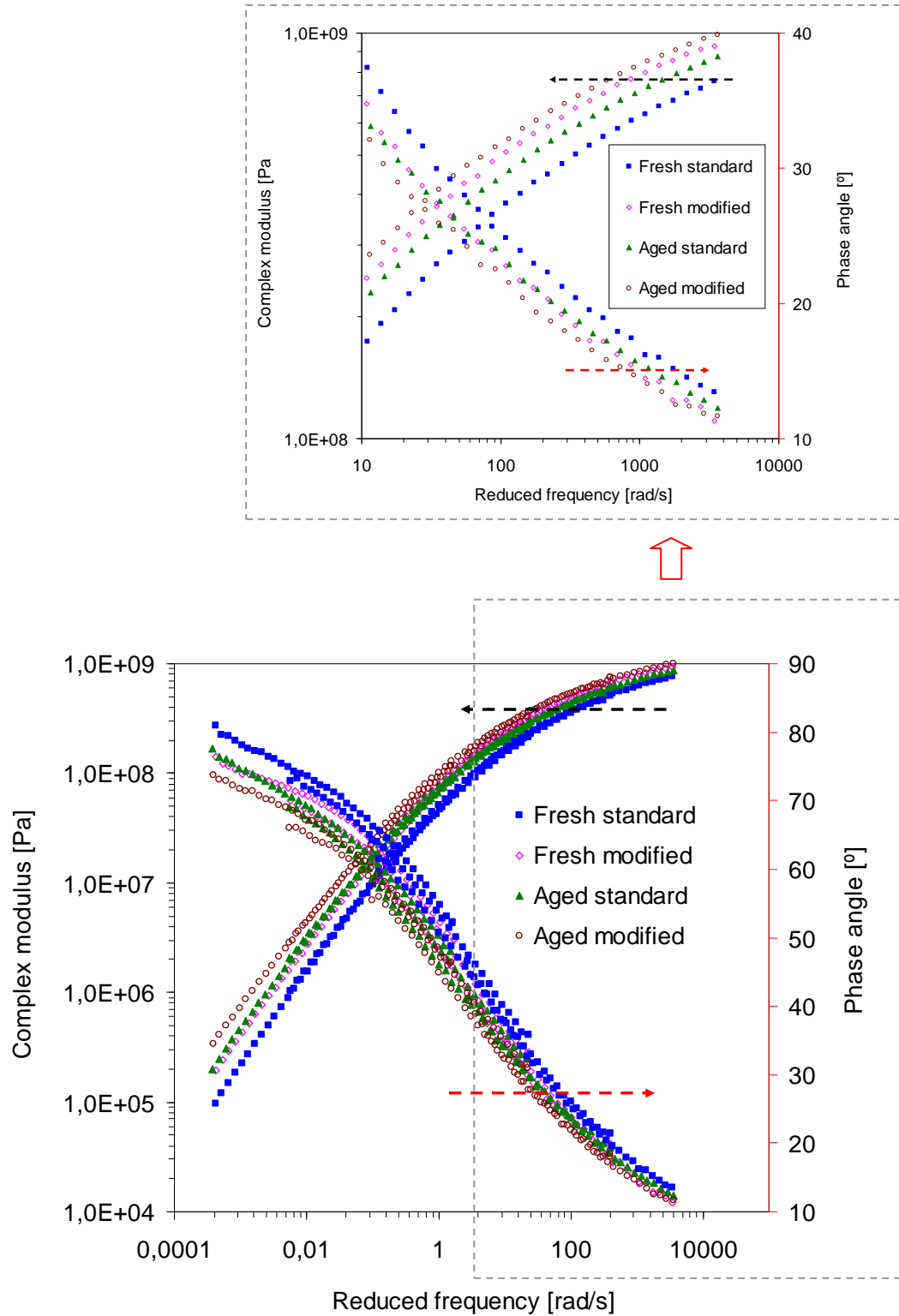


Figure 7.3.9 Master curves of standard and modified mortars before and after the ageing at a reference temperature of 20 °C

Table 7.3.3 shows the parameters fitting the master curves of the mortars. The change in G_{\max} , δ_{\max} , and δ_{\min} , due to the ageing and the modification is as expected. The process to construct master curve and the related model have been introduced in the section 6.2.3 of Chapter 6

Table 7.3.3 Model parameters in fitting master curves of complex modulus and phase angle

	Parameter	Fresh standard	Fresh modified	Aged standard	Aged modified
Shift factor	C_1	32.1	32.1	32.7	32.6
	C_2	250.3	251.1	250.7	251.8
Complex modulus	G_{\max}	4.63E+08	6.07E+08	5.45E+08	6.56E+08
	G_{\min}	0	0	0	0
	β	26.67	23.04	21.34	21.17
	γ	0.73	0.70	0.69	0.66
Phase angle	δ_{\max}	88.22	83.28	84.90	80.02
	δ_{\min}	11.57	10.40	10.93	10.36
	β	9.70	9.88	6.73	7.79
	γ	0.22	0.23	0.21	0.22

A ratio of the complex modulus after ageing to the one before ageing has been defined as an ageing index to the bitumen in previous chapter, and was adopted in this chapter to evaluate the mortar's ageing properties. Figure 7.3.10 shows the standard and modified mortars' ageing index as a function of reduced frequency. At the same frequency, the modified mortar exhibits a lower ageing index which means a better ageing resistance. It is believed that the barrier properties of clay layers to oxygen invasion play a main role in the improvement of the ageing resistance of the mortar. With increasing frequency, the difference between the two index curves gradually decreases. A value of around 1 is obtained at a maximum frequency of 1000 Hz.

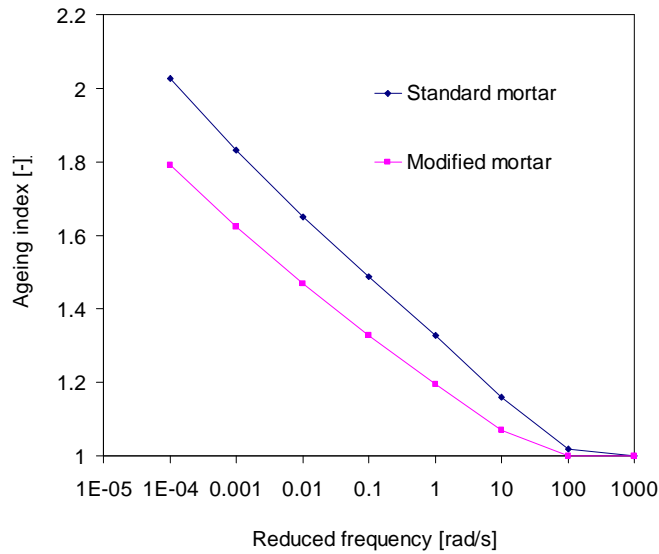


Figure 7.3.10 Ageing index as a function of reduced frequency for the standard and modified mortars

In this section, the DER method has also been adopted to define the fatigue life of the mortar. Figure 7.3.11 shows mortar's fatigue life lines as a function of shear stress. With respect to the fresh standard mortar, the ageing and the modification improved its fatigue life. Although the fresh modified mortar and the aged standard mortar showed almost the same rheological properties (see Figure 7.3.9), the former exhibits better fatigue resistance than the latter. Table 7.3.4 gives fatigue results of mortars at different shear stresses. Classic power law functions were fitted to these results and they are also listed in Table 7.3.4.

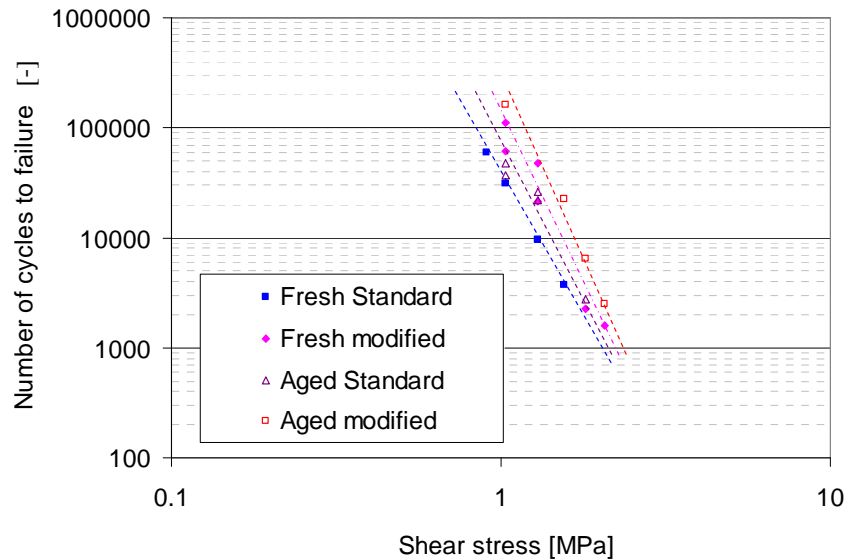


Figure 7.3.11 Fatigue life for the standard and modified mortars before and after the ageing, as a function of shear stress

Table 7.3.4 Fatigue results of mortar as a function of shear stress

Codes	Shear stress [MPa]	N_f	N_f as a function of shear stress
Fresh standard	0.9	60000	$y = 37067x^{-5.1957}$ $R^2 = 0.9997$
	1.0	31500	
	1.3	9600	
	1.6	3700	
Fresh modified	1.0	61000*	$y = 118055x^{-6.0513}$ $R^2 = 0.9500$
	1.0	110000	
	1.3	21500	
	1.3	47000	
	1.8	2250	
	2.1	1600	
Aged standard	1.0	37500*	$y = 60883x^{-4.7813}$ $R^2 = 0.9297$
	1.0	48000	
	1.3	22000	
	1.3	26000	
	1.8	2750	
Aged modified	1.0	160000	$y = 226323x^{-5.9331}$ $R^2 = 0.9848$
	1.6	22500	
	1.8	6500	
	2.1	2500	

* means the second fatigue failure mode shown in Figure 7.2.9, and is not taken into account in the fatigue data fitting.

To get a fundamental understanding on the change in fatigue behaviour, the fatigue life as a function of initial dissipated energy ($w_{initial}$) was plotted in Figure 7.3.12. The order of the fatigue lines is the same as that which is plotted as a function of shear stress in Figure 7.3.11. One can observe however that fatigue lines are much more susceptibility to $w_{initial}$ than to the shear stress. For example, a tiny change on $w_{initial}$ has a much greater effect on the change of fatigue life than a change in the shear stress level.

All mortar data were also fitted using the simple model (Equation 7.1.8) developed by Mo (2010). The model parameters are given in Table 7.3.5. As indicated by the correlation coefficient of R^2 , the model showed a good fit with the test data. It is observed that W_0 increases due to the effect of ageing and modification. The value of W_0 is in the same order of magnitude as those reported by Mo (2010) who used the same test configuration.

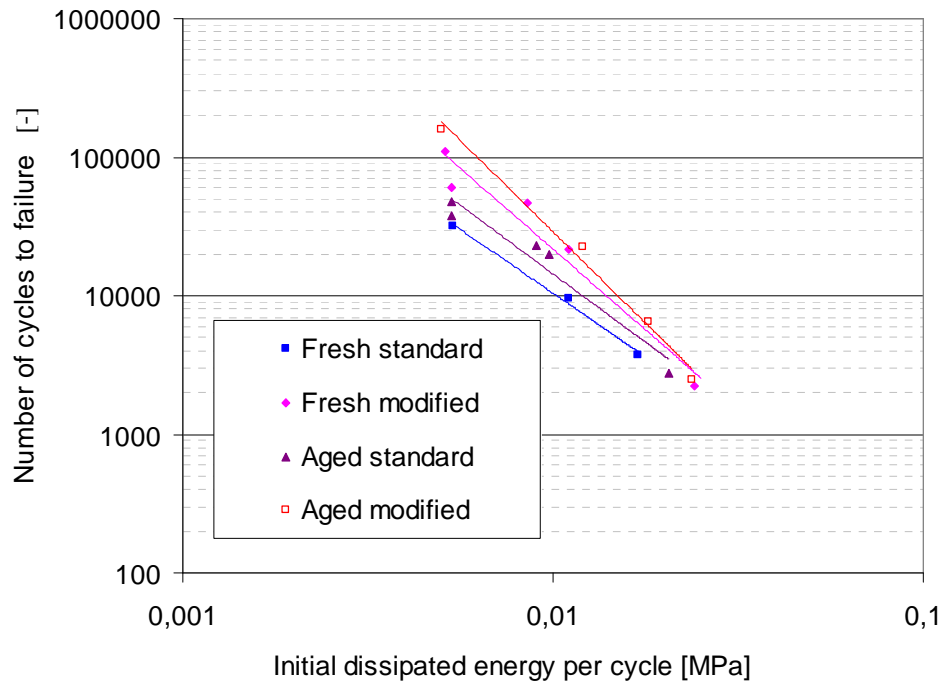


Figure 7.3.12 Fatigue life for the standard and modified mortars before and after the ageing, as a function of initial dissipated energy per cycle

Table 7.3.5 Model parameters based on initial dissipated energy

	Fresh standard	Fresh modified	Aged standard	Aged modified
W_0 [MPa]	0.64	0.72	0.89	0.93
b	2.23	2.27	2.11	2.30
R2	0.9942	0.8346	0.8991	0.9999

Figure 7.3.13 shows the relation between the complex modulus and the parameter ψ for the mortars. Compared with bitumens (Figure 7.3.8), ψ for the mortars shows more scatter at different loading levels. The nanoclay modification not only increases the modulus, but also ψ , an average value from 0.57 for fresh mortar to 0.67 for fresh one modified by the nanoclay. Although ageing also increases the modulus, it does not result in a big change in ψ , an average value of 0.56 for aged mortar and 0.63 for aged one modified by the nanoclay.

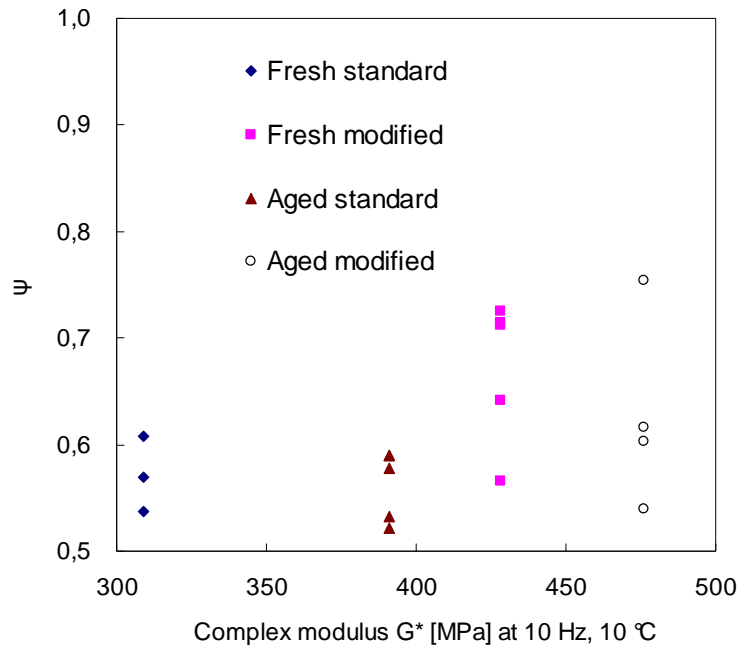


Figure 7.3.13 Relation between the complex modulus of the mortars at fatigue testing conditions and the parameter ψ

7.3.3 Mixture fatigue

Compared with the bitumen and mortar, the fatigue behaviour of the mixture was more complicated. Figure 7.3.14 shows how the specimens looked like after the test. It was observed that for most of them, a pure crack along the diametrical line had developed, which indicates that the horizontally indirect tensile played a main role in the fatigue failure.

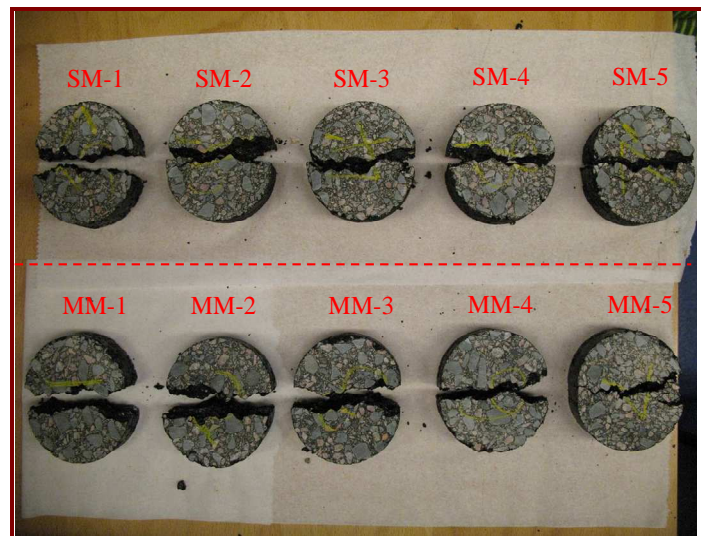


Figure 7.3.14 Fatigue failure outlines of all mixture specimens

Different crack propagation paths were also observed during the fatigue test. For example, when a tensile stress of 1.9 MPa was applied on specimen SM-1, the fatigue crack even propagated through the aggregates (Figure 7.3.15a). However, at a stress level of 0.5 MPa applied on specimen SM-5, it seemed that the fatigue crack mainly took place through the mortar (Figure 7.3.15b). Because of these different crack paths, it was concluded that the contribution of bitumen to the mixture's fatigue resistance was related to the load level.

There was a little bit of plastic deformation near the loading strip, which especially occurred at the lower load level. This deformation was due to stress concentrations near the loading strip, a phenomenon which has been described by Erkens (2002) (2002) through a finite element model.



Figure 7.3.15 Fatigue failure profiles on (a) the specimen SM-1 at a maximum loading of 1.9 MPa and (b) the specimen SM-5 at a minimum loading of 0.5 MPa

Figures 7.3.16a and b give typical fatigue curves at two stress levels for standard and modified mixtures. The vertical displacement was only recorded, since the horizontal displacement was out of the sensor's range during the fatigue test. Therefore, the DER can not be calculated in the mixture test. When the vertical displacement was used to characterize the fatigue, the fatigue process for each curve also consisted of three stages (specifically see Figure 7.3.16a). Heating played a main role during stage A. After the temperature was stabilized, the fatigue mainly took place during stage B. There was a rapid degradation due to the specimen's complete failure during stage C. In this study, the number of loading repetition for the first two stages was defined as the fatigue life. Standard and modified mixtures exhibited different fatigue curves at these two stress levels. Furthermore, more creep deformation can be observed during the stage B for standard mixture at a testing temperature of 5 °C. This indicates that the modified mixture has a higher resistance to permanent deformation.

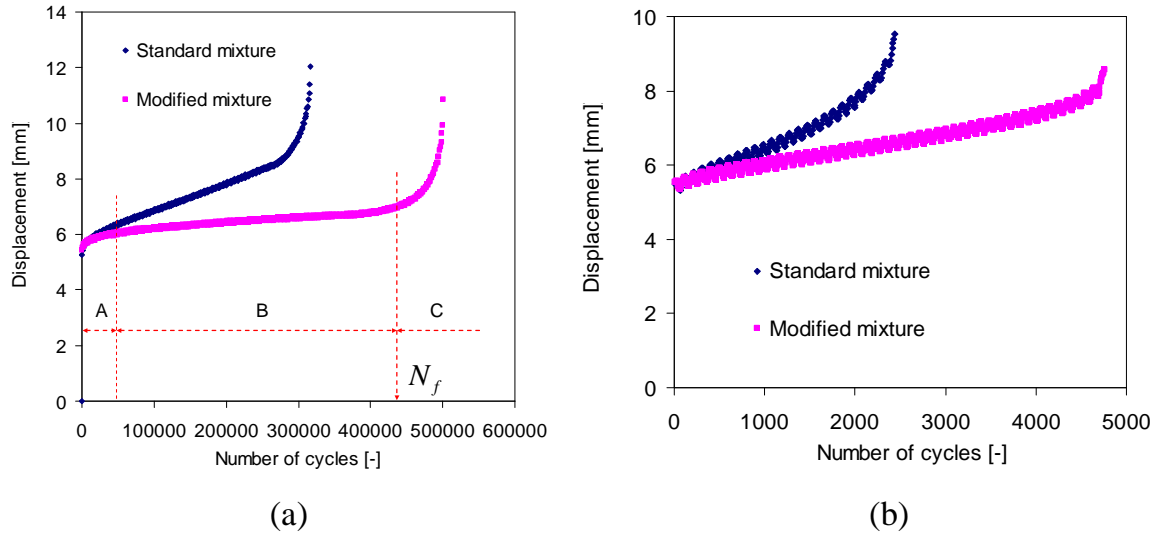


Figure 7.3.16 Fatigue curves of both mixtures at (a) a stress of 0.5 MPa and (b) a stress of 1.92 MPa

Figure 7.3.17 shows the fatigue lives for the standard and modified mixtures as a function of the indirect tensile stress. As one can observe, there is only a small difference in fatigue life between the standard and modified mixture. Compared with bitumen and mortar, the asphalt mixture was more heterogeneous, and its failure mechanism was more complicated, such as different propagation paths of the fatigue crack at different loading levels. The results show a limited positive effect of the modification on the fatigue performance of the mixture.

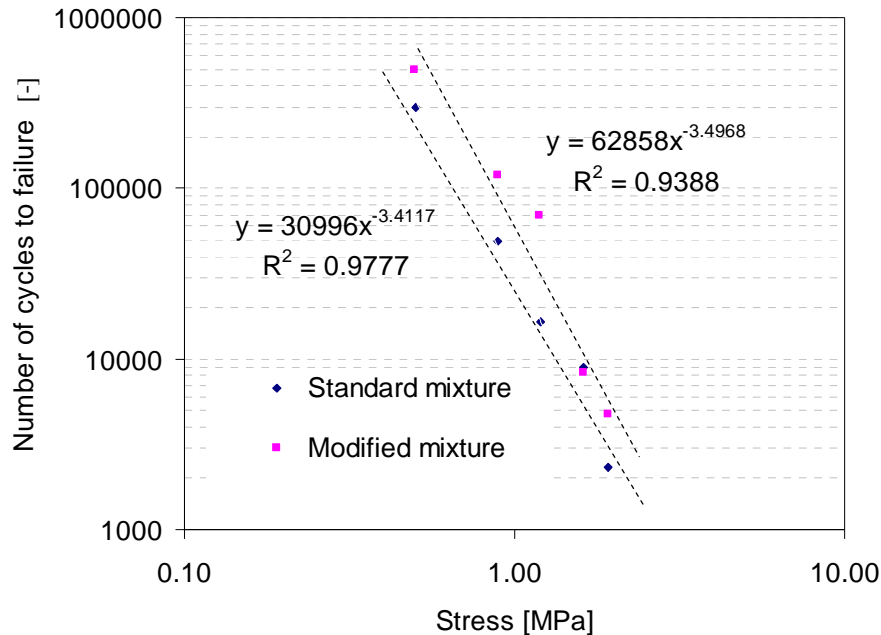
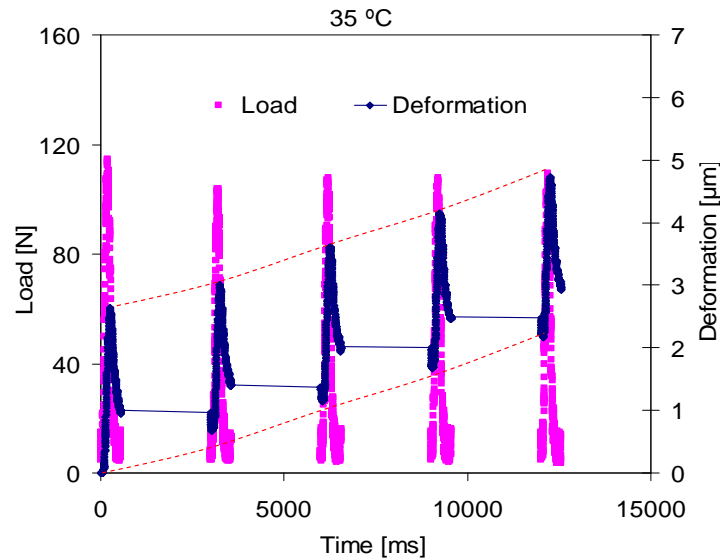


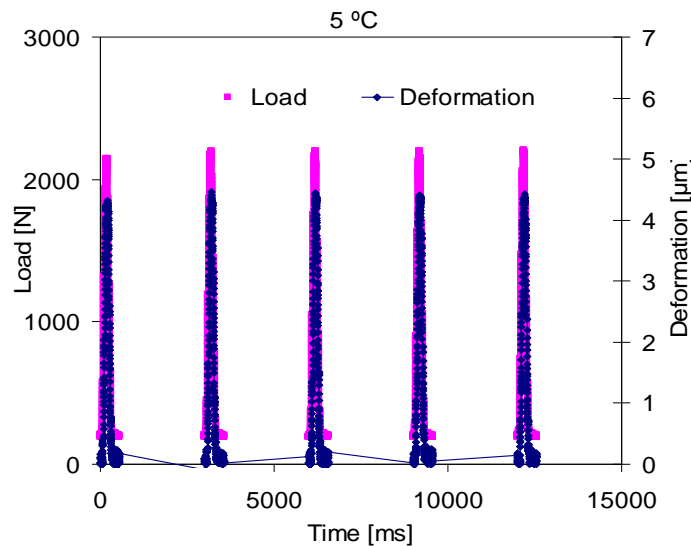
Figure 7.3.17 Fatigue life for standard and modified mixtures as a function of shear stress

7.3.4 Resilient modulus

The resilient modulus of the mixture at different temperatures and loading times were also determined. Figures 7.3.18a and b e.g. give a typical load and deformation response for the last 5 pulse cycles during the resilient modulus test at two temperatures. It was easier to find the accumulated permanent deformation at 35 °C than at 5 °C, which was due to a lower stiffness at a higher temperature. This indirectly explained why 5 °C was chosen for the fatigue test.



(a)



(b)

Figure 7.3.18 Load and deformation response for the last 5 pulse cycles during the resilient modulus test on the standard mixture at (a) 35 °C and (b) 5 °C

Figure 7.3.19 presents the load and deformation response for two mixtures, the standard and the modified, at the first pulse cycle during the resilient modulus test at 35 °C and 0.1 kN. Due to the viscoelastic properties of the asphalt mixture, there was a response lag between the load and the deformation. The modified mixture had a smaller lag (Δt_1) than that (Δt_2) of the standard mixture. Besides the type of mixture, this response lag also depends on the test temperature and the loading frequency. Lower temperature or higher loading frequency would lead to a smaller lag. After one pulse, a small amount of permanent deformation was accumulated. When compared to the standard mixture, the modified mixture exhibited a lower permanent deformation (Δd_1).

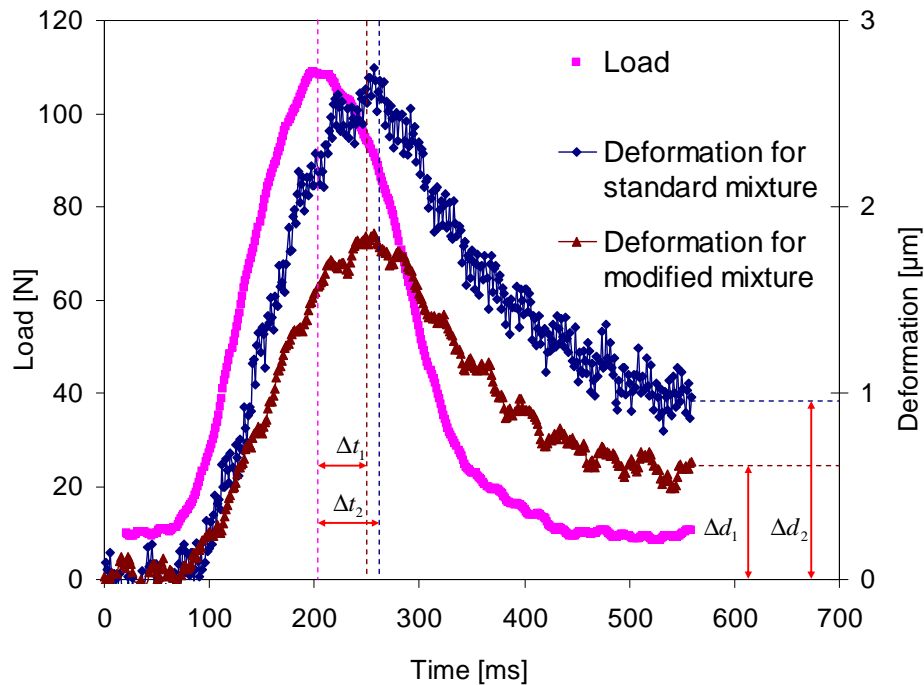


Figure 7.3.19 Load and deformation response for the mixture at the first pulse cycle during the resilient modulus test at 35 °C and 0.1 kN

Table 7.3.6 gives the resilient modulus results for the specimens of the standard and the Mt2 modified mixtures at different temperatures and pulse width. The resilient modulus was obtained by calculating an average for last 5 pulse cycles using Equation 7.2.9. An average increase of 18% in the modulus was observed as a result of the modification. Based on these results, the master curve at a reference temperature of 20 °C was established. The WLF function (see Equation 6.2.9 in Chapter 6) was adopted to obtain the shift factor a_T , and the sigmoid model (S-model) was used for curve fitting as follows:

$$S_{\text{model}} = S_{\text{min}} + \frac{(S_{\text{max}} - S_{\text{min}})}{[1 + (\frac{t_c}{t_{\text{red}}})^k]^{m_e/k}} \quad 7.3.1$$

where,

S_{model} = mixture stiffness, MPa,

S_{min} = minimum mixture stiffness, MPa

S_{max} = maximum mixture stiffness, MPa

t_c = location parameter with dimension of time, ms

t_{red} = reduced time, equal to the pulse width divided by a_T , ms, and

k, m_e = shape parameters.

Table 7.3.6 Resilient modulus results for the standard mixture and the modified mixture

		Standard mixture Resilient modulus [MPa]							
Temp. [°C]	Pulse width [ms]	Pulse 1	Pulse 2	Pulse 3	Pulse 4	Pulse 5	Mean	SD*	CV% [#]
5	63	6214	6196	6302	6281	6255	6255	187.32	3.19
	125	6283	6116	6084	6120	6177	6157	109.77	1.8
	200	6095	6380	6066	5739	6341	6125	264.73	4.3
	300	5498	5932	6089	6264	6173	5991	269.69	4.5
12.5	63	4198	4617	4495	4351	4485	4429	103.29	2.6
	125	4271	4698	4268	4287	4550	4415	108.62	2.77
	200	4062	4469	4319	4330	4426	4321	118.04	3.04
	300	4145	4559	4057	4145	4048	4191	61.38	1.66
20	63	3709	4080	3436	3615	3825	3733	190.95	5.74
	125	3564	3920	3677	3138	3225	3505	226.33	7.48
	200	3119	3430	2990	3285	2985	3162	129.51	4.67
	300	2794	3073	2973	2849	2856	2909	87.73	3.29
35	63	1625	1787	1268	1407	1309	1479	120.52	9.62
	125	1103	1214	1024	1123	911	1075	72.88	7.6
	200	1057	1163	988	930	905	1009	53.93	6.2
	300	978	1076	888	956	880	955	41.35	4.72

		Modified mixture Resilient modulus [MPa]							
Temp. [°C]	Pulse width [ms]	Pulse 1	Pulse 2	Pulse 3	Pulse 4	Pulse 5	Mean	SD	CV%
5	63	6968	6765	6910	6871	6864	6876	157.62	2.33
	125	6877	6839	6733	6873	6872	6839	109.57	1.63
	200	6825	6683	7056	6791	6585	6788	184.62	2.7
	300	6691	6635	6968	6590	6917	6760	138.7	2.03
12.5	63	5807	5917	5931	5985	5836	5895	64.99	1.1
	125	5078	5177	5230	5262	5405	5230	107.4	2.05
	200	5018	5236	5199	5160	5256	5174	84.64	1.64
	300	4550	4717	4790	4708	4806	4714	132.13	2.77
20	63	4693	4621	4888	4563	4718	4697	137.05	2.89
	125	4118	4203	4190	4064	4020	4119	109.41	2.63
	200	3566	3741	3613	3686	3676	3656	51.06	1.38
	300	3355	3465	3364	3336	3209	3346	81.53	2.44
35	63	1830	1791	1820	1991	1817	1850	105.71	5.42
	125	1401	1494	1409	1447	1483	1447	37.54	2.59
	200	1261	1179	1166	1157	1117	1176	47.34	4.03
	300	1052	1057	1063	1007	1029	1042	20.88	2

Here, * is Standard deviation, and # is coefficient of variation

Figure 7.3.20 shows model-fitting master curves of the resilient modulus for both mixtures, and Table 7.3.7 gives the parameters used in Equation 7.3.9. At loading times ranging from 0.1 ms to 10^5 ms, the order of magnitude of resilient modulus just changed from 3 to 4, which indicates that the mixture has a good temperature susceptibility resistance. In general, the modified mixture has a little higher modulus than the standard mixture over the whole range of loading times. The master curves overlapped a little bit at the long loading times. This could be caused by the model-fitting, and also reflects the complication of resilient modulus test at high temperatures. It is necessary to note that this change not only depends on the testing condition, but also on the internal structure of mixture itself.

Table 7.3.7 Modeling parameters in the WLF model and the S-model

Modeling parameters		Standard mixture	Modified mixture
WLF	C_1	40.0	32.7
	C_2	262.5	263.4
S-model	S_{\max}	11689.2	10102.9
	S_{\min}	101.2	37.8
	t_c	591014343.1	2978852.5
	k	-0.13	-0.20
	m_e	-1.40	-1.50
	R^2	0.9721	0.9929

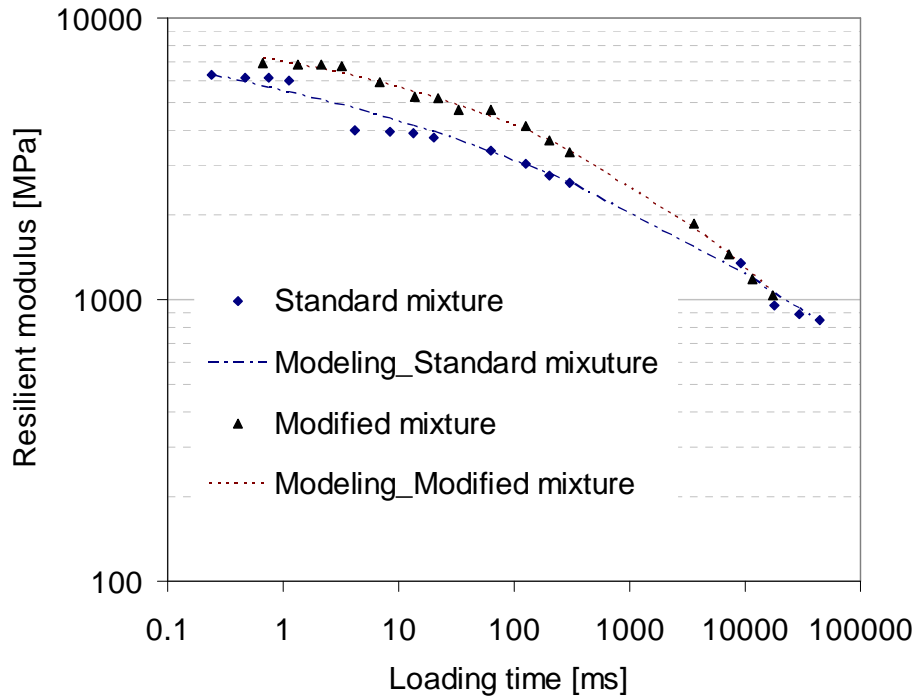


Figure 7.3.20 Master curve of resilient modulus at a reference temperature of 20 °C

7.4 Summary and conclusions

In this chapter, fatigue tests were performed on bitumen, mortar, and mixture. First, the cone and plate device was used to characterize the fatigue properties of the bitumen with and without the modification by two organo montmorillonite nanoclays Mt1 and Mt2. The results indicated that the nanoclay modification can change the fatigue life which was defined by the dissipated energy ratio (DER) in the stress controlled mode. It is believed that the interfacial interactions between the surfactants on the nanoclay and bitumen molecules play a key role in the improvement of the fatigue life. The surfactants on the nanoclay Mt1 contain straight carbon chains, and the surfactants on the nanoclay Mt2 own a straight carbon chains plus a phenyl. The reason for more improvement in fatigue properties by the Mt2 can be that the surfactants have a stronger interaction with bitumen which consists of all kinds of hydrocarbons in the terms of straight or branched chains, saturated rings, and aromatic rings.

Next, the standard mortar and the one modified by the Mt2 before and after the short time ageing were subjected to fatigue testing using a column specimen. The DER method has also been adopted in this case to define the fatigue life. Both ageing and modification did influence the fatigue properties of the mortar in the stress controlled mode. Although the ageing and the modification almost

contributed the same to the change in rheological properties of standard mixture, the latter improved its fatigue properties more. Meanwhile, the modified mortar showed a better ageing resistance than the standard one.

Finally, the indirect tensile fatigue test was adopted to characterize fatigue properties of a dense mixture with Mt clay. Only the vertical displacement of the specimen was only recorded to determine fatigue failure. There was a small difference in fatigue life between the standard and modified mixture. Compared with bitumen and mortar, the asphalt mixture is more heterogeneous, and its failure mechanism is more complicated, such as different propagation paths of fatigue crack at different loading levels. Although the results are positive, the improvement in fatigue life by modifying the asphalt mixture with nanoclay is not spectacular.

7.5 Reference

- Anderson, D. A., Y. M. L. Hir, et al. (2001). "Evaluation of fatigue criteria for asphalt binders." Transportation Research Record: Journal of the Transportation Research Board **1766**(-1): 48-56.
- Bahia, H., H. Zhai, et al. (2001). "Development of binder specification parameters based on characterization of damage behavior." Asphalt paving technology **70**: 442-470.
- Bodin, D., H. Soenen, et al. (2004). Temperature effects in binder fatigue and healing tests. 3rd Eurasphalt & Eurobitume Congress Vienna 1996-2004.
- Broek, D. (1991). Elementary Engineering fracture mechanics. Dordrecht, Kluwer academic publishers.
- Chomton, G. a. V., P.J. (1972). Applied rheology of asphalt mixes-practical applications. Third International Conference of the Structural Design of Asphalt Pavements, London.
- Erber, T., S. A. Guralnick, et al. (1993). "Hysteresis and fatigue." Annals of Physics **224**(2): 157-192.
- Erkens, S. (2002). Asphalt concrete response (ACRe): determination, modelling and prediction, Technische Universiteit Delft. **PhD thesis**.
- Ewalds, H. L. and R. J. H. Wanhill (1986). Fracture Mechanics, Edward Arnold and the Delftse Uitgevers Maatschappij, Delft.
- Gerritsen, A. H., van Gurp, C.A.P.M, van der Heide, J.P.J., Molenaar, A.A.A. and Pronk, A.C (1988). Prediction and Prevention of Surface Cracking in Asphalt Pavements. Proceedings of the 6th International Conference on the Structural Design of Asphalt Pavements. University of Michigan, USA. **1**: 378-391.
- Ghuzlan, K. A. and S. H. Carpenter (2000). "Energy-derived, damage-based failure criterion for fatigue testing." Transportation Research Record: Journal of the Transportation Research Board **1723**(-1): 141-149.
- Hopman, P. C., Kunst, P.A.J.C. and Pronk, A.C. (1989). A renewed interpretation method for fatigue measurement, verification of miner's rule. 4th Eurobitume Symposium. **1**: 557-561.
- Jin, J., L. Chen, et al. (2006). "An Analysis on Enhancement of Fatigue Durability of Polyurethane by Incorporating Organoclay Nanofillers." Macromolecular Materials and Engineering **291**(11): 1414-1421.
- Khedoe, R. N. and J. Moraal (2007). Sample preparation and laboratory testing for the LOT research program, Road and railway section, Delft University of Technology.
- Martin, A. E. (2006). "Combating pavement cracking." Texas transportation researcher **42**(3): 1.
- Medani, T. O. and A. A. A. Molenaar (2000). "A Simplified Practical Procedure for Estimation of Fatigue and Crack Growth Characteristics of Asphaltic Mixes." International Journal of Road Materials and Pavement Design **1**(4).

- Mo, L. T. (2010). Damage development in the adhesive zone and mortar of porous asphalt concrete. PhD thesis, Delft University of Technology. **PhD thesis**.
- Molenaar, A. A. A. (1983). Structural performance and design of flexible road constructions and asphalt concrete overlays Delft University of Technology. **PhD Thesis**.
- Molenaar, A. A. A. (1984). "Fatigue and reflection cracking due to traffic loads." Journal of the association of asphalt paving technologist **53**: 440-474.
- Molenaar, A. A. A. (2007). "Prediction of Fatigue Cracking in Asphalt Pavements: Do We Follow the Right Approach?" Transportation Research Record: Journal of the Transportation Research Board **2001**(-1): 155-162.
- Molenaar, J. M. M. (2002). Performance related characterisation of the mechanical behaviour of asphalt mixtures, Delft University of Technology. **PhD thesis**.
- Morrison, F. A. (2001). Understanding rheology, Oxford University Press, USA.
- Muraya, P. M. (2007). Permanent deformation of asphalt mixes, Delft University of Technology. **PhD thesis**.
- Paris, P. and F. Erdogan (1963). "A critical analysis of crack propagation laws." Journal of Basic Engineering **85**(4): 528-534.
- Poot, M., M. v. d. Ven, et al. (2008). Asphalt testing, Road and railway research laboratory, Delft University of Technology.
- Pronk, A. C. (1995). Evaluation of the dissipated energy concept for the interpretation of fatigue measurements in the crack initiation phase, The Road and Hydraulic Engineering Division (DWW), Netherlands.
- Raithby, K. D. a. S., A.B. (1972). Some effects of loading history on the performance of rolled asphalt Transport and road research laboratory, Crowthorne, England.
- Ray, S. S., M. Bousmina, et al. (2005). "Structure and properties of nanocomposites based on poly (butylene succinate-co-adipate) and organically modified montmorillonite." Macromolecular Materials and Engineering **290**(8): 759-768.
- Rolt, J. (2000). Top-down cracking: myth or reality. The World Bank Regional Seminar on Innovative Rehabilitation and Recycling Technologies, Amman, Jordan.
- Rowe, G. M. (1996). Application of dissipated energy concept to fatigue cracking in asphalt pavements, University of Nottingham.
- Santagata, E., O. Baglieri, et al. (2008). "Experimental investigation on the fatigue damage behaviour of modified bituminous binders and mastics " Journal of the association of asphalt paving technologist **77**: 851-884.
- Si, Z., D. N. Little, et al. (2002). "Characterization of microdamage and healing of asphalt concrete mixtures." Journal of materials in civil engineering **14**(6): 461-470.
- van Dijk, W. (1975). "Practical fatigue characterization of bituminous mixes." Asphalt paving technology **44**: 38-74.

Van Dijk, W., Moreaud, H., Quedeville, A. and Uge, P. (1972). The Fatigue of Bitumen and Bituminous Mixes. Third International Conference of the Structural Design of Asphalt Pavements, London.

8

CONCLUSIONS AND RECOMMENDATIONS

8.1 Introduction

In this chapter, the conclusions and recommendations that resulted from the research described in this thesis are presented. A more elaborate description can be found in the respective chapter.

8.2 Conclusions

Main conclusions with regards to the goal of this thesis are given below:

- It is possible to use the montmorillonite (Mt) to modify the bitumen. The modification effect depends on the type of Mt.
- The X-ray diffraction (XRD) results indicated that an intercalated structure for organo Mts was formed in the three base bitumens used in this study. The structure was corresponding to the aspect ratio calculated using the composite model. A phase separated structure of natural Mt was found in the base bitumen. Micro-CT images further proved that natural Mt acted like a conventional filler at micrometer level, probably due to its hydrophilic surface causing poor compatibility with the bitumen.
- The results show that organo Mts improve the short term ageing resistance of base bitumen. The barrier properties of Mt particles hindering the penetration of oxygen are the main reason for this improvement. Meanwhile, the reduction of volatilization of the oily components in the bitumen due to these barrier properties can be another reason.
- The Mts gave a less effective improvement in the long term ageing when using the PAV. Under tough testing conditions, an automatic accumulation of organo Mt platelets took place to reduce their surface area. This accumulation weakened the barrier properties of the Mts. Consequently, the improvement in the ageing became less. It is nevertheless believed that modifying bitumen with Mts can enhance the ageing resistance in the field because the physicochemical properties

of the Mt are very stable under field conditions and no accumulation will happen as occurred in the PAV.

-- It was difficult to evaluate the ageing effect on the chemical change of modified bitumens due to the interruption of the Si-O on the Mt to the FTIR spectra of bitumen. In comparison, rheological methods such as the DSR method are more effective to characterize the ageing properties of Mt modified bitumens.

-- The change in the viscosity of the bitumen modified by the Mt was attributed to two reasons: one was that the Mt platelets limit the flow of bitumen; another was that part bitumen molecules were confined to the two dimensional galleries of Mt clay. When imposing a shear stress on the bitumen at a liquid state, the Mt platelets orient themselves which results in the reinforcement of shear thinning, as well as a higher zero shear viscosity. This implies a good drainage resistance of the asphalt mix during transportation.

-- It was observed that the organo Mt modification increased the complex modulus accompanied by a decrease in the phase angle. Due to the high stiffness of the clay platelets, this modification contributed more to the change of the elastic part of bitumen's mechanical composition than that of loss part.

-- The results indicated that the nanoclay modification can change the fatigue life which was defined by the dissipated energy ratio (DER) in the stress controlled mode. The interfacial interactions between the surfactants on the nanoclay and bitumen molecules play a key role in the improvement of the fatigue life. Meanwhile, the modified mortar showed a better ageing resistance than the standard one.

-- Compared with bitumen and mortar, the asphalt mixture is more heterogeneous, and its failure mechanism is more complicated. Although the results are positive, the improvement in fatigue life by modifying the asphalt mixture with nanoclay is not spectacular.

8.3 Recommendations

From the experience obtained from this study, the following aspects appear important for further research:

-- Although the high-shearing mixing method is the most accessible one to prepare bituminous materials not only in the lab, but also in the factory, the results indicated that this preparation method did not result in an exfoliated structure for Mts in the bituminous matrix; just intercalated and phase separated structures were formed, depending on the type of Mt. To achieve an exfoliated state of organo Mt,

some other physical methods, such as melt intercalation and roll milling (introduced in Chapter 2) are recommended for future research

-- Adhesion failure results in the loss of bitumen or mortar from the aggregate (i.e. stripping). The presence of moisture is one of the main reasons. The Mt platelets can limit not only the penetration of oxygen, but also moisture. Therefore, it is recommended to characterize the moisture resistance of asphalt mixture. Besides, how the Mt can influence the adhesive strength between the bitumen and the aggregate is important to be investigated. The change in the surface energy of modified bitumen using the Wilhelmy plate method can give some indication.

-- To fundamentally understand how the Mt platelets interact with bitumen, it should be known which components or fractions of the bitumen are in the interlayer space of the Mt when its intercalated structure is formed. If the respective component or fraction of bitumen can be extracted and modified by the Mt, more detailed information could be obtained on the modification effect.

-- Because accumulation of the Mt platelets happens automatically when the modified is in liquid state, the standard PAV method is not suitable to simulate long term ageing of Mt modified bitumens. Therefore, it is necessary to design a new ageing method for this type of modified bitumen. Increasing the air/oxygen pressure and decreasing the film thickness of bitumen specimen are options. Whatever, the test specimen made of this type of bitumen should be in the same state as in the field.

Publications

International journals

1. **Gang Liu**, Martin van de Ven, Shaopeng Wu, Jianying Yu, and Andre Molenaar. 2011. Influence of organo-montmorillonites on fatigue properties of bitumen and mortar. *International Journal of Fatigue*, 33(12), 1574-1582
2. **Gang Liu**, Martin van de Ven, Shaopeng Wu, Jianying Yu, and Andre Molenaar. 2011. Organo-montmorillonite modified bitumens: studies on the structure and artificial ageing behaviours. *Journal of Applied Clay Science* in review.
3. **Gang Liu**, Shaopeng Wu, Martin van de Ven, Jianying Yu, and Andre Molenaar. 2010. Influence of sodium and organo-montmorillonites on the properties of bitumen. *Journal of Applied Clay Science* 49, 69-73.
4. **Gang Liu**, Martin van de Ven, Shaopeng Wu, Andre Molenaar, and Jeroen Besamusca. 2010. Characterization of Organic Surfactant on Montmorillonite Nanoclay to Be Used in Bitumen. *Journal of Materials in Civil Engineering*. 22(8), 794-799.
5. **Gang Liu**, Martin van de Ven, Shaopeng Wu, Jianying Yu, Andre Molenaar. 2010. A nanoindentation study on the rheological behaviour of bituminous binders. *Journal of Wuhan University of Technology*, 32, 47-50.
6. Shaopeng Wu, **Gang Liu**, Jianying Yu, Tingwei Cao. 2007. Investigations of Fatigue Characteristics of Porous Asphalt with Organomodified Montmorillonite Modified Asphalt. *Key Engineering Materials*, 348-349, 929.

International conferences

7. **Gang Liu**, Martin van de Ven, Shaopeng Wu, Jianying Yu, Andre Molenaar. Organo-Mt nanoclay, an alternative modifier to sustain the durability of asphalt pavement. Transportation Research Board 91st Annual Meeting. (Washington DC, America: January 22-26, 2012)
8. **Gang Liu**, Shaopeng Wu, Martin van de Ven, Andre Molenaar, Jeroen Besamusca. Modification of bitumen with organic montmorillonite nanoclay AES – ATEMA' Third International Conference on Advances and Trends in Engineering Materials and their Applications (Montreal, Canada: July 06-10, 2009).

Curriculum Vitae

PERSONAL

Name: Gang Liu
Date of Birth: 29th January, 1981
Place of Birth: Jingmen, Hubei, P.R. China
Marital Status: Married with Juan Tong on 8th, August, 2010
E-mail: Liugang102129@hotmail.com

EDUCATION

May, 2007 - Dec., 2011 PhD in the section of Road and Railway
Delft University of Technology.
Thesis entitled "Characterization and Identification of Bituminous
Materials Modified with Montmorillonite Nanoclay"

Mar., 2006 - Apr., 2007 Technical consultant in the pavement design and construction,
Administrative Agency of Chitong Asphalt Expressway, Inner
Mongolia

Sep., 2004 - Mar., 2006 M.Sc. (Road Materials and Engineering).
Wuhan University of Technology, P.R. China.
Thesis entitled "Study on Component Design and Properties of
Fibers Modified Porous Asphalt Mix "

Sep., 2000 - Jun., 2004 B.Sc. (Materials Science and Engineering).
Wuhan University of Technology, P.R. China.
Thesis entitled "Nondestructive Testing of Building Structures Using
Radar and Infrared Thermal instruments"

